Design and Performance Evaluation of a Low Concentrating Line-axis Dielectric Photovoltaic System

Nabin Sarmah

Submitted for the degree of Doctor of Philosophy

Institute of Mechanical, Process and Energy Engineering

School of Engineering and Physical Sciences

Heriot-Watt University

Edinburgh, United Kingdom

December 2012

Abstract

This thesis presents a detailed investigation of the design optimisation and performance analysis of a dielectric concentrator for building façade integration at high latitudes (>55°). Considering the seasonal variation of the sun's position at these latitudes, a concentrating photovoltaic (CPV) system with stationary concentrators of large acceptance angle and low concentration ratio is a suitable alternative to conventional flat plate photovoltaic (PV) modules. A well designed dielectric asymmetric compound parabolic concentrator (ACPC) is a suitable choice to achieve optimum range of acceptance angles and concentration ratio for building façade integration in the Edinburgh and higher latitudes.

A theoretical study of the optical performance shows that a truncated dielectric ACPC with acceptance half-angles of 0^o and 55^o (termed as DiACPC-55) is the optimum design, when compared to the dielectric ACPC designs with acceptance half angles of (0^o and 66^o) and (0^o and 77^o) in Edinburgh and higher latitudes. An increase in the range of acceptance angles is achieved by truncating the concentrator profile. Ray tracing simulations show the DiACPC-55 exhibits the widest range of acceptance angles compared to the other designs. The maximum optical efficiency of the DiACPC-55 is found to be 83%. In addition it is found to have a better intensity distribution at the receiver and a higher total annual energy collection, compared to the other designs. Thermal modelling of a CPV system with the DiACPC-55 concentrator shows that the solar cell and rear plate temperature can reach up to 41.6^oC for 1000 W/m^2 irradiance, when operating with an average ambient temperature of 10^oC.

The maximum power ratio of the CPV module (fabricated using the DiACPC-55 concentrator) to a similar non-concentrating counterpart is found to be 2.32, when characterised in an indoor controlled environment using a solar simulator. An average electrical conversion efficiency of 9.5% is measured for the entire range of acceptance angles. The optical loss analysis shows that incident light can escape from the parabolic sides and concentrator-encapsulation interface.

The outdoor characterisation of the CPV module with the DiACPC-55 concentrator shows that a maximum power ratio of 2.22 can be achieved on a sunny day. In comparison, a maximum power ratio of 1.9 is observed on a rainy day. These results

reveal that the designed dielectric concentrator is capable of collecting 68% of the diffuse radiation. The maximum electrical conversion efficiency of the CPV module in outdoor condition is found to be 9.4%. Module degradation due to the delamination of the solar cell is observed in the long term investigation study, which reduces the module efficiency to 8.6% on a clear sunny day.

The fabricated CPV system with the DiACPC-55 concentrator is found to be £190.3/m^2 cheaper than similar sized conventional glass-glass laminated modules. Therefore the cost of the CPV module is found to be £0.53/W_p cheaper than the conventional glass-glass laminated modules for building facade integration at high latitudes.

Acknowledgement

The journey of my PhD studies has been a defined experience to develop myself as an independent thinker and researcher. During the journey with success and failure, I have been accomplished by help and support of many people, without acknowledging them my thesis would be incomplete.

I am greatly indebted to my PhD supervisor **Tapas Mallick** for making this PhD possible. I cannot find the words to express my gratitude for your continuous guidance, encouragement and help during my PhD. Your support and supervision has been invaluable for me. I would also like to take the opportunity to thank my co-supervisor **Bryce Richards:** your suggestion and guidance have been invaluable. Your expertise and knowledge has always been helpful for me to rectify my mistakes and to learn new things.

I am thankful to the School of Engineering and Physical Sciences, Heriot-Watt University for providing the financial support and research facilities during my PhD. I am grateful to all the staff of EPS and specially Aftab, Rebecca, Alex, Karen, Josh, George and Cameron. I cannot forget all technicians Richards, Kenny, Alistair, Ian and Chris in the mechanical engineering workshop for their help in making my experimental hardware.

I would also like to take the opportunity to thank faculty members in department of Energy Technology, Tezpur University for their help whenever I needed. Dulon Konwar, Deben Baruah, D. Deka, S. Samdarshi, Rupam Kataki: your suggestion have been very helpful for me during my PhD. Special thanks to Sadhan Mahapatra, for his support and motivation during my M.Tech course and for guiding me to PhD.

I am grateful to all my fellow PhD students and Research Associates with whom I spent a lovely time and got help whenever I needed. I am thankful to Gavin, Dave, Laura, Bren, Lindsay, Efthymios, Gudrun, Pas, Nazmi, Ali, Mandy, Hasan, Jonathan, Sean, Dorothy, Dalila, Aritra and many others for your friendship and interesting discussions. I owe many of you especially for helping me in proof reading of my thesis and papers.

There is always a great support from all my friends in India and abroad. Pranjal, Gyan, Hanish, Kaustav, Hara, Panku, Devanka, Adi, Chandra, Rose and Ying: Thank you all.

I do not have enough words to thank my **Babu** and **Ma** for supporting me in everything. I am certainly blessed to have you as my parents. Thanks to my sister (Bunu): without your love and care it would be a difficult journey for me. Special thanks to Siva Da: your continuous support is greatly appreciated. Love you all!

ACADEMIC REGISTRY
Research Thesis Submission

Name*:*	Nabin Sarmah		
School/PGI:	School of Engineering and Physical Sciences		
Version: *(i.e. First, Resubmission, Final)*	Final	Degree Sought (Award **and** Subject area)	PhD Mechanical Engineering

Declaration

In accordance with the appropriate regulations I hereby submit my thesis and I declare that:

1) the thesis embodies the results of my own work and has been composed by myself
2) where appropriate, I have made acknowledgement of the work of others and have made reference to work carried out in collaboration with other persons
3) the thesis is the correct version of the thesis for submission and is the same version as any electronic versions submitted*.
4) my thesis for the award referred to, deposited in the Heriot-Watt University Library, should be made available for loan or photocopying and be available via the Institutional Repository, subject to such conditions as the Librarian may require
5) I understand that as a student of the University I am required to abide by the Regulations of the University and to conform to its discipline.

* *Please note that it is the responsibility of the candidate to ensure that the correct version of the thesis is submitted.*

Signature of Candidate*:*		Date:	14th December 2012

Submission

Submitted By *(name in capitals):*	NABIN SARMAH
Signature of Individual Submitting:	
Date Submitted:	14th December 2012

For Completion in the Student Service Centre (SSC)

Received in the SSC by *(name in capitals):*			
Method of Submission *(Handed in to SSC; posted through internal/external mail):*			
E-thesis Submitted (***mandatory for final theses)***			
Signature:		Date:	

Please note this form should bound into the submitted thesis.

Updated February 2008, November 2008, February 2009, January 2011

Content

Page No.

Chapter 7: Conclusions

List of figures

Page No.

List of tables

Page No.

Nomenclatures

Symbol	Definition	Unit
2a	Receiver length	m
A	Surface area	m^2
A_a	Aperture area	m^2
A_e	Area of envelop	m^2
A_r	Receiver area	m^2
C	Concentration ratio	
C_g	Geometrical concentration ratio	
C_{max}	Maximum concentration ratio	
D_i	Inner diameter of receiver tube of thermal collector	m
D_o	Outer diameter of receiver tube of thermal collector	m
F_R	Heat removal factor	
$F_{r\text{-}s}$	Fraction of heat radiation from receiver to source	J
$F_{s\text{-}r}$	Fraction of heat radiation from source to receiver	J
F_{ji}	View factor	
$F^{/}$	Collector efficiency factor	
G_a	Effective incident solar radiation on the aperture plane	Wm^{-2}
G_D	Direct solar radiation	Wm^{-2}
G_{diff}	Diffuse solar radiation	Wm^{-2}
G_G	Global solar radiation	Wm^{-2}
$H_t^{/}$	Total flux at the receiver	Wm^{-2}
I	Electric current	A
I_i	Intensity of a single ray	Wm^{-2}
I_o	Total intensity on the aperture	Wm^{-2}
I_{rec}	Intensity at the receiver	Wm^{-2}
$K_{\gamma\tau\alpha}$	Incidence angle modifier	
L_i	Path length of a single ray within concentrator	m

N	Number of surfaces	
N_u	Nusselt number	
P	Power	W
P_{max}	Maximum power	W
$Q_{r\text{-}s}$	Heat transfer from receiver to source	J
$Q_{s\text{-}r}$	Heat transfer from source to receiver	J
R	Distance of earth from sun	m
R_s	Series resistance	ohm
R_{sh}	Shunt resistance	ohm
T_b	Temperature of the bottom plate	^oC
T_r	Temperature of receiver	^oC
T_s	Temperature of source	^oC
U_L	Total heat loss co-efficient of flat plate collector	$Wm^{-2}C$
$U_{a/b}$	Heat loss co-efficient between cover and ambient	$Wm^{-2}C$
$U_{e/a}$	Heat loss co-efficient between receiver envelope and cover	$Wm^{-2}C$
$U_{r/e}$	Heat loss co-efficient between receiver jackets	$Wm^{-2}C$
V	Voltage	V
W	Half width of top cavity	m
Z	Vector function	
f	Focal length	m
h_{cond}	Heat transfer co-efficient for conduction	$Wm^{-2}K^{-1}$
$h_{cond,\ r\text{-}a}$	Heat transfer co-efficient for radiation between receiver and aperture	$Wm^{-2}K^{-1}$
h_{fi}	Heat transfer co-efficient between the fluid and inside the receiver tube	$Wm^{-2}K^{-1}$
h_{rad}	Heat transfer co-efficient for radiation	$Wm^{-2}K^{-1}$
$h_{rad,\ a\text{-}s}$	Heat transfer co-efficient for radiation between aperture and source	$Wm^{-2}K^{-1}$
h_w	Heat transfer co-efficient for convection	$Wm^{-2}K^{-1}$
j	Number of reflections	
m	Number of rays	
$\dot{m}$	Mass flow rate	Kgs^{-1}

n	Refractive index	
p	Pressure	Nm^{-2}
q	Charge of an electron	coulomb
$q_{in,i}$	Energy flux reflected from surface i	W
$q_{out,i}$	Energy flux reflected from surface i	W
r	Radius of curvature	m
u	Velocity in x-direction	ms^{-1}
v	Velocity in y-direction	ms^{-1}
z	Radius of curvature	m
α	Absorbance	
ε_a	Emmisitivity of aperture	
ε_e	Emmisivity of envelop	
ε_r	Emmisivity of receiver	
γ	Intercept factor	
k	Boltzmann constant	$m^2kgs^{-2}K^{-1}$
k_f	Thermal conductivity of fluid	$Wm^{-1}K^{-1}$
ρ_f	Fluid density	Kgm^{-3}
ρ	reflectivity	
τ	Transmittance	
τ_d	Transmittance of dielectric material	
τ_g	Transmittance of glass	
τ_r	Reflective component of unpolarised light transmission from a dielectric material	
η	Module efficiency	
θ_c	Angle of sun rays	Degree
$\theta_{max\ in}$	Maximum acceptance angle	
σ	Stefan-Boltzman's constant	$Wm^{-2}K^{-4}$
δ	Del operator	
∇	Laplace operator	

Abbreviations

AM	Air Mass
PV	Photovoltaic
LGBC	Laser Grooved Buried Contact
CIS	Copper Indium diselenide
CdTe	Cadmium Telluride
SEL	Stacked Element Layer
MJ	Multi Junction
MJ	Mega Joule
GaAs	Gallium Arsenide
InP	Indium Phosphide
GaSb	Gallium Antimonide
CR	Concentration Ratio
PV/T	Photovoltaic/Thermal
CPC	Compound Parabolic Concentrator
ACPC	Asymmetric Compound Parabolic Concentrator
CPV	Concentrating Photovoltaics
BIPV	Building Integrated Photovoltaics
BAPV	Building Attached Photovoltaics
BICPV	Building Integrated Concentrated Photovoltaics
SNP	Semi Non-Parabolic
EAC	Extremely Asymmetric Concentrator
MaReCo	Maximum Reflector Collector
ACPPVC	Asymmetric Compound Parabolic Photovoltaic Concentrator
FPSC	Flat Plate Static Concentrator
LSC	Luminescent Solar Concentrators
UV	Ultra-violet
PU	Polyurethane
PMMA	Polymethyle Methacrylate
ASTM	American Society for Testing and Materials
EVA	Ethylene Vinyl Acetate
CAD	Computer Aided Design
DiACPC	Dielectric Asymmetric Compound Parabolic Concentrator

BF	Borofloat
ND	Neutral Density
He-Ne	Helium-Neon
CAM	Computer Aided Manufacturing
2D	Two Dimensional
3D	Three Dimensional
CJC	Cold Junction Compensation
SE	Solar Energy
NI	National Instruments
OD	Optical Density
EMA	Ethylene Methyl Acetate
IAT	Inclination After Truncation
TAI	Truncation After Inclination
CFD	Computational Fluid Dynamics
HTC	Heat Transfer Co-efficient
EQE	External Quantum Efficiency
FF	Fill Factor
OE	Outdoor Experiment
FP	Flat Plate
NaREC	National Renewable Energy Centre
a-Si	Amorphous Silicon
c-Si	Crystalline Silicon

List of publications during this thesis work (to date)

Publications included in the thesis

Journal

N. Sarmah, B.S. Richards, T.K. Mallick, Evaluation and optimization of the optical performance of low-concentrating dielectric compound parabolic concentrator using ray-tracing methods, Appled. Optics., 50 (2011) 3303-3310.

N. Sarmah, B.S. Richards, T.K. Mallick, Design, development and indoor performance analysis of a low concentrating dielectric photovoltaic module, Applied Energy (submitted).

N. Sarmah, B.S. Richards, T.K. Mallick, Outdoor experimental performance analysis of a CPV modules with low concentrating dielectric concentrator for building integration, Solar Energy (In preparation).

Conference

N. Sarmah, A. Ghosh, T. K. Mallick, Indoor performance analysis of a low concentrating photovoltaic module for building integration, *In Proceeding of the CPV-8*, 26th - 18nd April, 2012, Toledo, Spain

N. Sarmah, T. K. Mallick, Development and characterisation of a low concentrating dielectric photovoltaic concentrator, *In Proceeding of the SWC-2011*, 28thAugust - 2nd September, 2011, Kasel, Germany

N. Sarmah, S. K. Natarajan, B. S. Richards, T. K. Mallick, Numerical investigation of thermal and electrical behaviour of concentrating photovoltaic module with low concentrating dielectric photovoltaic concentrator, *In*

Proceeding of the PVSAT-7, 6th-8th April, 2011, Heriot Watt University, Edinburgh, UK

N. Sarmah, B. S. Richards, T. K. Mallick, Design and performance evaluation of a prototype dielectric photovoltaic concentrator, *In proceeding of the PVSAT-6,* 24th-26th March, 2010, Southampton, UK

N. Sarmah, B. S. Richards, T. K. Mallick, Optimised Line Axis Dielectric Asymmetric Compound Parabolic Photovoltaic Concentrator: An Optical Performance Analysis, *In proceeding of the PVSAT-5,* 1st-3rd April, 2009, Wrexham, UK.

Publications not included in the thesis:

S. Maiti, N. Sarmah, P. Bapat, T. K. Mallick, Optical analysis of a PV-V trough system installed in Western India, Applied Optics (In press).

L. Micheli, N. Sarmah, X. Luo, T.K. Mallick, Opportunities and Challenges in micro-nano technologies for Concentrating Photovoltaic Cooling: a review, Renewable & Sustainable Energy Reviews (In press).

H. Baig, K. C. Heasman, N. Sarmah, T. K. Mallick, Solar cells design for low and medium concentrating photovoltaic systems, *In Proceeding of the CPV-8,* 26th - 18nd April, 2012, Toledo, Spain

H. Baig, K. C. Heasman, N. Sarmah, T. K. Mallick, Numerical modelling of a low concentrating photovoltaic system, Solar Energy Materials and Solar Cells (submitted).

Chapter 1

Introduction

Solar energy is the largest exploitable renewable energy source on earth. Statistically, the average solar energy incident on earth in one hour is more than the annual global energy demand. However conversion from solar energy to electrical energy is yet not cost effective enough to replace the conventional sources for power generation, due to the expensive solar cells. Concentrating solar photovoltaic systems can provide a solution by replacing expensive solar cells with inexpensive concentrator materials. For certain applications, like building integration, low concentrating systems can be an efficient way to generate higher power, while collecting the solar irradiance effectively, and using fewer solar cells compared with conventional building integrated photovoltaic (BIPV) modules. In this chapter, detailed introduction and the literature review of the concentrating photovoltaic system has been reported. Furthermore different state of the art BIPV technologies and previously reported concentrator designs for building integrated concentrating photovoltaic system has been discussed in details. The economics and the issues related to the BIPV and concentrating BIPV systems have also been reported.

1.1 Introduction

Energy is inevitably needed for human societies to sustain themselves and develop. With modernization of human civilization, energy demand is increasing day by day. Over hundreds of years, conventional sources, especially fossil fuel, were being used to fulfill the demand. The vast use of fossil fuels is creating social and environmental problems like climate change, environmental disasters and air pollution. In this energy scenario the demand for clean energy has increased and it has become important to use renewable sources for power generation [1-5]. The primary disadvantage of utilizing the renewable sources is the low conversion efficiency and high cost compared to the conventional sources. Solar and wind are the leading renewable sources compared to others like hydro, geothermal, biomass and tidal energy. The reasons for this attention towards solar and wind is the flexibility in installation of the system and zero pollution [6]. Furthermore, solar energy is the most exploitable renewable energy source. It is

reported that the annual energy consumption (4.1×10^{20} J) in 2001 was less than the solar energy incident on earth surface in one hour (4.3×10^{20} J) [7].

Solar energy, with its vast and essentially infinite fuel source, is playing a major role among the other renewable energy sources from the very early days. In normal household practice solar energy has been used for many decades for space heating and lighting. In the present energy scenario it has become important to utilise solar energy for industrial applications and for power generation along with conventional practices such as drying, day lighting and space heating. Nowadays with technological achievements solar energy utilisation has become more prominent. Solar energy can be collected as thermal energy and electrical energy as per the requirement. Considering the different operational condition and design, solar energy collection system for thermal and photovoltaic applications are studied separately as solar thermal collector and photovoltaic collector respectively.

1.2 Utilisation of solar energy in photovoltaics

The Sun is a gaseous sphere, which is 1.5×10^{11} m away from earth. Because of unceasing nuclear reactions, the Sun continuously emits energy that enables sustainable life on earth. From the very early days of human civilization solar energy has been used in different ways and for different application. The photovoltaic technology is the modern and advanced technology that converts solar energy directly into electricity, where a solar cell is the fundamental power conversion unit.

1.2.1 The Sun spectrum

The effective surface temperature of the sun is approximately 6000 K. Due to the continuous nuclear reaction the Sun emits electromagnetic radiation with a continuous spectrum, which matches that of a blackbody radiation at that temperature. The solar radiation reaches outside the earth atmosphere and it is measured in terms of power per unit area perpendicular to the direction of the Sun [8]. The internationally accepted extra-terrestrial radiation of the Sun is 1.353 kW/m^2. The spectrum of the Sun outside the Earth's atmosphere is called *air mass zero (AM0).* The Sun's spectrum continuously varies at the different places while travelling to Earth. The AM0 spectrum differs from the black body radiation at 6000 K, because of the different transmissivity on the Sun's surface for different wavelengths. In the same way, while entering the earth atmosphere

the spectrum changes because of absorption and scattering by different constituents of gas, water and dust particles. While entering the earth atmosphere the solar radiation is attenuated by 30% [9]. The attenuation of solar radiation inside the earth atmosphere depends on the path length of light travelled. So depending on the Sun's position in a particular location the spectrum of the sun varies due to the scattering and absorption effect of the atmosphere and has been termed accordingly for universal acceptance. When the sun is directly over head the spectrum is termed as AM1. With the change in sun position from overhead, depending on the angle to the overhead the air mass is give by [8, 10]

$$Air\ mass = \frac{1}{cos\theta} \tag{1.1}$$

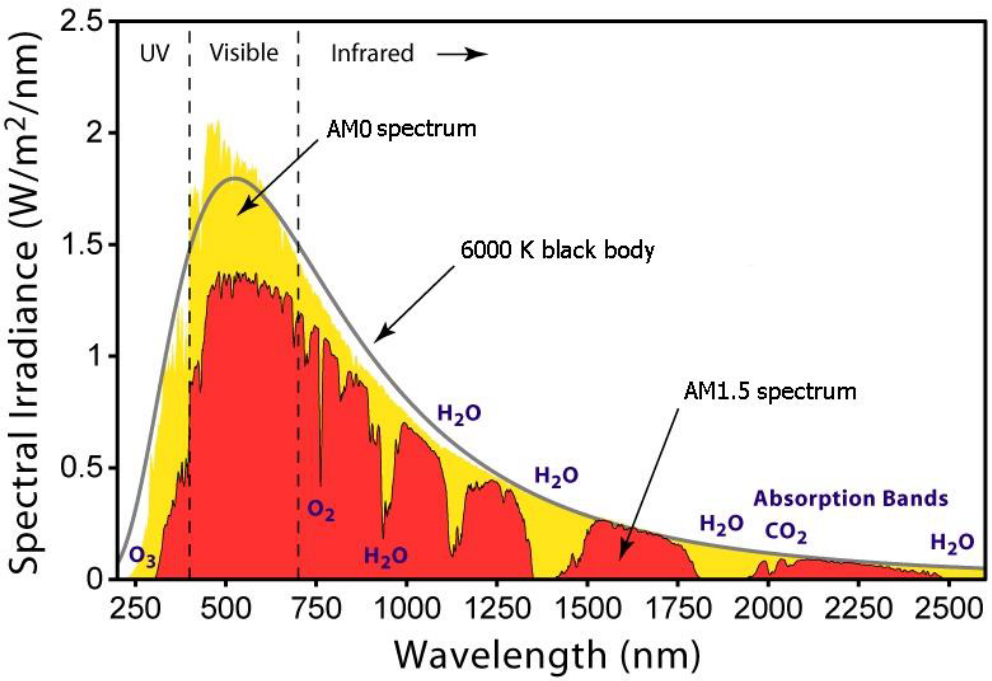

Figure 1.1 spectral distribution of sunlight with AM0 and AM1.5 spectrum [8, 10]

The spectrum of the sun when it is 60^o off overhead is termed as AM2 and so on. However for comparison of the different solar PV technologies a standard spectrum and radiation intensity has been adopted. The universally accepted standard terrestrial solar spectrum is AM1.5 and the radiation intensity is 1 kW/m^2. The spectral distribution of the Sun, AM0 and AM1.5 spectrum is shown in figure 1.1 [10, 11]

1.2.2 Direct, diffuse and global radiation

Above the Earth's atmosphere the solar radiation is incident directly from the sun. While entering the Earth's atmosphere the solar radiation scatters by the gas, vapour and dust. On the Earth's surface the radiation is scattered and reflected by the surroundings, which is termed as diffuse solar radiation. So the total radiation on a particular place on Earth is a combination of both direct and diffuse radiation. Even on a clear sunny day the contribution of diffuse radiation on a horizontal plane is 10-20%, depending on the location [11]. The diffuse radiation has a different spectrum than the direct radiation, and rich in short wavelengths. The global radiation is defined as the sum of direct and diffuse radiation on a surface at a particular location. In the common practice, the global radiation referred to the total sum of direct and diffuse radiation on a horizontal plane [10]. So to report the global radiation on a different surface other than horizontal, it is important to mention the plane as well. So the global radiation on a horizontal surface is given by [1, 12-15]:

$$G_G = G_D + G_{Diff} \tag{1.2}$$

where, G_G is the global radiation, G_D is the direct radiation and G_{Diff} is the diffuse radiation. In this thesis the terms direct, diffuse and global radiation referred to the internationally accepted definitions of these types of solar radiation.

1.2.3 Solar cell technologies

In the basic working principle of the solar cell, the incident light generates mobile charges within the semiconductor which can be separated by device structure or in the junction to produce an electric current (Figure 1.2) [8, 16, 17]. The operation of a solar cell is based on the junction of the p-type and n-type semiconductor in a solar cell. The junction can also be demonstrated as an interface of n-type and p-type semiconductor. When p-type and n-type semiconductor bring on contact, few surplus electrons near the junction in n-type will diffuse into p-type leaving behind positive charge in n-type.

The same takes place in p-type with diffusion of holes from p-type to n-type leaving behind negative charge in the p-type [18]. This will create a strong electric field at the junction. This field generates in the opposite direction to the electron-hole flow and balances further flow of the electron and holes. When light is incident on the solar cell,

electron-hole pair generates on the both side of the junction. The generated minority carriers of the both sides diffuse to the junction and are swept away by the electric field at junction, which produces a current. The equivalent circuit diagram of a solar cell is shown in figure 1.3 [19-21]

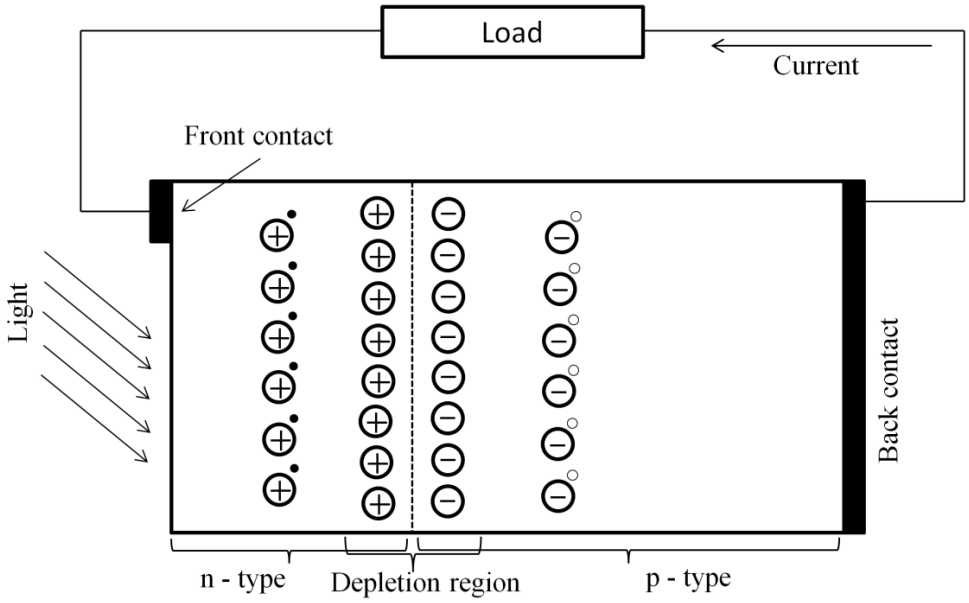

Figure 1.2 Schematic diagram of solar cell circuit [17].

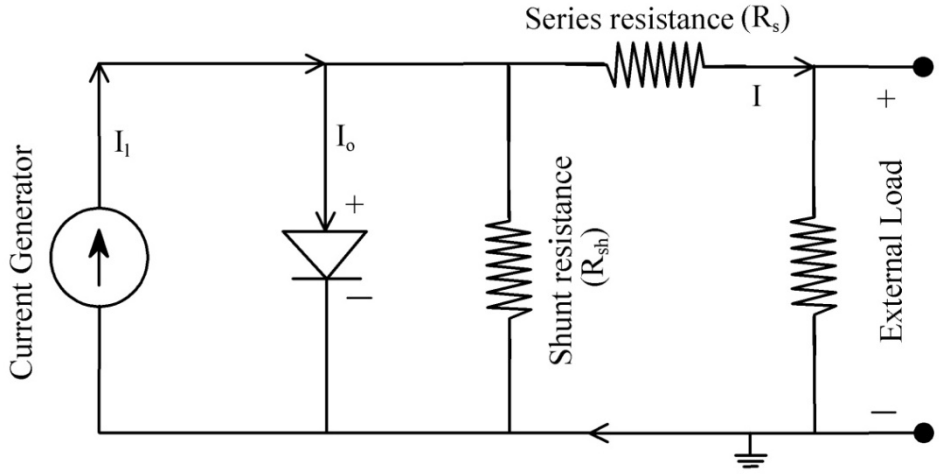

Figure 1.3 Equivalent circuit of solar cell [17].

The output current I is given by the difference of light generated current I_l and dark current I_d [19],

$$I = I_l - I_d \tag{1.3}$$

where, $I_d = I_o \left[exp\left\{ \frac{q(V+IR_s)}{KT} \right\} - 1 \right] - \frac{q(V+IR_s)}{R_{sh}}$, T is the cell temperature, K is the Boltzman constant, q is the charge of electron, V is the voltage across the cell, R_s is the series resistance and R_{sh} is the shunt resistance. Different solar cell technologies are available on the market. The solar cells are made of different materials and by different manufacturing processes. The conversion efficiency and life time also varies from the cell to cell depending on the technology.

1.2.3.1 Crystalline silicon solar cells

Crystalline silicon solar cells are used in 90% of the PV modules in the market to date. The popularity of the crystalline silicon solar cell can be put down to two reasons; a) silicon is a good semiconductor material with well-balanced chemical, physical and mechanical properties, and b) an established silicon processing technology is in place due to its use in the electronics industry [22]. Crystalline silicon solar cells are basically a monocrystalline or polycrystalline p-n junction. The cell base is a p-type silicon wafer of 300-500 µm thick. Taking into consideration the band structure of silicon, the n-type emitter is a thin layer, heavily doped to allow maximum possible light to pass through to the base and to reduce series resistance, respectively [23-27]. The indirect band gap of crystalline silicon is 1.7 eV, while the direct band gap is 3 eV [17]. A schematic diagram of the crystalline silicon solar cell is shown in figure 1.4 indicating screen printed silver fingers, back contact, p-type and n-type silicon.

Depending on the crystal size and structure the silicon wafer, crystalline silicon solar cells are separated in two groups: monocrystalline and multicrystalline silicon solar cells. The solar cell efficiency and cost vary because of the different crystal grain size and manufacturing processes.

- Monocrystalline silicon solar cells: Single crystal silicon is commonly grown by *Czochralski* process, in which "*a single crystal is drawn slowly out of a melt" [27]*. The dopant is usually introduced during this process to make it a p-type crystal. N-type dopant is then allowed to diffuse on to the p-type wafer to prepare the junction. To reduce the reflectivity, the front surface of the cell is textured and an anti-reflection coating is introduced. There are front contacts (as finger and bus-bars) and rear contacts to prevent the generated electrons from recombining and to achieve good conductivity. The maximum efficiency of the

monocrystalline solar cell reported recently is 25% [29]. The laser grooved buried contact (LGBC) process is a major breakthrough in monocrystalline silicon solar cell development in recent times [30, 31]. The performance of the LGBC cells has been maximized by minimal contact area, front and back surface texturing and a back surface field [30, 32]. Schematic images of a standard monocrystalline silicon solar cell and LGBC cell design is shown in figure 1.5. In most of the other manufacturing processes of solar cells the front contact is added by a screen printing process on top of the cell [33]. In LGBC manufacturing process, a laser is used to inscribe grooves into the cell where fingers for the front contact are deposited by electro-plating technique. This reduces the shading losses due to the fingers. Because of the controlled laser technique, the front contacts can be designed to take any shape if required, for any specific applications [34][35].

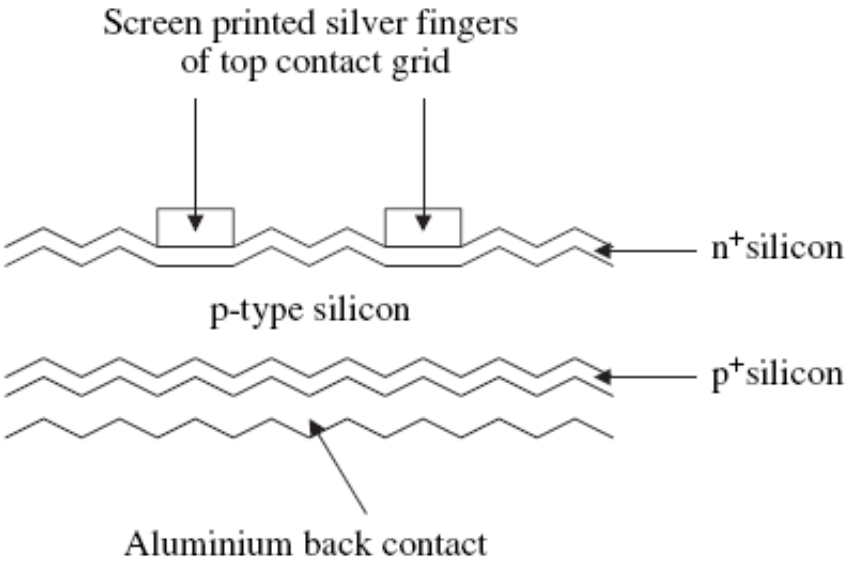

Figure 1.4 Schematic diagram of the crystalline silicon solar cell (cross sectional view) [28]

- Multicrystalline silicon solar cells: The commercial success of multicrystalline silicon solar cells can be noticed by increase in market occupancy from 30% to 48% of the world's photovoltaics market from 1998 to 2010 [22, 36]. The silicon wafer used is fabricated with a technique which allows silicon ingots with large columnar grains to grow from the bottom when solidifying molten silicon [22]. Different manufacturing and texturing techniques have been reported to improve the efficiency of the multicrystalline solar cells [37-40]. The

efficiency of the multicrystalline silicon solar cell is limited because of the minority carrier recombination. The recombination takes place due to the intragrain defect (impurities and precipitates) and dislocations.

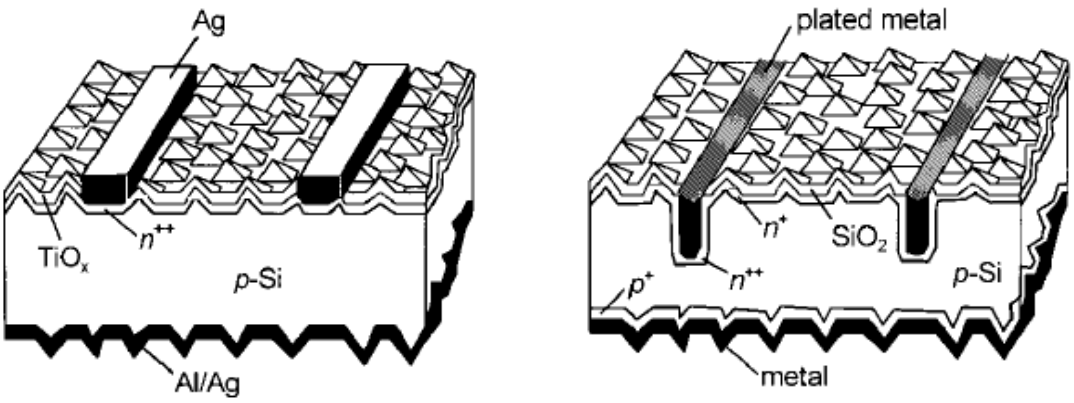

(a) (b)

Figure 1.5 Schematic image of (a) a screen printed crystalline silicon solar cell (b) LGBC crystalline silicon solar cell [41]

1.2.3.2 Polycrystalline thin film solar cells

The thin film solar cell is an alternative to silicon solar cells with cost and performance advantages [42-44]. Thin film solar cells have efficient material utilisation, potential for large scale manufacturing and better energy economy in terms of production [32, 45]. Different types of thin film solar cell with compound semiconductor approach have been mentioned below:

- Copper Indium Gallium Diselenide (CIGS): Copper Indium Selenide (CIS) and CIGS are emerging thin film semiconductors [46]. CIGS ($Cu(InGa)Se_2$) solar cell is the most promising solar cell technologies among the thin film solar cell family to achieve cost effective power generation. Long term stability is another important advantage of the CIGS solar cells [17]. The CIGS solar cell materials have advantages like satisfactory band gap for homojunction and heterojunction [28, 32], direct band gap transition minimises the minority carrier diffusion length and very stable electro-optical properties. CIGS solar cells can be manufactured by various deposition techniques, flash evaporation, sputtering, electrodepositing, spraying etc [47-49]. The thin film of the solar cell is deposited on a glass substrate and the necessary connections are made to

complete the cell [32]. The maximum efficiency of CIGS solar cell is reported to be 20.3% [29].

- Cadmium Telluride (CdTe): CdTe has a band gap near to 1.5 eV, which is optimum energy band gap for PV application [50]. A thin layer is enough to absorb the incident solar radiation, which leads to reduction in cost. The popular choice of the CdTe based solar cell is CdS/CdTe solar cell [51]. High efficiency CdTe based solar cells are manufactured by SEL processing [52]. Deposition of Cd_2SnO_4, Zn_2SnO_2, CdS, CdTe and back contact in sequence was reported to have maximum efficiency of CdTe based solar cell in 2002 [28]. Although CdTe based thin film modules have potential of low cost and large scale manufacturing, stability of the material is still an issue.

1.2.3.3 Dye Sensitised solar cell

Dye sensitized solar cells are photochemical cells, an alternative to all solid state solar cells. The basic structure of this kind of cell is a top electrode made by screen printing a layer of TiO_2 onto fluorine doped SnO_2 coated glass. A dye is applied to the TiO_2 which gives nice aesthetical properties. The electrodes in the bottom counter are made by a layer of pyrolithic platinum onto fluorine doped SnO_2 coated glass by a screen printing method [28]. Suitable electrolytic material is added between the electrodes. Sealing the sides to prevent the leakage of electrolyte materials completes the structure of the cell. The most successful type of cells in this category is 'Gratzel cells' [53]. Dye sensitized solar cells are also manufactured by pouring molting silicon through screens which makes small droplets of silicon to form electrodes [54]. The maximum efficiency of this kind of cell to date is reported to be 11.4% [29].

1.2.3.4 Organic solar cells

Cells made of organic material such as polymeric semiconductors, fullerenes and fullerene derivatives are catagorised as organic solar cells [55-57]. Due to the polymer materials, these cells are flexible and can be used for a wide range of applications [58]. The basic cell structure consists of three components: a) glass substrate coated with Indium tin oxide (this works as a transparent top electrode) b) a layer of organic material c) metal back contact. The advantages of organic solar cells are the simple deposition technique (spin coating) and less expensive material [59]. The maximum efficiency of this type solar cell is reported to be 10.6% [29].

1.2.3.5 Multijunction (MJ) solar cells

Single junction solar cells cannot absorb the entire photon incident within the solar spectrum, due to the limitation of band gap of the semiconductor materials. So there is a need for different coupling of junctions, each of different band gap values, to use the entire solar spectrum [60]. III-V material such as Gallium Arsenide (GaAs), indium phosphide (InP) and gallium antimonide (GaSb) are found to have excellent opto-electronic properties to manufacture high efficiency solar cells [28]. These direct band gap compounds have good optical absorption co-efficient and minority carrier lifetime. Theoretically ~72% conversion efficiency with 32 band gaps can be achieved with MJ solar cell [61]. In recent times a number of studies have been carried out to improve the efficiency of the multijunction solar cell [62-67]. The maximum efficiency of a triple junction GaP/InGaAs/Ge solar cell has been reported to be 41.6% for intensity of 364 suns [29]. However, current record efficiency of a multi-junction solar cell is reported to be 43.5%, using dilute nitride alloy for the lowest junction [68].

1.3 Solar energy collector

In general terms, a solar energy collector can be defined as a device that collects the energy of sun and converts it into a more usable form. The term collector refers to a system which includes receiver, concentrator, cover element and tracking element. The receiver constitute of absorber and insulation or cooling depending on the application. The concentrator directs the solar radiation from the large aperture area to the small area receiver area. The cover element is to protect the total system from degradation, dirt, corrosion and oxidisation. Tracking element is required to change the orientation of the collector according to the position of the sun. Tracking of the sun is essential for high concentrating solar collectors.

Terrestrial solar radiation of 1000 W/m^2 (average) is not enough for thermal application in industrial level and not economically attractive for photovoltaic operation because of low conversion efficiency of solar cell. Concentrating solar radiation leads to increase in flux density on a small receiver area. High flux density provides higher temperature for thermal application and higher electrical output in PV applications.

1.3.1 Solar concentrator

Solar concentrating systems constitute of an aperture area, receiver area and reflector/refractor. The aperture refers to the side of the concentrator through which solar irradiation enters the concentrating system. The receiver is the section where absorber is attached. The reflector or refractor is responsible for directing the radiation to the receiver. Different concentrator profile and design are used over the years for different applications to achieve high optical efficiency [69-79].

Considering the optics of the reflector or refractor the concentrators can be divided into two main categories: imaging and non-imaging concentrators [80, 81]. As the term defines concentrators with imaging optics forms an image of the sun on the receiver, like parabolic mirror, convex lens etc. Whereas concentrators with non-imaging optics do not form any image of the sun but only concentrate the solar irradiation over a specified area [82].

1.3.2 Concentration ratio

The term ‘concentration ratio’ can be described as the ratio of the energy flux at the receiver to the energy flux at the aperture of the concentrating system, which is primarily related to the area of the aperture and receiver of the system [10]. There are two definitions of concentration ratio: i) geometrical concentration ratio ii) Optical concentration ratio, the former is most commonly used [17].

1.3.2.1 Geometrical concentration ratio

The most commonly used definition for concentration ratio is the ‘geometrical concentration ratio’ which is defined as the ratio of the aperture area to the absorber area.

$$C_g = \frac{A_a}{A_r} \tag{1.4}$$

The theory of the concentration limit is established by using the radiative heat transfer between the two sources, the sun and the absorber [83].

As shown in figure 1.6, 'z' is the radius of the sun (S) and R is the distance of earth from sun. A_a and A_r are the area of the aperture and receiver respectively.

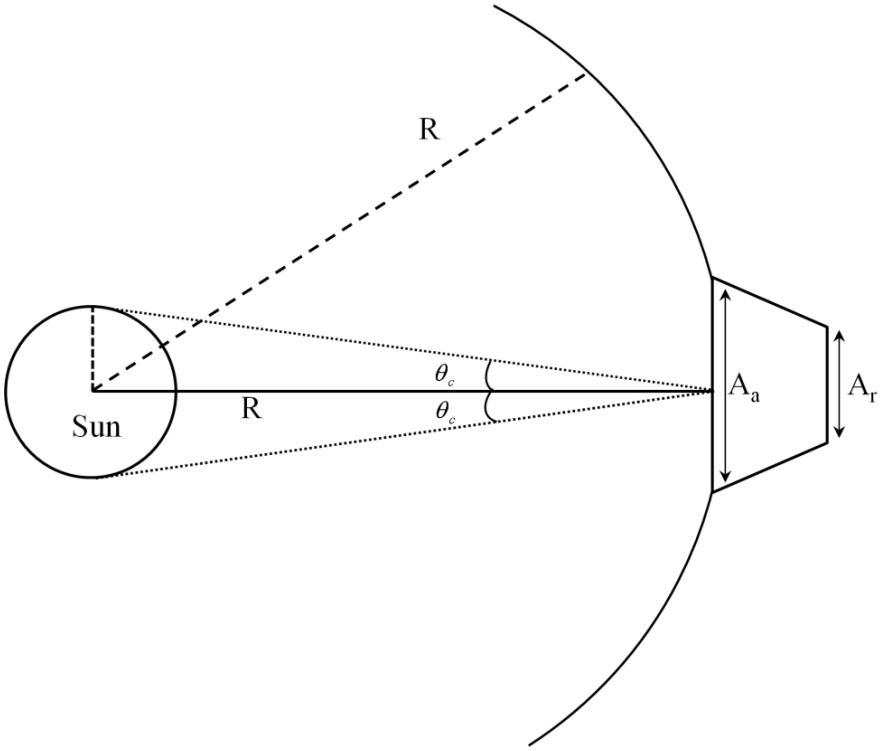

Figure 1.6 Radiation transfer from source to absorber through aperture [83]

Considering both the source (sun) and the absorber as black body with temperature T_s and T_r respectively, the amount of heat transfer from the source to receiver is

$$Q_{s-r} = Q_s F_{s-r} = A_a \frac{z^2}{R^2} \sigma T_s^4 \tag{1.5}$$

Where, $F_{s\text{-}r}$ is the fraction of the total heat radiation from the sun reaching the receiver, $F_{s\text{-}r} = A_a/4\pi r^2$

Again the amount of heat transfer from the receiver to source is

$$Q_{r-s} = F_{r-s} A_r \sigma T_r^4 \tag{1.6}$$

Where $F_{r\text{-}s} < 1$, Second law of thermodynamics states that there cannot be any heat transfer between two bodies of equal temperature. So for $T_r = T_s$

$$A_a \frac{z^2}{R^2} = F_{r-s} A_r \quad (1.7)$$

$$C = \frac{A_a}{A_r} = \frac{R^2}{z^2} F_{r-s} = \frac{F_{r-s}}{Sin^2\theta_c} \quad (1.8)$$

The maximum value that $F_{r\text{-}S}$ can have is unity, which gives

$C = \frac{1}{Sin^2\theta_c}$, for three dimensional concentrator (1.9)

In a two dimensional case it becomes;

$$C = \frac{1}{Sin\,\theta_c} \quad (1.10)$$

If the receiver is covered by dielectric medium of refractive index 'n', the maximum concentration ratio increases to;

$C = \frac{n^2}{Sin^2\theta_c}$, for three dimensional concentrators (1.11)

$C = \frac{n}{Sin^2\theta_c}$, for two dimensional concentrators (1.12)

1.3.2.2 Optical concentration ratio

Optical concentration ratio is also termed as 'flux concentration ratio' and 'intensity concentration ratio'. It is defined as the ratio of average energy flux on the absorber to the aperture of the system [17]. Since the energy flux on the receiver surface is not homogeneous, the average of the flux on the receiver is considered. In another approach local flux concentration ratio on the absorber can also be defined, which stated as the ratio of the flux at any point of the receiver to the aperture [84]. Optical concentration ratio is also termed as 'suns'. If the flux on the absorber is 5 times the flux on aperture, the concentration ratio is termed as 5 suns or 5X.

1.3.2.3 Limit of concentration ratio

The theoretical limit of concentration has been derived by optical method considering unit refractive index of the both input and output medium [82]. In non-imaging optics, when light rays enter the concentrator through aperture area of A_a with an angle less than $\theta_{max,in}$ and transmitted through the receiver area of A_r with an angle $\theta_{max,out}$, (as shown in figure 1.7) the concentration is given by [17],

$$C = \frac{A_a}{A_r} \le C_{\max} = \frac{\sin\theta_{\max out}}{\sin\theta_{\max in}} \quad \text{(for two dimensional cases)} \tag{1.13}$$

Since the $\theta_{max, out}$ cannot have value more than 90^o, so

$$C_{\max} = \frac{1}{\sin\theta_{\max in}} \quad \text{(for two dimensional cases)} \tag{1.14}$$

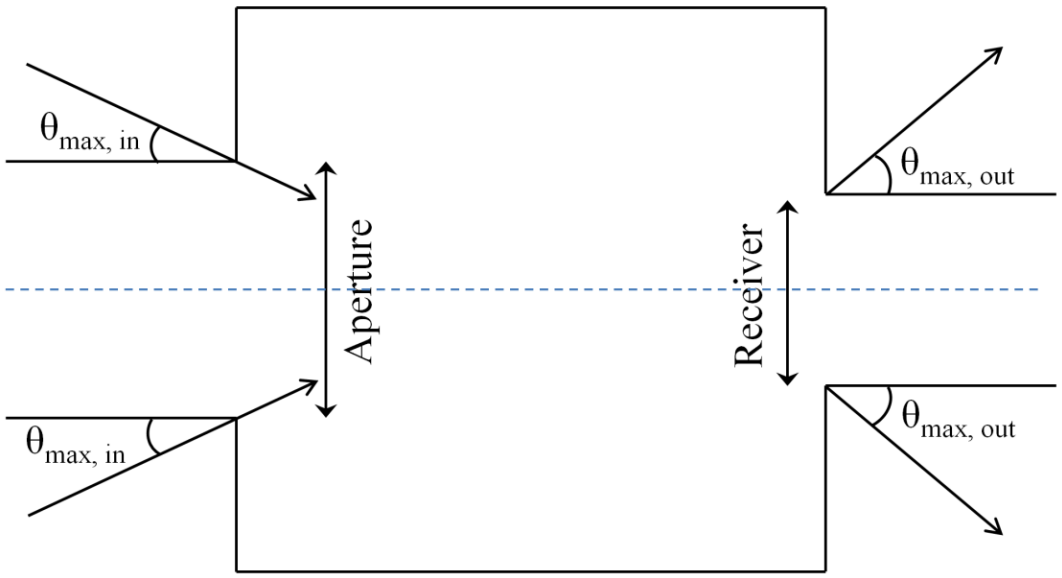

Figure 1.7 Schematic representation of concentrator optics

Also from the definition of geometrical concentration ratio, the maximum possible concentration ratio for 3-dimensional and 2-dimensional cases, given by equation (1.13) and equation (1.14) are

$$C = \frac{1}{\sin^2\theta_c} \quad \text{(for three dimensional cases)}$$

$$C = \frac{1}{\sin\theta_c} \quad \text{(for two dimensional cases)}$$

Thus with $\theta_c = 0.27^o$, the minimum half angle that solar radiation subtended on earth surface, the maximum possible concentration ratio that can be achieved for 3-dimensional case (or circular concentrator) is 45000 and for 2-dimensional case (or for linear concentrator) is 212 [10].

1.4 Concentrating collector properties

The performance of concentrating collectors is dependent on its optical and thermal properties. The parameters for the optical properties of solar collector are termed as 'optical efficiency' and 'angular acceptance'. The optical efficiency is defined as the ratio of solar radiation absorbed by the absorber to the radiation on the aperture. The 'angular acceptance' is defined as the fraction of a uniform beam of parallel rays incident on the aperture at an angle from the symmetry axis that would reach the receiver if the optics were perfect [85]. The thermal performance of the concentrating collector is characterized by the heat loss from the absorber to the atmosphere. The higher the heat losses the lower the efficiency of the collector for solar thermal application.

1.4.1 Optical properties of concentrating collector

The optical properties of the concentrating collectors vary with the geometry and configuration. The general concept that can be applied to all concentrating collectors is related to the radiation absorbed at the per unit area of the receiver. Several factors can influence the optical properties of the concentrating collector, including the properties of the material and the design of the collector. The general equation representing the optical properties of the concentrating collector can be written as [10];

$$S = G_a \rho (\gamma \tau \alpha)_n M_{\gamma \tau \alpha} \tag{1.15}$$

Where, S is the radiation absorbed per unit area of the receiver, G_a is the effective incident radiation measured on the plane of the aperture. ρ is the specular reflectance of the reflective type concentrators and transmittance of the refractive type concentrators. γ, τ, α are termed as intercept factor, transmittance of cover system on the receiver and absorptance of the absorber. In general, the effect of these three parameters treated separately; however these parameters can be considered as functions of the incident angle modifier as well. The intercept factor is defined as the fraction of the reflected radiation incident on the absorbing surface of the receiver. Normally the value of γ is greater than 0.9. The low concentrating non-tracking collectors can be designed to achieve intercept factor 1. The transmittance of the cover of the receiver and the absorptance of the absorber is the property of the material used; however these parameters can significantly depend on the angle of incidence. Radiation reflected or

transmitted from concentrator can reach the receiver with different incidence angles. So for detailed investigation of the transmittance and absorptance of the cover and absorber, optical modeling considering millions of rays as incident radiation is required. 'n' in the equation represents the number of components in the concentrating collector. Figure 1.8 shows a schematic diagram of a concentrating collector indicating the losses in the different components, which represents the different parameters of the equation 1.15.

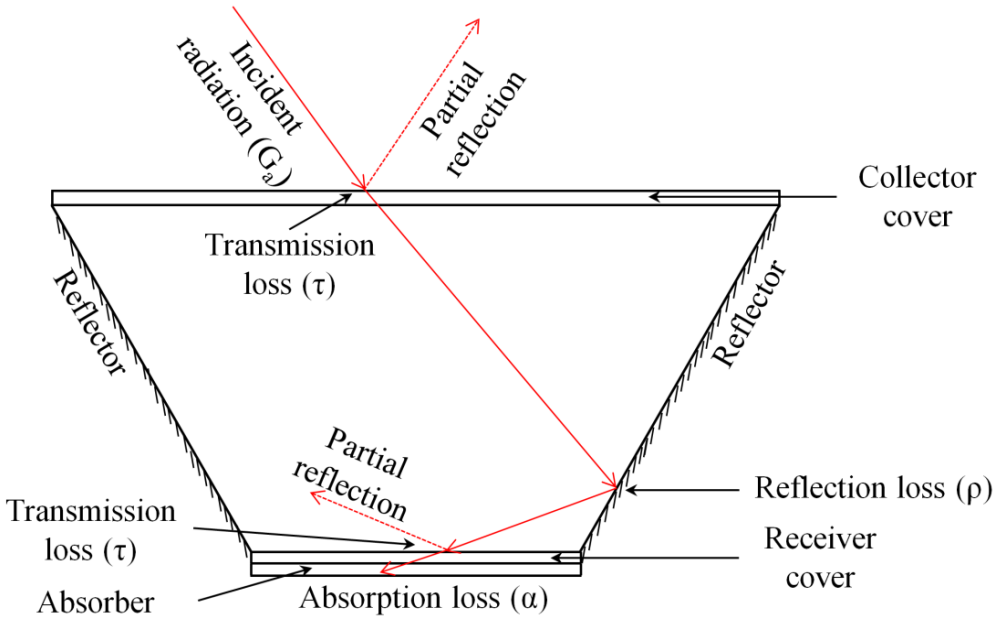

Figure 1.8 Schematic diagram showing the losses in a concentrating collector

For the concentrating collectors with secondary concentrators, the intercept factor of the secondary concentrators and the primary concentrator should be treated separately. The transmittance of the number of the receiver cover and the absorption properties of the different material layers of the absorber also need to be taken into account. $M_{\gamma\tau\alpha}$ is the incident angle modifier (IAM) used for deviation of the angle of incidence from the normal [10]. The IAM also demonstrates the effect of the incidence angle on the optical efficiency of the system, hence the can be considered as a function of intercept factor, transmittance and absorptance of the system and receiver. While all the functions of the IAM are treated separately, the value of IAM will be 1.

1.4.2 Thermal properties of concentrating collectors

The thermal performance of concentrating collector is largely dependent on heat loss from the receiver. The estimation of thermal losses from the receiver is complex due to the variable shape and design, high temperature, edge effect and compounded by the non-uniformity of the radiation flux on receiver. So every concentrating solar collector has a different design configuration should be treated separately, as their thermal behavior changes with their configuration.

The generalized thermal performance of concentrating collector can be represented by the flat plate collector. Collector efficiency factor $F^{/}$, the heat loss co-efficient U_L, and collector heat removal factor U_R determines the collector's overall useful gain [86].

The expression of heat loss co-efficient U_L for flat plate collector is given as;

$$U_L = h_w + h_{rad} + U_{cond} \tag{1.16}$$

For a receiver area A_r and aperture area A_a the expression of U_L can be written as

$$U_L = \left[\frac{A_r}{(h_w + h_{rad\ ,a-s})A_a} + \frac{1}{h_{cond\ ,r-a}}\right] \tag{1.17}$$

For flat plate concentrating system with cylindrical receiver, the inside and outside diameter and the heat transfer property of the material used will determine the collector efficiency factor. For a system with receiver tube of outer diameter D_o and inner diameter D_i the collector efficiency factor will be [87]

$$F^{/} = \frac{{}^{1}/_{U_l}}{\frac{1}{U_L} + \frac{D_o}{h_{fi} D_i} + \left(\frac{D_o}{2k} \ln \frac{D_o}{D_i}\right)} \tag{1.18}$$

Where, h_{fi} is the heat transfer co-efficient inside the tube and k is the thermal conductivity of the tube.

The heat removal factor is also an important parameter for determining the thermal performance of the concentrating system. For a flat plate collector, the expression for heat removal factor is;

$$F_R = \frac{\dot{m}C_p}{A_r U_L}\left[1 - \exp\left(\frac{A_r U_L F'}{\dot{m}C_p}\right)\right] \tag{1.19}$$

Where, $\dot{m}$ is the mass flow rate and C_p is the specific heat capacity of the fluid used. This expression for the different concentrating system will vary according to the geometry of the system and take on a more complex form. Detailed geometrical analysis of the concentrating system is necessary before analyzing the thermal performance of any collector.

1.5 Different types of solar concentrating system

The Solar concentrating systems are found to have different shape, design and different range of concentration ratio (CR) depending on the type of application. The details of concentration ratio are discussed in section 1.3.2. Solar concentrators are used in all the solar energy application including photovoltaics, thermal and photovoltaic/thermal (PV/T) systems [70, 88-98]. Different application of the solar concentrators depending on the concentration ratio is shown in figure 1.9.

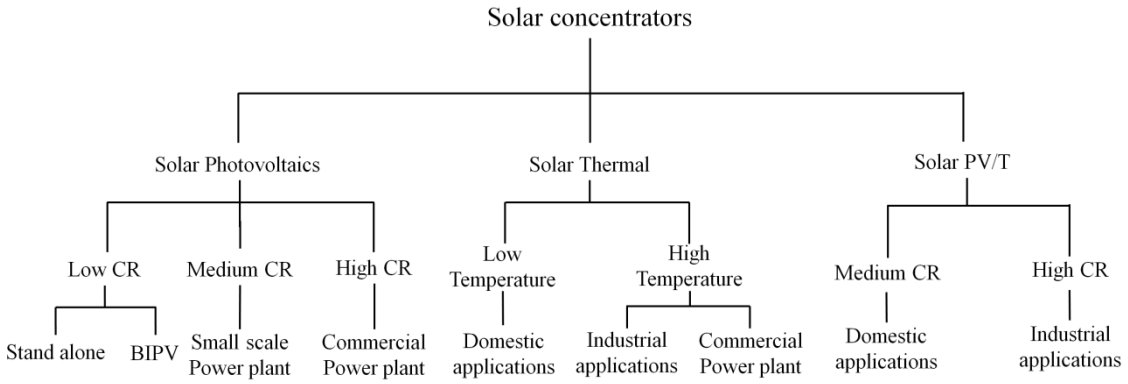

Figure 1.9 Different solar concentrators and their applications

The solar energy concentrating systems can be sorted into three categories depending on the concentration ratio as i) High concentrating system, ii) Medium concentrating system, iii) Low concentrating system. Figure 1.10 shows several concentrator configurations with different absorber designs. The concentrator configurations shown in figure 1.10 (a-c) are for low concentrating system. Whereas figure 1.10 (d-f) shows configurations used for medium to high concentrating system, which require tracking.

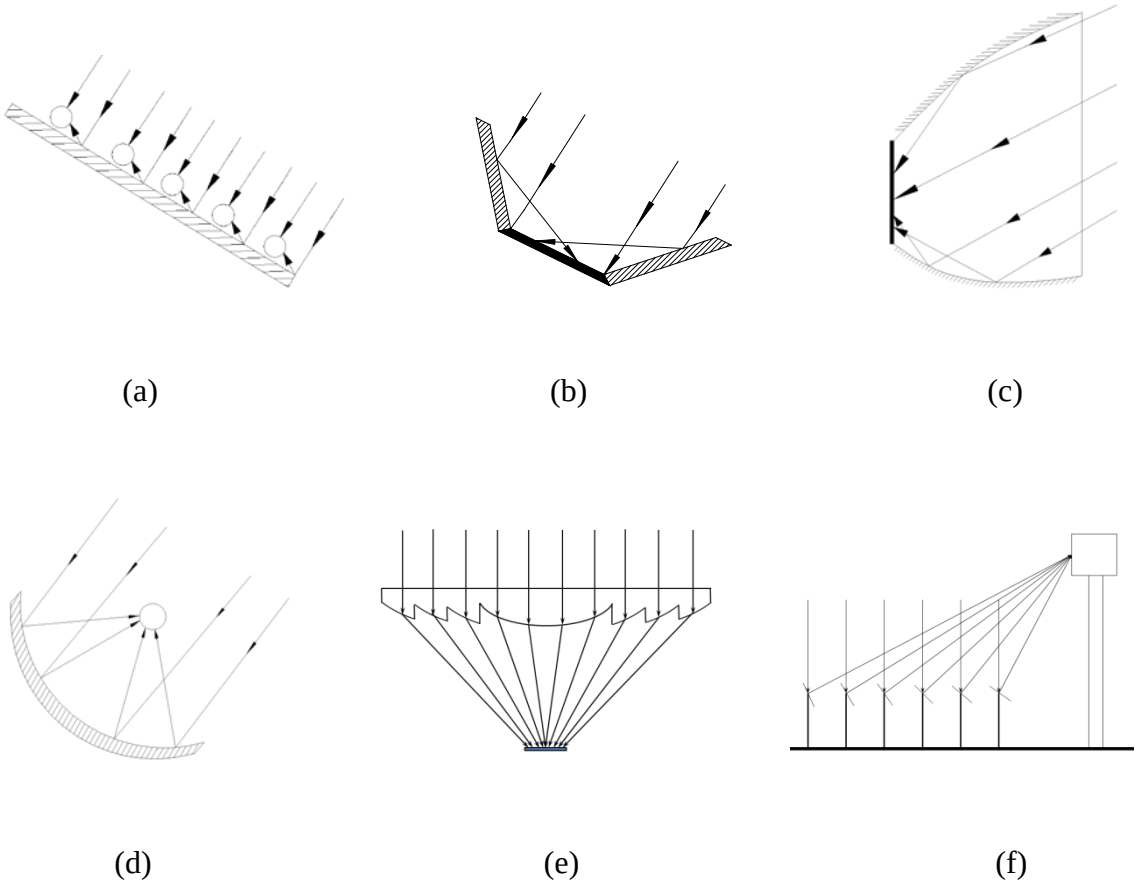

Figure 1.10 Different concentrator configuration: (a) tubular absorbers with diffuse back reflector (b) plane receiver with plane reflector (c) Asymmetric compound parabolic concentrator. (d) Parabolic concentrator (e) Fresnel lens (f) Heliostat

1.5.1 High concentrating system

High concentrating systems have a concentration ratio higher than 100. High density flux of solar irradiation can be obtained with this type of concentrating system. But the major disadvantage of this kind of concentrating system is the requirement of 2-axis tracking of the sun. Parabolic discs and lenses are mainly used to obtain high concentration [99-102]. Central receivers with heliostat fields reflecting the light towards the receiver are used to obtain high concentration [76, 103]. This type of concentrating system is popular in solar thermal power plants and in industrial processes where high temperatures are required. However, in recent times high concentrating systems are also used in CPV systems with multi-junction solar cells.

In high concentrating photovoltaic systems very small sized solar cell can be used as the spot size will be very small with high flux density. The reduced solar cell area results in

a decrease in cost of the power output significantly. However there is a need for a cooling system and special cell design for this kind of concentrating system.

1.5.2 Medium concentrating system

This type of system refers to a concentration ratio of 10X – 100X[10]. Such systems require one axis tracking of sun. Fresnel lens and parabolic reflector are used to achieve the concentration ratio [104-106]. For PV system with medium concentration range the cells have to be specially designed and cooling systems will be required for better efficiency.

1.5.3 Low concentrating system

The systems with a concentration ratio of 1X-10X are catagorised in this type. No essential tracking is required to achieve this concentration ratio [77, 107, 108]. Low concentrating systems are suitable for PV applications, which can be used without tracking and cooling requirement. Low concentrating systems use linear geometry concentrators and have the advantage to integrate in buildings or to use as a standalone system. Standard PV modules can be used with this type of concentrating system without much modification. CPCs of different configuration are popular designs for low concentrating system but other geometries are also in use [109]. The geometries that are suitable for low concentration photovoltaics include V-trough reflector, CPC type reflector, refractive CPC and linear Fresnel lenses.

1.6 Non imaging optics

Non imaging optics is concerned only with the transfer of light energy to the target without endeavoring for an image. This kind of optics is seen to be very useful in solar concentrator and illumination applications [110, 111]. In solar energy application the prime objective of the concentrator is to increase the power density of the radiation, which is popularly done by concentrating the light with the help of an image forming system. But the disadvantage with the image forming devices is optical aberration and requirement of large no of refracting or reflecting surfaces [82].

For construction of non-imaging concentrators Welford and Winston, 1978 estimated a principle for ideal concentrators that collect rays within their acceptance angles and rejects rays outside this angle. This principle states that the bundle of rays from one of

the extremes of the source has to be imaged into one of the extreme of the receiver and the other extreme of the source has to be into the other extreme of the receiver [112]. It was assumed that all the rays in the source within these extremes fall somewhere inside the collector [113]. In an ideal non-imaging concentrator, firstly the concentrator aperture is irradiated uniformly from a Lambertian source and then the absorber receives a uniform flux coming through the aperture.

1.6.1 Compound parabolic concentrator

The concept of the Compound Parabolic Concentrator (CPC) for solar energy applications are proposed in 1974 [114]. Since then many works have been reported to use CPC for both solar thermal and photovoltaic applications [115-121]. Compound parabolic concentrator can achieve the highest possible concentration for any acceptance angle compared to the flat mirrors, focusing parabolas and lenses [69]. A typical CPC consists of the two reflectors, which funnel all the radiation that is incident on the aperture within certain angles. The two reflectors in the left and the right hand side of the receiver are different parabolic sections mounted at certain angles. The focus points of the two parabolic reflectors are located at the two edges of the receiver. Figure 1.11 shows the cross-section of a CPC with the path of the extreme rays of the acceptance angle. All the light that is incident within the acceptance angle reaches the receiver. The parallel rays with extreme angle will be directed into the focus of the parabola that is at the edge of the absorber.

The equation of the CPC considering the figure 1.11 is given by

$$(r \cos \theta_{max} + y \sin \theta_{max})^2 + 2a (1 + \sin \theta_{max})^2 r - 2a \cos \theta_{max} (2 + \sin \theta_{max})z$$
$$- a^2(1+ \sin \theta_{max})(3+ \sin \theta_{max}) = 0 \qquad (1.20)$$

In polar co-ordinate the parametric equation becomes:

$$r = \frac{2 f \sin(\theta - \theta_{\max})}{(1 - \cos\theta)} - a^{/} \qquad (1.21)$$

$$z = \frac{2 f \cos(\theta - \theta_{\max})}{1 - \cos\theta}, \quad \text{where } f = a^{/}(1 + \sin\theta_{\max}) \qquad (1.22)$$

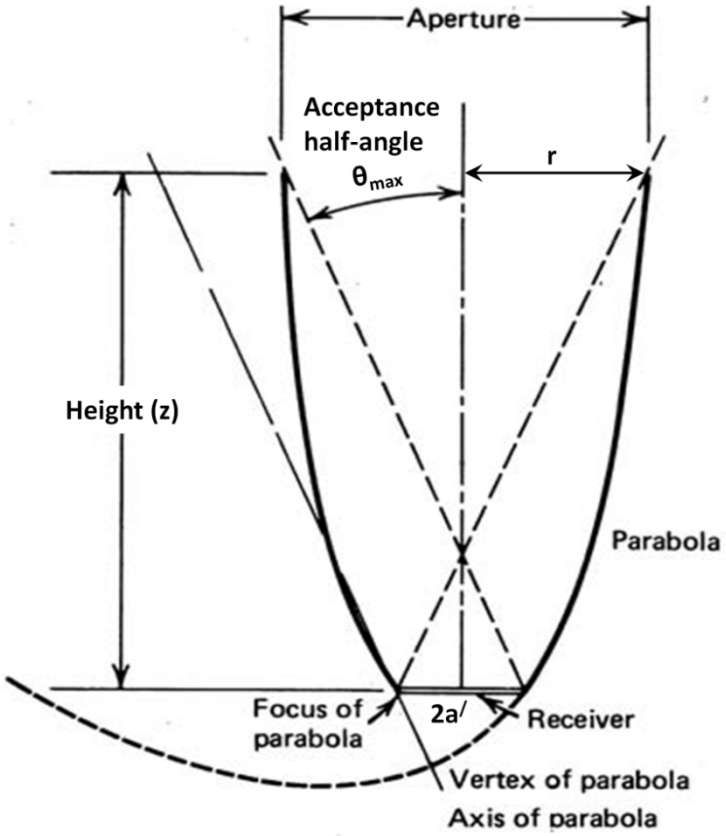

Figure 1.11 CPC showing the different parabolas and their focus points [10]

1.6.2 Asymmetric compound parabolic concentrator (ACPC)

The Compound parabolic concentrator with non-symmetrical design, i.e. with different acceptance half angles of the two parabolas, is termed as an Asymmetric compound parabolic concentrator. Figure 1.12 shows the cross sectional geometry of an asymmetric CPC with its extreme rays.

In fact symmetric CPCs can be considered as special approximations of ACPC with two similar acceptance half angles. This kind of design helps to meet the seasonal adjustment of the concentrator according to the position of sun without tracking requirements. Moreover because of design flexibility, ACPC can be modified according to the location and mounting [122, 123]. Symmetric CPCs have uniform concentration ratio independent of the solar incidence angle due to the symmetric aperture, whereas the effective concentration ratio of an ACPC (untruncated) changes with the incidence angle as the effective aperture varies [83].

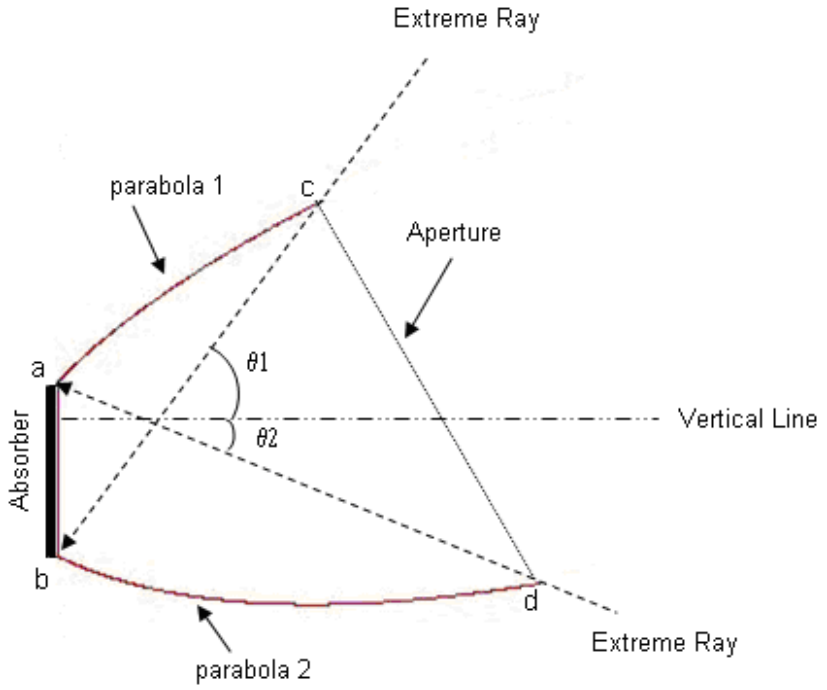

Figure 1.12 Schematic diagram of Asymmetric Compound Parabolic Concentrator

1.6.2.1 Truncation of ACPC

In spite of being the ideal concentrator, the major disadvantage of the CPC in practice is the large reflector area. It can be diminished by truncation of the reflector area, but results in a reduction in concentration ratio [124]. The top portion of the reflector does not intercept much radiation and it can be cut off without a significant drop in concentration ratio [125]. Study shows that (Figure 1.13) the range of the acceptance angle of the concentrator increases with truncation.

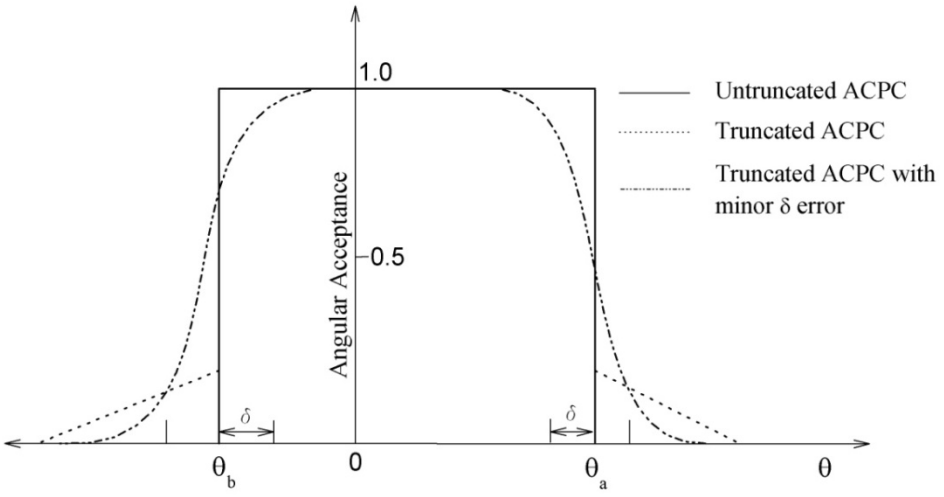

Figure 1.13 Variation of angular acceptance with increase in acceptance half angle after truncation [125]

Truncation of compound parabolic concentrator leads to the following changes in characteristics:

- Average number of reflection of a ray within acceptance angle θ_{in} to reach receiver decreases with truncation. This is desirable for uniform collector radiation.
- With truncation, a large amount of diffuse radiation is accepted by the concentrator. As the acceptance angle increases, it leads some extra rays to enter into the aperture of the collector [124]. Though these extra rays do not make a significant impact in practice for thermal applications, with higher truncation it may play a considerable role for PV applications.

1.6.3 Optical properties of ACPC

ACPC's can be operated without continuous or seasonal tracking for a low concentration ratio over an entire year. However orientation and design of concentrator varies from location to location. The major optical properties that ACPC exhibit are:

- All rays incident on the aperture within acceptance angle of the concentrator reach the exit end or receiver.
- Rays incident on the aperture outside the acceptance angle range will come out of the concentrator through the aperture after multiple reflections within the concentrator.

1.6.4 Thermal properties of ACPC

Thermal properties of ACPCs are associated to the heat transfer characteristics between the aperture, absorber, reflector plates and atmosphere. Thermal analysis of ACPC collectors considering only radiative and convective heat transfer between the components has been reported, which gives a reasonable first approach [125]. A detailed thermal analysis of a ACPC collector has been reported by Hsieh, 1981 [126]. However this model did not consider any absorption of solar or long-wave radiation at the reflector. The mathematical formulations were developed considering a ACPC cusp fitted with a concentric, evacuated double pipe as heat absorber. The thermal network for a CPC is shown in figure 1.14.

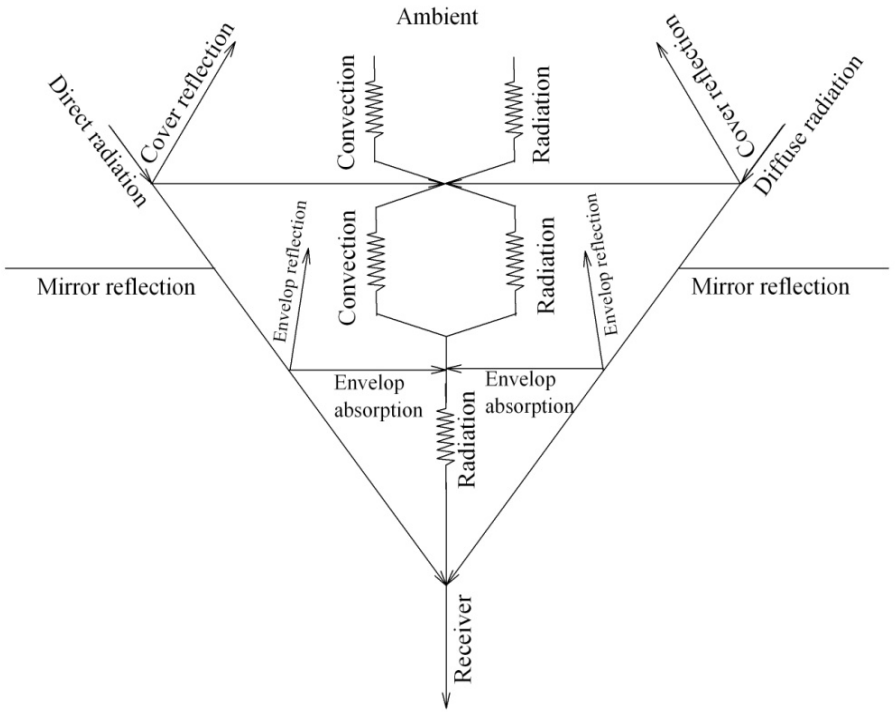

Figure 1.14 Thermal network circuits for ACPC collector [126]

The amount of useful heat that can be extracted from CPC collector is [126]

$$Q_u = H_t^{/} \tau_a \rho_m^{n} \tau_e \alpha_r \; fpA_a - U_L A_r (T_r - T_b) \tag{1.23}$$

Where $H_t^{/}$ is the total flux at the receiver, f is a correction factor accounting for multi-reflection contribution to absorbed energy and U_L is the heat loss co-efficient from the receiver jacket to atmosphere, which is found as;

$$U_L = \frac{1}{A_r}\left(\frac{1}{U_{r/e}A_r} + \frac{1}{U_{e/a}A_e} + \frac{1}{U_{a/b}A_a}\right)^{-1} \tag{1.24}$$

Where, $U_{r/e}$, $U_{e/a}$ and $U_{a/b}$ are the heat loss co-efficient between receiver jacket and envelope, receiver envelope and cover, cover and ambient respectively. The mathematical expression for these heat loss co-efficients has been derived from the thermal network in figure 1.13.

$$U_{r/e} = \frac{\sigma\left(T_r^{\,2} + T_e^{\,2}\right)\left(T_r + T_e\right)}{\frac{1}{\varepsilon_r} + \frac{A_r}{A_e}\left(\frac{1}{\varepsilon_e} - 1\right)} \tag{1.25}$$

$$U_{r/e} = \frac{\sigma\left(T_e^{\,2} + T_a^{\,2}\right)\left(T_e + T_a\right)}{\frac{1}{\varepsilon_e} + \frac{A_e}{A_a}\left(\frac{1}{\varepsilon_a} - 1\right)} + h_{e/a} \tag{1.26}$$

$$U_{a/b} = \varepsilon_a \sigma \frac{T_a^{\,4} - T_s^{\,4}}{T_a - T_b} + h_{a/b} \tag{1.27}$$

The convective heat transfer co-relation suggested in this model was

$$h_w = 1.32\left(\Delta T / 2p\right)^{0.25} \tag{1.28}$$

Where, ΔT the temperature difference between envelope and aperture cover and p is the radius of the envelope.

Thermal analysis of a ACPC has also been carried out by Prapas et al [127]. Different ACPC configurations were considered, taking into account of the energy absorption at the reflector. However, these were very initial approaches for thermal performance analysis. Major disadvantage of this model was to ignore the inclination effects of the collector and approximation of constant temperature at reflector.

Detailed theoretical and experimental investigation of heat transfer in ACPCs were carried out by Chew et al with a much more realistic approach [128, 129]. In the theoretical approach, finite element model was developed for a CPC with tubular receiver. The boundary conditions considered the receiver and cover as isothermal and reflector as adiabatic boundaries. The experimental investigation was carried out with an apparatus consisting of a 1-meter polystyrene block with internal profile lined with aluminum foil. The receiver was comprised of a copper cylinder enclosing an electrical heating element. Ten thermocouples at the receiver monitored circumferential and axial temperature variation and several were placed at the reflector. The heat transfer correlation was estimated in terms of Nusselt number as;

$$N_{u_H} = 0.44\left(\frac{H}{W}\right)^{\frac{1}{6.5}}\left(G_{r_H}.P_r\right)^{\frac{1}{4}} \quad \text{for} \quad 5\text{x}10^4 < \left(G_{r_H}.P_r\right) < 3\text{x}10^7 \tag{1.29}$$

Where, W is the half width of the flat top of the cavity. Study showed that convective heat transfer from the receiver plays a dominant role in the thermal performance of the solar collector system. In determining convective heat transfer at the surface, Nusselt number is the vital factor, which is a dimensionless quantity and defined as temperature gradient at the surface [130].

$$N_u = \frac{hL}{k_f} = \left.\frac{\partial T^*}{\partial y^*}\right|_{y^*=.0} \tag{1.30}$$

The Nusselt number correlations for convective heat transfer vary with design and configuration of the ACPC. Different Nusselt number correlations were reported for different ACPC configurations, these are found in literature as:

For tubular receiver enclosed eccentrically and collinearly within a large tube or CPC [87]

$$N_{u(r_{eq}-r_i)} = F_{ecc}\left(c\frac{r_{equ}}{r_i} - a\right)\left(G_{r_{(r_{equ}-r_i)}}\right)^b \tag{1.31}$$

For ACPC-type cavities with flat-plate absorber [131]

$$N_{u_H} = a\left(R_{a_H}\right)^c \tag{1.32}$$

For ACPC cavity considering angular inclination effect [132]

$$N_u = \frac{1}{\left(a + b\cos(\theta - 45)\right)} \times \left(\frac{H}{W_2}\right)^n G_r^{\,(c+d\cos(\theta-45))} \tag{1.33}$$

1.7 Concentrating photovoltaics

Photovoltaic technology has advantages such as, no emissions, low operating costs and excellent safety records. However the technology is not able to become leader in power generation. This is due to disadvantages like low energy density high installation cost and lack of economically efficient energy storage. The major barrier above all is the low conversion efficiency of expensive solar cells which increases the cost of per unit energy produced. One approach to decrease the cost per unit energy is by incorporating solar concentrators with solar cells. Incorporation of concentrating system in photovoltaic technology provides of the following major advantages:

- Concentrating photovoltaic systems can use concentrating solar cells, which have higher conversion efficiency of ~ 43.5% (multi-junction solar cell).
- High efficiency solar cell may not be cost effective for non-concentrating system, as total amount of power out is low, but may be cost effective for higher amount of output power with concentrating system.
- The application of comparatively low cost materials as concentrators will increase the power output of the same area of solar cell.

In the 1960s Wilson Solar energy Centre paved the way for research in solar concentrator systems for PV applications. The group worked with the parabolic disc concentrators, focusing on certain issues like reducing the series resistance and maintaining low cell temperatures. In 1965, Eugen Ralph proposed further approaches to the concentrating systems with low concentrating cones to high concentrating heliostat field in order to reduce the cost of energy production.

Different types of concentrating PV systems were explored during the period of 1976-1993, which boosted the research in this field. Reflecting discs, reflecting troughs, point focus Fresnel lenses, linear Fresnel lenses, luminescent concentrators, compound parabolic concentrator and small heliostat fields with central receiver were considered [17]. Among the variety in design of PV concentrators, refractive concentrators operated with Fresnel lens were popular in early days [133]. Fresnel lens offer more flexibility in optical design, which leads to greater uniform flux distribution at the receiver [134]. With the development of non-imaging optics both reflective mirrors and refractive lenses are in use as solar PV concentrators.

The performance of different PV concentrating systems varies depending on the design and geometry of the concentrators. Different techniques, materials and configurations have been proposed and researched to optimise efficiency of the concentrators in different applications. Examples of CPV system are discussed in the following sections.

1.7.1 CPV system with low concentration ratio

One of the examples of low concentrating PV system is ARCHIMEDES system. The ARCHIMEDES concentrating system consists of a V-trough reflecting type concentrator for low concentrating applications. This concentrating system is designed

to be installed in medium to large scale photovoltaic power stations. Two of this kind of concentrating systems have been installed in Germany with a couple of demonstration prototypes in Crete Island and in Spain [107]. The geometry and prototype of ARCHIMEDES concentrating system is shown in figure 1.15.

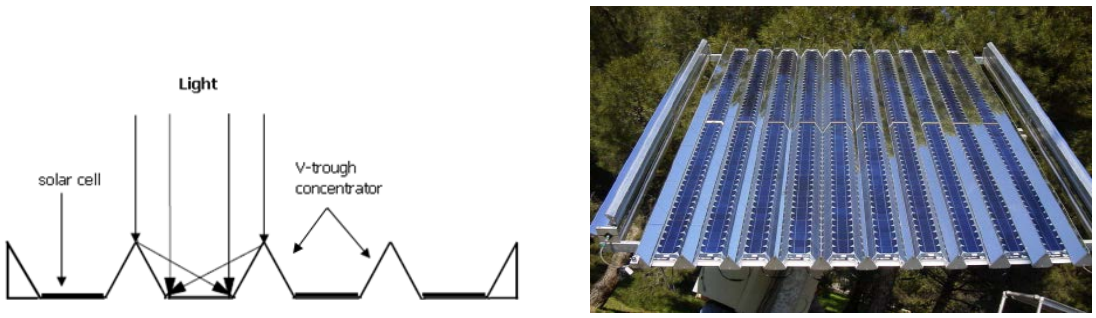

(a) (b)

Figure 1.15 (a) Schematic view of ARCHIMEDES concentrator (b) Arial view of ARCHIMEDES concentrating system [107]

The main characteristics of ARCHIMEDES concentrating system are [107]:

- The V-trough concentrator geometry is being used to achieve 2X geometrical concentration ratio, which implies that the aperture area is double of solar cell area.
- Structural and tracking requirement has been designed to use thermo-hydraulic passive tracking with high acceptance angle and low concentration ratio.
- Only direct irradiation on the aperture is counted for concentration though the system accepts both direct and diffuse radiation.
- A tracking accuracy of about $\pm 3^{o}$ is enough for this kind of concentrating system.
- The specific annual array yield (In kWh per installed of PV modules) of ARCHIMEDES concentrating PV-system is about twice that of a conventional fixed tilted system.

Post installation studies shows that the operational temperature is comparable to a conventional non-concentrating system. The ARCHIMEDES system can be 40% more cost effective for water pumping compared to non-concentrating PV counterparts.

Energy and economic analysis shows that it has a potential of generating 3000-3500 kWh per year in southern Europe.

1.7.2 CPV system with medium concentration ratio

The EUCLIDES© is a medium range CPV system with 20X-40X concentration ratio. It incorporates one kind of reflective parabolic trough concentrator [105]. The EUCLIDES© concentrating system consist of concentrating profile with reflected mirrors, concentrating cells encapsulated into receiving module, one-axis tracking system and heat sink [135, 136]. The collector of the EUCLIDES© has a split mirror arrangement to build the parabolic troughs (Figure 1.16 (a)). The concentrating system has been installed for power generation in the 480 kW_p EUCLIDES©-THERMIE demonstration plant in 1998 (Figure 1.16 (b)).

That was the world largest power plant using concentrating solar energy for photovoltaics at that time. The EUCLIDES©-THERMIE plant consists of 14 arrays, 84 meters long, each with 140 linear parabolic mirrors and 138 receiving modules connected in series [137]. The mirrors are laminated with 3M acrylic silvered auto-adhesive film. The parabola is selected with non-imaging optics criteria and the mirrors are put into the shape with two aluminium ribs. The optical efficiency of the system is found to be 89% and 95% of collected light reaches the 20mm strip of solar cells [135].

(a) (b)

Figure 1.16 (a) EUCLIDES© concentrating system (b) Partial view of PV field with EUCLIDES© concentrating system in EUCLIDES©-THERMIE demonstration plant [135]

1.7.3 CPV systems with high concentration ratio

The Aminox concentrating system is a high concentrating system of effective concentration ratio 250-1000, having two axis tracking. It is a large-area concentrating system including modules with concentrating optics for individual cells. Refractive concentration technology is used with Fresnel lens profile. The Fresnel lens is made up of 4 mm acrylics having anti-reflection coating. The system characteristics of the 25kW installed Amonix PV concentrating system is given in table 1.1 and the working principle an image of the mega module is showing in figure 1.17 (a) & (b).

Table 1.1: System characteristics of a 25 kW mega module configuration of Amonix concentrating system [139]:

Rated power output	25 kW ac @850 W/m^2
Collector size	55 ft x 44 ft x 2.5 ft
Aperture lens area	1960 ft^2 (182 m^2)
Number of cells	5,760 cells
Operating voltage	277/480 volts ac
System efficiency	Dc=18%, ac=16%

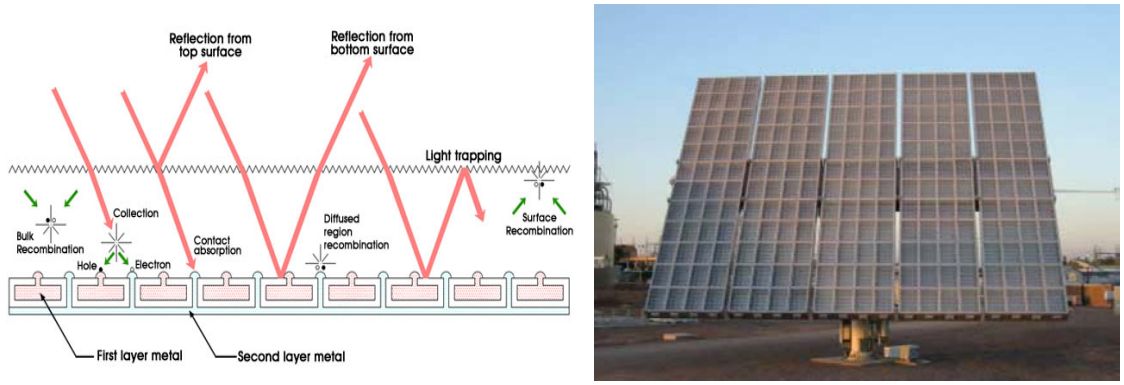

Figure 1.17 (a) Schematic representation of Amonix concentrator technology (b) The Amonix corp. 25 kW, Fresnel lens-illuminated PV concentrating system [138]

Leutz et al [134] designed a low concentrating non-imaging Fresnel lens concentrator following the edge ray principle and evaluated the performance by ray trace analysis for PV applications. In another study the same group designed a Prism-array-concentrator module and calculated the optical collection efficiency for the annual solar irradiation in

Tokyo. Maximum optical collection efficiency of 82% has been reported with this type of concentrator, configured with a flat reflector. A solar PV concentrating system with one axis tracking has been designed and developed to achieve geometrical concentration ratio of 300X [140]. Generally two-axis tracking is required to achieve such a high concentration ratio, but the reported concentrating system designed with two stage concentrators manage to achieve the level with polar oriented axis tracking. In this concentrator design a parabolic trough mirror is used in the first stage and 3-dimensional compound parabolic concentrator in the second stage. The first stage parabolic trough concentrator has a concentration ratio of 39.7X, which is followed by the second stage of 3-dimensional compound parabolic concentrator with a concentration ratio 7.7X. Summary of few concentrating photovoltaic system in market and prototype stage is given in table 1.2

Table 1.2 List of the different CPV systems installed commercially and in prototype stage

CPV Systems	**Concentration Ratio**	**Concentrator Geometry**	**Company/Institutes**
Amonix	250 - 1000	Fresnel lens, Pedestal	Amonix, USA
Butterfly	1100	Fresnel lens, Pedestal	Alitec, Italy
Saturno	700	Refractive type	CBF engineering, Italy
SolFocus	1000	Small mirror, Pedestal	SolFocus, USA
MegaWattSolar	20	Reflective linear, Pedestal	MegaWatt Solar, USA
Skyline	14	Reflective linear	Skyline Solar, USA
F-CPV	15	Reflective linear, floating	Solaris Synergy, Israel
EUCLIDES	40	Reflective linear	UPM, Spain
ASPIS	10	Fresnel lens, linear	ASPIS project
ClearPower	3	Refractive type, static	Stellaris, USA
Archimedes	2	Reflective linear, One axis tracking	UPM, Spain and ZSW, Germany
LCOC	7	Reflective linear	SunPower, USA
JXC	3	Reflective linear mirror	JX Crystal, USA

1.8 Issues related to CPV systems

Although several designs have been reported for CPV systems, certain issues arise during feasibility and installation. Incorporation of tracking system, choosing of proper concentration ratio to minimize the temperature effect and manufacturing issues to withstand outdoor weathering are few of them.

1.8.1 Tracking and non-tracking system

As the high concentrating photovoltaic system mainly exploits only direct solar radiation, tracking of sun comes into play to focus direct solar radiation over the year. The tracking requirement in a CPV system is dependent upon the concentration ratio of the system. The tracking mechanism leads to high installation cost and need regular maintenance, which makes it irrelevant for building façade integration and stand-alone applications. However integration of tracking in CPV systems designed for power plant application is an economically viable option with increased power output. The certain issues related to the tracking system requirement can be summarized as:

- For high concentration (C_g > 100), there is a need of two-axis tracking. In this kind of system very small size solar cells can be used, as the spot size will be very small with high flux density. But two axis tracking involves complex mechanical arrangement, which will increase the initial installation cost.
- For a medium concentrating system (C_g =10-100), one axis tracking is sufficient. Horizontal axis of rotation or polar axis rotation is configured for one axis tracking.
- No essential tracking is required for low concentrating system (C_g < 4). However for a concentrator with concentration ratio higher than 4, tracking is needed to collect solar irradiation over the day, since the range of acceptance angle decreases with the increase in concentration ratio. Development of suitable static concentrating system will be interesting from a commercial point of view as it replaces the tracking requirement with higher efficiency and enhances the performance of the existing PV market.

Whereas in the early days the tracking mechanism depended on a solar sensor and tracking motors, most of the modern tracking system uses microcontrollers, which increases the efficiency of the tracking system. The challenges with the tracking system

include designing of tracker to survive in worst climate such as a storm and designing of tracking system to work in different locations.

1.8.2 Mismatch in solar cell

The term mismatch in solar cells refers to the condition that causes difference in I-V characteristic of individual solar cells in a module. Mismatch in solar cell can lead to a decrease in total power output of a module. In general mismatch occurs with material mismatch, misalignment of the optical element and cell, electrical characteristic and non-uniformity of radiation in solar cell. There are two type mismatch found in solar cell [141]:

1. **Intrinsic mismatch**: Intrinsic mismatch occurs due to the designing error and variation of grade in solar cell materials. Small variation of individual solar cell quality can create current mismatch from individual cells in the same solar irradiation. Improper design may cause non-uniform heat removal from solar cell, which creates variation in temperature of individual solar cell. This contributes to significant mismatch.

2. **Transient mismatch**: Transient mismatch occurs due to external factors such as tracking errors, misalignment of solar cell and optical elements, non-uniform heat dissipation of module and uneven shading by dust and dew. Tracking error causes variation in illumination on solar cell between optimally illuminated and minimally illuminated. Uneven shading by dust and dew causes uneven distribution of radiation in individual cells. Permanent degradation of materials of module also causes mismatch in the solar cell.

Proper design of the module and tracking system, concerning in radiation distribution on solar cell and habitual cleaning of the module reduces the mismatch in solar cell.

1.8.3 Temperature effect on CPV system performance

The solar cell temperature in a CPV system increases with the increase in concentration of solar radiation. This results in the increase in temperature of the solar cell while operated without cooling compared to the flat plate modules. The increase in operating temperature of the solar cell causes decrease in cell efficiency [110, 142-144]. The

amount of current generated by a solar cell is given by equation (1.3), $I = I_l - I_D$ where and I is the current at the load, I_I is the light generated current at the solar cell and I_D is the dark current. In ideal case, the dark current I_D can be expressed as

$$I_D = I_o \left[exp \frac{qV}{KT} - 1 \right] \tag{1.34}$$

However, under the influence of parasitic resistances in the solar cell, the equation becomes

$$I_D = I_o \left[exp \left\{ \frac{q(V+IR_s)}{KT} \right\} - 1 \right] - \frac{q(V+IR_s)}{R_{sh}} \tag{1.35}$$

Where T is the operating temperature of solar cell, R_s is the series resistance and R_{sh} is the shunt resistance of the solar cell. At open circuit voltage (I=0), the light generated current will be flowing through the diode and the equation for open circuit voltage can be written as

$$V_{oc} = \frac{KT}{q} ln \frac{I_{sc}+I_o}{I_o} \tag{1.36}$$

Since I_{sc} >> I_o, this equation can be written as near approximation to

$$V_{oc} \approx \frac{KT}{q} ln \frac{I_{sc}}{I_o} \tag{1.37}$$

This equation of open circuit voltage indicates that the V_{oc} is logarithmically reciprocal to the reverse saturation current (I_o). With the increase in temperature the intrinsic carrier concentration increases and this leads to an increase in reverse saturation current and eventually increase in dark (recombination) current. Due to the increase in dark current the open circuit voltage of the solar cell decreases. In another effect due to the increase in temperature the band gap of the material decrease, which results increase in photocurrent, since photon with lower energy can be absorbed. However the gain in I_{sc} cannot compensate the loss in V_{oc}, which results overall decrease in power output of the solar cell.

It has been found that with per degree increase in temperature, single crystal silicon solar cell electrical efficiency decreases by absolute 0.5% [145]; whereas the negative thermal co-efficient of the thin film solar cell is found to be better than the crystalline silicon solar cell with a value of -0.2% (absolute) per degree increase in temperature

[17]. If the solar cell temperature exceeds certain limit, it can lead to long-term degradation of the cells [142, 146]. The long term exposure to the high temperature can degrade the ohmic contract between the fingers (or bus bars) and the solar cell wafer. This can increase the series resistance of the solar cell significantly and can decrease the conversion efficiency. Long term exposure to high temperature can also destroy the anti-reflective coating and can result high optical loss resulting decrease in power output. Presence of impurities in the silicon wafer can cause severe consequences on material properties of the semiconductor material while expose to the high temperature. While working with a triple junction cell at irradiation 1000W/m^2 on a 1000X CPV system, it is required to dissipate 56W/cm^2 heat energy for optimum performance [147]. So to maintain low operating temperature cooling mechanism should be integrated in high and medium concentrating systems. Both active and cooling techniques are used with concentrating photovoltaic systems to maintain the operating temperature [148-152]. For low concentrating systems the increase in temperature is relatively low, which does not create significant change in efficiency.

1.8.4 Manufacturing issues of CPV system

Solar concentrating systems face challenges with manufacturing issues, even those with excellent optical properties. The greatest challenge includes the selection of material for the concentrator, materials for tracking system and integrating with existing standard modules [68].The manufacturing requirement of CPV system includes [153];

- Selection of material: Selection of long durable material compatible with solar cell. Another norm includes low cost and less weight. Proper dielectric material may be a suitable option to fulfill those criteria.
- Application of dry and solid material: Dry and solid material should be preferred for concentrator fabrication and cooling system, which results low maintenance requirement of the system.
- Less moving parts: The system should be constructed with less moving parts to avoid mechanical failure. System should be enclosed as much as possible to protect from climatic hazards.
- Low cost and fast manufacturing process: The construction or manufacturing process of the concentrator and system components should be easy, low cost and fast for commercial deployment [17].

1.8.5 Economics of photovoltaic concentrators

The cost of the concentrating PV module reduces because of the reduction in the expensive solar cell area and in last ten years the solar industry has been boosted with growth in the CPV industry. During recent time the investment in CPV is in the order of $1 billion [68]. Whereas the PV market is growing in gigawatt range, concentrating PV has started production in hundred of megawatt per year. With technological development the conversion efficiency of the solar cell has also increased in the last decades. The summary of solar cell conversion efficiency over a decade is shown in figure 1.18. The maximum solar cell efficiency of any type of solar cell reported so far is 43.5%. This efficiency is achieved with a multi-junction solar cell while using with highly concentrated solar radiation (1000×). The multi-junction solar cells are expensive compared to the crystalline Si solar cells, which is the most popular solar cell in the market. The maximum efficiency of the crystalline Si solar cell is reported to be 25%.

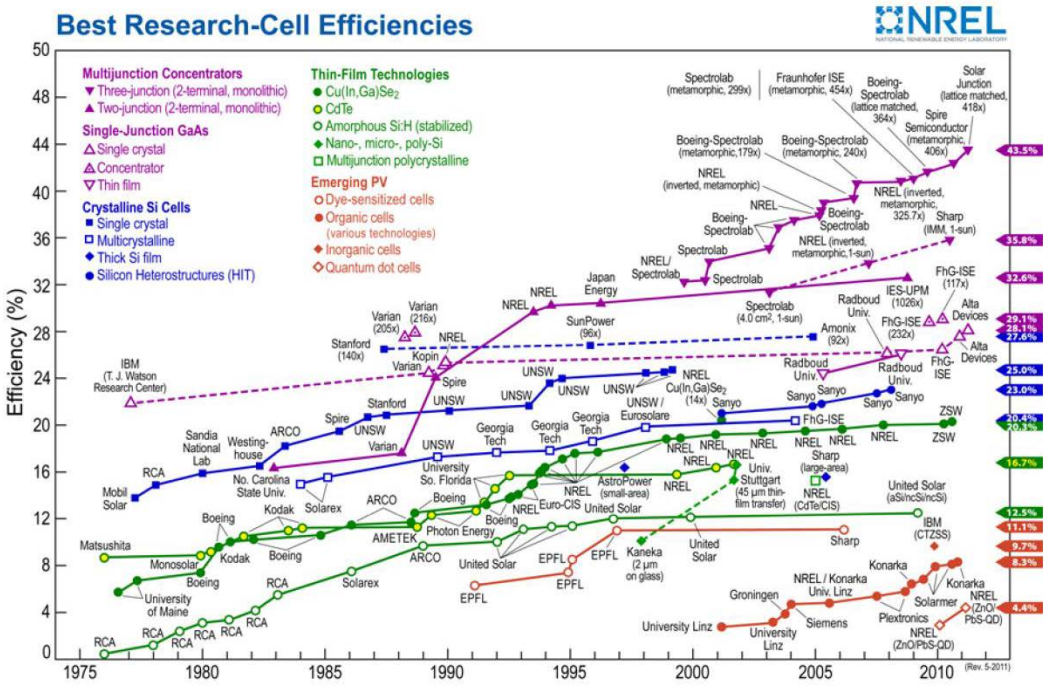

Figure 1.18 Summary of best conversion efficiency results of solar cell efficiencies over last 25 years [68]

The cost analysis of concentrating PV module shows that the cost of concentrating module is directly dependent on the solar cell cost and concentration ratio. If the solar cell costs range from \$0.10 cm^{-2} to \$5.00 cm^{-2} and assuming cost of lens and reflecting

concentrator is \$30 m^{-2} and the rest of the concentrator module is an additional \$70 m^{-2}, then cost of less than \$200 m^{-2} for entire module are possible, which will be more than \$500.00 m^{-2} without concentrating system [133]. Whereas most of the recent flat plate PV systems have energy payback periods of 3 years, the energy payback period study for the high concentrating PV system FLATCON estimated a number as low as 8 – 10 months, including losses in transportation, balance of system and system loss, energy utilization in system manufacturing [154]. The study was performed with high concentrating solar cells with a conversion efficiency of 36.9%. This is an impressive result for the concentrating PV market. With an increase in conversion efficiency of concentrating solar cell, the concentrating system is going to play a vital role in cost reduction of photovoltaic power output.

1.9 Building integrated photovoltaics

The PV industry is growing at a very fast rate during this decade with the development of the PV efficiency and deployment of PV applications. One such area of PV deployment is building integrated PV systems. The buildings play a significant contribution to the global energy balance accounting for 20-30% of the total primary energy consumption of industrialized countries [155]. Earlier, energy conscious efforts in building design only limited to thermal insulation or ventilations for human comfort with minimum use of energy. So the focus of the study was mainly concerned with energy savings in the building instead of energy generation. Today the proven technology of photovoltaics has made engineers think about designing building that can generate energy using PV modules. Building designers have come up with different approaches to using PV modules in buildings, making PV modules a part of a building while generating electricity. The use of photovoltaics in buildings can have two approaches: Building Integrated Photovoltaics (BIPV) and Building Attached Photovoltaics (BAPV) [156]. “BIPV are considered as a functional part of the building structure, or they are architecturally integrated into the building design” [156]. BIPV replaces the conventional building materials such as roof tiles, shingles and even facades [157, 158]. BAPV is referred to the photovoltaic modules attached to the building structure as an add-on without replacing any functional part of the building. An example of BIPV and BAPV is shown in figure 1.19. Most popular form of BAPV is the rack-mounted PV panel. BAPV is used mostly in old building without compromising the structure of the building. However the term ‘BIPV’ is accepted to refer the PV modules attached to building either as integral part or an add-on to the

buildings and the term BIPV is used in this thesis to represent both types of PV module installations in building.

(a)

(b)

Figure 1.19 Example of (a) BIPV and (b) BAVP system on the roof of buildings

In the recent times, BIPV is gaining popularity from both architectural and economical aspects while designing and constructing a new building. While replacing the conventional building materials as weather protective building envelop, BIPV generates power required for household applications and extra power can be feed into the grid [159]. Also BIPV is an alternative to the land use for PV module installations for power generation [160]. Especially for urban and sub-urban locations, BIPV can be a suitable choice as micro-power plant. In summary the BIPV has the following advantages [155]:

a) No additional land area needed for PV installations as the building component is used for module mounting. Densely populated urban and sub-urban areas can be highly benefited.
b) Can avoid the additional infrastructure for installation of PV modules.
c) Transmission and distribution losses of electricity can be minimized because of the on-site power generation to use in the buildings.
d) Can provide power to the all or the major part of the electricity consumption in the building during the daytime, thus reduces the electricity bills
e) Conventional building materials can be replaced with PV modules, enhancing the payback period of the PV installation
f) Can improve aesthetic appearance of a building with cosmetic layer of PV modules in a innovative way
g) Can reduce the planning cost

For BIPV, the roof and the facades are considered to be the best options. The PV modules can be installed over the entire roof and facades, giving maximum exposure to the solar radiation (figure 1.20). However apart from conventional façade and roof integration, BIPV can also be used as semi transparent windows, skylight, semi transparent roof, building exterior cladding panel etc [158, 161-163].

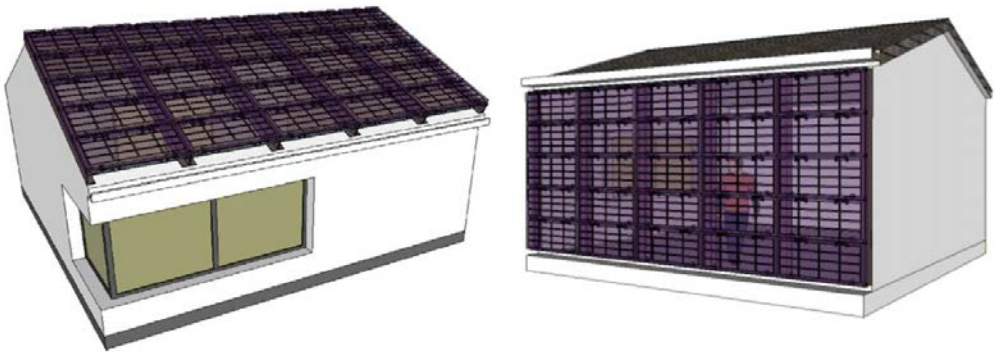

Figure 1.20 Architectural designs for BIPV in roof and façade of a building [164]

The roof is considered to be a perfect location for BIPV because of low shading probability, inclination of the roof matching to the required inclination for PV modules and cost of the roof is reduces by the use of PV modules[165, 166]. The roof integrated BIPV modules are roof tile slats for flat roofs or shingles. The later one is used for tilted roofs, which is a standing seam unit [158]. Several BIPV modules for roof integration have been designed and reported. The "SOLBAC" [167], "SOFREL" [168], "PowerGuard" [169], "SUNSLATE" [170] are few examples of different kinds of roof and façade tiles for BIPV. These BIPV tiles are mostly silicon solar cell based and a few of them come with integrated contact bar, diode etc. There are several BIPV modules developed with the same shape and size with the conventional tiles for easy replacement [171-174]. Few BIPV roof tiles like the "solar tile" were developed to integrate into clay roof tiles [175]. Other interesting modules for BIPV roof application are the glass roof integrated PV systems [176, 177]. These semi transparent glass roof integrated PV tiles, which can be useful in the countries like UK to use daylight effectively; however the comfort and glazing can be an issue.

1.9.1 BIPV in facades

Along with the roof tiles, building facades are also getting much interest because of the flat surface, which provides a more optimal cell positioning. The BIPV in façade can be

used as semi-transparent façade to use the daylight more effectively and power generation. There are basically two types of BIPV for façade integration: "PV glass curtain walls and PV metal curtain walls" [158, 178, 179]. In the first one, specially designed glass-glass laminated modules with different coloured solar cells can be used instead of glass curtain walls. While in the later ones inclined PV modules in a panel are arranged. The other BIPV options for facades integration with different aesthetic and architectural aspects are [180]:

a) Shading: This is the simplest type of BIPV, but can result in excellent gain of solar energy. The PV modules are mounted in an angle while providing shadow to the windows or walls; and at the same time maintaining the view to the outside and day-light inside the building. Schematic of a BIPV module for shading and photograph of a building with BIPV as shading are shown in figure 1.21.

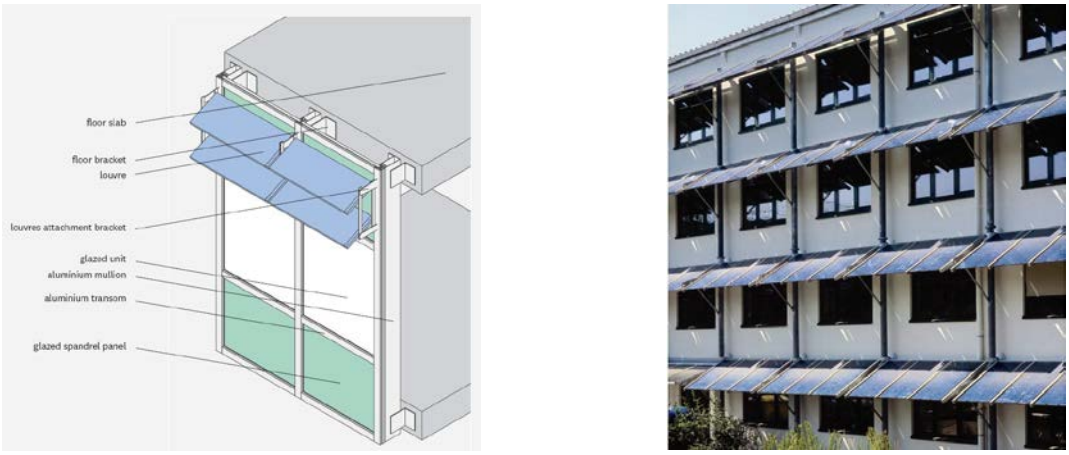

(a) (b)

Figure 1.21 (a) Schematic image of a BIPV module to use as shading (b) Photograph of a building with BIPV modules as shading [180]

b) Rainscreen overcladding: In this type of BIPV system, PV modules are used as the outer leaf of the building walls overcladding, while the inner leaf can be any conventional material as an air barrier [181]. Outer surface of the wall with PV modules can provide a nice look to the building while generating power at the same time. Figure 1.22 shows a schematic image of a BIPV module to use as rainscreen

overcladding and photograph of a building with PV modules as rainscreen overcladding.

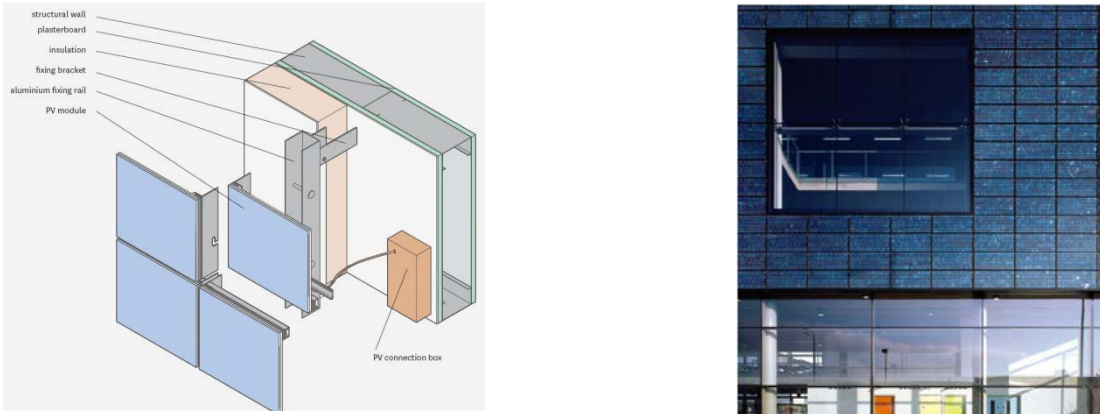

(a) (b)

Figure 1.22 (a) Schematic image of a BIPV module to use as rainscreen overcladding (b) Photograph of a building with PV modules as rainscreen overcladding [180]

c) Curtain walls: In this type of BIPV approach PV modules are constructed as curtain wall and can be installed either in the vision area or in the opaque walls depending on the type of PV modules. Glass to glass laminated modules with polycrystalline silicon cells placed with adequate spacing is a popular curtain wall choice as BIPV. Schematic image of a BIPV module to use as curtain wall of a building and a photograph of a building with integrated PV modules as curtain wall is shown in figure 1.23.

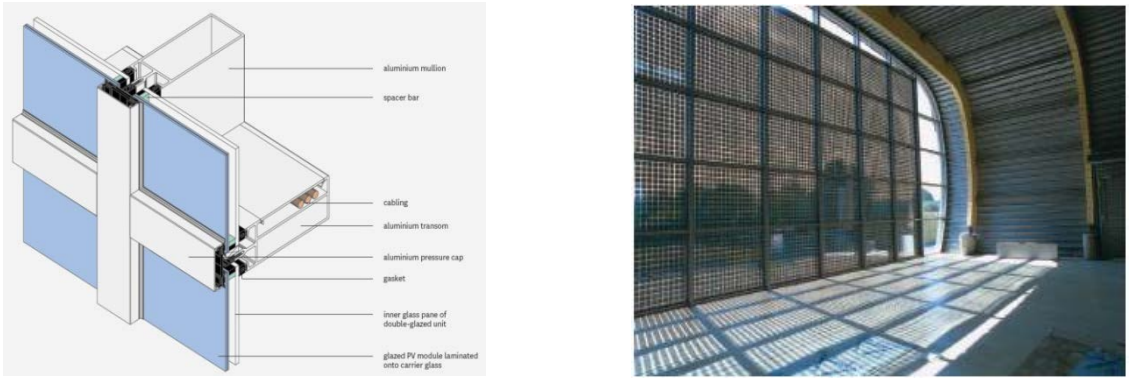

(a) (b)

Figure 1.23 (a) Schematic image of a BIPV module to use as curtain wall of a building (b) Photograph of a building with integrated PV modules as curtain wall [180]

d) Double screen façade: The double screen façade is also referred to as ‘building in building’, since the inner screen of the façade is separated by a significant distance to the outer screen. The BIPV modules are used as outer screen of the facades. The façade design is to balance the seasonal fluctuation of the heat, cold, light and wind as well as acoustic noise with an optimum ventilated system of air for different seasons. Figure 1.24 shows schematic diagram of a PV module to use in a double screen façade and a photograph of a building with PV modules

(a) (b)

Figure 1.24 (a) Schematic diagram of a PV to use in a double screen façade (b) Photograph of a building with PV modules as one component of double screen facade [180].

a) Atria and canopies: In this kind of BIPV arrangement, the modules are integrated in the horizontal or sloping facade of the building. Unlike the roof tiles, the atria and canopies arrangement can be used as single or double glazed systems, with PV modules on the outer surface. Depending on the requirement, the PV modules can be used either in the spandrel area or visional panels by integrating into stick-system skylights. Schematic image of a BIPV module to

use as atria of a building and a photograph of a building with integrated PV modules as atria is shown in figure 1.25.

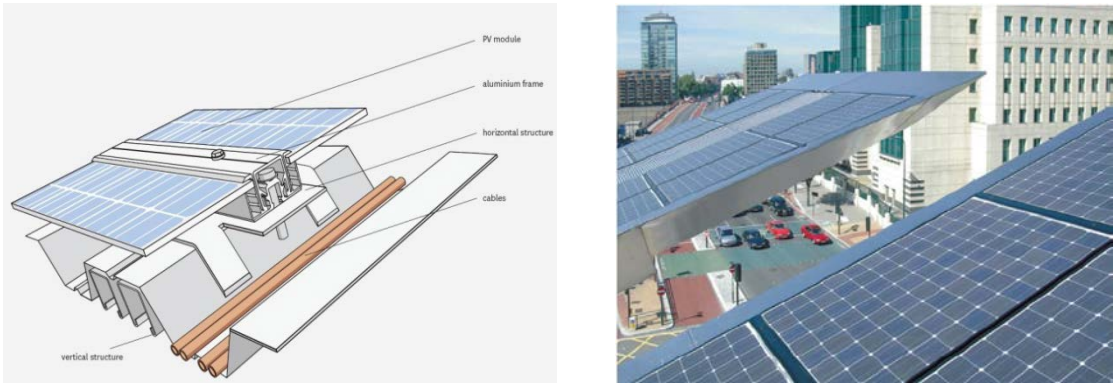

(a) (b)

Figure 1.25 (a) Schematic image of a BIPV module to use as atria of a building (b) Photograph of a building with integrated PV modules as atria [180]

1.9.2 Economics of BIPV

BIPV is considered a significant part of the global solar energy market with an expected growth from $\$1.8\times10^9$ in 2009 to $\$8.7\times10^9$ in 2016 as reported by a consulting firm NanoMarkets, New York [157, 182]. With the decrease in PV module prices and the increase in production (figure 1.26) the market of the BIPV is expected to grow as well.

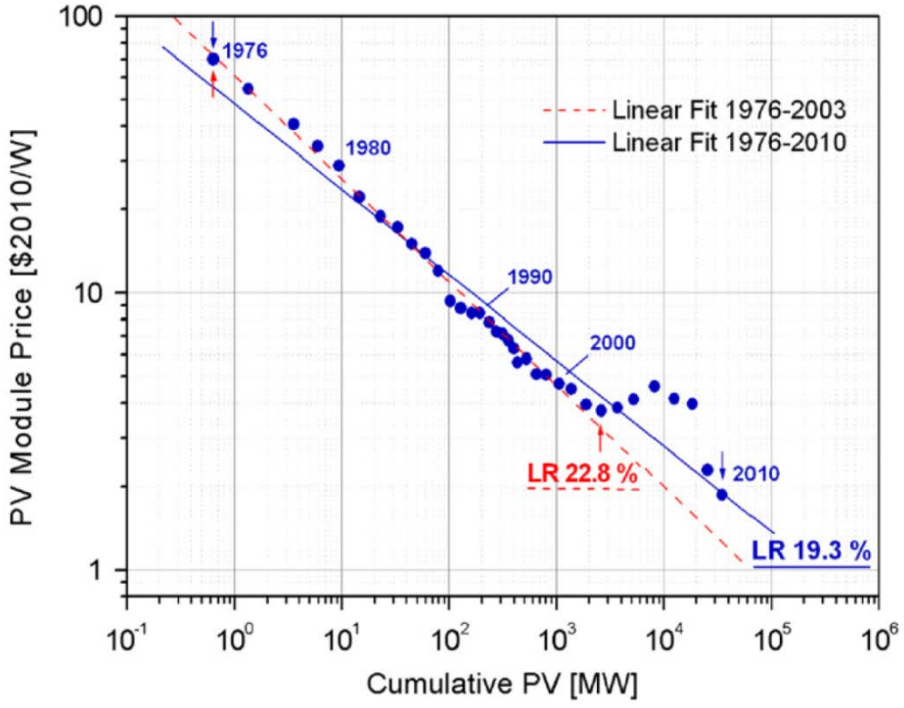

Figure 1.26 Learning curve of the production and cost of the PV modules from 1976 to 2010 [183]

While the annual growth rate of the PV industry is over 45% for last 15 years, the BIPV is playing a significant role in this growth [183]. As can be seen in figure 1.27, the annual production of the PV module has increased significantly from 33% to 45% after the roof-top program [183].

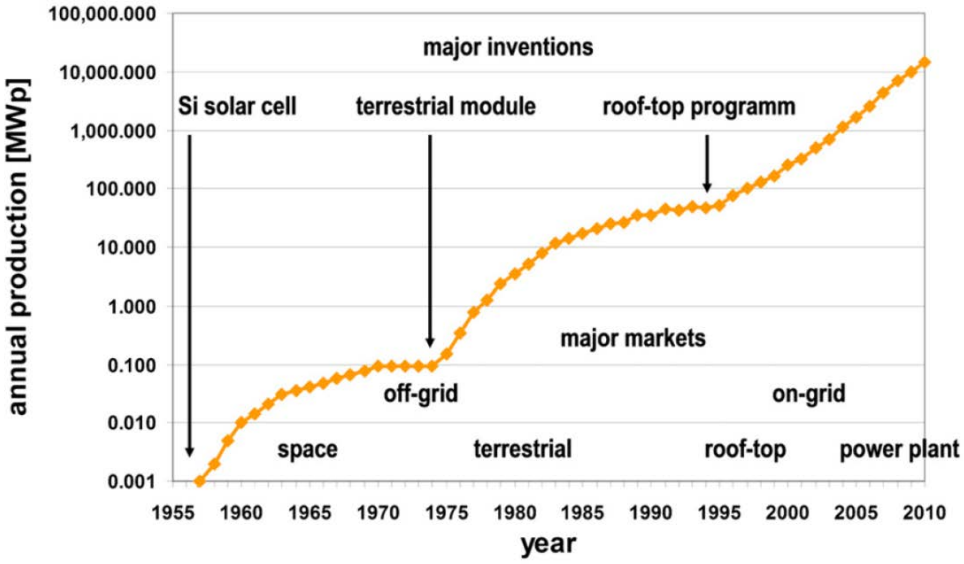

Figure 1.27 Market segment for production of the PV modules over the years with major innovations [183]

In Europe, a 39.2% growth in BIPV market during 2007-2014 is expected in terms of installed capacity (figure 1.28). During this time the BIPV market is expected to be reaching 260.44MW of installations with a value of €1185.9 million [184]. While the new PV technologies are emerging for BIPV, crystalline silicon solar cells still have the dominant role in BIPV of European market. As shown in figure 1.29, 90% of the BIPV modules are made of crystalline solar cells, with 50% contribution from mono-crystalline cells and 40% of poly-crystalline solar cells. Along with the market growth of BIPV, it is important to consider the payback period of the renewable energy systems. In most of the European countries the maximum payback period of a PV module is expected to be below 10 years [157] which is possible because of the subsidies. In Switzerland, the energy payback period of a small PV power plant of $3kW_p$ is found to be a maximum 3.5-4.5 years for mono-crystalline solar cells [157, 185]. In the United Kingdom the payback period of $2.1.kW_p$ installed BIPV system is found to be only 4.5 years [186] even though the annual solar energy incident is very low.

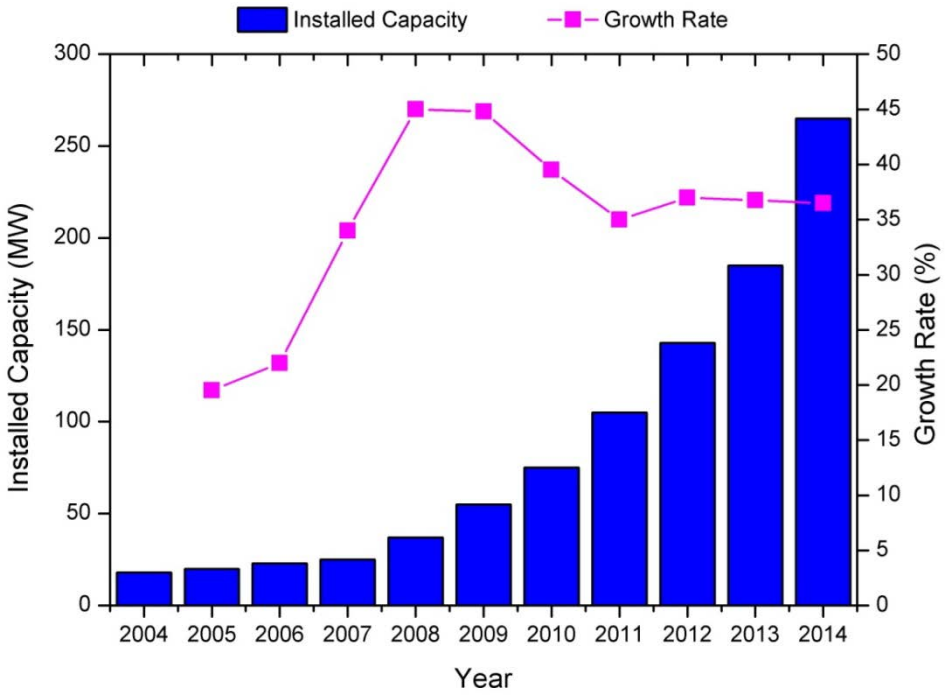

Figure 1.28 BIPV market predictions in Europe in terms of installed capacity during 2007-2014 [184]

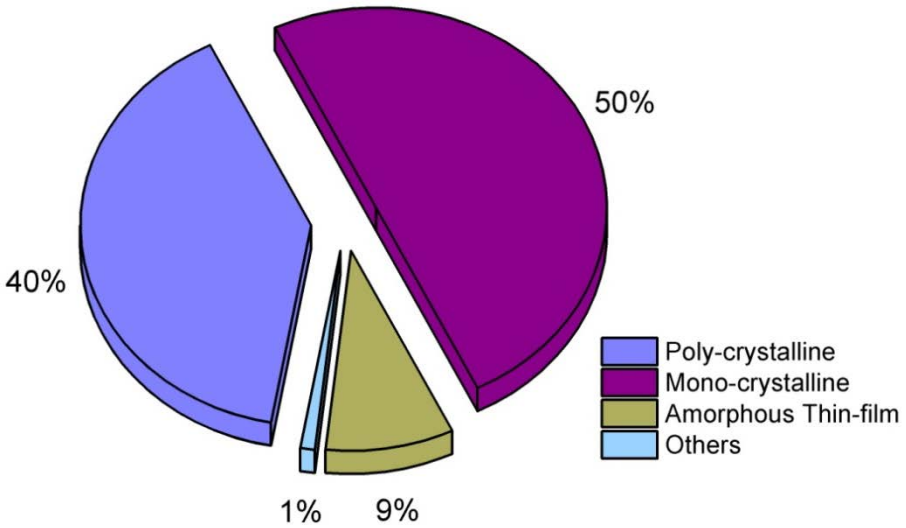

Figure 1.29 BIPV market shares of the different PV technologies in Europe [184]

1.10 Building integrated concentrating photovoltaics

Building integrated concentrating photovoltaic (BICPV) system can be a suitable alternative to BIPV to achieve lower cost of the energy output and subsequently reducing the energy payback period. The design of the BICPV system however needs to be state of the art to compete with the growing market of BIPV. An optimum concentrator and system design is an issue for BICPV, to use as an active component of

a building replacing conventional building material [187]. Depending on the concentrator design the BICPV system can be installed on the roof or the façade of building. BIPCV system design needs to fulfill certain requirements to be accepted by architectures for building integration [188, 189]:

- Architecturally and aesthetically pleasant design with excellent range of material and colour
- Suitable dimensions for natural integration in buildings
- Innovative design for modern buildings as well as highlighting conformity to the context of building

1.10.1 Concentrator designs for BICPV

BICPV concentrators are static type to eliminate the tracking requirement and to increase the range of acceptance angle. A tracking system in a BICPV system introduces more complexity to the construction of the building. A number of static concentrator designs suitable for BICPV system have been reported so far. For different receiver location the concentrator design changes accordingly [190]. Asymmetric non imaging concentrator designs are found to be promising for BICPV to eliminate the issue of the seasonal variation of sun position [69, 114]. Because of the asymmetric design and the wide range of acceptance angles, the concentrators are capable of collecting a large fraction of diffuse radiation as well.

A ‘Semi-nonparabolic (SNP) concentrator’ concept has been proposed by Millls et al in 1976 with design flexibility [191]. Even though the concentrator design required frequent tracking, it has lead to a new chapter of asymmetric concentrator design. An extremely asymmetric concentrator (EAC) has been reported with low manufacturing cost and fixed maximum concentration ratio [192]. Figure 1.30(a) shows ideal extremely asymmetric concentrator. Analytical expression for the geometrical characteristics of non-ideal EAC showed that for a fixed concentration ratio, the maximum range of acceptance angles could be achieved. However, the number of reflections for a ray to reach the receiver is high, which results increase in optical loss. With minor modification in ideal EAC and by using the Winston-Hinterberger curve as reflector geometry, non-ideal or nearly-ideal EAC was developed as shown in figure 1.30(b) [193]. In this kind of concentrating system the receiver is located relatively near

to the reflector to achieve large acceptance angle for the rays reflected from reflector [158, 193] and minimises the average number of reflection taken to reach the receiver.

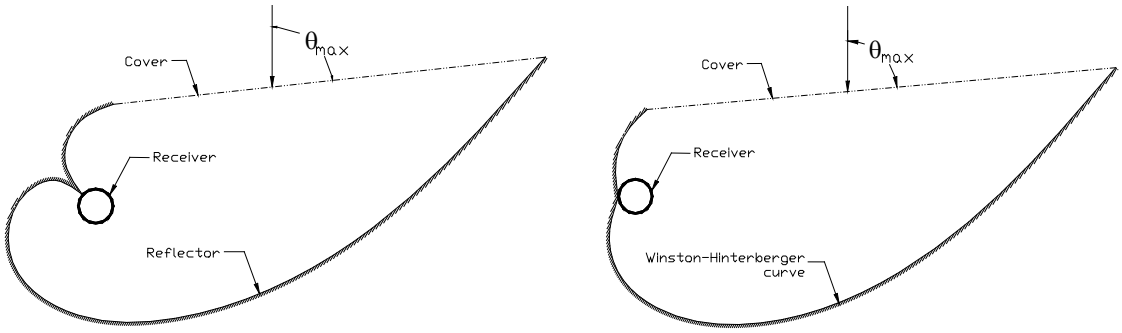

(a) (b)

Figure 1.30 (a) An ideal extremely asymmetric concentrator (EAC) [192] (b) A nearly ideal extremely asymmetric concentrator (EAC) [193]

A solar concentrator with variable output was proposed considering the variation of load for cooling and heating during winter and summer. The asymmetric non imaging concentrator designs are proposed to achieve maximum output in summer and winter varying the orientation of mounting and the receiver position. This concentrator is termed as 'sea shell' concentrator [83], which is a single parabola with maximum half angle of 36^{o}, allowing collection time of 7 hours in summer. The schematic design diagram of the 'sea shell' concentrator for different concentration in summer and winter is shown in figure 1.31 [85, 158, 194]

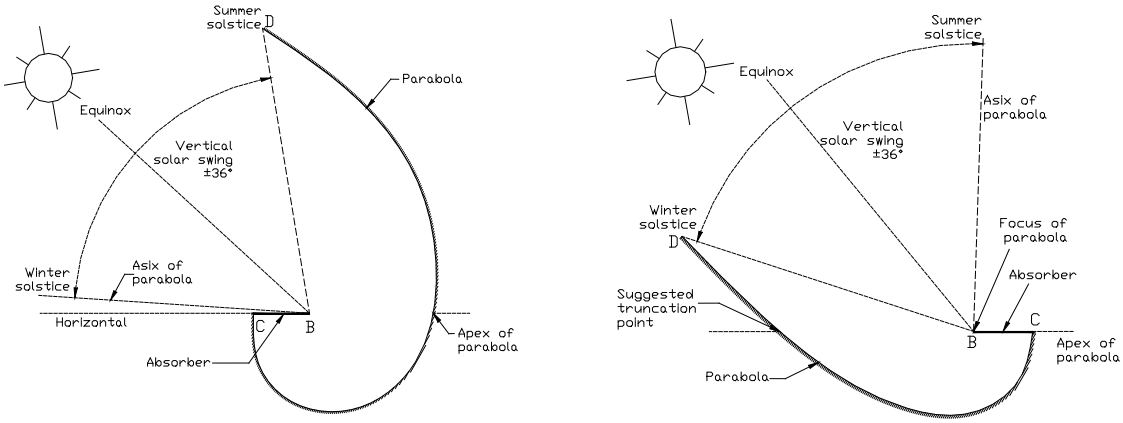

(a) (b)

Figure 1.31 Stationary 'sea shell' concentrator design and mounting for (a) summer (b) winter

For high latitudes, asymmetrically truncated parabolic concentrators are most preferable for maximum yield, because of the asymmetric radiation over the year. The "Maximum Reflector Collector (MaReCo)" with different design configurations for stand-alone and building roof or wall installations has been reported [195]. The cross sectional schematic diagram of the MaReCo concentrator for standalone applications, roof integration and building façade integration is shown in figure 1.32 [195-197] All the concentrator designs are to use bifacial solar cells for higher efficiency of the system. The maximum optical efficiency of this type of system is reported to be 56%[196]. The same group reported the radiation distribution in the absorber surface of the MaReCo and developed a method for determining the annual average optical efficiency factor for the collector at different absorber mounting angles [197].

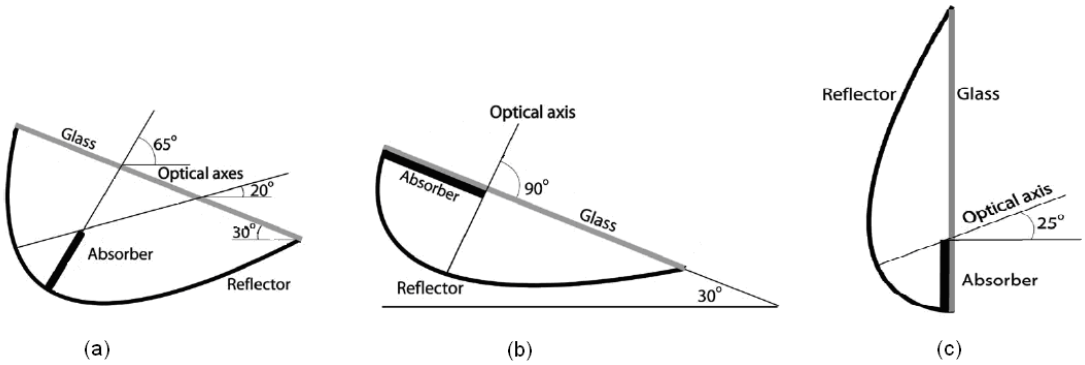

Figure 1.32 MaReCo design for (a) Stand alone with aperture tilt 30^o (b) Roof integration of tilt 30^o (c) Wall application. [196]

A detailed study on design and performance of a non imaging asymmetric compound parabolic photovoltaic concentrator (ACPPVC) is reported for BIPV (facade) application in UK [85]. The concentrator is designed with half acceptance angles (0^o & 50^o) and geometrical concentration ratio of 2. The schematic diagram of the ACPPVC concentrator design and the photograph of a CPV module with ACPPVC concentrator are shown in figure 1.33. The maximum optical efficiency of this reflective type ACPPVC concentrator is found to be 85.2% over the range of acceptance angles. Experimental analysis shows an increase in power of 62% (power ratio 1.62) compared to the similar non-concentrating counterpart [108]. Increase in temperature of the back plate and the ohmic losses resulted in a lower reducing the power output than anticipated [198].

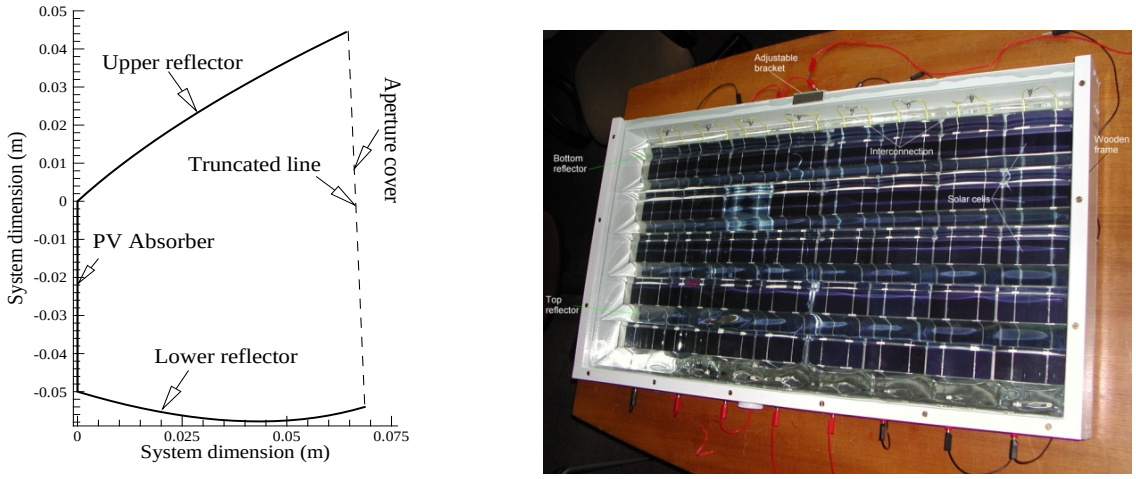

(a) (b)

Figure 1.33 (a) Schematic design diagram of ACPPVC and (b) Image of the CPV module with ACPPVC concentrator for building integration

Non-imaging static concentrator lens to achieve concentration ratio 2.0 and lens efficiency 94% were developed utilising refraction and total internal reflection for use in Sydney [199]. The range of acceptance angles of this lens type concentrator is found to be $\pm 60^{o}$ in the east-west direction and $\pm 25^{o}$ in north south direction. The annual average concentration ratio of this concentrating system was found to be 1.88.

Roof tiles with static concentrators using bifacial solar cell can be a suitable alternative to the conventional roof tiles [200-202]. The front surface of the designed roof tiles is cover with glass, while the rear surface has tilted grooves with reflective material. The grooves are designed to reflect the light from the rear surface, which totally internally reflected to reach the solar cell. The concentrator design and the light behaviours inside the concentrator are shown in figure 1.34. The concentration ratio was estimated to achieve 3.6 after considering all the absorption losses at the cavity and reflection losses from the rear surface, while the designed concentration ratio was 4. The efficiency of the prototype roof tile is found to be approximately 15%, which is lower than the anticipated value of 17-18%, mainly because of the poor performance of the rear reflector surface [200]. Similar concentrator design with varying concentration ratio has been investigated for optimum design [202]. A 1kW flat plate roof tile concentrating system with 16% efficiency has been reported for building roof integration [201]. The

concentrating system is designed to achieve a concentration ratio of 2 on the bottom surface and 1.5 on the top surface.

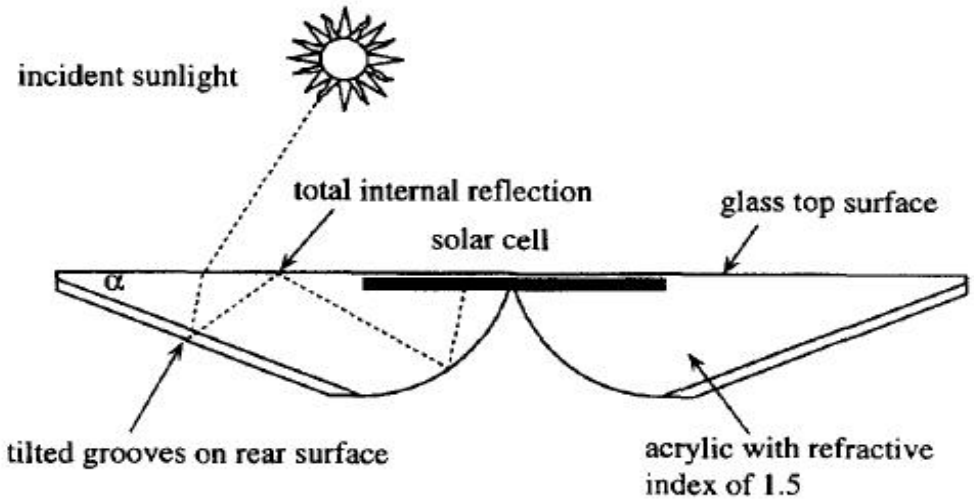

Figure 1.34 Schematic diagram of PV roof tiles with static concentrator [200]

Another flat plate static concentrator (FPSC) for both monofacial and bifacial solar cells has been reported with concentration ratios of 1.5 and 2, respectively [89, 203, 204]. The concentrator has a sub-millimeter V-groove reflector placed in between the solar cells. The v-grooved reflectors are specially designed, so that the light reflected from the v-grooved channels again totally internally reflects from the cover glass without escaping. The schematic diagrams of the concentrating system for monofacial and bifacial solar cells are shown in figure 1.35. The designed concentrating systems are reported to have optical efficiency 87.6% and 85.6% respectively for the systems with monofacial and bifacial solar cells. Outdoor testing of the FPSC module for bifacial solar cells resulted in 1.23 times higher short circuit current density compared to the conventional module.

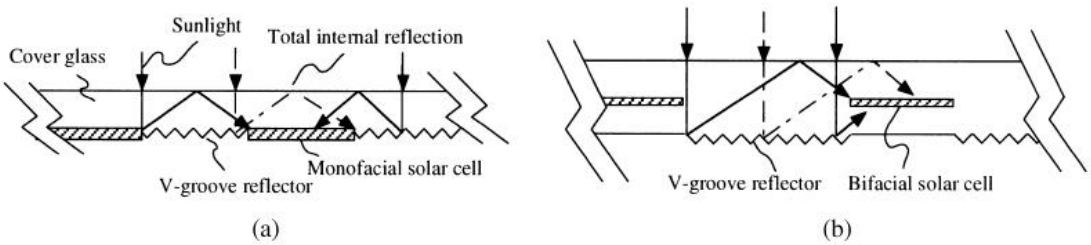

Figure 1.35 Schematic cross sectional diagram of FPSC module for (a) monofacial cell (b) bifacial cell [204]

A parabolic concentrating wall element to use with a $Cu(In,Ga)Se_2$ based module was designed and characterized for building façade integration was reported by Brogren et al, 2003 [205, 206]. The height of each of the reflectors and cell segments is 55cm, while the focal length of the parabolic reflector is 15.4cm. Schematic diagram of the concentrating system and an image is shown in figure 1.36.

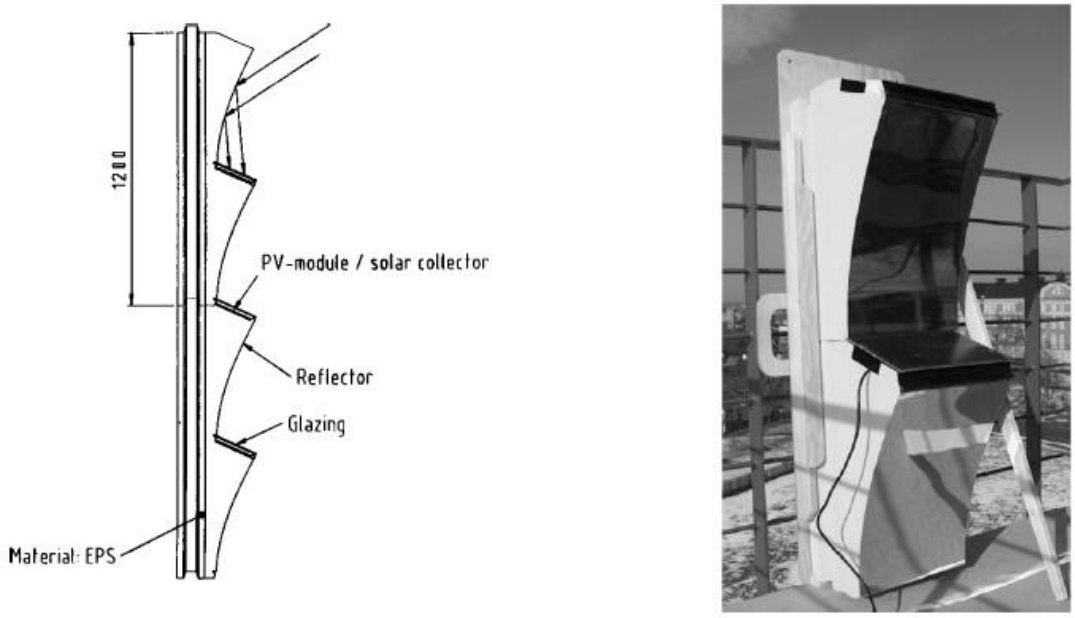

(a) (b)

Figure 1.36 (a) Schematic diagram of the PV wall element with parabolic concentrator (b) Photograph of the prototype PV wall element with concentrator [206]

The system is designed for 3x concentration ratio to accept radiation incident between 25^o and 90^o of the south projection angles. However an experimental result showed only a 1.9 times increase in power compared to a similar non-concentrating module; which is due to the optical losses in the system [206]. The optical efficiency of the concentrating system is found to be 76% at an effective solar height of 40^o. Further optimisation study of this type of concentrating system has been carried out, to achieve a concentration ratio from 2.96 to 4.65 depending on the inclination of the module and the optical axis of the concentrator [207]. Simulation results with the data of solar irradiation in Stockholm, Sweden, shows that the system with 2.96 concentration ratios, 25^o module inclination and 20^o concentrator inclination can achieve 72% higher electrical power than that of a vertical reference module.

Stationary dielectric non imaging solar concentrators have the advantages of a wider range of acceptance angles with higher concentration ratio, compared to the reflective type concentrators [208]. Since the dielectric concentrator uses total internal reflection, higher optical efficiency can be expected, minimising reflection losses when compared to reflective type concentrators [209] [199, 210]. A study with a dielectric asymmetric compound parabolic concentrator (ACPC) showed that it is possible to achieve over 90% optical efficiency for a wide range of acceptance angles. Even outside the range of acceptance angles, the dielectric concentrator can have an optical efficiency of over 40% [209]. A Prototype Photovoltaic Façades of Reduced Costs Incorporating Devices with Optically Concentrating Elements (PRIDE) system was designed as a stationary (non-tracking) concentrating system. The basic design of the PRIDE concentrator is a truncated asymmetric compound parabolic concentrator, manufactured with dielectric material having good optical properties. In the first generation, the PRIDE concentrator was designed for 3mm and 9mm wide monocrystalline silicon solar cell, while the 2nd generation PRIDE concentrator is designed for use with 6mm wide Saturn solar cells. The geometry and prototype of 2nd generation PRIDE concentrator is shown in figure 1.37.

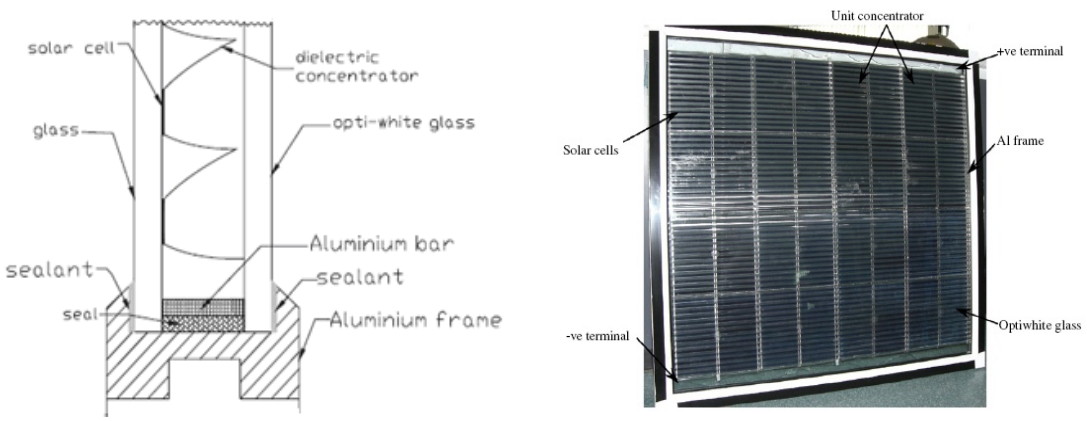

(a) (b)

Figure 1.37 (a) Schematic cross-sectional view of 2nd generation PRIDE concentrator (b) Second generation dielectric PRIDE concentrator module [211]

The main characteristics of PRIDE concentrating systems are [211]:

- PRIDE concentrators use total internal reflection, which reduces the reflection losses.

- Due to refraction at the aperture the effective incidence angle reduces, which results in an acceptance of a wide range of solar incidence angle with high geometrical concentration ratio than similar design counterparts.
- This concentrator is designed as a low concentrating system for application in building facades.
- Transmission losses were minimized by using dielectric material of low extinction co-efficient and reducing path length of the rays within the dielectric material.
- 81% optical efficiency can be achieved for a wide range solar incidence angles.

The CPV module with the PRIDE concentrator achieves a power ratio of 2.01 while the designed geometrical concentration ratio was 2.45. The electrical conversion ratio of the CPV module is reported to be 10.2% during outdoor characterisation. In large scale production the CPV modules with 2nd generation 3kW PRIDE concentrators can potentially reduce the cost of the energy output by 40%, when compared to the non-concentrating module [211].

Another type of concentrating system for BIPV is the luminescent solar concentrators (LSC). The luminescent solar concentrators use the concept of spectral shift to concentrate the incoming solar radiation. The luminescent concentrator consists of flat plate of polymer material containing luminescent material e.g. organic dye or quantum dot. These luminescent materials absorb part of incident radiation and emit it with a spectrum matching the spectral response of solar cell. Application of luminescent concentrator has the following advantages over geometrical concentrators:

1. Luminescent concentrators can collect both direct and diffuse radiations effectively.
2. Low cost transparent polymer material can be used.
3. Can avoid the bulky set-up of geometrical concentrators.

The working principle of the LSC concentrators and LSC concentrator illuminated by UV-light is shown in figure 1.38. The luminescent material in LSC should absorb the entire wavelength of solar irradiance up to 950 nm and should emit within the 950-1000 nm range for maximum performance of the concentrator. However the efficiency of the

LSC PV system is found to be low compared to the geometric concentrators, because of higher optical losses and material instability.

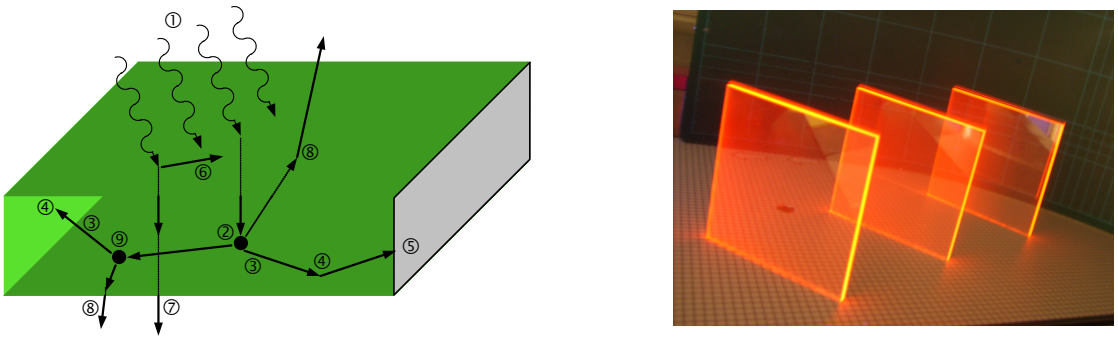

(a) (b)

Figure 1.38 (a) Schematic representation of working principle of LSC (b) Luminescent Solar concentrators illuminated by UV-light [212]

The highest efficiency of the LSC modules is reported to be 6.7% and 7.1% using GaInP and GaAs cell respectively [213, 214]. The first design used a two bonded sheet concept, while the next used mixed dye concept. However the highest efficiencies are achieved with very small size modules (2cm x 2cm x 0.6cm and 5cm x 5cm x 0.5cm respectively) and using a diffuse reflector [215].

1.11 Aims and objectives of the project

The aim of this project work is to optimise the dielectric ACPC design and to carry out extensive performance analysis to fulfill the gap between the earlier research and the commercial deployment of the dielectric CPV modules for BICPV application. Detailed literature review of photovoltaic concentrators, specifically with low concentration ratio reveals that there is a need of detail investigation for concentrator design optimisation and performance analysis to use it with the building integrated photovoltaic systems. Several concentrator designs have been proposed for BICPV application in different location. However the concentrator designs are restricted due to the large variation of the sun position during different seasons in the high latitudes. Few researchers have proposed different concentrator designs for different seasons. In practice, it is not convenient to change the concentrators from a BICPV system for different seasons. Earlier studies showed that the low concentrating asymmetric concentrator design is suitable for building integration in higher latitudes and ACPC is found to be as the most

suitable option than the other counterparts. Low concentrating systems evade tracking requirements and make the concentrator suitable for building integration, roof applications and standalone systems in remote areas. ACPC has advantages such as distribution of the collected radiation within the receiver area (as non-imaging optics) and design flexibility to adjust the range of acceptance angle for different locations. Earlier studies on the reflective type ACPC show that, the height of the concentrator increases substantially to achieve a wide range of acceptance angle with a specific concentration ratio. Also the reflective loss from the parabolic surface further reduces the overall optical efficiency of the system.

The thesis highlights the use of suitable dielectrics as concentrator material in ACPC's, which offer the following advantages over the concentrator with reflecting mirrors:

- The acceptance angle increases with the introduction of dielectric material.
- Higher concentration can be achieved for a wide range of acceptance angles.
- Total internal reflection of the light from the parabolic edges of the concentrator reduces the reflection losses
- Avoiding use of reflection materials from the concentrator walls leads to a reduction in cost of the system.
- Dielectric ACPC can collect higher diffuse radiation than the reflective counterparts. It was observed that dielectric ACPC systems offer 25% increase in comparison to the reflective system.

In spite of the huge advantages, detail optimisation study and performance analysis of the dielectric concentrators for building integration has not been carried out so far owing to the lack of intensive developments in BIPV concentrators in the past; however, the interest towards this technology is catching up slowly. Referring to the initial experimental investigation of the PRIDE concentrator [211], this study has been undertaken for theoretical optimisation and detail analysis of the dielectric ACPC concentrator for BICPV application.

The following objectives of this project are underlined for systematic optimisation study and performance analysis of the designed dielectric concentrators and fabricated CPV modules:

- Detail theoretical optical performance analysis of different design configurations of dielectric ACPC using a ray trace model in terms of the optical efficiency and energy flux distribution at the receiver.
- Design optimisation of the dielectric ACPC based on the annual energy collection of the concentrator while using with BICPV for higher latitudes ($>55^{o}$).
- Component level investigation on the optical performance and optical loss.
- Optimisation of the manufacturing criterion of the CPV module with dielectric concentrator and minimisation of the optical losses at different component level.
- Extensive performance analysis with the variation of solar incidence angle.
- Real time outdoor characterisation of the of the CPV modules.
- Cost analysis of the CPV module compared to the commercial flat plate modules.

In this study an optimisation study has been carried out with three different asymmetric compound parabolic concentrators made of dielectric material with good optical properties and resistance to outdoor weather for long term exposure (section 3.2). A theoretical study of the optical performance and the thermal behavior of the concentrators has been undertaken to find out the optimum concentrator design. An optimised concentrator has been characterised by a set of indoor and outdoor experiments. The indoor experiments include spectroscopic study of the manufactured concentrator and electrical characterisation of designed photovoltaic concentrating system in a controlled environment, with a solar simulator. Outdoor experiment has been carried out to investigate the performance of the concentrating system in real environment. Manufacturing cost analysis and the cost per watt peak power generation of the CPV module is carried out to compare with the cost of the conventional flat plate modules for BIPV.

1.12 Conclusion

This literature review includes a detailed study of the basic introduction to solar concentrators, with special interest in solar PV concentrators. A detailed literature study has been made into recent research scenarios of the PV concentrators. With an introduction to the non-imaging optics, different configurations of the asymmetric compound parabolic concentrator have been reported. Several PV concentrating systems

that are in operation and in the prototype stage were discussed. Issues relating to the PV concentrating system, e.g. manufacturing issues, temperature effect are detailed. An economic analysis shows that the application of concentrating system will significantly reduce the energy payback period and cost per unit energy production. The literature review also reveals that there is the need to optimise the design of PV concentrator for application such as roof tiles, building façade, and stand alone structures. Low concentration PV concentrators with no-tracking requirement will be ideal for those applications. The incorporation of low concentrating PV concentrators in conventional modules results higher output, without compromising the conversion efficiency of solar cell.

Based on the literature review the present work has been undertaken for detail investigation on design and performance analysis of the dielectric ACPC concentrator. Both theoretical and experimental investigation has been underlined for both concentrator design and CPV module fabrication. This work is expected to achieve a milestone in research of dielectric concentrators and enhances the progress in commercial deployment of BICPV.

Chapter 2

Materials and methods

This chapter provides details of the materials; manufacturing process of the dielectric concentrator; and characterisation technique for performance analysis of the concentrating photovoltaic (CPV) modules. This chapter also details of the design and fabrication of the solar simulator for module characterisation, including calibration of some reference devices such as photodiodes to measure indoor light intensity from the solar simulator.

2.1 Concentrator material

The basic requirement of the dielectric concentrator material is to have excellent transmission properties. Different solar cells have different spectral response ranges. So the transmission properties of the clear dielectric material needs to be considered taking into account the range of spectral response of the solar cell. Another requirement of the dielectric material is strength and rigidity, to retain the shape and the profile of the concentrator. Polymer materials having very low flexural and tensile strength cannot retain the form under mechanical stress, which, in turn, can destroy the geometrical shape of the concentrator. In this PhD project a major part of the study has been carried out by the dielectric concentrator manufactured by clear polyurethane. For comparison, the performance study has been carried out using acrylic material as well. However the manufacturing processes of the dielectric concentrator using these two materials are different.

2.1.1 Polyurethane

In this study the performance analysis of the designed dielectric concentrator has been carried out with clear polyurethane. The major use of polyurethane is as foam. Polyurethane has also been in use in industry as a coating material because of its toughness and chemical resistance. However in those application there was no specific requirement of clear polyurethane with good transmission properties. Clear polyurethane has been used for indoor sculptures and decorative items. Previously the

clear polyurethane for PV applications has been investigated as a host material in luminescent concentrators [216]. The chemical composition of polyurethane is given below

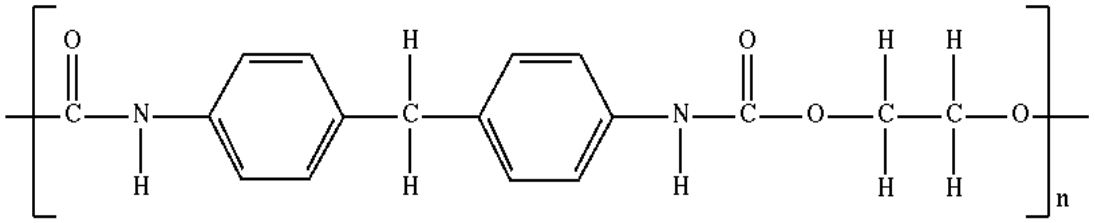

The reaction of polymerisation of the polyurethane can be written as [217]

$$\mathrm{nOCN(CH_2)_6NCO + nHO(CH_2)_6OH \rightarrow -((CH_2)_6 - NH - CO - O(CH_2)_6 - OCONH)_n -}$$

The polyurethane considered in this project is clear polyurethane called crystal-clear® from Smooth-on®. The urethane is supplied as two parts, Part-A and Part-B, which need to be mixed in a ratio 10:9 respectively to get a final polyurethane product. The basic properties of the crystal-clear® polyurethane are [218]:

1. Optically clear, suitable for applications requiring optical clarity
2. Low viscosity of Part-A and Part-B, to ensure easy mixing
3. Cures at room temperature and atmospheric pressure
4. Cures with very negligible shrinkage
5. Cured, cast final product is not brittle
6. UV resistance for long term exposure to outside weather

The crystal-clear series product comes with 4 products to use for different thickness and hardness requirements. The ‘crystal-clear 200’, is suitable for the required thickness of the designed concentrator and has good flexural strength. The technical specification of the physical and mechanical properties of the ‘crystal-clear 200’ is shown in table 2.1.

Table 2.1 Physical and chemical properties of the Polyurethane material [218]

Properties	**Specifications**
Cure Time (Hours)	16 hours
Mixed Viscosity (cps)	600 (ASTM D-2393)
Specific gravity (g/cc)	1.036 (ASTM D-1475)
Tensile strength (psi)	2,500 (ASTM D-638)
Flexural strength (psi)	10,650 (ASTM D-790)
Compression strength (psi)	6,385 (ASTM D-695)
Shrinkage (in./in.)	0.001 (ASTM D-2566)
Shore D Hardness	80 (ASTM D-2240)

2.1.2 Polymethyle methacrylate (PMMA)

Clear PMMA has excellent optical and weather resistance properties for use as a solar concentrator. Fresnel lens made of PMMA are a popular choice in commercial high concentrating systems. The chemical composition of PMMA is shown in figure 2.1

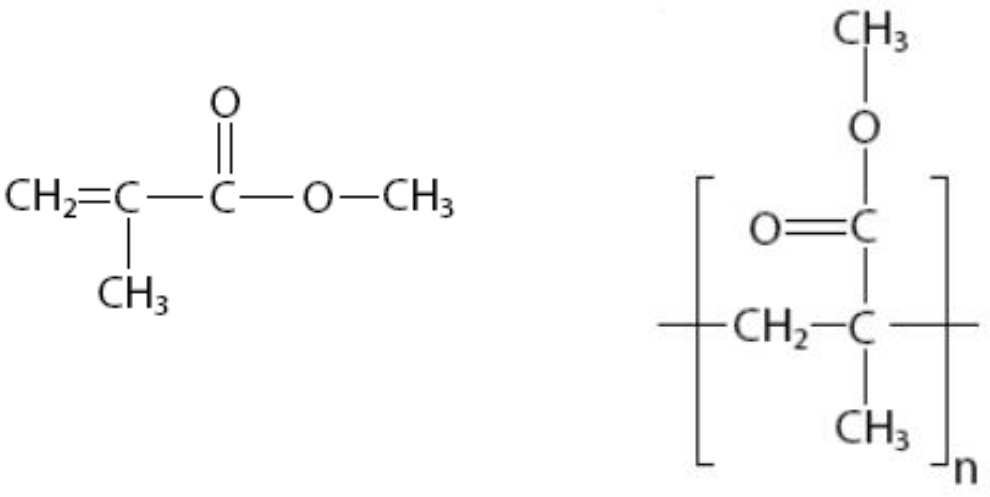

(a) (b)

Figure 2.1 Chemical composition of (a) MMA monomer (b) PMMA polymer

The density of the PMMA is 1.19gm/cm^3, which is 20% higher than the density of the MMA monomer. This change is density causes shrinkage of the PMMA during the curing process. The average refractive index of PMMA is 1.49 and the absorption co-

efficient of 1.4 cm^{-1} within the wavelength range 350-1000 nm, which makes it a suitable material for solar photovoltaic application.

2.2 Encapsulation material

Encapsulation material is used in photovoltaic modules to increase the lifetime of the solar cell by protecting them from moisture ingress and weathering [219]. The encapsulation material needs to have very good transmission properties in the UV-visible wavelength range, to minimise the optical losses. For commercial PV modules, the encapsulation material is expected to have low modulus and stress relieving properties. However for CPV application, especially for dielectric concentrating systems, the encapsulation material should also have good adhesion properties, to hold the dielectric concentrators on top of the solar cells. Ethylene vinyl acetate (EVA) is the most popular encapsulation material in commercial PV modules, because it is a cost effective material having good optical properties in the UV-visible range [220]. Encapsulation with EVA is carried out by laminating sheets of glass and EVA using a laminator. The solar cell is laminated between cover glass and a rear-plate with EVA sheet in between the layers. However, for dielectric CPV systems, the lamination process of encapsulation of the solar cell cannot be used, as the dielectric concentrator is sited in between the solar cell and the cover glass. So an alternative material, with good transmission and adhesion properties, is required which can be cast on top of the solar cells and can also be used as a strong adhesive material to hold the dielectric concentrators on top of the solar cells. Silicone encapsulant materials are found to be a suitable alternative to EVA due to following properties [221]:

1. The modulus of the silicon elastomer is low and consistent with that of EVA for a wide temperature range. The low modulus provides mechanical stress relief for the solar cells in the photovoltaic module
2. It has high temperature stability. Many of the properties of the silicone elastomer remain unchanged from 40^{o} to 150^{o}. So even for high temperature peaks there will be no degradation
3. Silicone elastomers are hydrophobic, while permeable to gas and vapour. This results in transmission of water vapour trapped in the interface and a low moisture pick up.
4. Silicone elastomers can adher strongly to various substrates including glass. This assists in protection of the solar cell from moisture and corrosion.

5. Silicone elastomers are known as very good electrical insulators and flame resistant polymers.
6. Silicone elastomers have high durability and low degradation in outdoor conditions. PV modules with silicone encapsulant from Dow-corning have been reported to have very satisfactory performance over 25 years.

The encapsulation material used in the project is the silicon elastomer from Dow-corning which is commercially known as Sylgard-184. Dow-corning has a range of different clear and transparent materials in sylgard series. Among those materials Sylgard-184 is found as suitable option having features such as, viscous liquid, room-temperature curing, high tensile strength, and good flame resistance [222].

2.3 Solar cell

The solar cells used in this project are mono crystalline silicon solar cells manufactured by the Laser Grooved Buried Contact (LGBC) process. The performance of normal crystalline silicon solar cells get worse with increase in concentration ratio. However, the LGBC crystalline solar cells can perform very well up to a concentration ratio of 100X [223-227]. The cells used in this project were originally manufactured by BP SOLAR known as SATURN solar cells. SATURN solar cells were manufactured by an electrolytic copper-plating process, to reduce the processing time and effluent treatment cost [228]. The average solar cell efficiency has been reported to be over 16% with fill factors higher than 75% [228]. These cells have been manufactured with dimensions 116mm×6mm. The cell has fingers on both sides for efficient collection of the electrons emitted. An image of the few cells used in this project is shown in Figure 2.2. The SATURN solar cells were designed with optimum finger spacing for concentration ratios greater than 10X [229]. In each solar cell of 6 mm wide, the finger spacing is 1mm, to fit 6 fingers along the width of the solar cell. A schematic diagram of fingers and the bus bar of the solar cells are shown in figure 2.3. The bus bar is a series of fingers closely spaced together. Due to the length of the solar cell, two bus bars have been used to solder the tabbing. Those bus bars are created along the width of the solar cell, connecting the fingers to bridge the connection network.

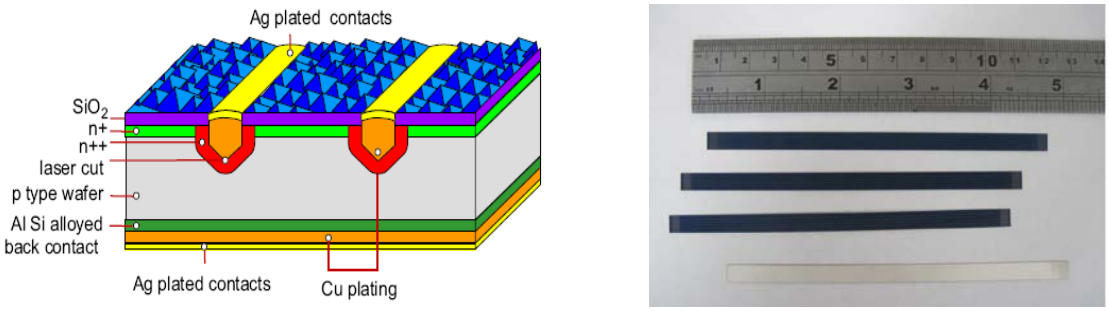

(a) (b)

Figure 2.2 (a) Schematic representation of the SATURN solar cell [229] (b) Photograph of the crystalline silicon solar cells used in this study

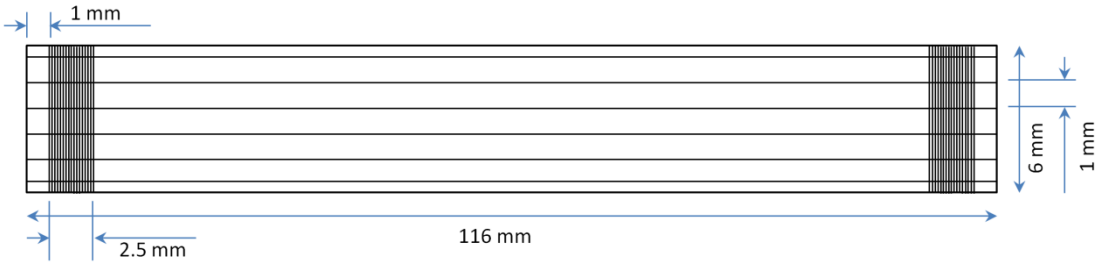

Figure 2.3 Dimension and bus bar details of the LGBC crystalline silicon solar cells used in this project

2.4 Concentrator manufacturing process

In this project, the performance analysis of the designed concentrator has been carried out using a dielectric concentrator manufactured from polyurethane. The concentrator was manufactured by casting of clear polyurethane in a predesigned mould with the concentrator profile. The casting process to manufacture the concentrator is detailed in the following sections

2.4.1 Casting of the Concentrator unit

2.4.1.1 Fabrication of the mould

The mould was fabricated in the workshop at Heriot-Watt University using a specially-designed cutter, with the concentrator profile. The tungsten tip cutter was custom-manufactured by an external company. The material for the mould was chosen as aluminium for a smooth surface finish. While steel could have provided a better surface finish, aluminium was chosen taking into consideration the cost and limitations of

facilities at Heriot-Watt University. The profile diagram and images of the specially-designed cutter are shown in Figure 2.4.

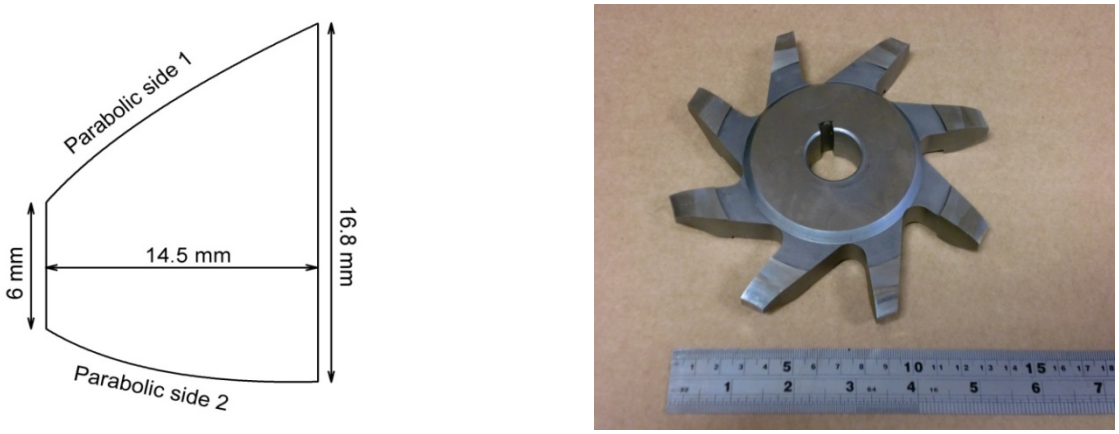

(a) (b)

Figure 2.4 (a) Cutter profile for mould construction (b) Image of the cutter

At first, the mould was fabricated to manufacture two concentrator troughs as one unit. However, there were some issues with achieving flat aperture surface with two troughs as one concentrator unit, which are described in the following section. An image of the first mould to manufacture two concentrator troughs as one unit and the manufactures concentrator using the mould are shown in figure 2.5.

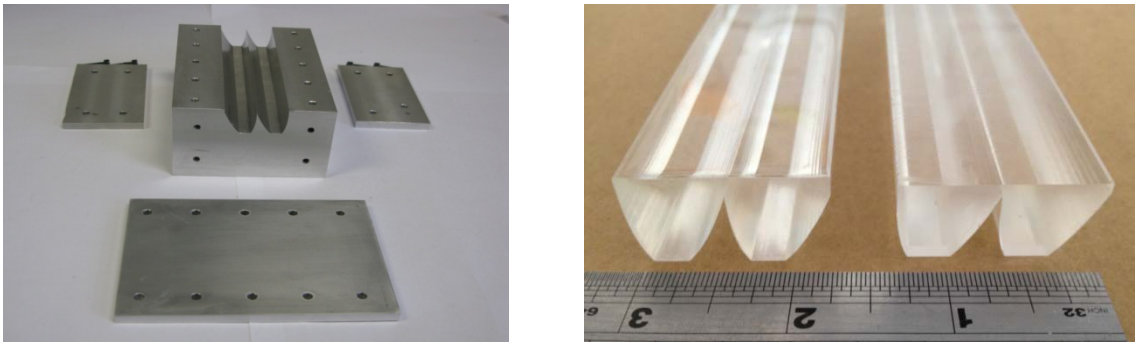

(a) (b)

Figure 2.5 (a) Mould with two troughs for manufacture of the concentrator unit having two trough (b) Dielectric concentrator having two troughs in one unit

A second mould was designed and fabricated to manufacture 10 concentrator troughs as one unit. The CAD design diagram showing the dimensions of the different sections of the mould and an image of the mould is shown in figure 2.6 (a) & (b).

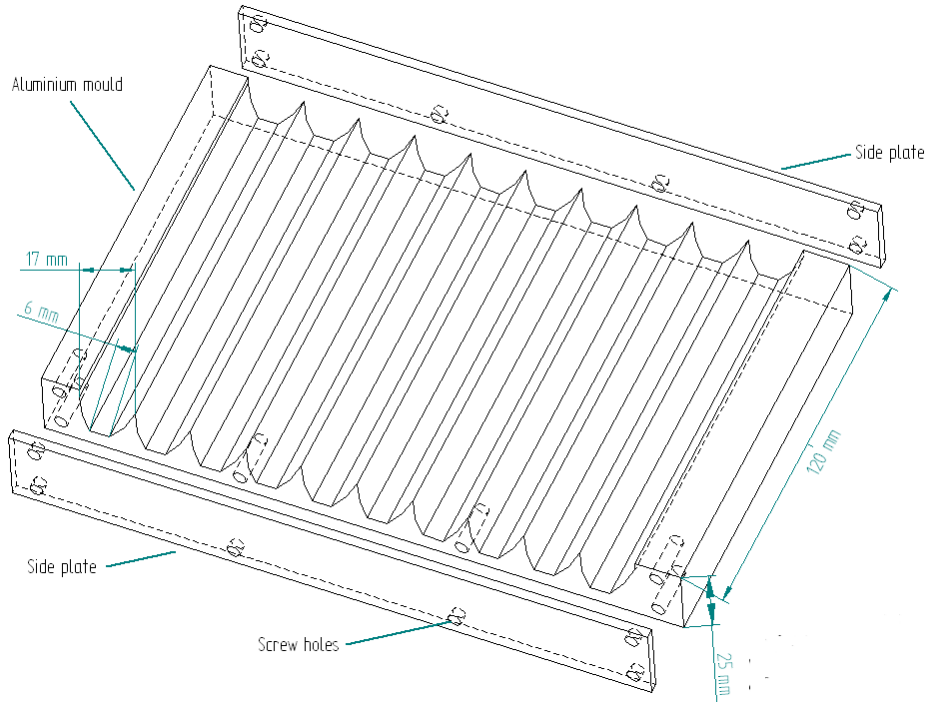

(a)

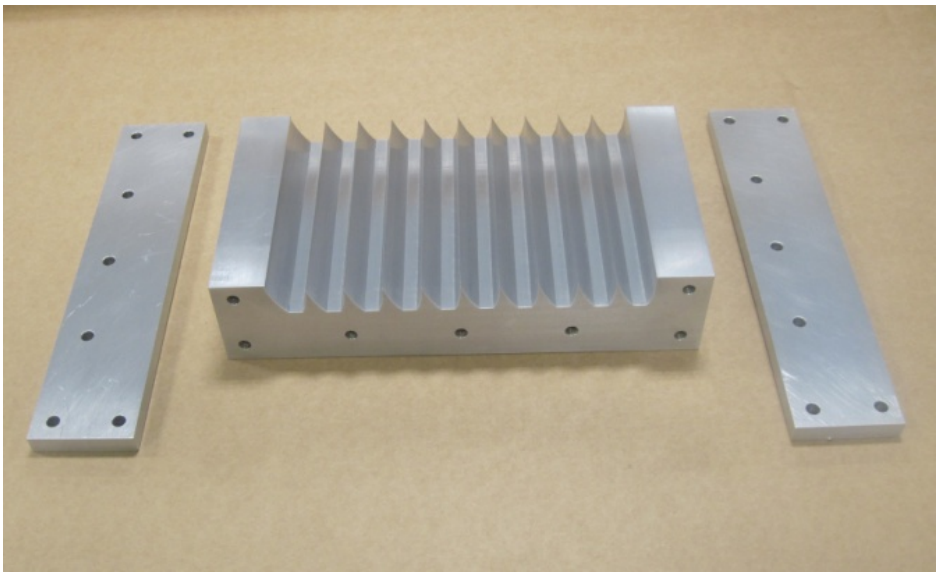

(b)

Figure 2.6 (a) Schematic diagram of the mould with 10 troughs (b) Image of the final mould used to manufacture a concentrator unit with 10 troughs.

However, the side troughs of the unit needed to be machined to achieve a flat aperture surface, which is described in the following section. The number of troughs in one concentrator unit is restricted to avoid any mechanical structural defect that may arise

with ageing; for example bending, which can cause separation (delamination) of the solar cell and the concentrator. In earlier studies, it was observed that with long term exposure in an outdoor environment, the dielectric concentrator (PRIDE concentrator) units with larger numbers of troughs, could bend along the length of the concentrator, which caused delamination [230]. The mould is designed to have the top surface open during curing of the dielectric material.

2.4.1.2 Casting process

The casting of the 'crystal clear 200' polyurethane is a simple process, as the material cures at room temperature and pressure. High quality clear plastic can be achieved without a post-curing process. During the casting process, the aluminium module is cleaned and dried properly to avoid any moisture being trapped inside the cast polymer. A universal mould release from Smooth-on® is used on the mould to prevent the polyurethane getting stuck in the mould while curing. This mould release is a specially formulated oily substance suitable for releasing moulds from polyurethane. The mould release is supplied as an aerosol, to be sprayed from 30 cm, to create a thin layer on the mould. To break the surface tension and to minimise air entrapment the layer of mould release is brushed over the surface using a soft brush. The release agent is then allowed to dry for half an hour before pouring the monomer mixture for casting. During this time the monomer mixture of the polyurethane is mixed in preparation for casting.

The urethane monomer is supplied as part-A and part-B to cast clear polyurethane. Part-A is dicyclohexylmethane-4, 4/-diisocyanate, and part-B is a plasticiser blend. The part-A is toxic in nature, so safety measures need to be taken while handling the product and mixing the two parts. Weighing and mixing of the two parts were carried out in the ventilated chamber of a fume cupboard. The supplied part-A and part-B were added as per the instruction, in the ratio 10:9 by weight [218]. The blend was stirred well to mix the two parts symmetrically. A magnetic stirrer could have been used to reduce physical effort and ensure good mixing, but considering the viscosity of the material and the rapid curing, manual stirring was found to be better for this material. 5 minute of stirring was sufficient, as there was then no sign of liquid monomer in the cured concentrator unit. During the mixing of part-A and part-B, air bubbles were generated, which needed to be eliminated from the mixture before pouring in the mould. Air bubbles in the dielectric concentrator can cause scattering of light which would increase the optical losses. A powerful vacuum chamber was used to eliminate the air bubbles.

The mixture was kept at 1MPa vacuum for 5 minutes, which brought all the trapped air bubbles to the surface and away from the mixture. During this process, the mixture started curing very rapidly and after 5 minutes in vacuum chamber the increase in the viscosity of the material caused problems in pouring into the mould. So the mixing and the elimination of air bubbles needed to be finished within 12-15 minutes, to allow a smooth pouring of the mixture into the mould. The mixture was poured slowly into one place of the mould, to avoid any possibility of air being trapped in the liquid. The mixture flowed to all the troughs smoothly filling the mould. The complete set-up was left at room temperature and pressure for 24 hours for curing, and to achieve hardness.

2.4.1.3 Post curing processes

The post-curing of the dielectric concentrator involves machining and polishing of the concentrator units to achieve a flat aperture surface. Even though the polyurethane shrinks negligibly, due to the surface tension, the cast concentrator units do not have flat aperture surfaces at the sides and edges. The schematic diagram of this curved surface is shown in figure 2.7.

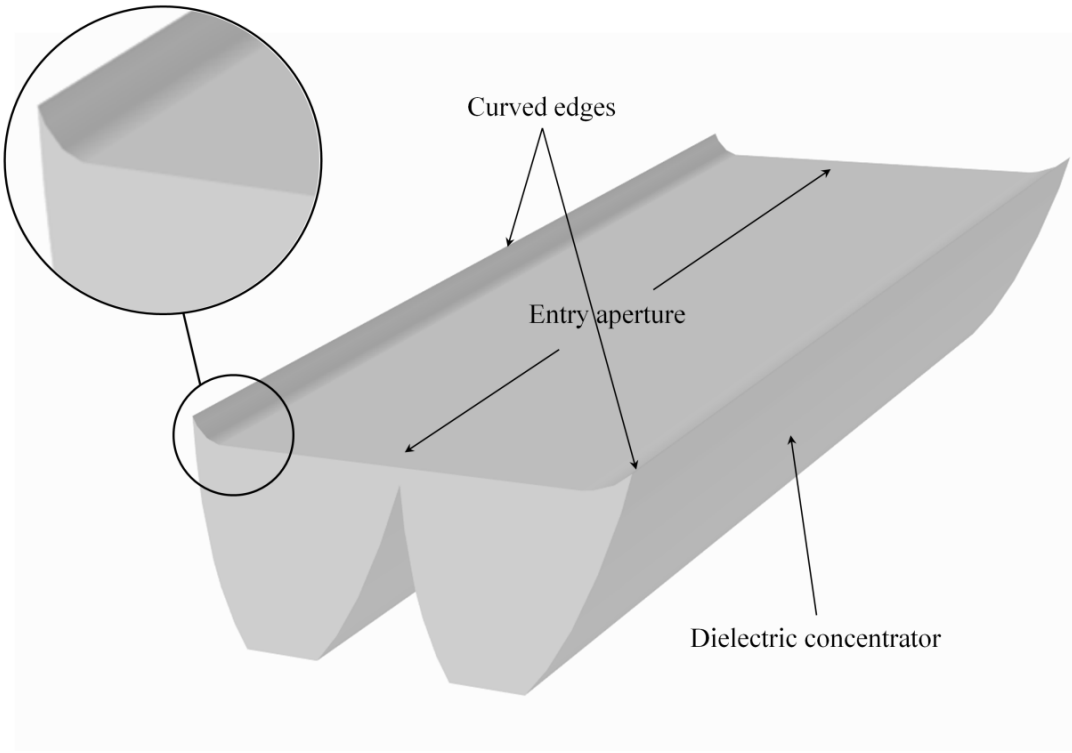

Figure 2.7 Schematic diagram of the one concentrator unit of two troughs showing the curved surfaces at the edges

At first, the aperture surface was polished to achieve flat surfaces for the concentrator units of having two troughs. The surface polishing was carried out using a diamond edge polisher, which resulted in a smooth surface finish. The single point diamond cutter rotating at approximately 7000 rpm takes out a thin layer of the material, leaving a polished surface. Figure 2.8 shows the polisher and the diamond cutter [231]. The surface of the concentrator needs to slide manually pressing across the rotating blade. Since the aperture surface of the concentrator unit was almost equal to the radius of the cutter, the polished surface was left with marks of the rotating cutter. These marks caused scattering on the aperture surface, resulting in a reduction in the optical transmission of the concentrator. So another approach was considered to avoid polishing, by manufacturing a concentrator unit with 10 troughs and machining the two side troughs.

(a) (b)

Figure 2.8 (a) PMMA polisher from Mutronics (b) Inset image of the diamond cutter used in the polisher

The second mould was designed to manufacture 10 concentrator troughs as one unit. The mould was designed to be 2mm longer than the length of the cell. To remove the curved surfaces of all the sides of a concentrator unit, first the two sides across the length have also been machined to take out the curved section. This made the concentrator length similar to the solar cells. After that two side troughs of the concentrator was removed. So the end product was a concentrator unit with 8 troughs having flat aperture surface and length matching the solar cell. One unit of the dielectric concentrator after post curing processes is shown in figure 2.9.

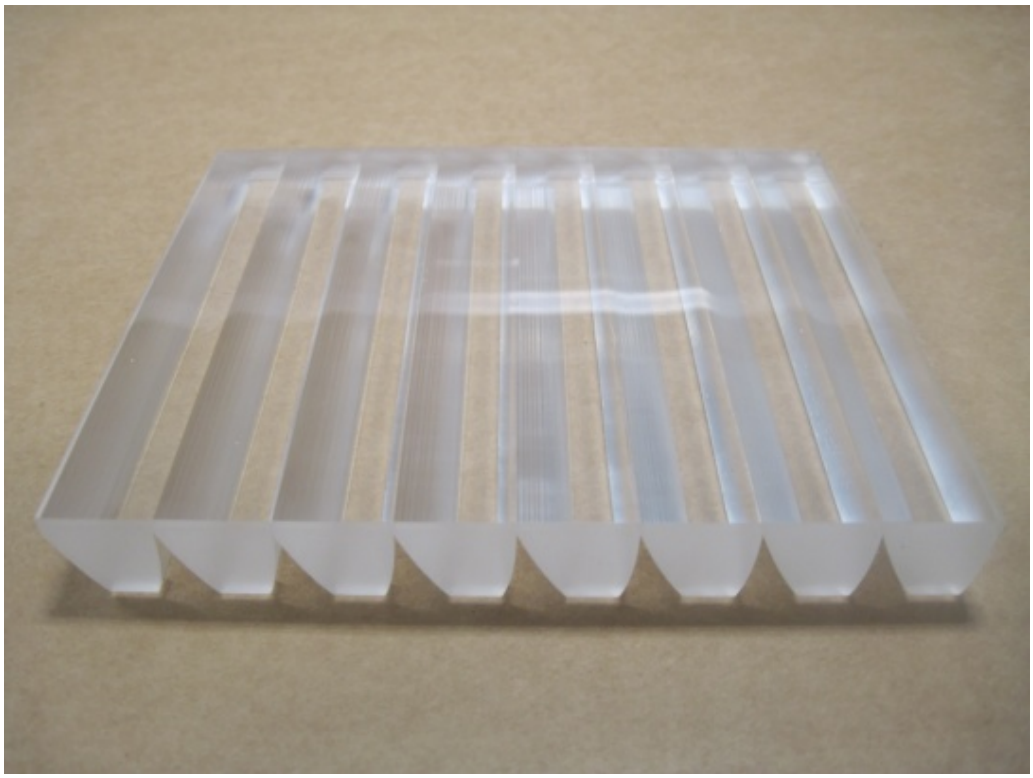

Figure 2.9 Image of eight concentrator troughs forming a concentrator unit after the post curing process

2.4.2 Machining of casted PMMA sheet

The concentrator was fabricated by machining a cast clear PMMA sheet with a specially-designed cutter, to achieve a concentrator profile as shown in figure 2.10 (a) The cutter is designed to cut groves in a commercial PMMA sheet of 15mm thick. This process has two advantages:

- It is an easy and quick process to achieve the designed ACPC profile on a casted sheet
- Cast PMMA with excellent optical properties can be used.

Casting of PMMA to manufacture the designed concentrator whilst maintaining the desired profile is very challenging, due to shrinkage. The photograph of the manufactured concentrator unit is shown in figure 2.10 (b). This process can result low cost manufacturing of the dielectric concentrators using PMMA. However this manufacturing process leads to a rough parabolic surface of the concentrator (compared to the casted concentrator), which can result higher optical losses.

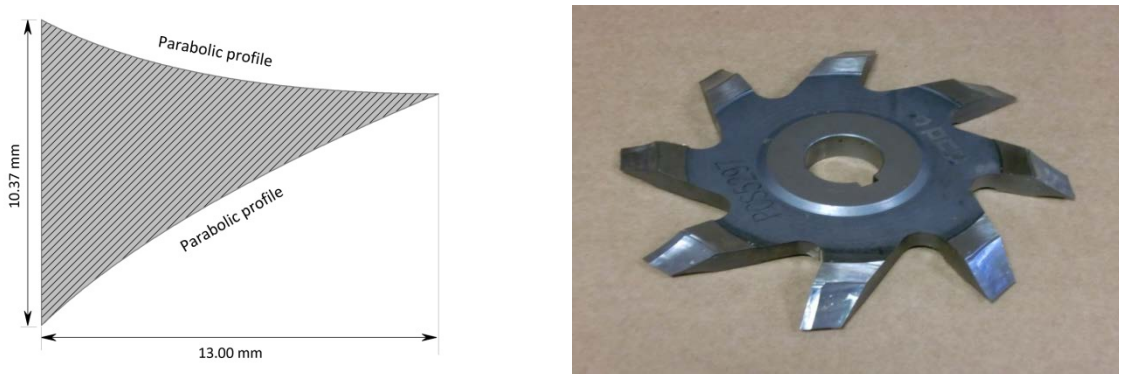

Figure 2.10 (a) Profile of the cutter to make trough in PMMA sheet and (b) Image of the cutter

2.5 Solar cell soldering and interconnection

In the construction of solar modules, solar cells are electrically connected by thin tin plated copper strips. These connection strings are soldered to the solar cells with connections either in series or in parallel, as required. The BP SATURN solar cells used in this project are designed to have soldered front and rear contacts [228]. Figure 2.3 shows the, the bus bars on the two sides of the cells for front tabbing. On the back side of the cell (positive side), the tabbing can be attached at any convenient point. High temperature soldering can damage the cells, so low temperature soldering was used. It is very important that the spacing between the solar cells matches the separation of the receiver in a concentrator unit. Misalignment between solar cell and receiver results in higher optical losses, and reduces the performance of the solar cell significantly. To maintain the spacing between the solar cell connections, a jig was constructed with a thermally-insulating plastic material. Figure 2.11 shows the schematic diagram of the spacing between solar cells and a photograph of the jig showing the cell position. The jig also helps to keep the tabbing in a straight line, so that the receiver of the concentrator fits precisely on top of the solar cell. The electrical connection of the solar cells is done by the following procedure:

- The tin coated copper tab was cleaned and cut to a length of 21mm, to connect two cells in a spacing of 11mm. It is important to ensure that the connector pieces are straight.
- The soldering iron rod, with a temperature controlled unit, is heated to 300^{o}C and maintained that temperature.

- A small amount liquid flux is used on the tip of the both ends of the connector piece for controlled and effective use of soldering material.
- A small amount of solder is applied with the help of the soldering rod on both ends of the connector piece. It is important not to use excessive solder, as this can overflow during tabbing with the cells, causing a short-circuit. The excessive use of solder can also increase the series resistance of the module.
- The solar cells are placed in the jig and connection to the negative terminal of the cells is made
- After connecting the negative terminals of the solar cells, the cells are placed upside down in the jig to connect the positive terminals.
- The same procedure is followed to connect cells in each string. Each string is placed on the rear plate for either parallel or series connection, depending on the requirement of the modules.

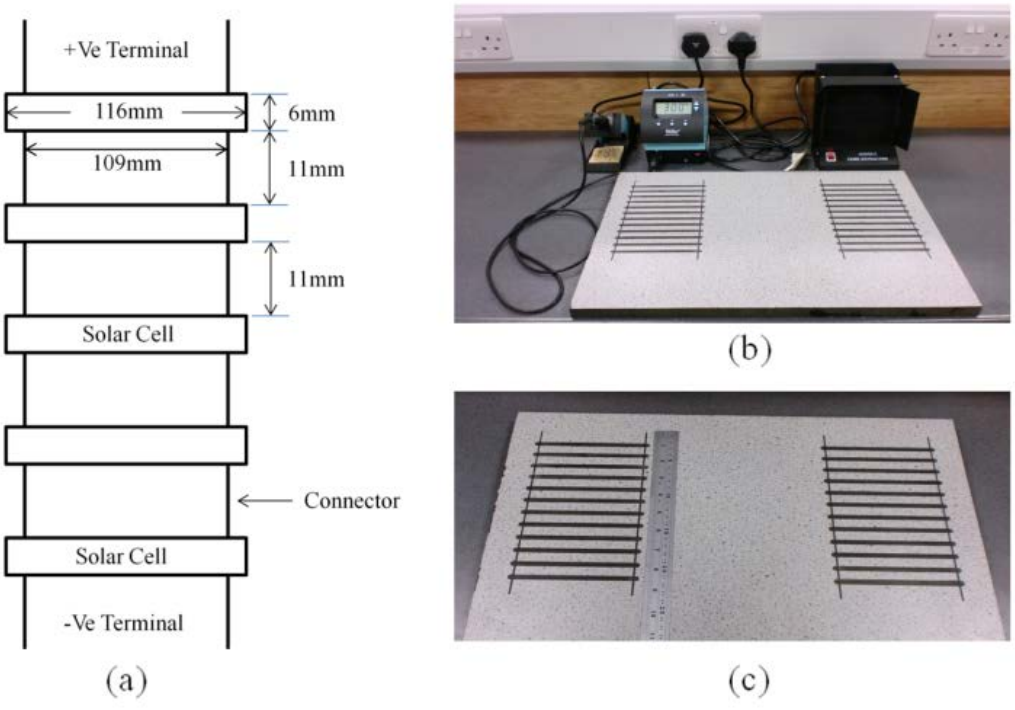

Figure 2.11 (a) Schematic diagram of the solar cell spacing in a CPV module using dielectric concentrator (b) Set-up for solar cell soldering (c) jig for solar cell connection

2.6 Assembly of components and fabrication of CPV modules

Four different types of module have been fabricated for indoor and outdoor testing. The large size modules were constructed to investigate the amount of error resulting from

fabrication on a large scale. A schematic diagram of the CPV module assembly is shown in figure 2.12. The CPV modules were constructed as follows:

- Checking short-circuit connections in each string of solar cells
- Positioning of the rear substrate and the strings of solar cells
- Preparation and application of the encapsulation material
- Positioning of the concentrator units on top of the solar cells
- Framing of the CPV module and electrical short-circuit check

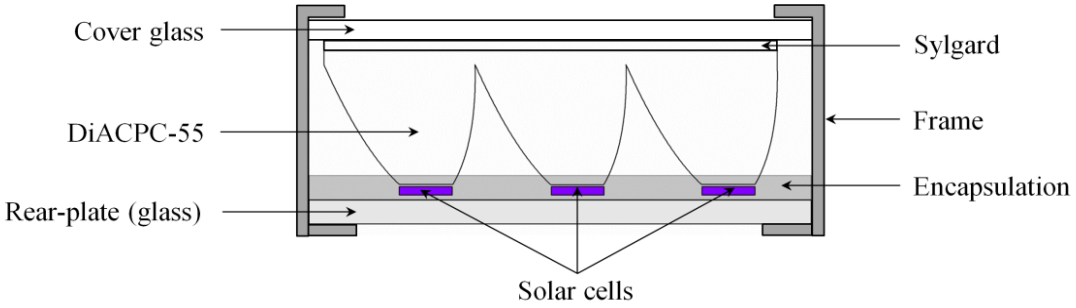

Figure 2.12 Cross-sectional schematic diagram of the CPV module showing different components.

2.6.1 Short-circuit inspection of the solar cell connections

It is very important to check for short-circuits in a string of solar cells. If there is a short circuit, a cell will not function correctly and the total power output will be affected. To test for this the continuity between solar cells was checked using a digital multimeter offset to electrical continuity check. The series resistance was measured to ensure that each cell had the same properties. After checking for short circuits, short circuit current and open circuit voltage of all the strings were checked to confirm same output.

2.6.2 Position of the rear substrate and strings of solar cell

The glass plate that was used as rear substrate was positioned on a horizontal plane and levelled to ensure uniform distribution of the encapsulation material. The glass was cleaned and dried to eliminate of dirt and grease. The strings of solar cells were placed in a prearranged layout on the glass sheet. For the modules with more than one string of cells, a gap of 5 cm was allowed between the strings, to provide sufficient space to position the concentrator units, which were placed on top of the solar cells. With everything in position, two long tabbing strips were soldered in place for parallel

connection of the positive and negative terminals of the strings, giving output terminals of the module.

A gasket of silicon rubber was placed at the boundary of the rear-plate, to prevent overflow of the encapsulation material. The gasket was 2 mm thick and 10mm wide silicon rubber, with the same outer dimension as the rear-plate. The gasket was clamped to the rear-plate and due to its physical compression stuck very well to the glass preventing leakage of the encapsulation material.

2.6.3 Preparation of encapsulation material

The encapsulation material, Sylgard-184, was cast on top of the rear-plate (figure 2.12) of the solar cell assembly. It is supplied as a base and curing agent in two separate containers. As per the instruction from manufacturer, the base and curing agent were mixed in a 10:1 ratio by weight. The base and curing agent were thoroughly mixed by stirring manually for 10 minutes. During the mixing air bubbles appeared. A gentle agitation of the liquid for 10 minutes and allowing it to set for another 10 minutes was adequate to get rid of most air bubbles. Volatile compounds are released when mixing curing agent and base, so all weighing, mixing and stirring were carried out in a fume cupboard and wearing nitrile gloves. After 20 minutes of pre-treatment, the mixture was placed in a vacuum chamber to eliminate the rest of the trapped air bubbles inside the mixture. The mixture was allowed to expand and then to settle to its original volume by creating and releasing a vacuum. Repeating this process 3 to 4 times reduced all visible air bubbles. The preparation of the encapsulation took approximately 30 to 35 minutes, depending on the amount of air bubbles introduced during stirring.

Before pouring the encapsulation material onto the rear-plate of the solar cell assembly, a primer was applied to the solar cell and the glass. The primer used in this project is Dow-corning primer-92-023 [232]. This specially formulated primer is used to mitigate surface cure poisoning. The primer enhances the adhesion between the Sylgard and a wide variety of surfaces, including glass and metal. The liquid primer was applied gently, using a soft brush and allowing 10 minutes to dry. If left for longer than 10 minutes, the primer starts to form white pigment; so as soon the primer dries, the prepared encapsulation material is poured onto the rear-plate and solar cell assembly.

The Sylgard-184 cures at room temperature or can be heat cured to speed up the curing process. The curing time at room temperature is approximately 48 hours. Curing also can be carried out at 100^{o}C, 125^{o}C and 150^{o}C for 35 minutes, 20 minutes and 10 minutes respectively. In this project, the sylgard was allowed to cure at room temperature for all the modules, because the concentrator units need to be placed on the solar cells before the Sylgard cures, in order to hold the concentrator in place. Room temperature curing was carried out to avoid any misalignment of the concentrator receiver and the cell that could have been occurred during heat curing.

2.6.4 Integration of concentrator units

The concentrator units are incorporated into the rear-plate and solar cell assembly after the uncured encapsulation material is in place. After pouring the encapsulation material it is allowed to increase in viscosity for 5 to 6 hours before the concentrators are put in place. If the concentrators are positioned just after pouring the encapsulation material, the thickness of the Sylgard layer between cell and concentrator is found to be too thin causing delamination problems. This is described in the following experimental results section. After 5 to 6 hours the viscosity of the Sylgard is sufficiently high to put the concentrator in place. Further delay results in high viscosity and sticky Sylgard, which creates problems in aligning the concentrator receiver and the solar cells. The concentrators are placed on top of the Sylgard gently, aligning the solar cell and the receiver. Due to the layer of Sylgard, the concentrator can be moved with a gentle manual force to adjust the position, without damaging the solar cells below. When all the concentrator units are in place, the Sylgard is allowed to cure completely for at least 48 hours at room temperature. The Sylgard is compatible to polyurethane, metal and glass, creating a strong adhesion between concentrator, rear-plate and solar cell. Thus the Sylgard works very well as both encapsulation material and binding material to hold the dielectric concentrators in a CPV module.

2.6.5 Framing of the CPV module

CPV modules that are fabricated for extensive outdoor testing are only framed permanently. Small prototypes are fabricated with only one concentrator unit and no framing is required for indoor characterisation. The framing is required to the CPV modules fabricated for outdoor testing for the following reasons:

- Structural rigidity
- To protect from environmental degradation
- To protect the front glass cover and rear plate from mechanical shock
- Suitable electrical connection

The fabricated modules are enclosed in an aluminium frame with a front cover glass sheet. The frame is constructed using L-shaped cross-section. The “L” section is 39mm high and 13mm wide. A schematic diagram of the height of the arms of the angle and an image of the frame is shown in figure 2.13.

(a) (b)

Figure 2.13 (a) Dimensions of the aluminium section used to construct frames for CPV modules (b) An image of the frame

The length and width of the frame were designed to fit the pre-ordered cover glass and the assembled CPV. The low-iron content borofloat (BF) glass was first put inside the frame and sealed. A shock-absorbing sealing tape was used between the cover glass and the aluminium frame to prevent the glass breakage by mechanical shock. The assembled CPV module was placed inside the frame with the aperture facing the cover glass. The positive and negative terminals of the module were taken out through small holes in the frame that were sealed later, using a rubber sealant. Once everything is inside the frame, the rear-plate was sealed to the frame using silicon sealant CT-1, which is suitable for use outdoors. The sealant prevents moisture and water leakage into the module. CT-1 sealant exhibits thermal expansion; so can tolerate expansion and contraction due to

diurnal variations in temperature. An image of the different process steps is shown in figure 2.14

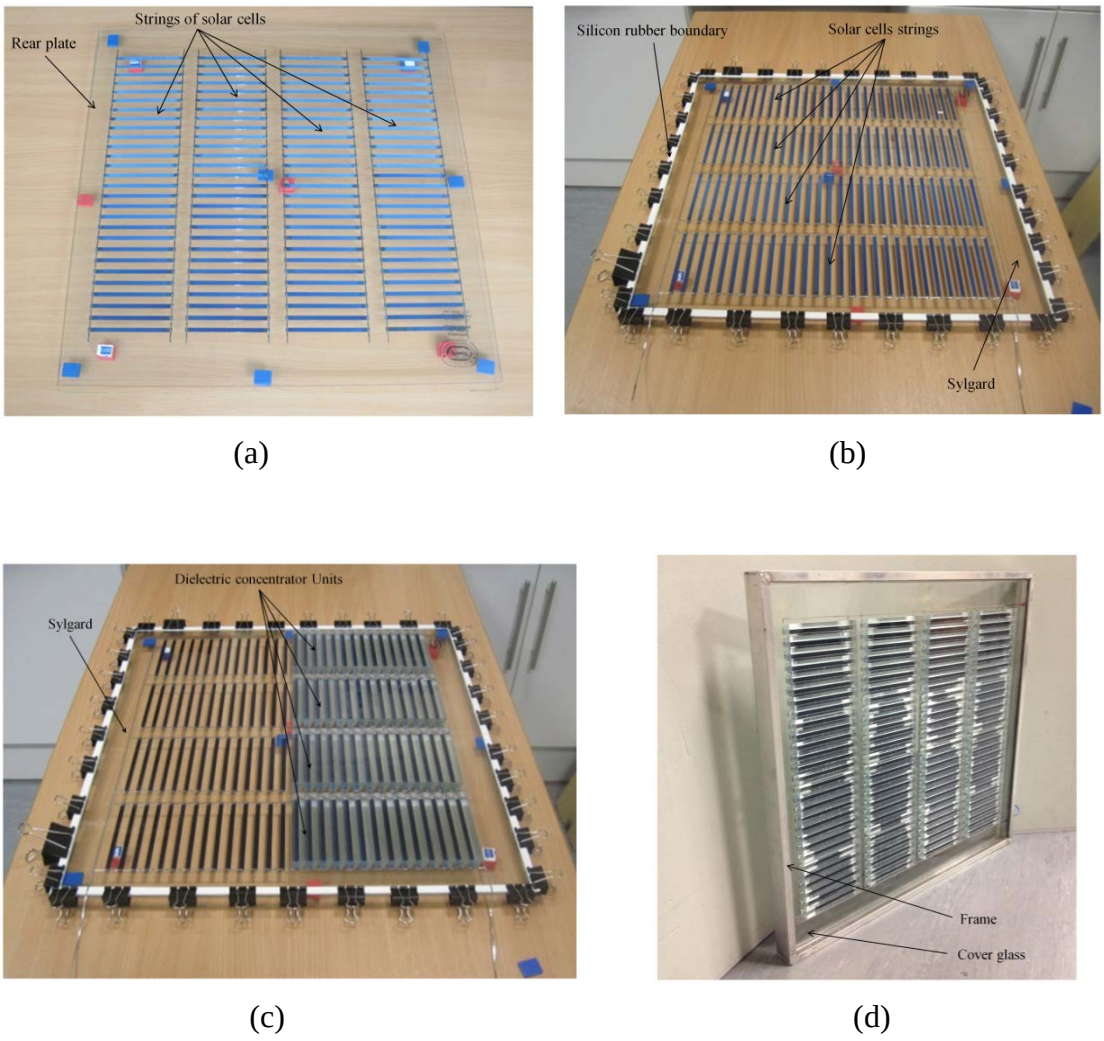

Figure 2.14 CPV module fabrication process steps (a) solar cells strings on a rear glass plate (b) Rear plate and solar cell with uncured encapsulation material (sylgard) (c) Integration of concentrator units on top of the solar cells (d) Complete CPV module with aluminium frame.

2.7 Different prototype modules

2.7.1 First prototype module for indoor characterisation

The first prototype module for indoor characterisation was fabricated using three concentrator units, each one having 2 troughs. This module was used for initial characterisation of the concentrator. The concentrator used in this module did not have flat aperture surfaces, since no post curing process was carried out. After measuring the

performance of this module, the post curing process was adopted and the mould to manufacture 10 concentrator troughs as one unit was employed, which is described in Section 2.4.1.1 and 2.4.1.3. The first prototype was fabricated with two strings of three solar cells in series. This module was manufactured using a standard 2mm thick window glass as cover glass in a non-permanent frame. Figure 2.15 shows the images of the first prototype module.

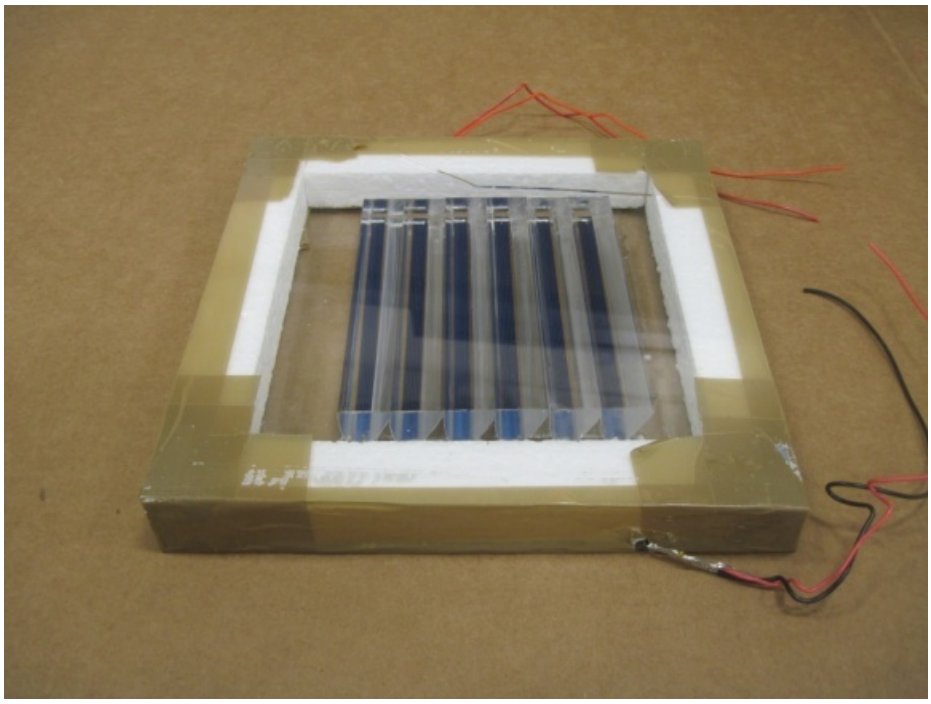

Figure 2.15 First prototype CPV modules with two solar cells as prepared for indoor characterisation

2.7.2 Second prototype CPV module

The second prototype module was constructed for detailed indoor characterisation using one unit with 8 concentrator troughs. The size of the module was 150×170mm, with an effective aperture surface area of 158 cm^2. The fabrication process for all the PV modules was similar as described in section 2.6. However, a few modifications were made in this second prototype in order to carry out detailed investigation of the concentrator performance. Ray-trace analysis of the concentrator and concentrating system showed that a major optical loss occurs at the air-dielectric interface of the aperture and cover glass. This is because of the cover glass was not optically coupled with the aperture of the concentrator. For indoor performance analysis of the CPV module, a module was fabricated with a glass optically coupled to the aperture of the concentrator.

Optical coupling was achieved by use of the encapsulation material (Sylgard-184). The Sylgard mixture was prepared following the procedure described in section 2.6.3 and poured on a low-iron content BF glass. The aperture of concentrator unit was placed on this; clamped to sandwich the Sylgard in between glass and the concentrator, and allowed to cure for at least 48 hours at room temperature and pressure. This creates excellent optical coupling between the glass and the aperture of the concentrator. This concentrator with optically-coupled cover glass was used to fabricate a CPV module for indoor characterisation. An image of the CPV module with optically coupled glass is shown in figure 2.16

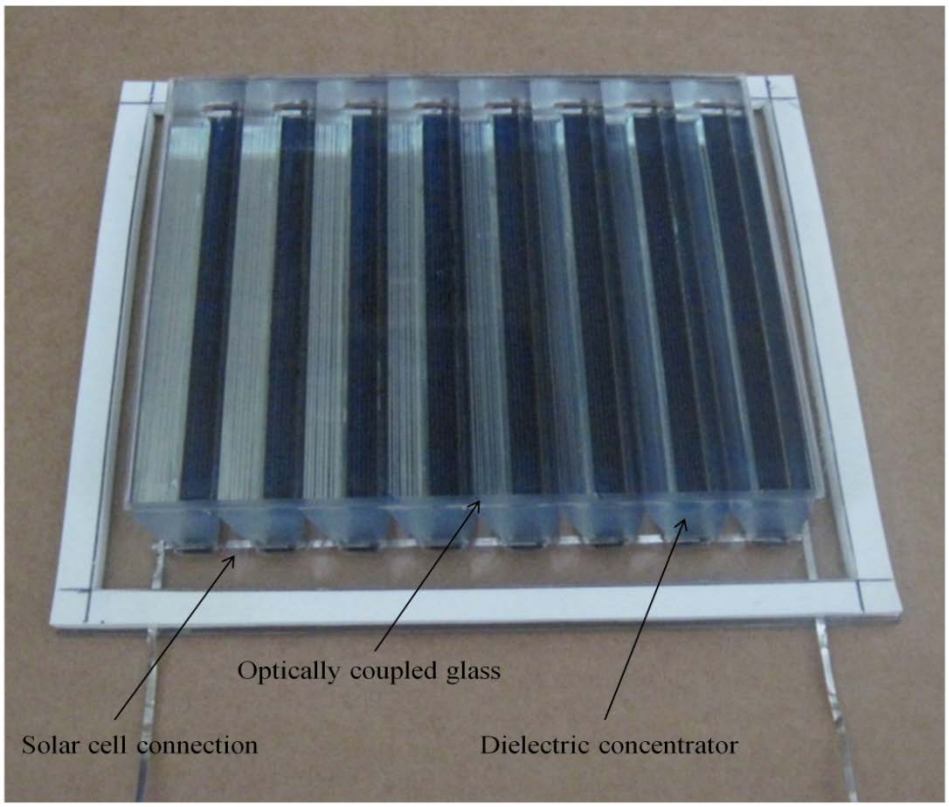

Figure 2.16 Second prototype of CPV module with optically coupled cover glass

In another modification, the second prototype module was constructed with and without reflective films at the parabolic surfaces of the concentrator in contact with the encapsulation material as shown in figure 2.17. It was observed in an initial experiment that at the concentrator-encapsulation interface of the CPV module, light can escape and cause higher optical loss. This loss can be minimised by incorporating a thin reflecting film of 2mm width on the parabolic sides, inside the encapsulation material next to receiver. Reflective films of 2mm width and 116mm length were cut from a sheet of

commercial reflective film specially manufactured by ReflecTech® to use in solar concentrators [233]. The reflective film has one self adhesive side. The reflective films work with two fold advantages; preventing direct contact of the encapsulation material with the parabolic sides of the dielectric concentrator and reflecting the light from those sections of the parabolic sides to the receiver.

The modules with reflective films were expected to reduce the optical loss in the CPV system and to enhance the performance for the range of acceptance angles of the concentrator.

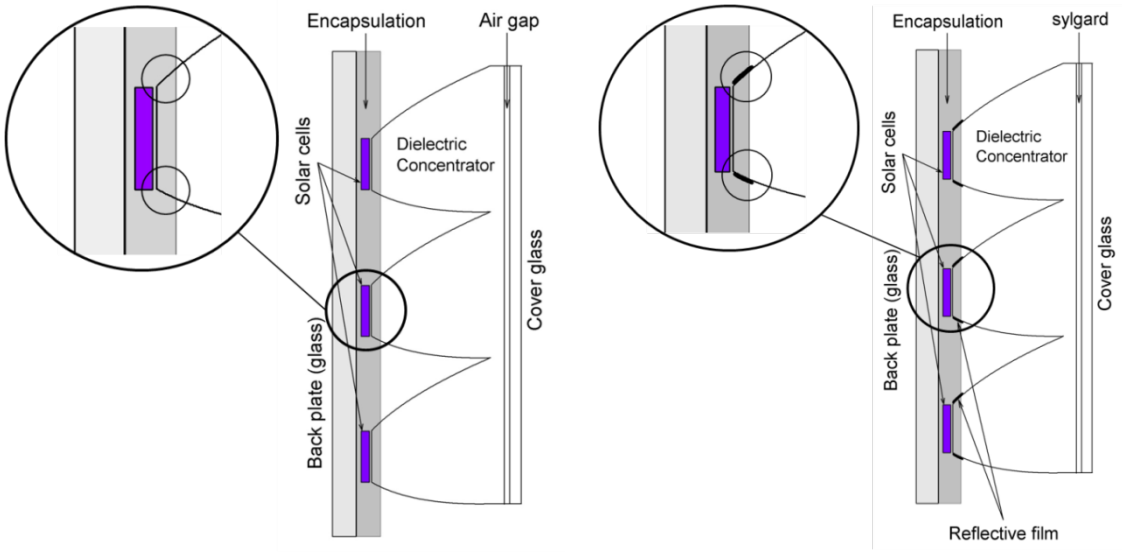

(a) (b)

Figure 2.17 Schematic diagram of the CPV module (a) without reflective film and optically coupled cover glass (b) with reflective film and optically coupled cover glass

2.7.3 Third prototype CPV module

The third prototype CPV modules were constructed to analyse performance in both in outdoor environment, and using a large area solar simulator. The module sizes of the third prototype were 300mm×300mm. These modules were framed using low-iron content glass. The complete frame was sealed with sealing agent to prevent moisture and air ingress. Images of the third prototype are shown in figure 2.18.

Figure 2.18 Photograph of the third prototype CPV module

2.7.4 Fourth prototype

The fourth prototype CPV module with dielectric concentrator was constructed to monitor long term energy output and performance in an outdoor environment at Edinburgh, UK. The module was 600mm×600mm in size. Four parallel strings of 28 solar cells in series were connected to get a maximum operating voltage of 12V and to generate a 2A current at a solar irradiation of one Sun. The module was constructed with 16 concentrator units in total, 8 of which have 8 troughs and 8 with 6 troughs. An image of the fourth prototype module is shown in figure 2.14 (d).

The concentrator units used in this module were modified by incorporating strips of reflective film, as described in Section 2.7.2, to reduce at the optical loss at concentrator-encapsulation interface. The specifications of the different prototype modules fabricated during this project for performance analysis are given in table 2.2. Three flat plate modules (FP-1, FP-2 and FP-3) were constructed to compare with the performance of the CPV prototype modules. The flat plate modules were non-concentrating counterparts of the CPV prototype modules. FP-1 is the non-concentrating counterpart with the same module area as CPV-1. Similarly FP-2 and FP-3 are the non-concentrating counterparts of CPV-S1 (and CPV-S2) and CPV-T1 (and CPV-T2) respectively.

Table 2.2 Specifications of the different prototype CPV modules used in the project for performance analysis

CPV Prototypes	Name	Dimension (mm)	Specifications	Type of Test
First prototype	CPV-1	170 × 170	- Concentrator without post curing process	Indoor
Second prototype	CPV-S1	150 × 170	- Concentrator after post curing process - Cover glass not optically coupled - Optical loss at the concentrator-encapsulation interface	Indoor
	CPV-S2	150 × 170	- Concentrator with post curing process - Optically coupled cover glass - Reflective film at concentrator-encapsulation interface	Indoor
	CPV-S3	150 × 170	- DIACPC-55 concentrator manufactured from PMMA - Cover glass not optically coupled - Optical loss at the concentrator- encapsulation interface	Indoor
Third prototype	CPV-T1	300 × 300	- Concentrator with post curing process - Air gap between cover glass and concentrator aperture surface - Optical loss at concentrator-encapsulation interface	Indoor/ Outdoor
	CPV-T2	300 × 300	- Concentrator with post curing process - Air gap between cover glass and concentrator aperture surface - Reflective film at concentrator-encapsulation interface	Outdoor
Fourth prototype	CPV-4	600 × 600	- Concentrator with post curing process - Air gap between cover glass and concentrator aperture surface - Reflective film at concentrator-encapsulation interface	Outdoor

2.8 Experimental methods

A detailed investigation of the performance of the designed concentrator was carried out through a series of experimental characterisations. All the components in the CPV module were investigated for optical and spectroscopic properties. The prototype CPV modules of different aperture areas were investigated in both indoor and outdoor environments to compare with similar non-concentrating counterparts.

2.8.1 Spectroscopic analysis

The spectroscopic analysis of the different components is an important characterisation to investigate detail performance of the concentrators. The spectroscopic analysis was carried out to find transmittance of the optical components and the external quantum efficiency of the CPV module. The transmission spectrum can indicate the absorption losses in the optical components within the spectral response of the solar cell. The external quantum efficiency of the solar cell and the module is used to evaluate the effect of incorporating the concentrator and the encapsulation with the solar cell.

2.8.2 Transmission study

The spectroscopic analysis of the different components of the CPV module was carried out using a Perkin Elmer Lambda 900 UV-Vis spectrometer [234] . This instrument is capable of scanning a material for transmittance, reflectance and absorption properties within a wavelength range from 200nm to 3000nm at 1 nm intervals. The Lambda 900 UV-Vis-NIR spectrometer used in this study is shown in figure 2.19. A light beam from a light source is allowed to pass though a monochromator and filters before reaching the sample. The monochromatic light reaches the detector after passing through the sample to measure the transmittance or absorption properties of the material. The sample is placed in a sample holder and the transmittance is measured with reference to air. Once the spectral transmittance of the sample is measured, the absorption coefficient of the sample is calculated using Beer-Lambert law [235]:

$$T = (1 - R)^2 e^{-\alpha t} \qquad 2.1$$

Where, T is the transmittance of the material, R is the reflectance with air boundary, α is the Napierian absorption coefficient and t is the thickness.

Figure 2.19 The Perkin-Elmer UV-Vis-NIR spectrometer at Heriot-Watt University

2.8.3 External Quantum efficiency

The spectral response and quantum efficiency are properties, which are used to understand the current generation, recombination and diffusion mechanisms in a solar cell. *"The spectral responsivity is measured in units of current produced per unit incident power"* [11]. Typically, spectral response is calculated using the short circuit current, which is usually same as the generated photocurrent. External quantum efficiency (EQE) can be measured by spectral response of the solar cell using the equation [17]

$$QE(\lambda) = \frac{qS(\lambda)}{\lambda hc} \tag{2.2}$$

Where, QE is the quantum efficiency, q is the charge of an electron, $S(\lambda)$ is the spectral response, λ is the wavelength, h is Plank's constant and c is the speed of light. The EQE of the bare cell and cells in CPV modules were measured using a Bentham spectral response set-up. The EQE measurement set-up is shown in figure 2.20. The spectral response of the solar cell was scanned for a range of wavelengths. Light from a source was directed through a monochromator and filter before illuminating the sample under test. The set-up was first initialised with a calibrated photodiode, before measuring the spectral response of the cell. The spectral response was measured under a biased light from a xenon lamp.

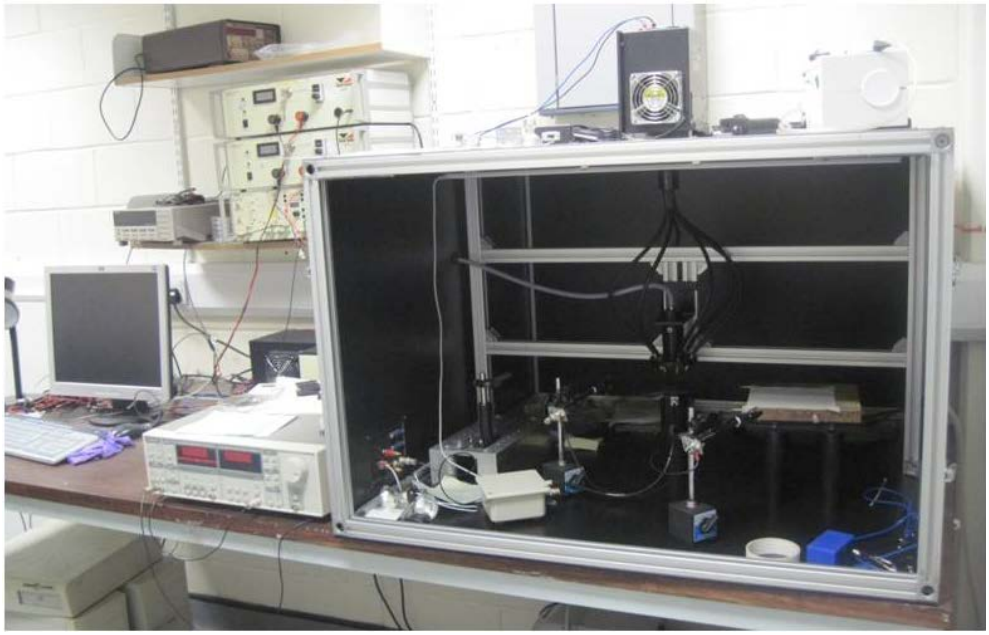

Figure 2.20 The spectral response set-up at Heriot-Watt University

2.8.4 Scattering and optical loss analysis

Optical losses are the main source of reduction on power output in concentrating photovoltaic systems. The other losses in a CPV system include resistive losses; mismatch losses and reduction in power output with temperature. The resistive losses can be reduced by using high-quality inexpensive conducting materials, which are commercially available. These can be further minimised with good connectors and well-structured electrical joints, when tabbing the solar cells. The mismatch loss from a solar cell can be controlled and minimised by using cell from the same batch of solar cells, with similar properties. In this project, the mismatch loss from solar cells was expected to be negligible, since cells from the same batch were used in the modules. A small amount of mismatch loss in a CPV system can occur due to non-uniform distribution of the energy flux at the receiver. The non-uniform distribution of energy flux at the receiver of the concentrator resembles the effect of shading on the solar cells, where localised flux is lower. The reduction in total power output of a CPV system with increase in temperature of solar cell is also a considerable loss. Concentrated light incident on a solar cell is expected to lead to higher temperatures than for the non-concentrating counterpart. With increase in temperature, the open circuit voltage and the fill factor eventually decrease to reduce the total power output of the system. However in low concentrating systems with concentrating ratio of 2-3X, the losses due to rise in temperature of the module is not significantly high and the effect of the temperature can be ignored. Out of all the losses in a CPV module, the optical loss within the

concentrator plays the most significant role in reducing the total power output. In well-designed reflective-type concentrators, assuming that all the rays incident on the aperture can reach the receiver, optical losses can occur due to the reflective losses at the reflectors and front glass; and absorption losses from other components, including the encapsulation material. However, the roughness of the reflective surface can cause scattering of the reflected rays. In dielectric concentrators, the scattering and escaping of light need to be investigated in detail, as the light is directed to the receiver by total internal reflection. So any minor machining error and surface roughness can make the light to escape or scatter during reflection.

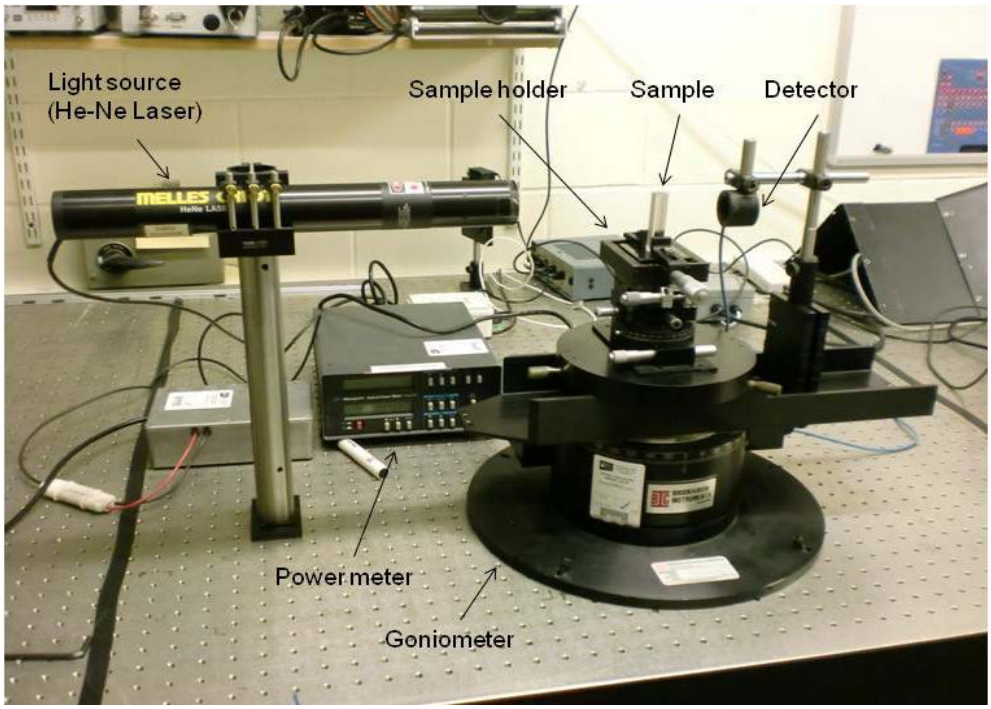

Figure 2.21 Photograph of the customised goniometer set-up

The investigation of the optical losses caused by the light escaping from the parabolic surface of the manufactured concentrator was carried out using a goniometer set-up. The goniometer set-up was modified for use with a solid dielectric concentrator. The goniometer set-up used in this study is the BI-200sm from Brookhaven Instruments is shown in Figure 2.21. It was primarily designed for liquid samples. In the modified set up, only the basic goniometer with rotating arms was used, without the PMT (photomultiplier tube) sensor. The sample holder was placed on the top plate, which could rotate 180^{o}. The sensor/detector was placed on a rotating arm which could also be rotated 180^{o}, to scan across the sample. Both the sample plane and the rotating arm rotate around a virtual axis at the centre of the sample holder. The whole set-up was

levelled and fixed on an optical table using bolts. The detector was mounted on the rotating arm at the same height as the sample holder. A Helium-Neon (He-Ne) laser was used as the light source which was mounted on a frame and placed 60cm away from the sample. The laser could be kept closer to the sample if required, but in this custom-made set-up the laser was kept 60cm away to make the handling of the instruments and set-up easier. The beam size of the laser is of radius 2mm, with a slit of radius 0.5 mm used to reduce the beam size. Reducing the beam size helped in accurate positioning of the beam at the different points, across the aperture width. The detector was a silicon-based detector calibrated with a Newport power meter for 620nm, which was the wavelength of the light from the He-Ne laser. To prevent the detector from becoming saturated, a neutral density filter (ND-4) of transmittance 0.01% was used in front of the detector. The power of the laser beam was reduced when it transmitted through the concentrator sample directly, or on reflection. This reduction in power shows the optical and scattering loss in the concentrator. The concentrator sample is placed on a sample holder at the centre of the plate, which can be rotated along the same axis as the rotating arm. The sample holder is on an x-y stage which can be moved in a perpendicular direction to the beam. The concentrator aperture is moved across in a perpendicular direction to examine the optical losses for the light incident at different aperture positions. Keeping the source constant, the plane of the sample is rotated to change the incident angle of the beam on the aperture surface.

Correct initial alignment of the light source, concentrator and detector were very important. Since the source and the rotating goniometer set-up were not attached together, the alignment was done mechanically first, followed by optical imaging. The laser and the detector were placed at the same height, so that the light beam was transmitted through the concentrator sample to the detector. The detector was aligned perpendicularly to the beam path by manual observation of the maximum power on the power meter. The aperture surface of the dielectric concentrator was aligned perpendicular to the beam by observing the partial reflection from the air-dielectric interface. With correct alignment there was no image of the light beam near the source. The schematic diagram of the alignment of the goniometer se-up for optical and scattering loss analysis is shown in Figure 2.22.

The detector is kept at an optimal distance of 20cm from the receiver of the concentrator. With detector is placed further away, a fraction of the scattered light could

not reach the detector, causing problems in analysing the scattering losses. If the detector was moved closer to the receiver, due to the small angular distance the detector can sense rays for a wide range of incident angle. This creates difficulties in scrutinising the angle and position of the rays coming out of the receiver; since the detector was 0.3mmx0.3mm size and a steady output power was observed for the wide range of incidence angles. The custom manufactured goniometer set-up was operated manually to obtain the data showing scattering loss across the dielectric concentrator sample. For each incidence angle, the beam of light was directed to different positions on the aperture surface. For each aperture position the detector arm was rotated for 270^{o} to detect the reflected light coming out of the receiver; the scattered light; and light escaping through the parabolic sides.

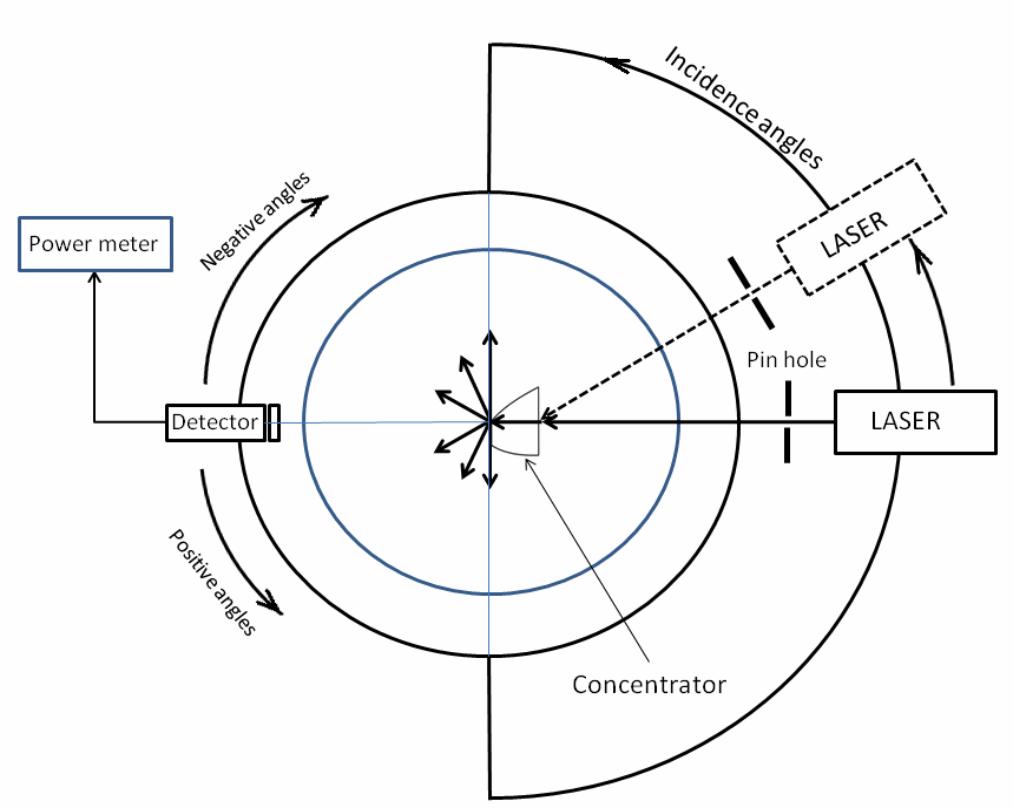

Figure 2.22 Schematic diagram of goniometer set-up showing the direction of the detector angle and angle of incidence

2.8.5 Concentrator profile investigation

The accuracy of the manufactured concentrator profile was compared with the design specifications. In manufacturing a concentrator unit there are several process step involves which can lead to manufacturing errors and the profile of the concentrator can

be deformed. To investigate the profile of the concentrator, a study was undertaken using a surface profile scanning machine named 'cyclone' from Renishaw® [236]. The Cylone is use for scanning unknown profiles with high speed data acquisition system. The machine uses a sensor probe (SP620) to touch the surface, calculating the co-ordinates of the touch points using a CAM (computer-aided manufacturing) software package. A detailed surface profile was obtained by scanning 100 data points over a 10cm distance. The specification of the cyclone scanning machine is given in table 2.3 and the image of the set-up of the scanning machine and the sensor probe is shown in figure 2.23.

Table 2.3 Specification of the cyclone scanning machine

Properties	Specification
Axial travel	600mm × 500mm × 400mm (nominal)
Accuracy	50 µm
Resolution	7 µm
Scanning rate	140 points per second
Sensor head resolution	5 µm

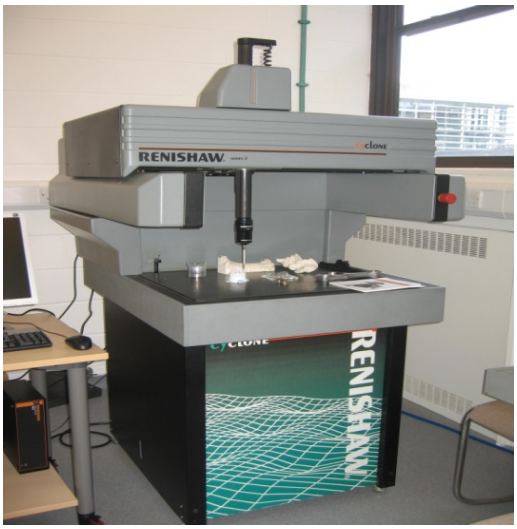

(a)

(b)

Figure 2.23 Photograph of the Renishaw cyclone set-up for profile scanning and (b) the sensor probe SP620

For scanning the 2D profile of the DiACPC-55 concentrator, the concentrator was placed on the sample holder table. It was important to achieve vertical alignment of the concentrator sample to eliminate any measurement error. An incorrectly-mounted sample would have led to measured data points in a different plane, giving incorrect profile information. Once the sample was properly mounted, the probe was allowed to touch one surface point of the concentrator to create an origin for measurements. In the next step, the data points are collected by moving the probe across the profile of the concentrator.

2.9 Indoor characterisation of CPV prototypes

In photovoltaic research, solar cells and the modules are characterised in a controlled indoor environment to find the best performance. Indoor performance analysis gives the flexibility of working under fixed irradiation conditions, while varying the other parameters. The performance of the designed dielectric concentrator in the CPV module was analysed in a controlled indoor environment using solar simulators. Two solar simulators are used for two different size modules. The schematic diagram of the indoor characterisation set-up is shown in figure 2.24.

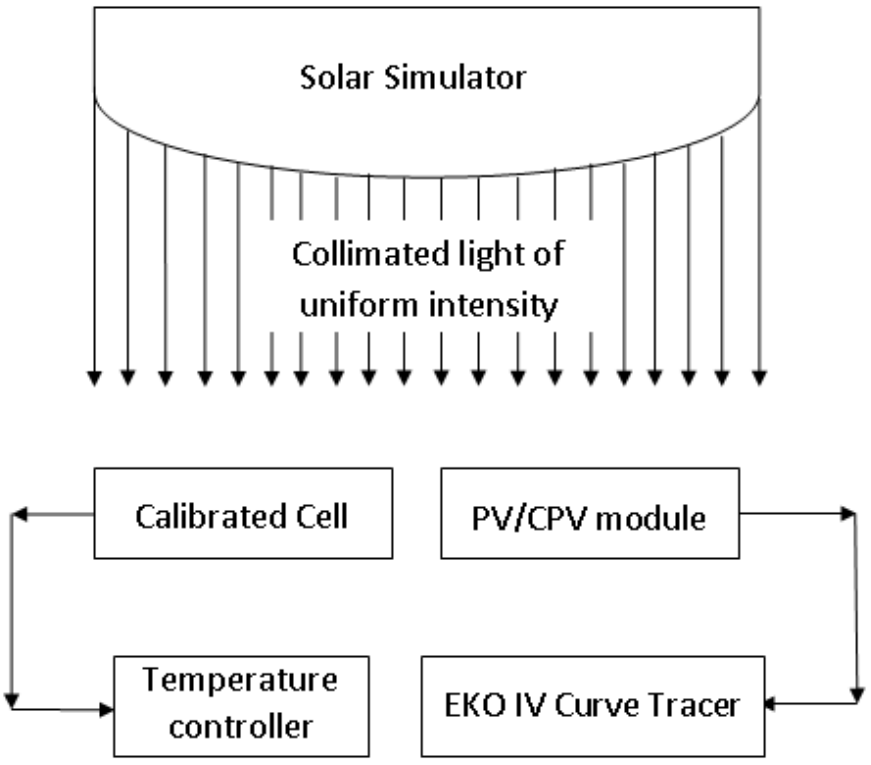

Figure 2.24 Schematic representation of the indoor characterisation set-up

2.9.1 Performance analysis of CPV modules with a small area solar simulator

The performance of the CPV modules were analysed using an ABET class-A solar simulator [237] in Heriot Watt University. The solar simulator consisted of a xenon lamp and a filter to provide an AM1.5 solar spectrum. This solar simulator had maximum illumination area of 156×156mm for a nominal working distance of 200mm. It had an uniformity of irradiation higher than 95%. The solar simulator was bolted on an optical bench and levelled during the installation. The solar simulator spectrum was found to be a very close match to the AM1.5G solar spectrum.

To characterise the CPV module under the solar simulator, the second prototype modules (CPV-1, CPV-S1, CPV-S2 and CPV-S3) were used. The size of these CPV modules fits well within the uniformly illuminated area of the solar simulator. The modules were characterised for different angles of incident and radiation. Since the incident angle of the irradiation from the solar simulator could not be changed, the different incident angles were realised by changing the inclination of the CPV module. Figure 2.25 shows the photograph of the set up to change the inclination angles of the modules for indoor characterisation.

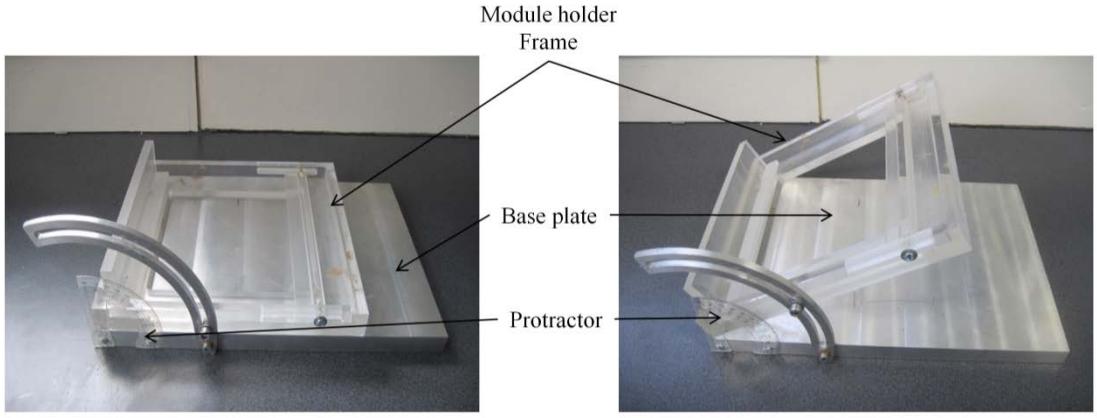

(a) (b)

Figure 2.25 Images of the set-up for inclination of CPV modules during indoor characterisation showing (a) Horizontal & (b) 30^{o} inclination

The set-up consisted of an aluminium base plate, attached to an acrylic frame by a hinge. The acrylic frame could be rotated across the axis of the hinge to change the inclination angle of the modules. The acrylic frame was designed to fit modules up to

200mm×200mm, by incorporating a moving bar. To allow natural convection from the back of the module, the frame was constructed with acrylic bars, not a continuous sheet. A protractor was attached at the junction of the acrylic frame and the aluminium base. This was used to estimate the inclination angle. However for fine adjustment of the inclination angle, a digital protractor was used. This digital protractor was accurate within ± 0.5^{o}. To characterise the modules for each inclination angle, the inclination angle was measured using the digital protractor, placed on a piece of glass on top of the frame. The digital protractor showed the horizontal surface at 0^{o} and inclination angles for any deviation from the horizontal.

The IV-curve measurement of the fabricated CPV module was carried out using an IV curve tracer from EKO [238]. It had a maximum rated power measurement for PV devices up to 300W, with maximum voltage and current ranges of 300V and 10A. This instrument was very efficient for both indoor and outdoor characterisation of PV/CPV modules, using two different software packages. The software package was very user-friendly for calculate of crucial parameters such as, maximum power; fill factor; open-circuit voltage; short circuit current; and short circuit current density from the IV curve during the experiment. The working principle of this instrument was to apply a biased voltage to the photovoltaic modules and to measure the current-voltage output from the module. The biased voltage was varied by a microcontroller through the range of values to be measured. The change in voltage and current output gives the IV curve of the module. The IV-tracer MP-160 works with a 4-wire connection, 2 positive and 2 negative terminals. One pair of positive and negative connections were used to apply a biased voltage and the other pair were used to sense outputs from the module.

To start the experiment, the solar simulator was switched on for one hour to warm up enabling a steady energy flux to be achieved over the illumination area. The shutter was kept closed during this time. Once the solar simulator had warmed up, the light intensity at the working plane and area was measured using a calibrated photodiode. The calibration process of the photodiode for the ABET solar simulator in Heriot-Watt University is described in the section 2.12. Since the light intensity in the illumination area from the solar simulator was height depended, the temperature controlled photodiode set-up was placed at the same height as the modules under test. The light intensity from the solar simulator at the photodiode plane was adjusted by increasing or

decreasing the current to the xenon lamp in the solar simulator. After adjusting the light intensity, the photodiode was replaced by the modules to be characterised.

For each set of readings for a given light intensity and inclination angle, IV measurements were taken for both non-concentrating and CPV modules. The performance of the CPV module was compared with that of the non-concentrating module for each desired inclination angle. This direct comparison of non-concentrating and concentrating modules for a particular inclination angle eliminated common optical losses that would have arises with increase in inclination angle. The complete indoor characterisation set-up with the ABET solar simulator is shown in figure 2.26

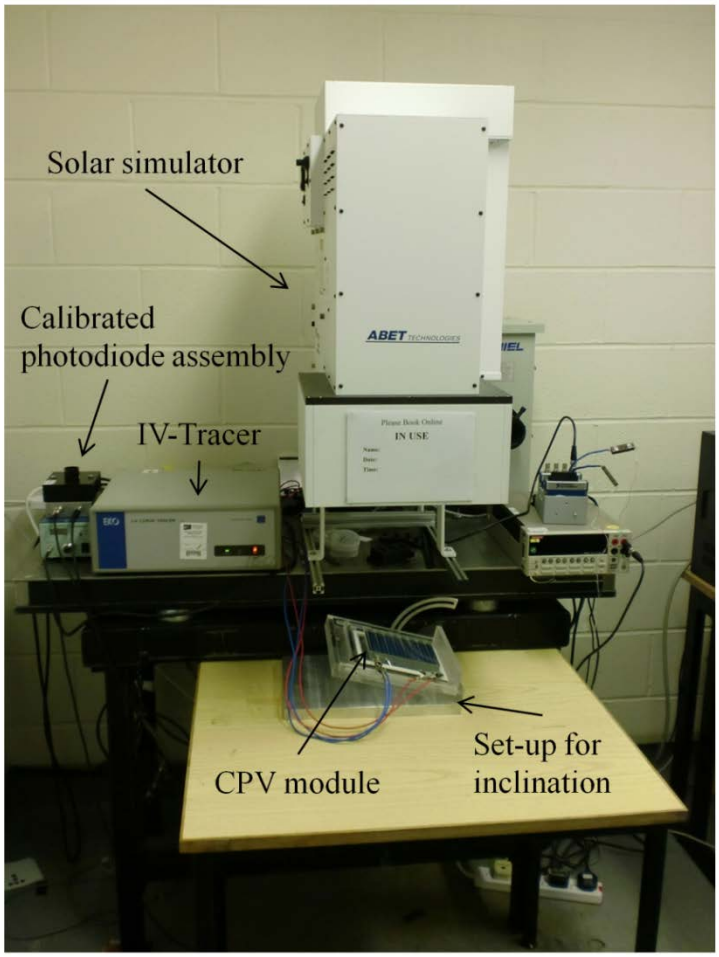

Figure 2.26 Indoor IV characterisation set-up for CPV modules using the ABET solar simulator

2.9.2 Performance analysis of CPV module large area solar simulator

One of the third prototype modules (CPV-T1) was characterised using the in-house large area solar simulator. The fabrication details and the specification of the large area

solar simulator are described in the following section. Large area CPV modules were characterised to investigate the performance of scaling scaled-up CPV modules and to compare IV measurements with those of non-concentrating systems in the same experimental set-up. Even though the spectrum of the in house simulator was not very close to sun spectrum, this study could provide a good comparison between non-concentrating and concentrating modules in order to analyse the performance of the dielectric concentrator in the CPV module.

The set-up for the characterisation of the CPV modules using the large-area solar simulator was similar to the set-up for ABET solar simulator. The IV-tracer and a data-logger were used to get the IV-data and temperature of the module respectively. The data logger used in this set-up was the Keithley Integra series (2700) data acquisition system. The Keithley data logger had built-in cold junction compensation (CJC). A multiplexer 7700 with 20 channels for voltage and 2 channels for current was used in this study. The voltage channels could be used for temperature measurements using thermocouples. Temperature measured by the thermocouples connected to the rear-plate of the CPV module and non-concentrating module was feed into the data logger for continuous monitoring and data collection. Figure 2.27 shows the CPV module characterisation set-up using the large area solar simulator.

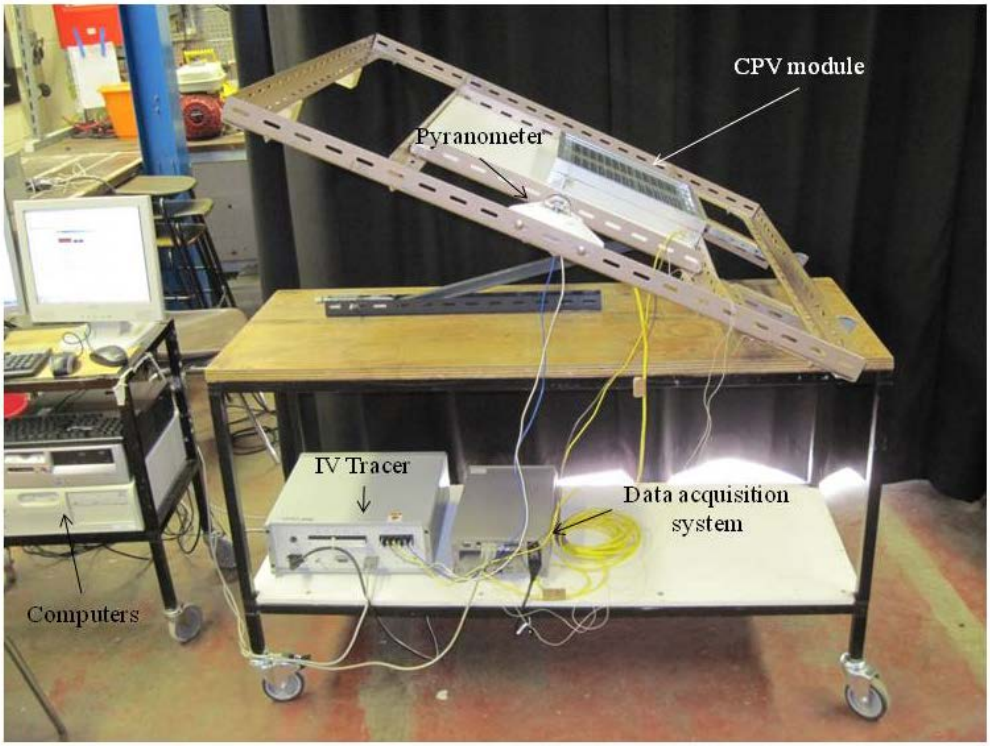

Figure 2.27 Indoor IV characterisation set-up for use with the large area solar simulator

Before collecting the IV and temperature data, the light intensity from the solar simulator was measured using the calibrated photodiodes. The intensity was measured at the same height as the modules under test. Since the non-uniformity of the light intensity was within ±10%, several readings were taken across the illuminated area to obtain an average intensity value. Proper safety measures were to be taken while working with this solar simulator, to prevent damage to skin and eyes by the high intensity light: welding goggles to block UV-light; thick full-body clothing and sun hat to prevent skin damage from UV light.

2.10 Outdoor characterisation of CPV prototypes

The outdoor characterisation of the CPV modules was carried out to investigate the actual performance under sunlight and with diurnal change in solar spectrum. The initial outdoor testing was carried out on the roof of Heriot-Watt University. Detailed outdoor characterisation was undertaken in the solar energy (SE) test site at Heriot-Watt University, Edinburgh (55.9N, 3.2W).

(a) (b)

Figure 2.28 (a) Location of the SE test-site on Heriot-Watt University campus (b) Photograph showing the open field of the test site without obstacle for shading

The SE test site is an open field, with no shading from trees or buildings. The location of the SE test site and the photograph of the open field around the test site are shown in figure 2.28. It was observed that direct sunlight in the morning (just after sunrise) cannot reach the module for around one hour due to the tree line approximately 200 metres away. The modules were mounted on a set-up which can be inclined as required.

Figure 2.29 shows the outdoor characterisation set-up in the SE test site at Heriot-Watt University.

Figure 2.29 Outdoor characterisation set-up at the SE test site of Heriot-Watt University

To characterise the CPV module and to compare the performance with its non-concentrating counterpart, a module selector (MI-520) switching device from EKO was connected to the IV tracer. This switching device was compatible with the IV-tracer for continuous characterisation of 12 modules at a time [239]. Each channel of this module selector could be customised for maximum rated voltage and current of the module under test. Four pyranometers and one pyrhaliometer were connected to the data logger to measure solar irradiation on the plane of the modules and on the horizontal plane. One pyranometer on the plane of the modules was connected to the IV-tracer and the rest were connected to the data logger. The solar radiation data from the pyranometer was used by the IV-tracer to calculate the fill factor and electrical conversion efficiency of the system. To calculate the direct and diffuse radiation accurately, a sun-tracker from Kipp & Zonen was used in this study. The sun-tracker was "SOLYS 2" with an option to mount a pyrhaliometer, which tracked the sun to measure direct radiation. It also had a top mounting plate for positioning the pyranometers [240], and a shading assembly to create shadow on two pyranometers placed on specified positions for measurement of diffuse radiation. The shading assembly and the pyrhaliometer were

connected to the tracking frame and the sensor, which moves with the sun. The system has an integrated GPS receiver, which automatically configures the location, time and the solar position giving an accuracy within 0.1^{o}. The positioning accuracy increases with the use of a "sun sensor", achieving accuracy up to 0.02^{o}. The sun tracker initially tracked the sun based on GPS-based information, fine tuning its angle by use of the "sun sensor" when the solar irradiation was higher than 300 W/m^2. All the pyranometers used in this study were CMP-11 from Kipp & Zonen. These pyranometers use temperature compensated detector technology, to generate voltage, which can be converted to solar irradiation by use of a sensitivity factor. The spectral range of the pyranometer was 285nm to 2800nm and was capable of measuring maximum solar radiation up to 4000 W/m^2 [241]. A cable was connected to the waterproof socket in the pyranometer to measure the output voltage and solar irradiation. Figure 2.30 shows the image of the sun tracker with pyranometers and pyrhaliometer. The pyrhaliometer used with the sun tracker was the CHP-1from Kipp & Zonen. This pyrhalimeter has spectral range of 200nm to 4000nm and it can also measure solar irradiation up to 4000 W/m^2.

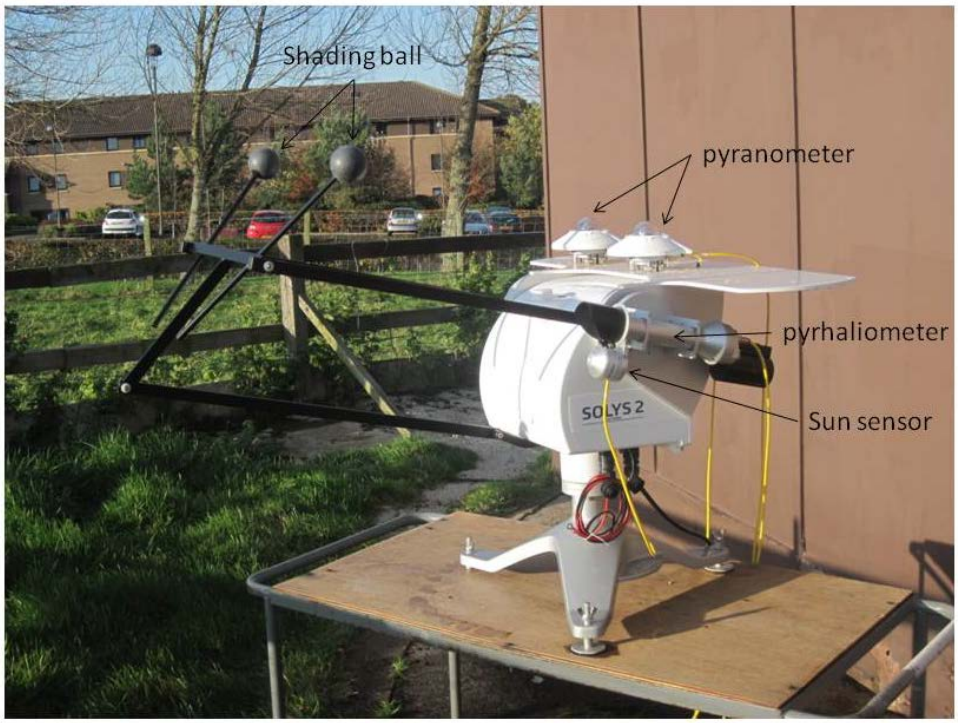

Figure 2.30 The sun tracker with pyranometers and pyrhaliometer at the SE test site of Heriot-Watt University

For collection of the temperature and solar irradiation data, a high speed data acquisition system from National Instruments (NI) was used in this study. The NI data logger

contained a chassis for insertion of different NI modules for measurement of different parameters such as voltage, current and temperature. Different modules from NI are available for different parameters depending on the rating of the device under test. The measured data was collected through a data cable from the chassis. A LabView programme was written to collect the data. One 24 bit, 16 channel voltage module was used to collect temperature and the solar irradiation data. The block diagram of the outdoor characterisation set-up and the set-up of the instruments used for data collection is shown in figure 2.31 and figure 2.32.

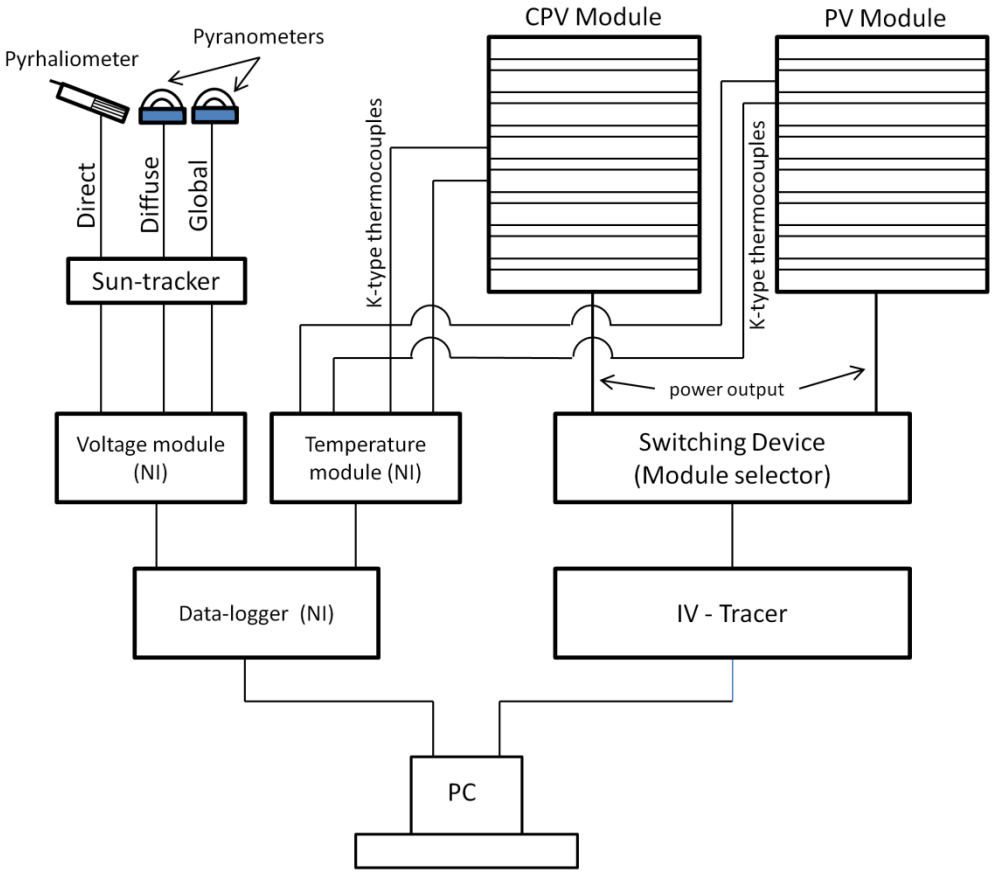

Figure 2.31 Block diagram of the outdoor characterisation set-up for CPV modules

The fourth prototype CPV module (CPV-4) was used to analysis long term performance. The module was mounted vertically on the outdoor characterisation set-up. The data for power output of this module is being collected from 1st of March 2012. The performance of the module will be continued to monitor to investigate the long term performance and degradation. Similar characterisation set-up for outdoor characterisation of the CPV module as described earlier in this section is being used for this long term performance analysis.

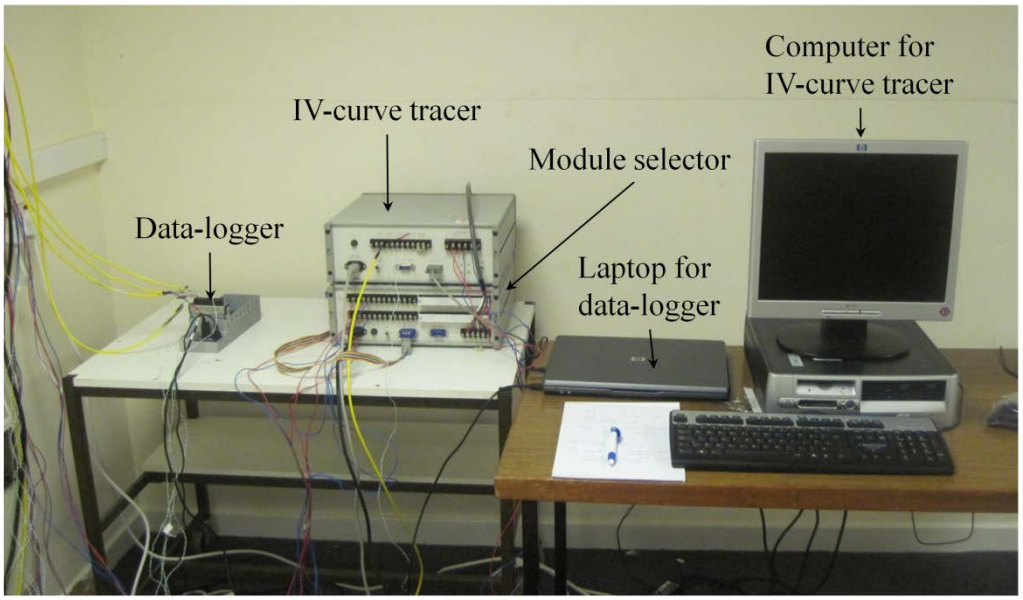

Figure 2.32 Image of the instrumental set-up used for outdoor characterisation of CPV module

2.11 Construction of a large area solar simulator

A large area solar simulator is of use in detailed characterisation of PV/CPV modules. Small area solar simulators are ideal for solar cell and small prototype module characterisation comes with highly collimated light and homogeneous distribution of light. In a large area solar simulator, large area PV/CPV modules can be characterises, to compare the performance with commercial modules. Normally multiple light sources are used in large area solar simulator to increase the illumination area. So, in some cases the uniformity of intensity distribution and collimation of the light have to be compromised.

2.11.1 Design of a continuous solar simulator for CPV application:

The basic design considerations of a solar simulator include:

- Selection of a light source with spectral distribution matching the solar spectrum
- Provision of intensity variation as required from a minimum value to a maximum above the solar terrestrial irradiation (1200W/m^2).
- Uniform distribution of the light intensity over the illuminated area.
- Collimated rays.
- Selection of an appropriate spectral-correction filter

2.11.2 Selection of the light source

It is very difficult to generate light that is an exact match to the spectrum of solar radiation. All the lamps that are used as light source in solar simulator have spectrum that nearly matches sun with addition of proper filters. Tungsten filament lamps, metal halide lamps, xenon-mercury arc lamps, high pressure xenon lamps are used as light sources for solar simulator. While the xenon lamps are found to be the most suitable light source for solar simulators with spectra very close to the solar spectrum compared to other sources; metal halide lamps are also very good competitors to xenon lamp for this particular application. A literature review and technical data shows that metal halide lamps are suitable for continuous radiation and have long life-times. Metal halide lamps of 1200 watt from OSRAM were chosen as the source lamps for this study. A Comparison of the spectral distribution of HMI 1200 lamps with solar spectra is shown in figure 2.33. Considering the availability of lamp wattage and area of illumination, it is decided to use more than one source with parabolic reflectors. The number of sources was decided by the optical study and reflector profile for each source. The structural dimensions of the lamp are shown in Figure 2.34 and the technical information of the lamp is given in table 2.4

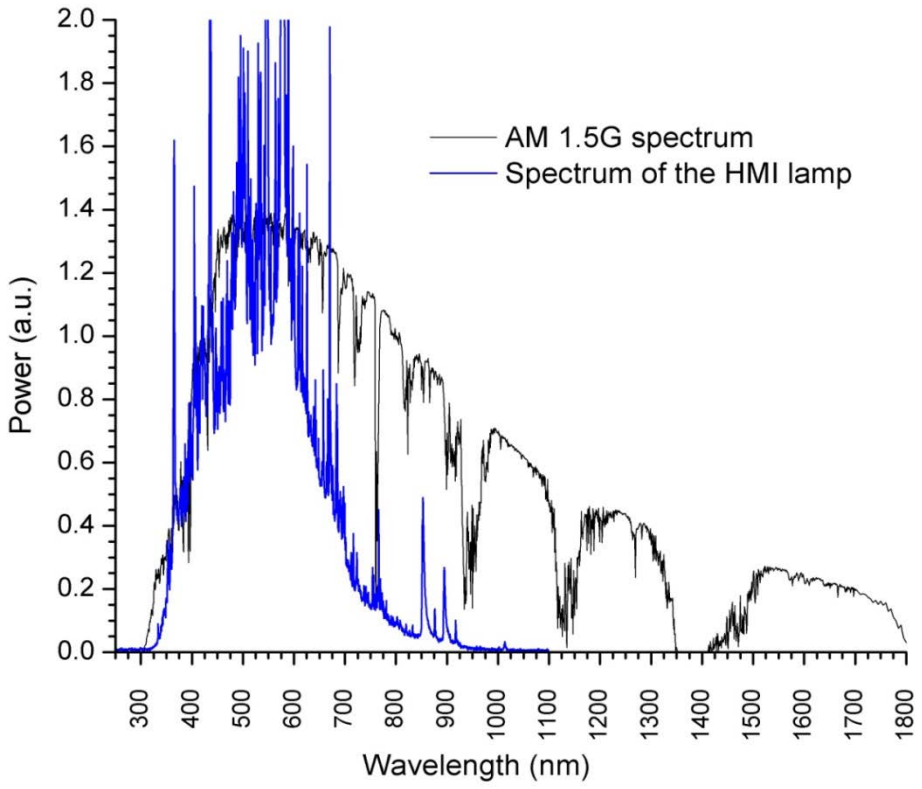

Figure 2.33 Comparison of the spectrum of HMI 1200 lamp and AM1.5G sun spectrum

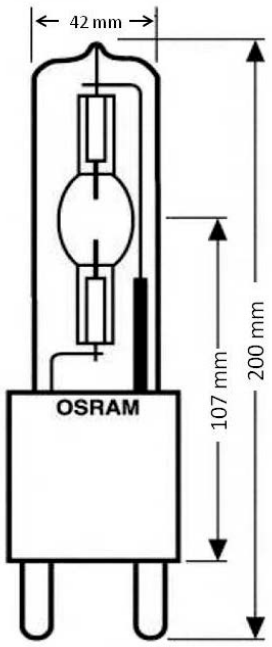

Figure 2.34 Physical and geometrical characteristics of HMI 1200 W/SEL lamp

Table 2.4 Properties of the OSRAM HMI 1200 W/SEL lamp [242]

Properties	**Value**
Rated Lamp Wattage (W)	1200
Ignition Voltage (kV)	5
Luminous flux (lm)	110,000
Colour Temperature (K)	6,000
Light arc length (mm)	10
Average service life (h)	1000

2.11.3 Reflector design optimisation

The reflectors in a solar simulator play a vital role in achieving collimated light with a homogeneous intensity distribution over the illuminated area. It is known that any light emitted from the focus of a parabola is reflected parallel to the axis of symmetry of the parabola. A light tool design software 'Optics Lab' was used to optimise the parabolic profile of the concentrator and the power of the light source [243]. The study was carried out for the illuminating area at a distance of 2 metres away from the source. The parameters of the reflector were chosen to attain a Gaussian intensity distribution from a

lamp with a reflector, so that the partial overlap of the intensity from nearby lamps generated a homogeneous distribution of intensity over the illuminated area. Three parameters: radius of curvature; diameter of the opening end; and position of source within parabolic reflector were taken into consideration to determine the parabolic reflector design. The values of the parameters were chosen with a realistic approach for the available fabrication facilities.

A study was carried out for diameters of the opening end of 175 mm, 200 mm 225 mm and 250 mm. For each value of opening end, the radius of curvature and position of the source were examined to give a homogeneous intensity of light. The radius of curvature was examined for the values from 70mm to 120 mm in 10 mm increments; and the position of the source at 30 mm, 35 mm, 40 mm, 45 mm and 50 mm from the vertex of the parabola. A schematic ray trace diagram of a single source, with a parabolic reflector of 34 mm focal length, placed at 40 mm from the source is shown in figure 2.35

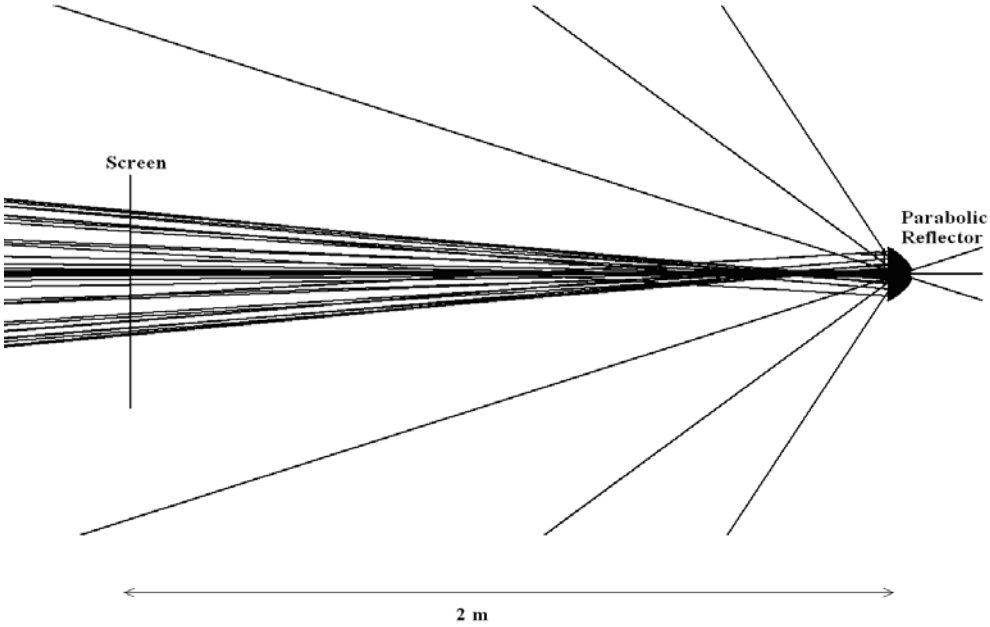

Figure 2.35 Schematic ray trace diagram (with 70 representative rays) of a single source with a parabolic reflector of 34 mm focal length and opening end diameter of 200 mm.

A Gaussian distribution of intensity from each lamp was desirable, to achieve a homogeneous intensity over the illuminated area, by overlapping of edge intensities. The study revealed that a reflector with radius of curvature 65 mm (equivalent to a focal length of 34 mm); diameter of open end of 200 mm; and distance from source to

reflector 40 mm is suitable to achieve a desired Gaussian distribution of intensity at 2 m from the source. A 2D view of the Gaussian distribution of intensity over the illuminated area is shown in figure 2.36. The illuminated-spot diameter from one source is found to be 460 mm, with a maximum intensity of 1311W/m^2 at the centre of the illuminated area, 2 metres away from the source. The intensity distribution across the diameter of the illuminated area from one source, with the designed parabolic reflector on a screen at 2 metres distance, is shown in figure 2.36. The modeling results for intensity distribution over the illuminated area of 1m × 1m is shown in figure 2.37

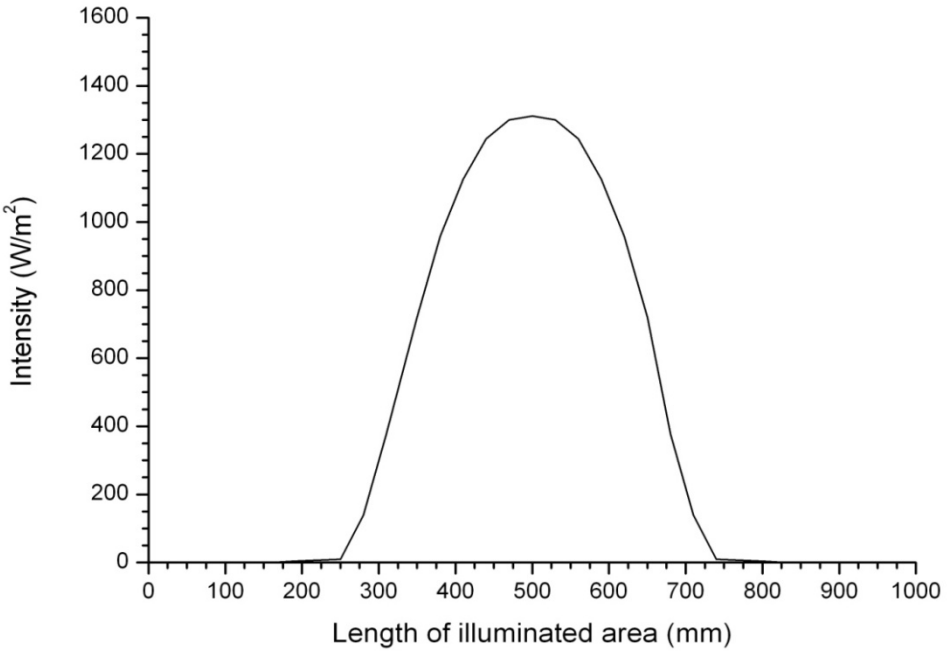

Figure 2.36 Intensity distribution across the diameter of the spot illuminated by a single (lamp) source with a parabolic reflector of 34 mm focal length and open end diameter of 200 mm.

The intensity is estimated for the maximum rated wattage of light (1200 watt), 40% conversion efficiency from electricity to light energy and 95% reflectivity of the inner side of the reflectors. However, in practical scenario, the light intensity is likely to be less than the theoretical estimated vales due to the lower reflectivity of the reflectors and variation in conversion efficiency. The maximum collimation of the rays over illuminated area was found to be 7.6^o.

The experimental intensity mapping of the illuminated area showed that the light was well distributed within a 750mm×750mm area. The maximum intensity was found to be

851W/m^2, with a minimum of 778W/m^2 within that area (measured with CMP-11 pyranometers). The non-uniformity within the 700mm×700mm area was 8.5%. The intensity distribution contour within the area is shown in figure 2.38.

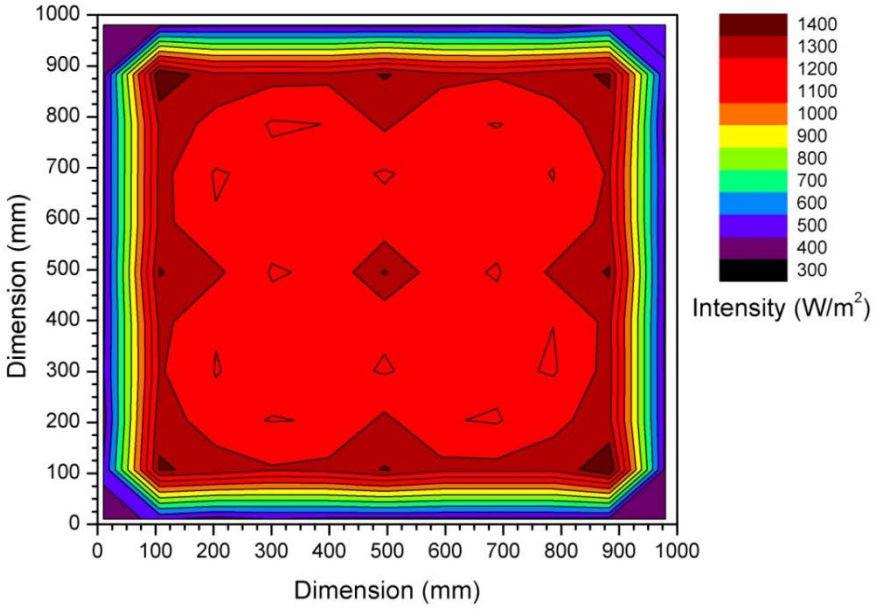

Figure 2.37 Expected intensity distributions from the solar simulator over one square meter area (optical simulation result)

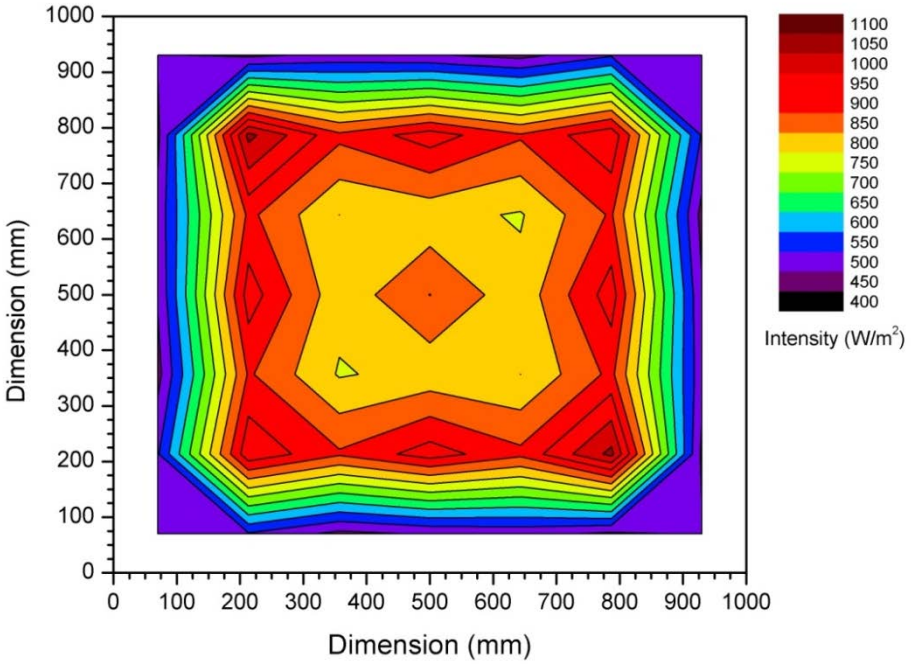

Figure 2.38 Intensity distribution contours of the measured intensity over the illuminated area of the solar simulator

The intensity drops sharply to 500 W/m^2 at the edges of the 1000mm×1000mm area. Though the intensity distribution is very close to the modeling results, the maximum intensity is found to be very low, which is due to the lower reflectivity of the parabolic reflectors. Future work has been proposed to improve the reflectors through use of a high reflective coating, to increase the intensity.

2.11.4 Solar simulator fabrication

2.11.4.1 Base plate construction

The base plate for fixing of the source lamps and reflectors was constructed from aluminum bars of 50mm × 50mm cross-sectional area and 2mm thick aluminum sheet. The positioning of lamps was crucial to achieve a homogeneous distribution of intensity. The drawing showing the positioning of the lamp bases is shown in Figure 2.39.

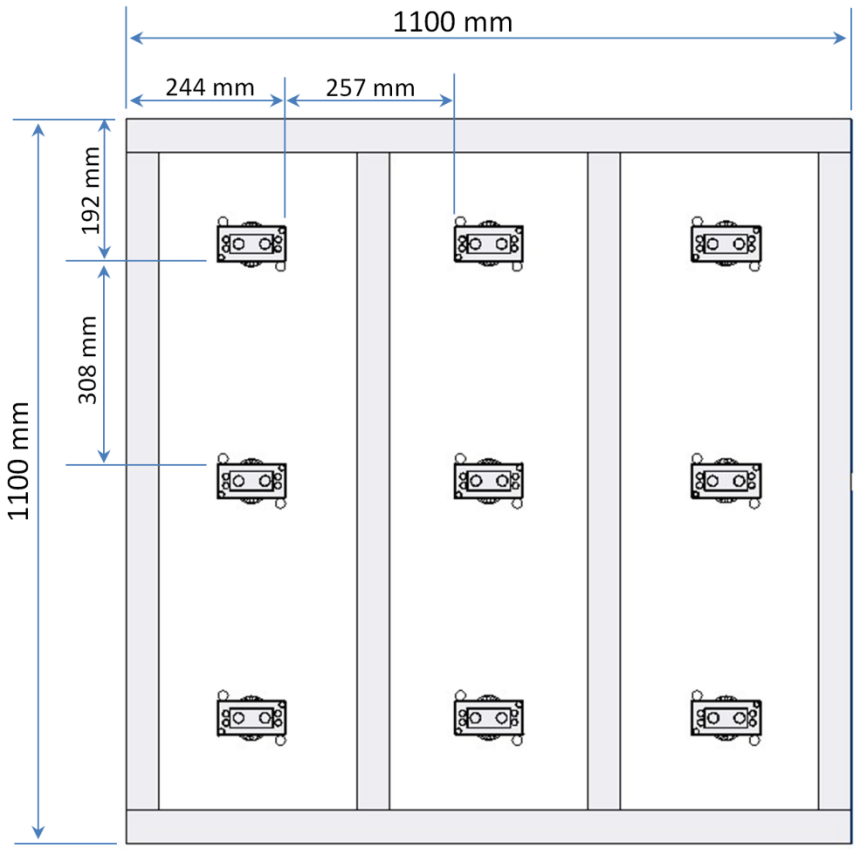

Figure 2.39 Schematic design and dimensions of the base plate and arrangement of the lamps.

The optical performance study showed that light from a single source irradiates a circular area of diameter 460 mm. From the intensity distribution along the diameter of illuminated area of a single source, it was found that overlapping of 100 mm of the illuminated spots from the two consecutive sources gives a homogeneous distribution along the joining axis. So three lamps separated by a distance 360 mm, were placed in one side. The lamp bases were screwed on to the base plate, and the reflectors were mounted on another movable plate to adjust the distance from the source.

2.11.4.2 Manufacturing of the reflectors

The parabolic reflectors were manufactured by metal spinning process of aluminum by an external manufacturer. Metal spinning can provide a high accuracy of profile and good surface finish. An aluminum coating was applied on the inner surface of the reflector to achieve reflectivity of about 85%. Aluminum was chosen because of cost, light weight and longer life-time without corrosion. Aluminum grade 1100 was used for this purpose. The cross-sectional dimensions of a reflector are shown in Figure 2.40

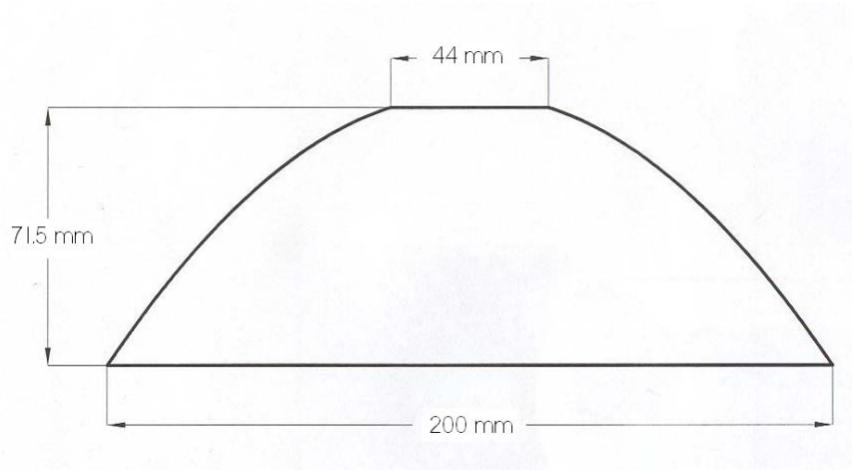

Figure 2.40 Cross sectional drawing of parabolic reflector for each source lamp

2.11.4.3 Mounting of the base plate

The base plate was mounted on a movable shaft. This provided flexibility to position the base-plate at the desired height when needed. A braking system in the slider was used to keep the plate stationary. The base plate was attached to the sliders with a bearing, to provide the necessary inclination. The whole system was mounted on a floor at a height of 2.5 metres. The entire electrical components including ballast and ignitor for the HMI lamps were placed in a restricted area near the base plate for safety. Figure 2.41 (a) and

(b) show the CAD drawing of the designed solar simulator and a photograph of the solar simulator, respectively.

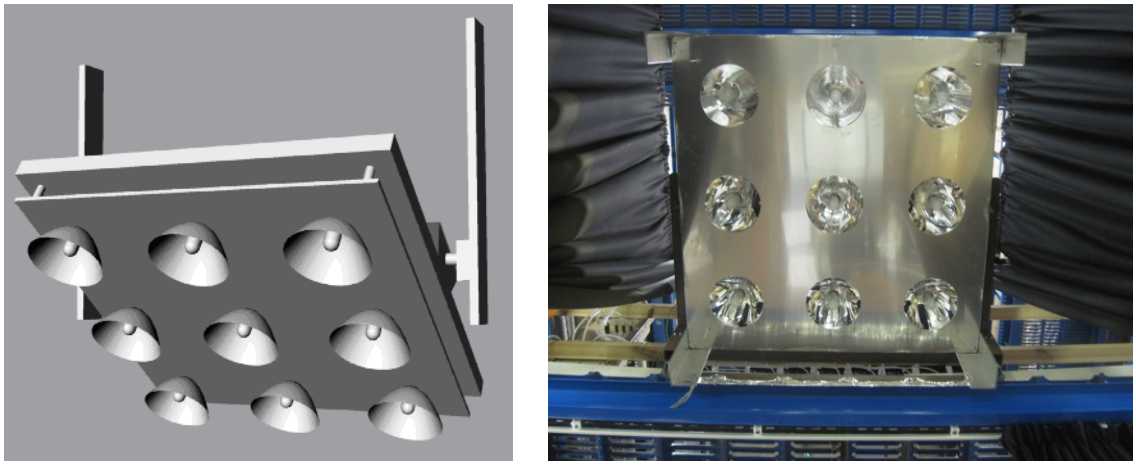

(a) (b)

Figure 2.41 (a) 3D CAD drawing of the mounted solar simulator plate (b) Photograph of the in-house built large-area solar simulator at Heriot-Watt University

2.11.4.4 Light intensity controller

The light intensity from the lamps was controlled by a dimming circuit. The electrical circuit for the lamp is shown as a block diagram in Figure 2.42. The lamps could be dimmed to 60% of the maximum light intensity, providing a flexibility to work with different light intensities.

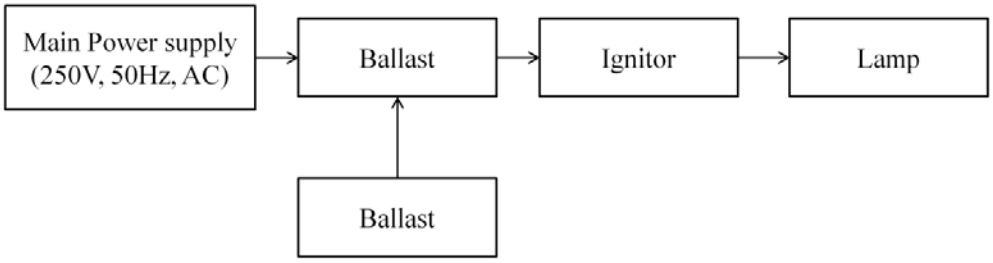

Figure 2.42 Block diagram of electrical circuit for lamp with intensity control

2.12 Calibration of photodiode

It is important to measure the flux density or the light intensity from a solar simulator on the working plane. Normally, for outdoor solar intensity measurements, different

pyranometers are used. For indoor characterisation of the photovoltaic devices with a solar simulator, the pyranometers are not considered to be a promising choice, because of the nature of the light spectrum in use. The pyranometers are calibrated for a range of solar radiation from 250nm to 4000nm, while the spectrum considered for silicon solar cell characterisation in a solar simulator is only from 250nm to 1200nm. So in standard practice, a calibrated solar cell is used to measure the light intensity of 1 sun on the working area, which has a spectral response within the range of 250-1200nm. However, a calibrated photodiodes can also be used for this. So a silicon photodiode assembly was constructed and calibrated, to use as a reference, to measure the light intensity from the solar simulator at Heriot-Watt University.

2.12.1 Photodiode specifications

The silicon photodiode had similar spectral response to the silicon solar cells. The spectral response range of this photodiode was from 190nm to 1100nm. Two S3477 series silicon photodiodes from Hamamatsu, of active area 5.8×5.8 cm (S3477-03) and 2.4×2.4 cm (S3477-04) were used to calibrate for 1000W/m^2 radiation intensity from the solar simulators [244]. To prevent the photodiode from reaching saturated short circuit current under the intensity of 1000W/m^2, a reflective type neutral density (ND) filter of optical density 3 (OD-3) was used, reducing the light intensity on the photodiodes [245]. The spectral response of the photodiode and the spectral transmission of the ND3 filter are shown in figure 2.43 (a) & (b).

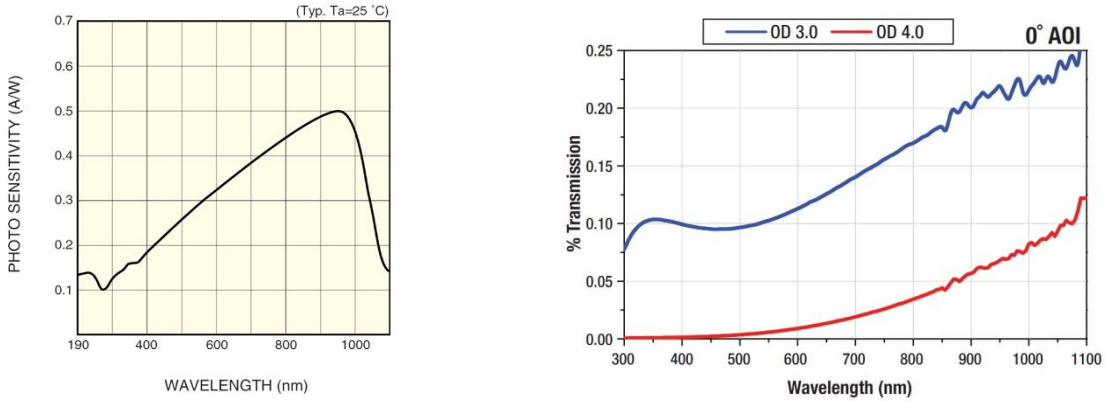

(a) (b)

Figure 2.43(a) Spectral response of the photodiode (b) Transmission of reflective-type ND filter of optical density 3 [245]

To use the calibrated photodiode as a reference to measure light intensity from a solar simulator, it was important to maintain a constant temperature. With change in temperature the short circuit current and open circuit voltage of the silicon photodiode varies for the same light intensity. The S3477 series photodiode sensors have an in-built thermistor, to sense the photodiode chip temperature; and the complete photodiode is combined with a thermoelectric cooler to maintain the temperature.

2.12.2 Fabrication of the photodiode assembly

The photodiode assembly contained a photodiode sensor with a thermistor, heat sink, and a temperature controller. The photodiode was mounted on a customised heat sink with holes for the photodiode pins. The heat sink with the photodiode was then mounted on a box with sockets for electrical outputs of the photodiode, temperature sensor and thermoelectric controller. The photodiode dimensions and photograph of the photodiode assembly are shown in Figure 2.44.

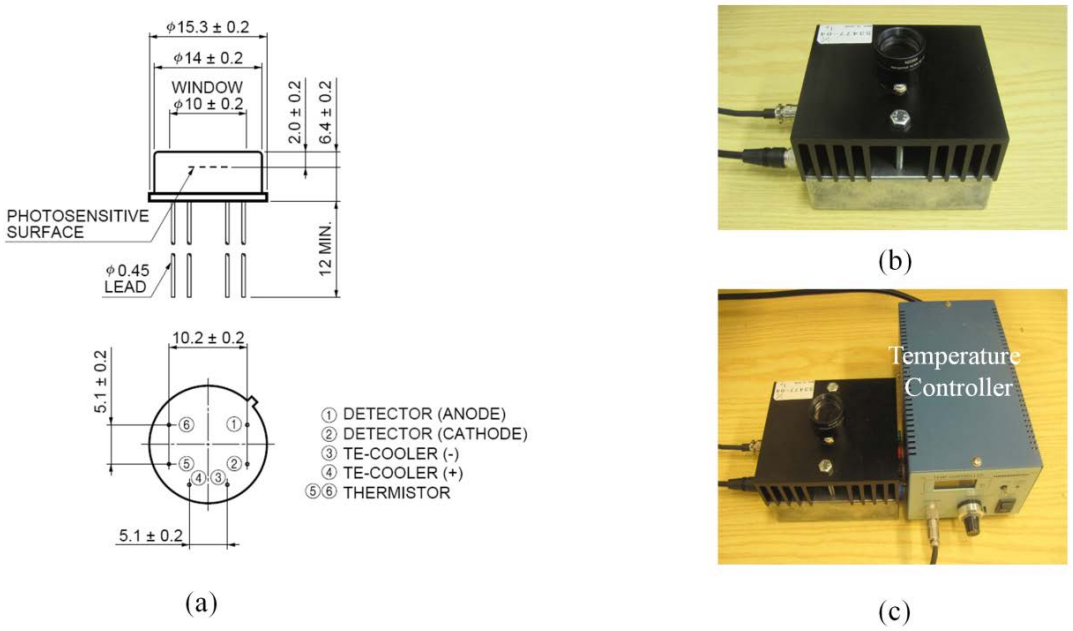

Figure 2.44 (a) Structural and geometrical dimensions of the photodiodes [244] (b) Photograph of the photodiode assembly (c) photodiode assembly with the temperature controller

The temperature controller used in this assembly was C1103-04 from Hamamatsu [244]. The basic principle of this temperature controller was to adjust the current flow through the thermoelectric cooler. The required temperature could be set easily by

adjusting the control knob. The basic circuit diagram of this temperature controller is shown in Figure 2.45

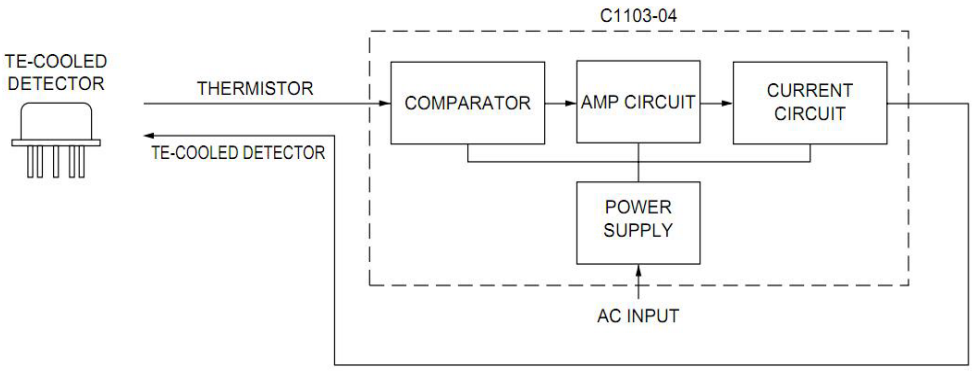

Figure 2.45 Circuit diagram of the temperature controller used in the photodiode assembly [244]

2.12.3 Calibration process

A silicon solar cell calibrated by the Fraunhofer Institute for Solar Energy Systems ISE, Germany was used as the reference to calibrate the photodiode. The following steps were used to calibrate the photodiode

1. The solar simulator was switched on for 2 hours to attain stable irradiation and spectrum
2. The reference solar cell was placed on the working plane in the middle of the illuminated area.
3. The temperature of the reference cell was monitored and the IV data was collected at 25^{o}C as per the measurement standards for the reference cell.
4. The IV data was compared to the supplied data of the reference cell for the intensity 1000W/m^2. The light intensity of the solar simulator was adjusted by adjusting the current flow to the lamp in the solar simulator.
5. Step 3 & 4 were repeated to get the IV data of the reference cell to match the supplied value.
6. Once the IV data of the reference solar cell was matched to the supplied value, the reference solar cell was replaced by the photodiode, and the IV-characteristic of the photodiode was measured at 20^{o}C.
7. The short circuit current measured from the photodiode was used as a reference for 1000W/m^2 light intensity of the solar simulator.

The calibrated value of the short circuit of the photo diode (at 20^oC) is used as the standard to measure $1000W/m^2$ radiation intensity from the solar simulator at Heriot-Watt University. In future for any change in light intensity from the solar simulator, the photo diode was used to calibrate the solar simulator to achieve $1000W/m^2$ radiation intensity.

2.13 Conclusion

Different materials, manufacturing methods and calibration processes used in this project have been described. Clear Polyurethane was used to manufacture the dielectric concentrators. The manufactured concentrators were an optimised design for use in higher latitudes ($>55^o$).

Prototypes of different sizes were fabricated for performance analysis of the designed dielectric concentrator. Different sizes of prototype were required to characterise the CPV module in indoor and outdoor conditions; and to investigate possible losses due to scaling-up. The different properties of the different components, such as spectral response for the solar cell; transmission of the concentrator and encapsulation material used in the CPV modules were investigated.

The indoor characterisation of the CPV module for different incident angles of irradiation has been described. The characterisation set-up was fabricated for a specific characterisation process for dielectric CPV modules. A photodiode set-up was assembled and calibrated for use as a reference, to measure light intensity while working with a solar simulator. A large area solar simulator was designed and developed to characterise large area PV/CPV modules. The developed solar simulator had a working area of 750mm×750mm, uniformity of intensity distribution within ±10%, and collimation within 7.6^o.

The outdoor characterisation set-up was developed in the SE test site at Heriot-Watt University. Meteorological data, including solar radiation, both direct and diffuse was collected using a sun-tracker. A high speed data acquisition system was used in the study to collect the solar radiation data, temperature and IV specifications of the CPV modules.

Chapter 3

Design optimisation and theoretical performance analysis of dielectric concentrator

This chapter provides details of theoretical performance analysis and optimisation of dielectric photovoltaic concentrator suitable for building façade integration in the higher northern latitudes (>55^o). Three concentrator designs with equal concentration ratio and different half acceptance angles are taken into consideration for the optimisation study. The concentration ratio for all the concentrators is kept constant in order to compare the optical performance in terms of angular acceptance, optical efficiency and energy flux distribution. The study has been carried out for the change in transverse incidence angles; with variation of sun position over a year in high latitudes. This study also provides details of tilt angle optimisation. Basic thermal modelling and the effect of temperature on the electrical performance of the CPV module are also reported.

3.1 Introduction

Ray trace analysis is a promising technique for evaluation of the optical performance of concentrators. A given number of rays can be traced to represent direct and diffuse solar radiations on a concentrating system. With proper reflection and refraction conditions, traced rays can be used to predict the characteristics of light within the concentrators. Incorporation of reflection and transmission losses with the ray tracing represents a real picture of optical performance of the concentrator.

In present ray trace analysis all incident rays are assumed to be parallel and carry an equal amount of energy. The vector form of reflection and refraction law of light is considered in the ray tracing, which is given by the following equations [80]

Law of reflection

$$\vec{r}_{refl} = \vec{r}_{inc} - 2\left(n.\vec{r}_{inc} \right)n \tag{3.1}$$

Law of refraction

$$n_r.\vec{r}_{refr} = n_i\,\vec{r}_{inc} + \left(n_r\,\vec{r}_{refr}.n - n_i\,\vec{r}_{inc}.n \right)n \tag{3.2}$$

The basic assumptions that have been considered in this ray trace modelling are as follows:

(i) All the rays follow the basic principles of reflection and refraction, i.e. all the rays are specular and follow Snells law of refraction.

(ii) All the rays under consideration follows the Fermat's principle of minimum distance and time i.e. all the ray will choose the minimum path length and time to travel from one point to another. For a rays travelling from point A to B, it can be mathematically represented as $\int_A^B L(x,y)dt = 0$, where L(x, y) is the path length between A and B.

(iii) The second order shape factor and the possible diversion of the rays after one or multiple reflection have not been considered in this study.

3.2 Concentrator design

In this optimization study three Dielectric Asymmetric Compound Parabolic Concentrator (DiACPC) design has been considered. The designed concentrators are termed as DiACPC-55, DiACPC-66 and DiACPC-77 having acceptance half angles (0^o & 55^o), (0^o & 66^o) and (0^o 77^o) respectively. The design process of the concentrators in consideration is detailed in the following steps:

i. Three ACPC profiles of acceptance half angles (0^o&33^o), (0^o&37^o) and (0^o&40^o) are generated.

ii. Dielectric material is introduced within this profile which eventually reduces the acceptance angles because of the untruncated structure.

iii. Subsequently, these preliminary dielectric profiles are truncated by 68%, 55% and 40% respectively to achieve the acceptance half angles (0^o&55^o),

(0^o&66^o), and (0^o&77^o), which are referred to as DiACPC-55, DiACPC-66, and DiACPC-77, respectively. These truncations result in a geometrical concentration ratio 2.82 for each concentrator. The change in acceptance angle with truncation of the dielectric concentrator is shown in figure 3.1. The effect of the truncation on angular acceptance is presented in the following section.

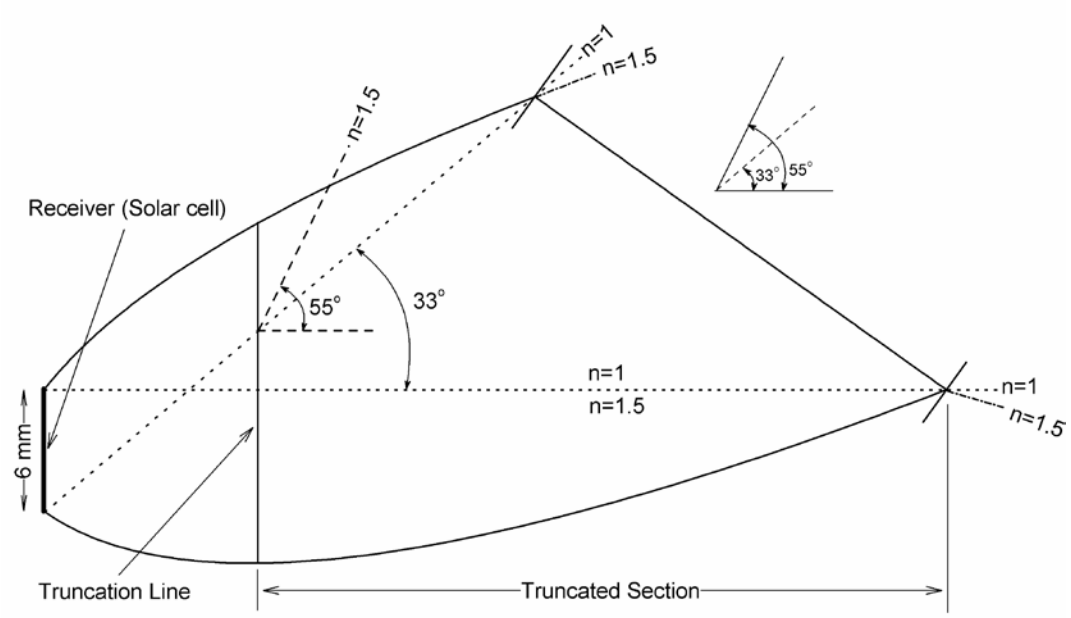

Figure 3.1 Schematic cross-sectional diagram of the design of DiACPC-55. The change in acceptance of extreme rays with refractive index is shown with the values of 'n'

The general characteristics of the designed profiles are as shown in table.3.1. The concentrators are designed for 6 mm wide crystalline solar cells. The co-ordinates of the reflector profile are generated by an in house PASCAL program by following the parametric equation [85]:

$$x = (at^2 - a)\cos\theta + 2at\sin\theta \tag{3.3}$$

$$y = (at^2 - a)\sin\theta - 2at\cos\theta \tag{3.4}$$

The design criteria of the concentrators in this thesis work was chosen based on the concentration ratio and optimised solar cell design, which builds from the initial unoptimised design of the dielectric ACPC systems and is an attempt to solve the engineering issues around it viz. efficiency, cost and longevity of the system. The work

was carried out considering theoretical modelling predictions and their experimental validation through rigorous indoor and outdoor measurements of electrical power output of CPV module.

Table 3.1 Geometrical characteristics of Dielectric concentrators

Concentrator profile	**DiACPC-55**	**DiACPC-66**	**DiACPC-77**
Acceptance half angles	0^o & 55^o	0^o & 66^o	0^o & 77^o
Receiver width (mm)	6	6	6
Aperture width (mm)	16.92	16.95	16.9
Concentrator height (mm)	14.4	16.5	19.3
Concentration ratio	2.82	2.82	2.82
Truncation (%)	68	55	40

The dimension of the solar cell, specifically the width of the solar cell (6mm) was optimised in earlier studies [211] to use with the concentration ratio of 2-3. A limitation of earlier design was that with the decrease in cell width, the edge losses in the CPV system increased, which reduced the overall efficiency of the system. With the increase in solar cell width, the height of the concentrator increases significantly to achieve the required concentration ratio with same range of acceptance angle. So the solar cell design and dimension has been kept same with the previous experimental study of the dielectric concentrator [211].

In this investigation, the acceptance half angles of all the three designs were chosen based on the studies earlier reported and the maximum solar altitude angle in Edinburgh, where the outdoor experimental investigation were to be carried out. The maximum solar altitude angle in Edinburgh is 55^o at solar soon on a solstice (21^{st} of June) and the minimum solar altitude angle is 0^o. So the acceptance half angle of one concentrator design is considered to be (0^o and 55^o). The acceptance half angle of the second concentrator design is chosen in accordance with the PRIDE concentrator previously reported as 0^o and 66^o; The third concentrator is designed with acceptance half angles (0^o and 77^o), to investigate the effect of change in the range of the

acceptance angle, to cover the entire range of variation. The concentration ratio 2.82 is chosen for this study, keeping in mind the height of the concentrators and range of the acceptance angle. To achieve the range of acceptance angle (0^o and 77^o) with higher concentration ratio, the height of the concentrator increases substantially. This also limits the truncation of the complete profile of the concentrator. Furthermore the solar cell used in this study has shown best performance within the concentration ratio 2-3 [211]. So it can be concluded that the choice of the design parameters taken in this study are subjective to the previous dielectric ACPC design, architectural/ aesthetic interests of the design for BIPV and the location itself. Moreover the manufacturing issues related to the CPV system with the dielectric concentrator is another factor in deciding the design parameters of the concentrators as it can impact the stability and their integration into the building envelope.

3.3 Material selection

Highly transmitting dielectric polymer materials such as EVA and EMA are widely used in PV industries as encapsulation materials, to provide structural support and optical coupling between cover glass and solar cells in PV module. With the development of CPV systems, dielectric materials are of interest in refractive type CPV modules as a lens material to reduce the cost and weight of the CPV system. These polymers require excellent transmission properties to reduce the optical losses in a CPV system. The chosen dielectric material to be used as a concentrator also requires a higher mechanical strength compared to the encapsulation materials to maintain its geometrical profile and shape. Furthermore, durability of the polymer material in a CPV system needs to be matched with the solar cells, which normally comes with a guarantee of around 25 years from the manufacturer. The major challenge is the photo degradation of the clear polymer by the UV component of the solar radiation. Several materials such as acrylic, polycarbonate and polystyrene are of interest as lens and concentrator material. All these dielectric polymer materials exhibit excellent optical properties and mechanical strength, but have very poor resistance to outdoor weathering for long term exposure, apart from acrylic (PMMA) and polyurethane. PMMA has excellent transmission properties and resistance to the photo degradation [246]. Adding an UV stabilizer to the polymer, the photo degradation can be reduced to increase the life time of the materials. On the other hand, addition of UV-stabilisers limits the UV part of solar spectrum (< 400nm) from reaching the solar cell which reduces the power output.

The theoretical study has been performed using acrylic as the concentrator material and low-iron soda-lime glass as the cover material. However in search of alternative material to the acrylics, the experimental study in this project has been carried out primarily with the clear polyurethane. A low cost, low absorption coefficient and suitable refractive index matching to glass are further advantages of the acrylic material as a PV concentrator. Studies have been carried out with refractive index value of 1.5 for both glass and acrylic. The average absorption coefficient over the spectrum of 350 nm – 1000 nm, of the dielectric material is considered to be 1.9 m^{-1} (for PMMA material supplied by Lucite) and of low iron glass to be 4.1 m^{-1} [211]

3.4 Concentrator reference system

The theoretical optical performance and optimisation study has been carried out with a single trough of the designed dielectric concentrators. The concentrator is positioned with 'axis of the concentrator' in east-west direction. The 'vertical axis' of the concentrator is parallel to the building façade with zero inclination and the aperture surface of the concentrator is considered to be facing south (figure 3.2). The theoretical optical performance has been investigated with a 2D profile of single trough concentrator design. The incidence angle of the solar ray incident perpendicular to the surface of the aperture and axis of the concentrator are considered as 0^o, positive towards the anti-clockwise direction and negative towards to the clockwise direction in the vertical plane as shown in figure 3.2. The inclination angle of the concentrator is also considered positive towards the anticlockwise direction and negative towards clockwise direction in the vertical plane.

3.5 Ray trace analysis of the DiACPC system

In house developed ray trace codes were used to evaluate the optical performance of the designed concentrators. The co-ordinates of the concentrator profile are fed in to the ray trace codes and the properties of the materials in each component were defined. The software generates co-ordinates of each ray for each change in directions. These co-ordinates were fed into the graphics software 'Techplot [247] to draw the ray trace diagrams. All the incident parallel rays are generated 5 mm from the aperture surface. The total incident energy flux at an instance of the incident radiation on the aperture is considered to be 600 W/m^2 (average annual direct solar radiation in Edinburgh), which is divided equally among the total incident rays considered. 50000 rays were traced in 1^o interval over the aperture in this theoretical study.

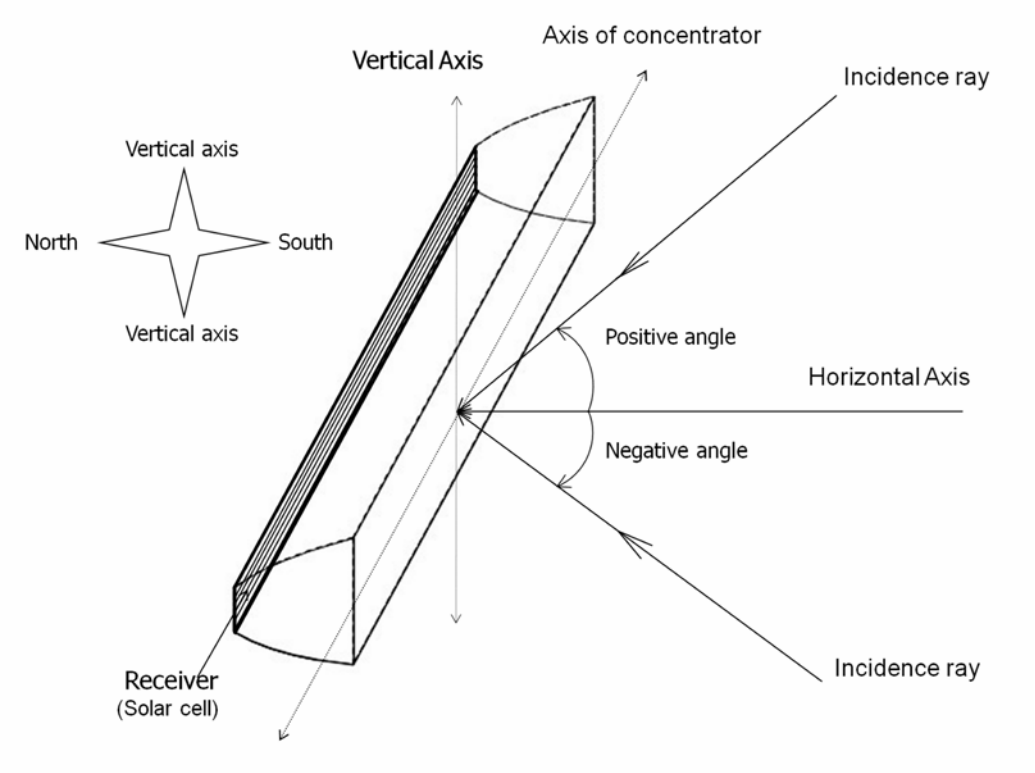

Figure 3.2 Concentrator reference system showing the positive and negative incidence angles for building façade integration.

The codes are developed to examine every intersection of each ray with the concentrator for refraction and total internal reflection criteria. The number of rays that reaches the receiver and the energy losses in each intersection have been calculated for angular acceptance, optical efficiency and energy flux distribution studies. The angular acceptance of a solar concentrator is defined as the fraction of light incident at different angles collected by the concentrator, without taking into account of the optical losses within the concentrating system. The optical efficiency estimates the fraction of the incident energy on the aperture that reaches the receiver considering all the possible losses. The light ray incident on the aperture of the concentrating system will enter the concentrator with a surface reflection component at air-glass interface. The possible behavior of the rays entering the concentrator is (see figure 3.3):

i. Reaches receiver with one or more reflections within the concentrator (Ray 1)
ii. Reaches the receiver without any reflection (Ray 2)
iii. Escape from the concentrator through the aperture after two or more reflections (Ray 3)
iv. Escape from the concentrator through the parabolic sides (Ray 4)

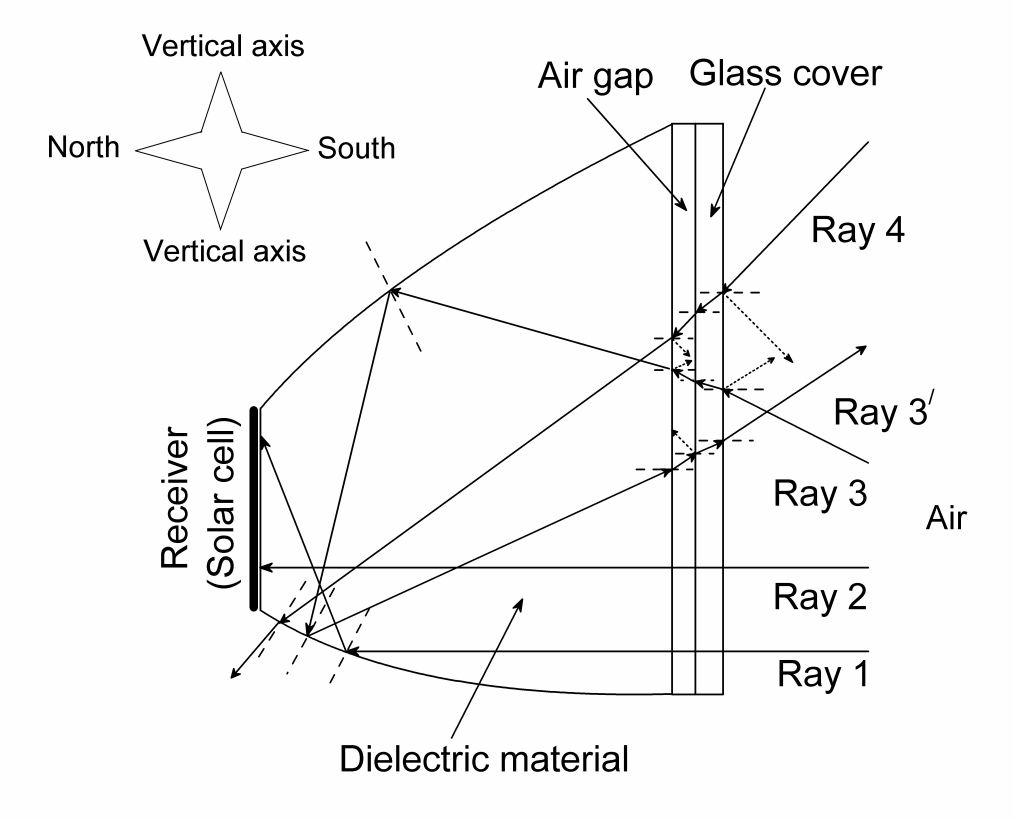

Figure 3.3 Cross-sectional schematic diagram of possible behaviour of incident solar radiation within a dielectric concentrator.

3.6 Comparative ray trace diagram of DiACPC-55, DiACPC-66 and DiACPC-77

The ray trace diagram of the DiACPC-55, DiACPC-66 and DiACPC-77 along with the untruncated version for 10^{o} incidence angle is shown in figure 3.4, 3.5 and 3.6 respectively. It can be observed that with the increase in range of the acceptance half angle the height of the untruncated profile of the concentrator (along the x-direction in figure 3.4 – 3.6) decreases. This eventually reduces the aperture area and the concentration ratio. However, in the final design of the concentrators (after truncation) the height of the DiACPC-55 is found to be less than DiACPC-66 and DiACPC-77.

The change in position of the collected rays on the receiver can be also be visualised in the ray trace diagrams of the designed concentrators for both untruncated and truncated profiles. It can be observed that, in the untruncated version incident rays are reflected from the lower parabolic section, while after truncation the surface of reflection for most of the ray changes. For reflecting type concentrators it is not expected to change in the parabolic surface of reflection. The refraction of light at the inclined aperture surface of the untruncated concentrator profile leads to this change.

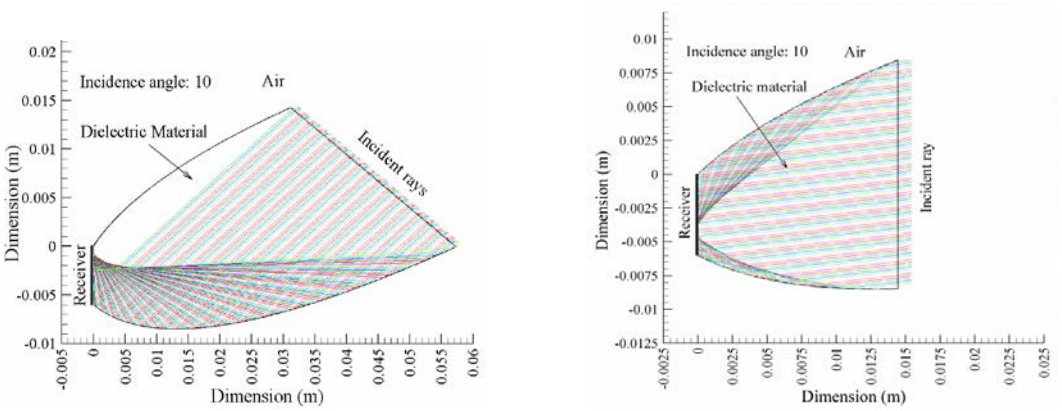

(a) (b)

Figure 3.4 Ray trace diagram of (a) Untruncated DiACPC-55 (b) Truncated DiACPC-55 for the rays with incidence angle of 10^{o}

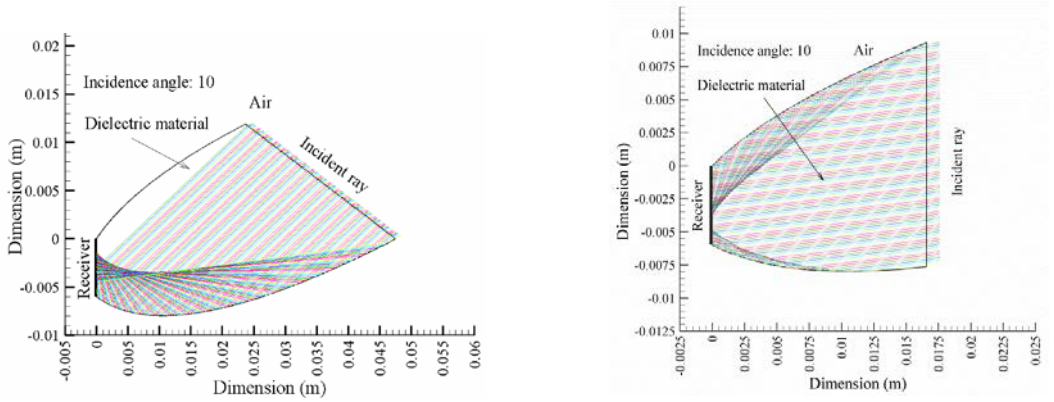

(a) (b)

Figure 3.5 Ray trace diagram of (a) Untruncated DiACPC-66 (b) Truncated DiACPC-66 for the rays with incidence angle of 10^{o}

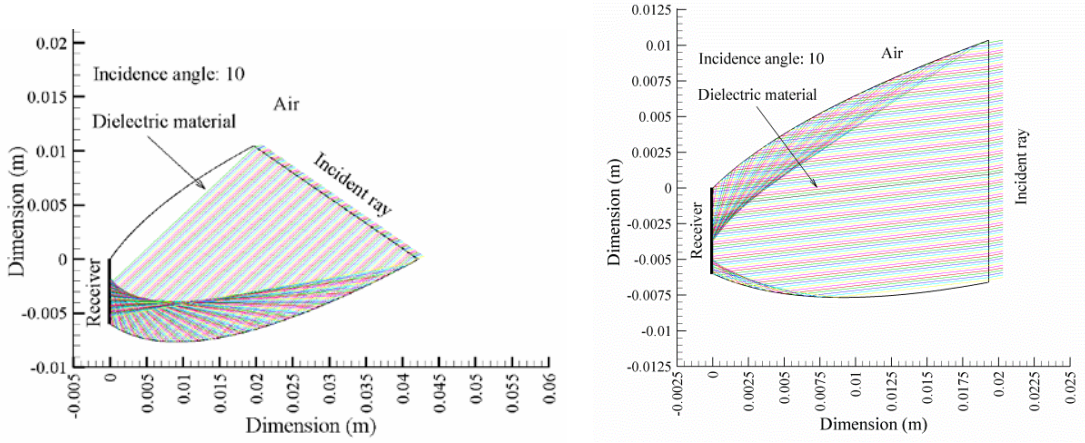

(a) (b)

Figure 3.6 Ray trace diagram of (a) Untruncated DiACPC-77 and (b) Truncated DiACPC-77 for the rays with incidence angle of 10^{o}.

3.6.1 Ray trace diagram of the truncated DiACPC-55

Ray-trace analysis of the DiACPC-55 shows that the designed concentrator can collect all the radiation incident on the aperture surface within the angles 0^o and 55^o. For incidence angles higher than 55^o and less than 0^o only a few rays without any reflection reach the receiver. The interception of the receiver in DiACPC-55 by the ray's incident with 5^o, 25^o, 45^o and 60^o is shown in figure 3.7.

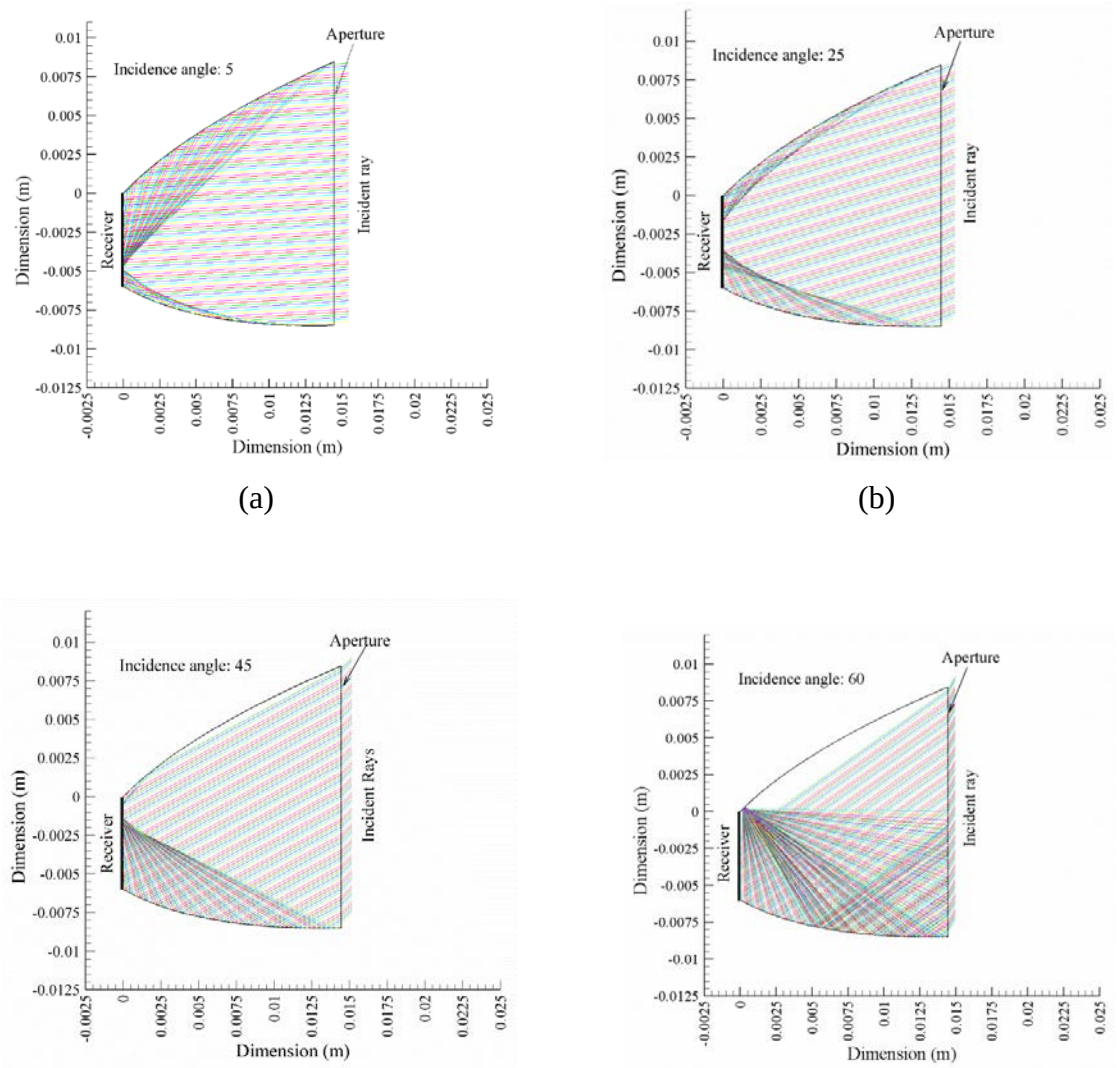

Figure 3.7 Ray trace diagram of a DiACPC-55 with 100 representative ray incident at an angle (a) 5^o (b) 25^o (c) 45^o and (d) 60^o.

It can be observed that with increase in incidence angle the number of reflections from the lower parabolic side increases. For incidence angle 60^o, which is higher than acceptance half angle 55^o, few rays are escaping from the parabolic sides or leaving the

concentrator aperture after multiple reflections within the concentrator as shown in figure 3.7(d). These ray trace diagrams will aid in visualising the phenomenon of change in distribution of energy flux at the receiver and optical efficiency of the concentrator which will be discussed in the following sections.

3.6.2 Ray trace diagram of DiACPC-66

The ray trace diagram of DiACPC-66 follows a similar behaviour to DiACPC-55, other than the distribution of rays at the receiver. The ray trace diagram of DiACPC-66 with 100 representative rays incident with an angle 5^o, 25^o, 45^o and 60^o is shown in figure 3.8. Since all the incidence rays considered are all within the range of the acceptance half angles of DiACPC-66, no rays are observed escaping the system for these angles.

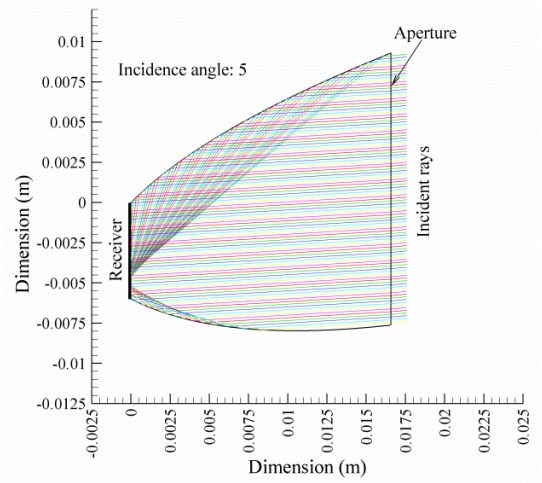

(a)

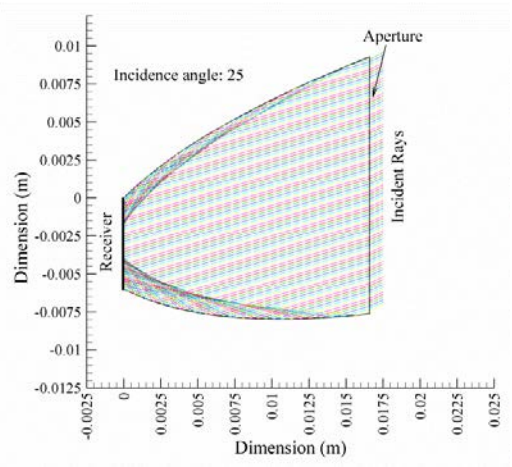

(b)

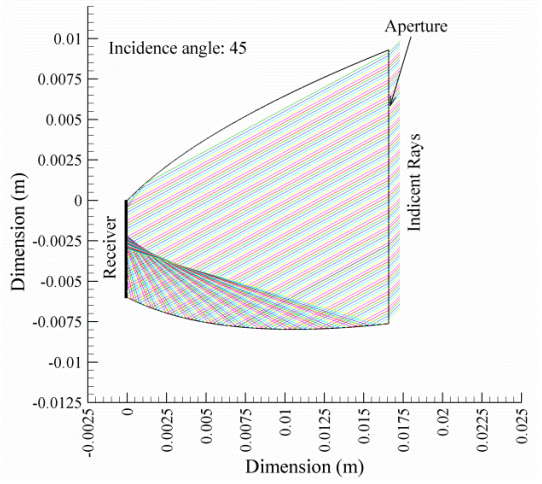

(c)

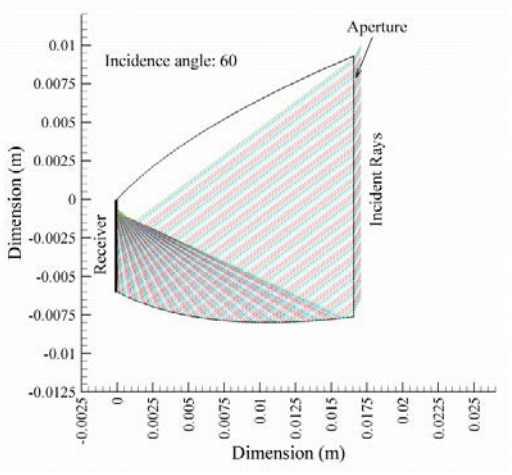

(d)

Figure 3.8 Ray trace diagram of a DiACPC-66 with 100 representative ray incident at an angle (a) 5^o (b) 25^o (c) 45^o and (d) 60^o

3.6.3 Ray trace diagram of DiACPC-77

The variation in distribution of rays and change in the number of reflections from the two parabolic sides of DiACPC-77 can be seen in figure 3.9. It can also be observed that due to the change in profile geometry the number of reflections from the lower parabolic sides decrease in DiACPC-77 compared to DiACPC-55. This variation of ray distribution will result in a difference of intensity distribution on the receiver. The flux distribution on the receiver is discussed in further detail in section 3.10.

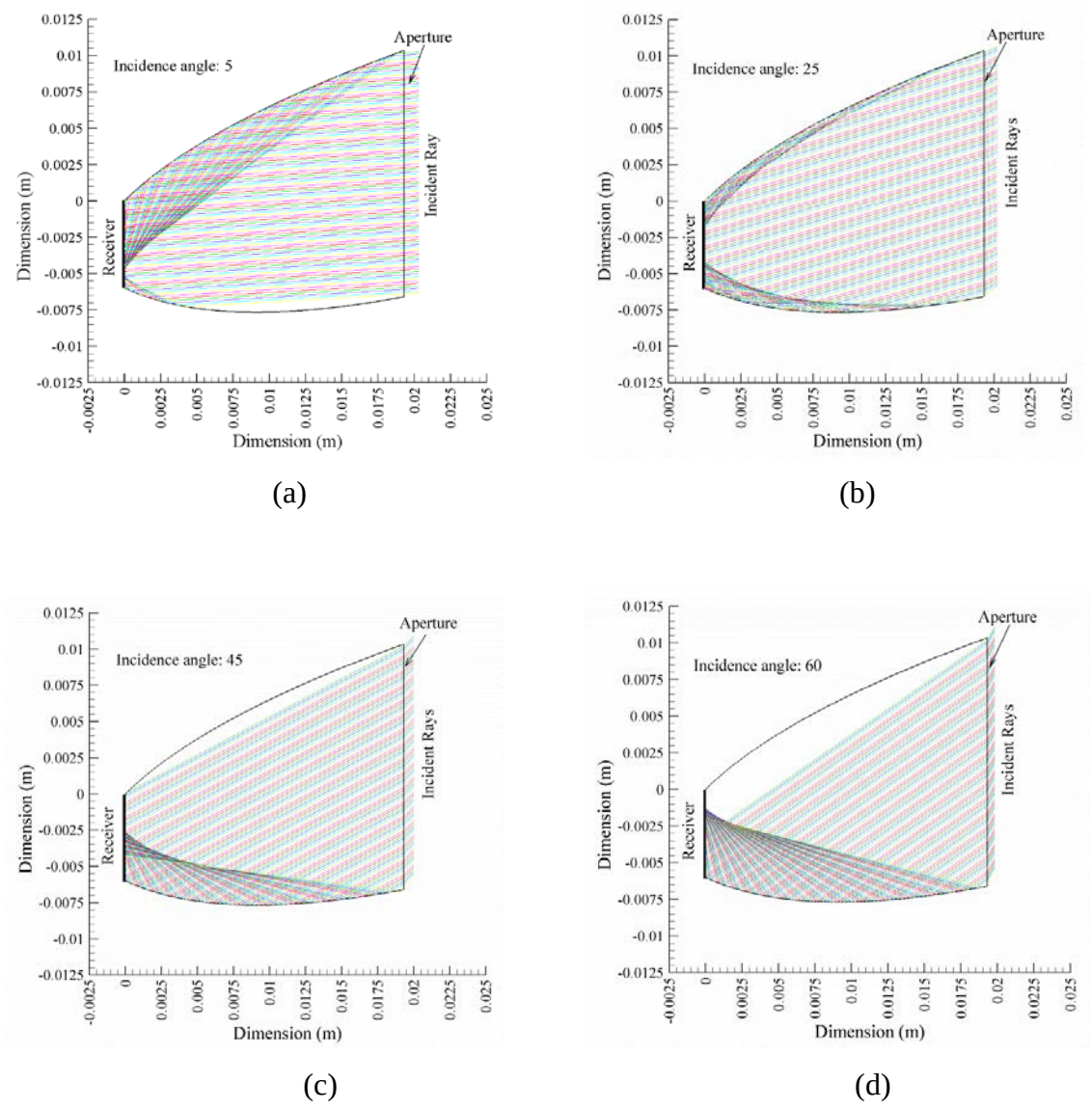

Figure 3.9 Ray trace diagram of a DiACPC-77 with 100 representative ray incident at an angle (a) 5^o (b) 25^o (c) 45^o and (d) 60^o

3.7 Angular acceptance and optical efficiency DiACPC concentrators

Angular acceptance and optical efficiency has been studied for a range of incidence angles from -90^o to +90^o. Truncation and inclination of the concentrator affect the angular acceptance and optical efficiency of the dielectric concentrating system. The truncation and inclination effect on angular acceptance and optical efficiency of dielectric concentrators is detailed in section 3.7.1 and section 3.7.2 respectively.

3.7.1 Truncation Effect on the angular acceptance

The truncation of the dielectric concentrators changes the aperture profile which increases the range of the acceptance angles significantly. It is found that, with 68% area truncation, the range of the acceptance angles of DiACPC-55 increased by 2.2 times compared to the untruncated profile (figure 3.10). The effect of the change in aperture profile after truncation causes the half acceptance angles and its range to change. The range of the acceptance half angles changes and shifted, because of the change in aperture profile after truncation. The angular acceptance study shows, both DiACPC-55 and DiACPC-66 can collect radiation up to a maximum incidence angle of 89^o; while no rays with an incidence angle higher than 79^o are able to reach the receiver of DiACPC-77, as shown in figure 3.11 & 3.12. It has been observed that the radiation incident within the range of acceptance half angles is concentrated on to the receiver without escaping from the dielectric-air interface of the parabolic sides. The simulation results show that all the designed concentrators can collect all the rays entering within the range of acceptance half angles, which means 100% angular acceptance for the respective range of the acceptance half angles. However, the angular acceptance drops significantly to less than 50%, outside this range, for both positive and negative angles. The angular acceptance of DiACPC-55 is found to be 29% for the incidence angle 56^o, decreasing to 12% for 89^o in the positive direction. The untruncated profiles of the concentrators were designed primarily to accept direct solar radiation incident with positive angles (with one half acceptance angle 0^o). However truncation of the profile and introduction of dielectric material enables the concentrators to collect irradiation from negative angles because of asymmetric mounting of the two parabolic sections. The enhancement of angular acceptance in negative direction of these dielectric concentrators is entirely depended on the amount of truncation. For negative directions, DiACPC-55 can collect radiation up to -50^o, with 49% angular acceptance at -1^o ,which drops to zero at -50^o (figure 3.10). This enhancement of angular acceptance in the negative direction will play a significant role in collecting diffuse radiation.

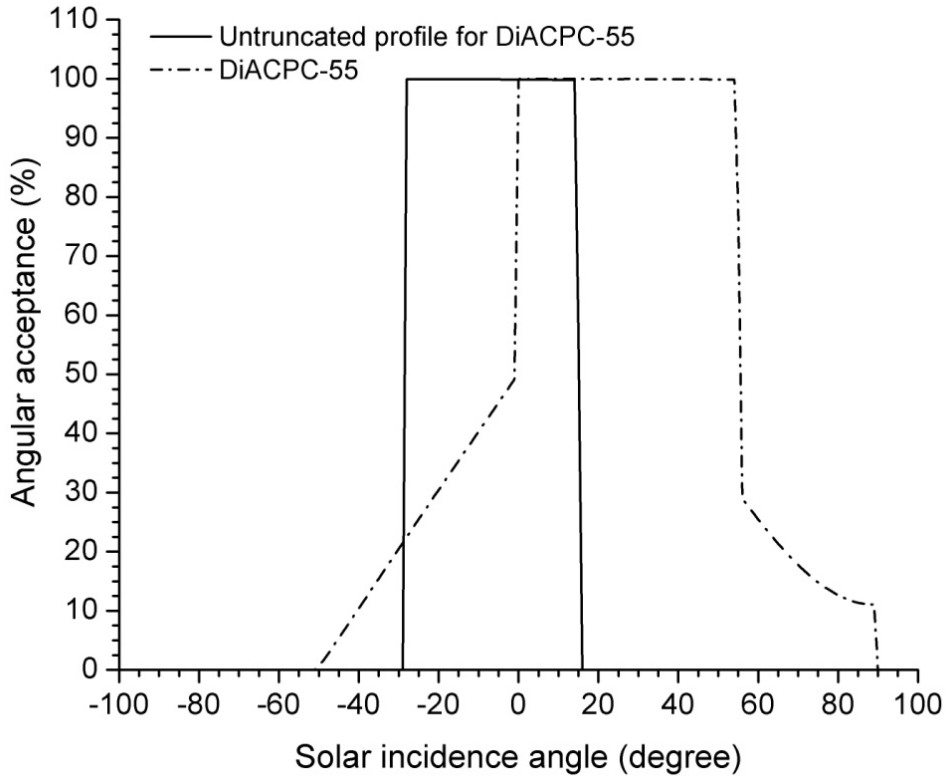

Figure 3.10 Angular acceptance of untruncated and truncated DiACPC-55 for incidence angle -90^{o} to 90^{o}.

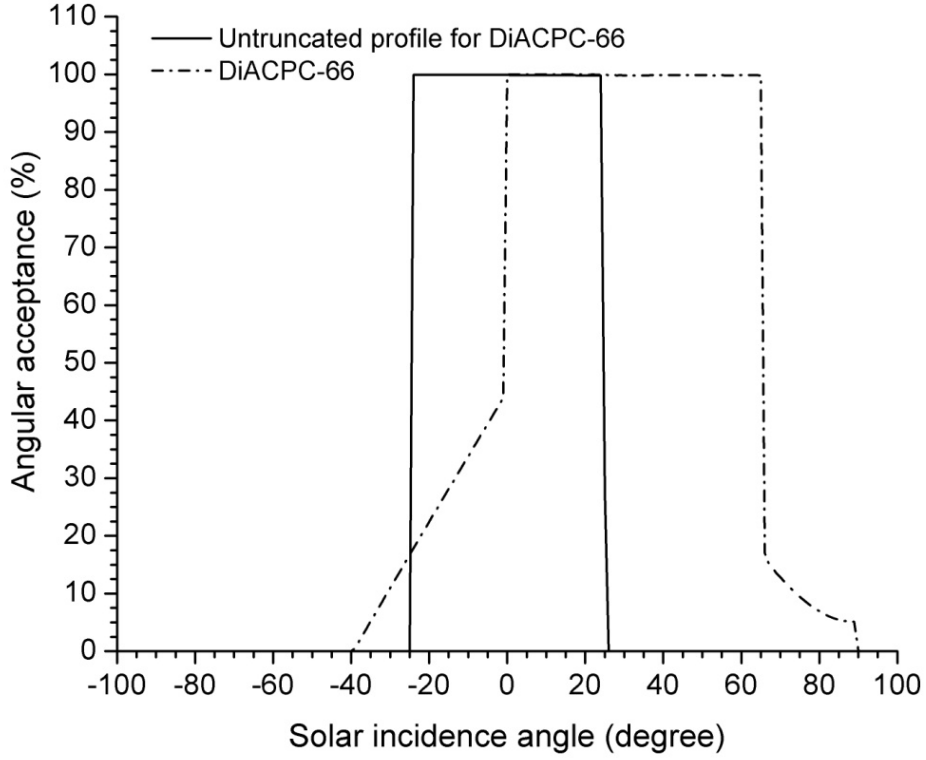

Figure 3.11 Angular acceptance of untruncated and truncated DiACPC-66 for incidence angle -90^{o} to 90^{o}.

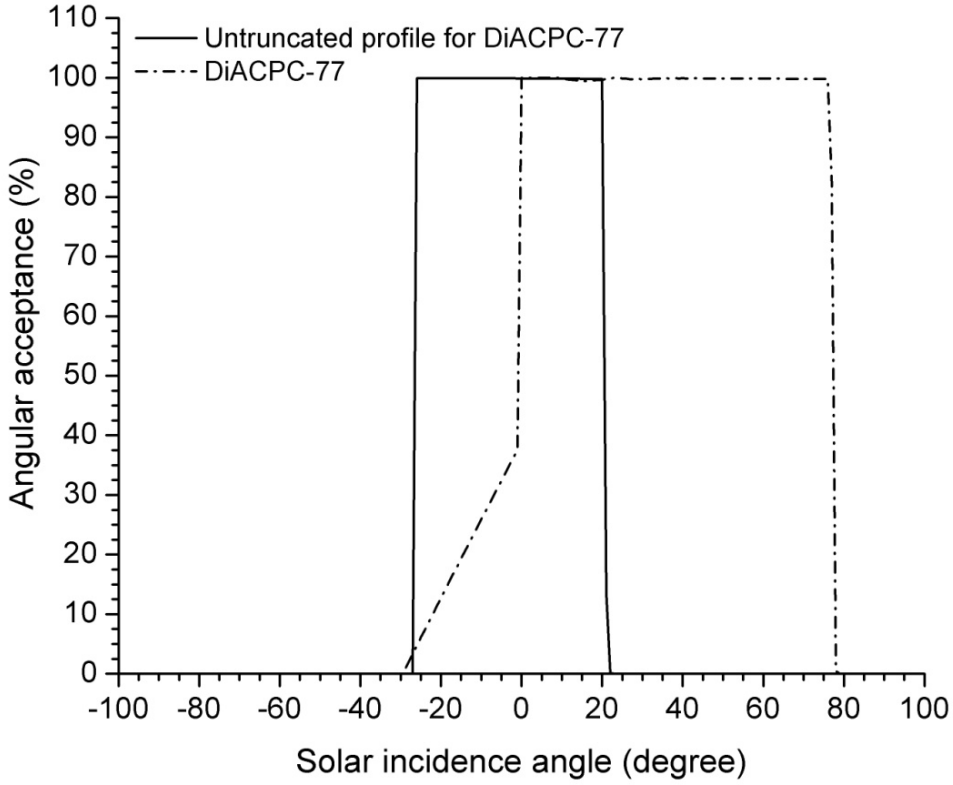

Figure 3.12 Angular acceptance of untruncated and truncated DiACPC-77 for incidence angle -90^o to 90^o.

3.7.2 Optical efficiency of truncated DiACPC systems

The optical efficiency estimates the fraction of the incident energy on the aperture that reaches the receiver. The optical efficiency accounts for all possible reflection and transmission losses on the aperture cover and within the dielectric material of the concentrator. Since the cover glass and the dielectric concentrator are not encapsulated, a possible air gap between these two is considered as realistic approach to account this lack of optical coupling. A significant part of the transmission losses occurs from the cover glass because of the partial reflection of unpolarised incident radiation at the air-glass-air-dielectric interface [10]. The optical efficiency is a function of the angle of the incident light and the path-length within the dielectric material and is calculated from Eqn. (3.5) [10],

$$\eta(\theta) = \sum_{i=1}^{m} \frac{I_i \tau_r \exp\left(-\dfrac{\alpha L_i}{\cos\left(\sin^{-1}\left(\sin\theta / n\right)\right)}\right)\rho^j}{I_o} \qquad (3.5)$$

where θ is the incident angle, I_i is the intensity of a single ray (W/m^2), I_o is the total intensity at the aperture (W/m^2), τ_r represents the reflective component of unpolarised light transmission, α is the absorption coefficient (m^{-1}), n is the refractive index of the dielectric material and glass, L_i is the path length of a single ray within concentrator, ρ is the internal reflectivity from the parabolic sides, j is the number of reflections and m is the number of rays

The optical efficiency study of the designed concentrators shows that a maximum of 83% can be achieved for radiation incident perpendicular to the aperture (0^o incidence angles) resulting in a minimum optical loss of 17% within the system. The major part of this loss is due to the reflection losses at the air-glass interface, which increases with increasing incidence angle. A detailed study of the losses, considering the parallel and perpendicular component of the unpolarised solar radiation [10] shows that the reflection losses at the air-glass interface contributes 13% of the total loss for the radiation incident perpendicular to the aperture. The other 4% is contributed by the absorption losses in the cover glass and concentrator material. For DiACPC-55 the optical efficiency is almost constant (83% optical efficiency) within the acceptance half angles of the concentrator (figure 3.13). The optical efficiency of the concentrators DiACPC-66 and DiACPC-77 are found to be 82.4% and 81.7% for radiation incidence perpendicular to the aperture, which drop for incidence angles higher than 55^o. For an incident angle of 60^o, the optical efficiencies of DiACPC-66 and DiACPC-77 are found to be 73.1% and 72.1% respectively (figure 3.14 & 3.15), which are poor values for a low concentrating application. These results show that, although the concentrators DiACPC-66 and DiACPC-77 are suitable for collecting solar radiation up to 89^o and 79^o incident angles respectively (figure 3.14 & 3.15), the drop in optical efficiency for higher incidence angles represents no practical use of the radiation accepted for incidence angles higher than 55^o.

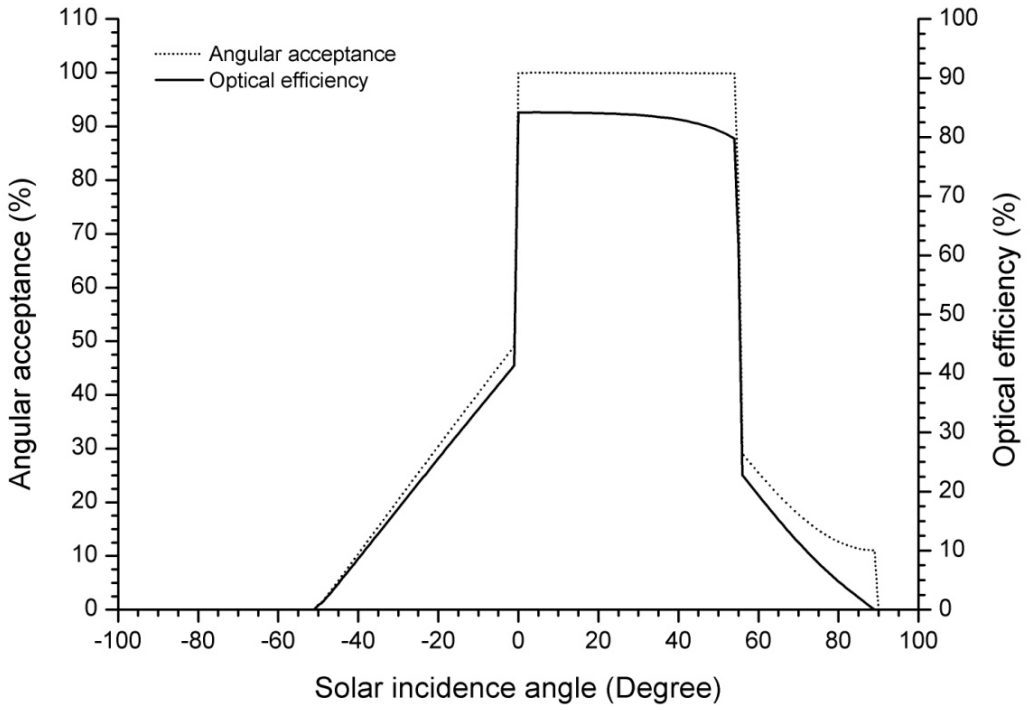

Figure 3.13 Angular acceptance and optical efficiency of truncated DiACPC-55

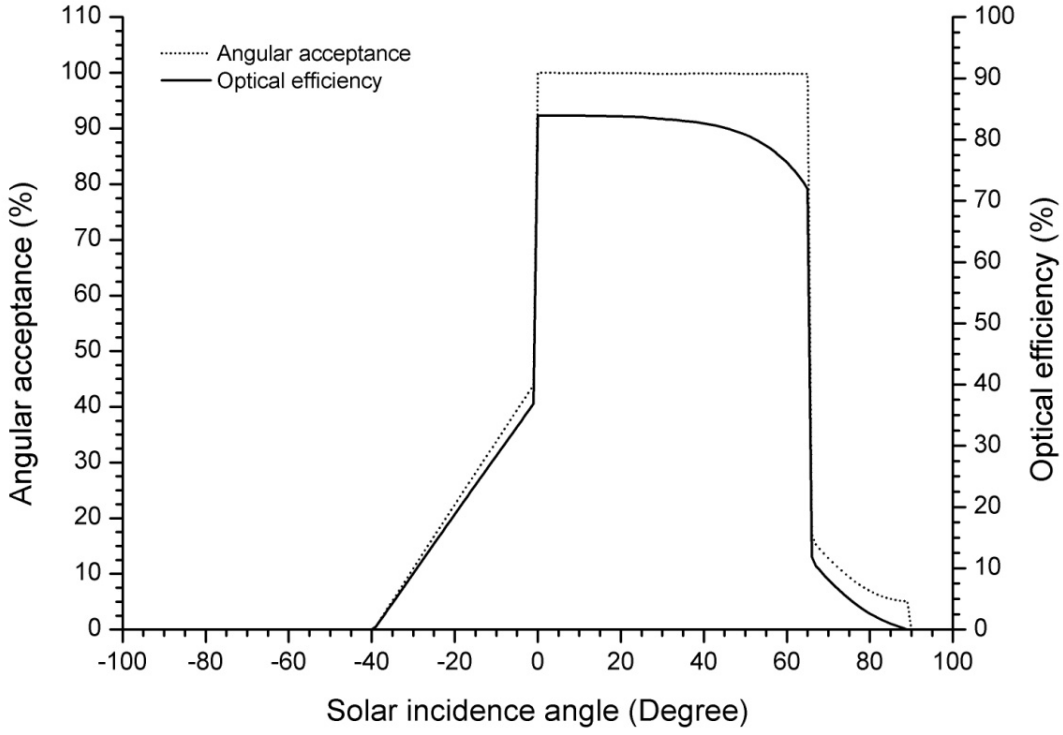

Figure 3.14 Angular acceptance and optical efficiency of truncated DiACPC-66

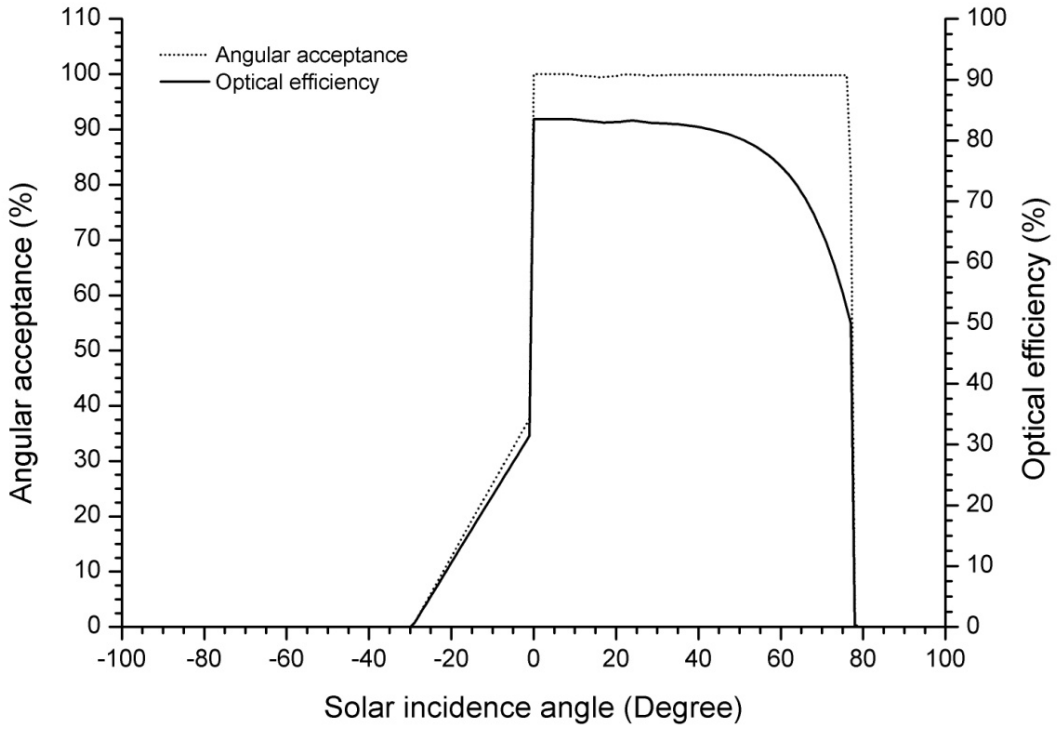

Figure 3.15 Angular acceptance and optical efficiency of truncated DiACPC-77

3.8 Inclination effect on angular acceptance and optical efficiency

The inclination effect on the optical performance is studied with two kind of inclination: (i) Inclination after truncation (IAT) and (ii) Truncation after inclination (TAI). For IAT, the whole system including concentrator, solar cell and front glass cover is inclined by various angles. In this inclination the profile of the concentrator doesn't change. In TAI the concentrator has been made after inclination. So only the receiver is kept at an inclined angle, but rest of the system remains vertical. In this kind of inclination, the profile of the concentrator is changed. The geometrical difference of IAT and 'TAI is shown with ray trace diagram in figure 3.16 (a & b). Optimized inclination of the concentrator may lead to an improved positioning to accept a wider range of incident radiation. Angular acceptance and optical efficiency characteristic have been studied for inclination angles 5^o, 10^o, 15^o and -5^o. The study shows that the IAT of the concentrator doesn't change any characteristic of the angular acceptance other than that the curve shifted in the direction of inclination depending on the inclined angle.

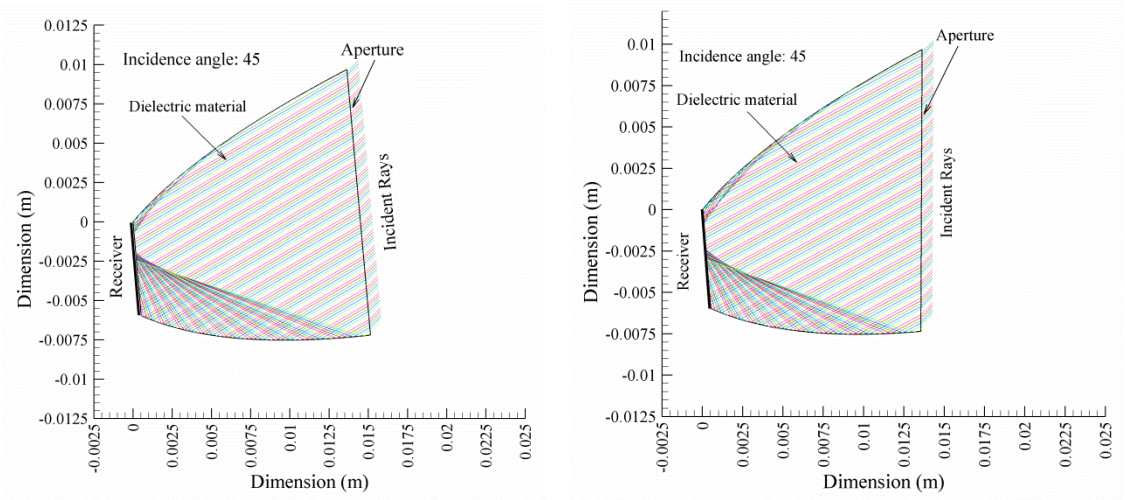

(a) (b)

Figure 3.16 Representative Ray trace diagram for (a) 5^o inclination after truncation. (b) Truncation after 5^o inclination with DiACPC-55.

In the case of TAI, the angular acceptance curve shifted towards the inclined direction; the acceptance range was also found to be increasing with positive inclination. For DiACPC-55, with 5^o inclination the range of acceptance angle increases by 13% and accepts all the rays within incident angles 8^o to 70^o. The maximum decrease in optical efficiency within the acceptance angles is only 13.2% which is considered acceptable due to the gain in angular acceptance. For DiACPC-66 and DiACPC-77 the range of acceptance angle increased by 24.2% and 6.4% with 5^o inclination. However, the optical efficiency decreases very sharply for higher angles, which makes no practical use of increased acceptance angle. The inclination study carried out for higher inclinations (10^o and 15^o) shows that although there is an increase in range of acceptance angles of DiACPC-55; however, sharp decrease in optical efficiency makes no practical use of this gain. For negative inclination the range of the acceptance angle decreases and for DiACPC-55 with -5^o inclination, acceptance half angles shifted to -7^o and 45^o which is a 5.5% decrease on zero inclination. The comparative estimation of change in angular acceptance and optical efficiency with 5^o inclination of DiACPC-55 is shown in figure 3.17 - 3.19.

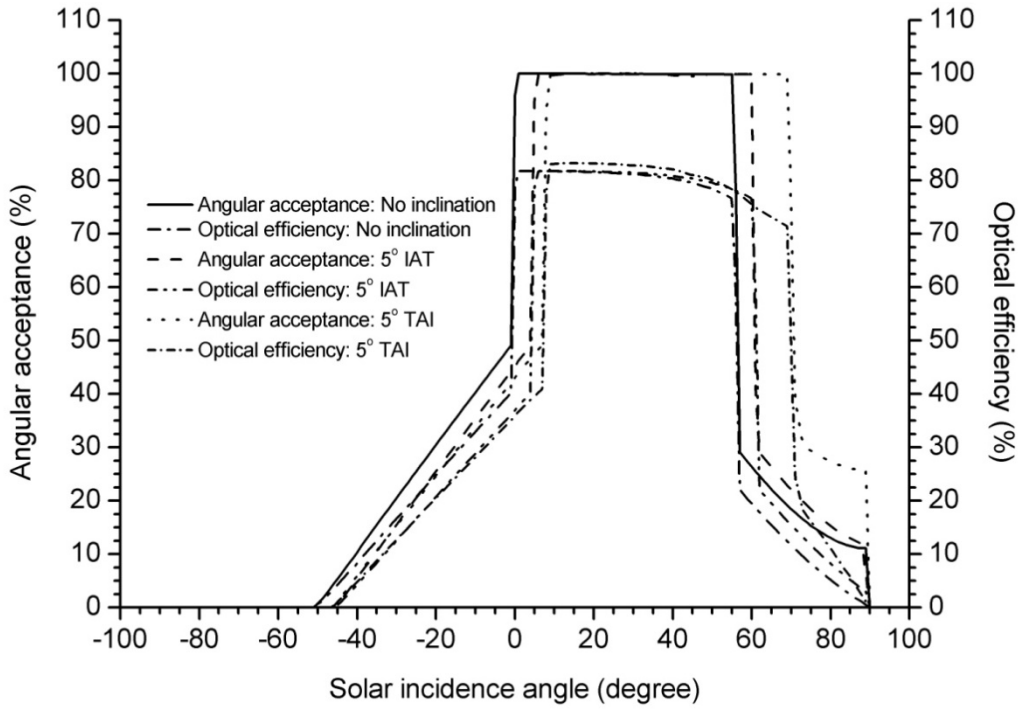

Figure 3.17 Comparative angular acceptance and optical efficiency of DiACPC-55 with no inclination, 5^{o} inclination after truncation and truncation after 5^{o} inclination.

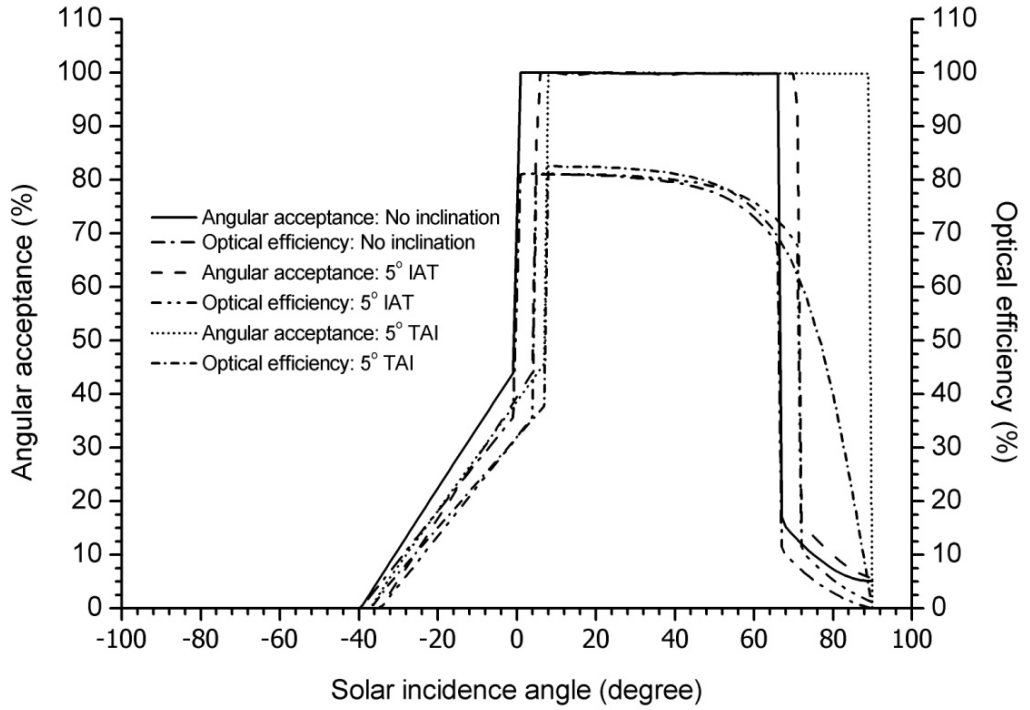

Figure 3.18 Comparative angular acceptance and optical efficiency of DiACPC-66 with no inclination, 5^{o} inclination after truncation and truncation after 5^{o} inclination.

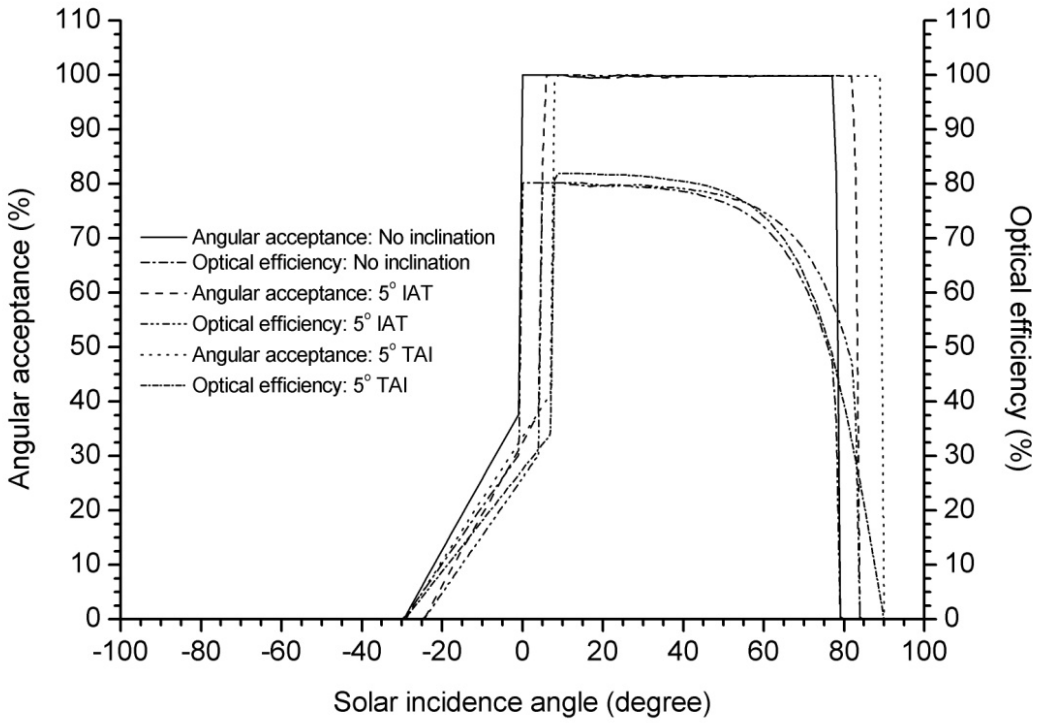

Figure 3.19 Comparative angular acceptance and optical efficiency of DiACPC-77 with no inclination, 5^o inclination after truncation and truncation after 5^o inclination.

3.9 Energy flux distribution at receiver

The biggest advantage of non-imaging concentrators for CPV application is the ability to distribute the collected energy over the receiver, without a sharp image of sun at one point. A homogeneous flux distribution over the solar cell area is desirable for higher electrical efficiency and output of the PV system. Inversely an inhomogeneous distribution causes reduction in fill factor and PV electrical efficiency. Although it is very difficult to design a solar concentrator to obtain a uniform radiation distribution over the receiver area, the non-imaging concentrator can achieve a good distribution of concentrated radiation at the receiver.

3.9.1 Energy flux distribution at receiver due to direct irradiation

For the designed DiACPC's, the concentrated radiation is well-distributed over the receiver for a wide range of incident angles, but a sharp peak of energy intensity can be observed at some points for direct solar radiation, as shown in figure 3.20, 3.21 and 3.22. However the distribution of energy flux and position of the peak at the receiver changes with the incidence angle and asymmetric profile. The peaks become sharper for the incident radiation close to the acceptance half angles because of the light reflected

from the parabolic surfaces is concentrated at the edge of the receiver (along the x-axis in figure 3.20). The energy flux at the receiver of the concentrator is calculated from Eqn. (3.6), [10] considering a direct insolation of 600 W/m^2 for the chosen location of Edinburgh [248]

$$I_{rec} = I_o - \sum_{i=1}^{m} (\tau_g I_i + \tau_d I_i + j\rho I_i) \tag{3.6}$$

In Eqn. (3.6), I_{rec} is the intensity at the receiver (W/m^2), I_o is the total intensity at the aperture (W/m^2), I_i is the intensity of a single ray (W/m^2), τ_g is the transmittance of glass, τ_d is the transmittance of dielectric material, ρ is the internal reflectivity from the parabolic sides, j is the number of reflections and m is the number of rays. The shift of intensity peaks at the receiver of DiACPC-55, with increase in incidence angle is shown in figure 3.20. A similar characteristic of intensity distribution at the receiver of DiACPC-66 and DiACPC-77 can be observed in figure 3.21 and figure 3.22 respectively. Although the distribution is found to be better for DiACPC-77 for a range of incidence angles from 0^o to 55^o than DiACPC-55; the optical efficiency results for this concentrator has limited it's application as a building façade CPV system in the desired location. The energy distribution for the incident rays outside the acceptance angle is quite flat with a much lower intensity, as only a few direct rays (without any reflection) can reach the receiver. The study reveals that even though the intensity distribution at receiver of the concentrator is not homogenous, due to the non imaging property of the concentrator, the collected energy is distributed across the whole receiver area for wide range of incidence angles. The sharp intensity peak of DiACPC-55 varies from 9907 W/m^2 to 5140 W/m^2 corresponding to the incidence angle 45^o and 25^o. This gives a clear indication that the non-uniformity varies with seasonal variation of the sun's position resulting in better performance during autumn and spring compared to winter and summer.

Comparison of the intensity flux distribution of the DiACPC-55, DiACPC-66 and DiACPC-77 for incidence angle 25^o is shown in figure 3.23. The minor peak is in the same position for all the three designs because of the same acceptance half angle 0^o; however the major peak has shifted with a change in the other acceptance half angle of the concentrators.

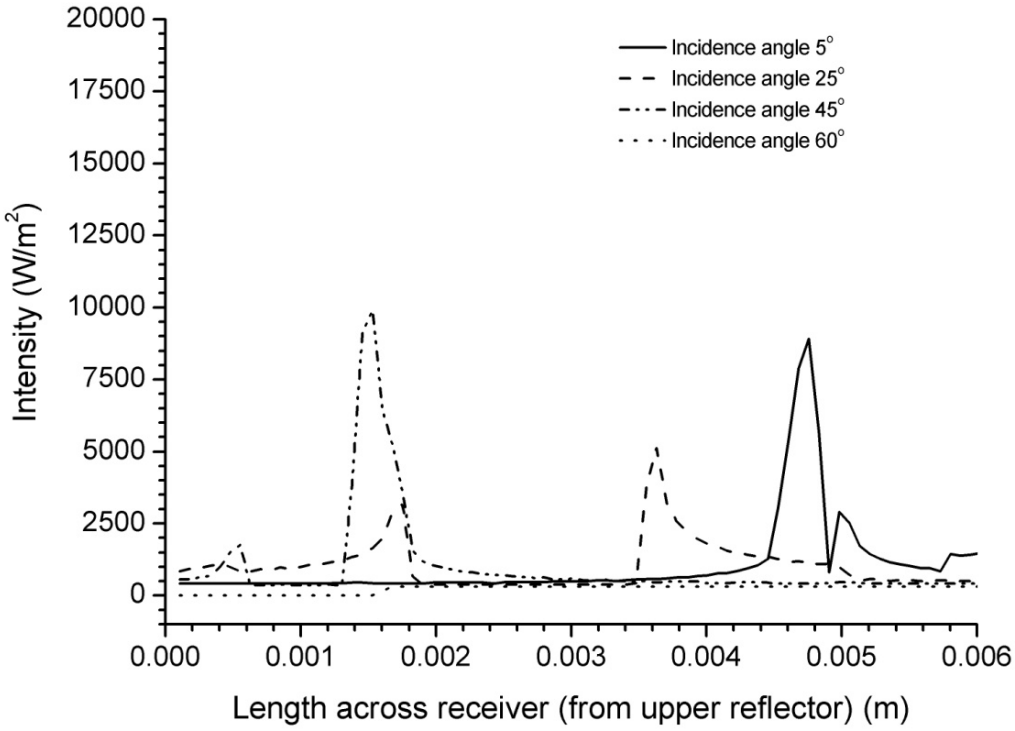

Figure 3.20 Energy flux distribution on receiver of DiACPC-55 for incidence radiation 5^o, 25^o, 45^o and 60^o.

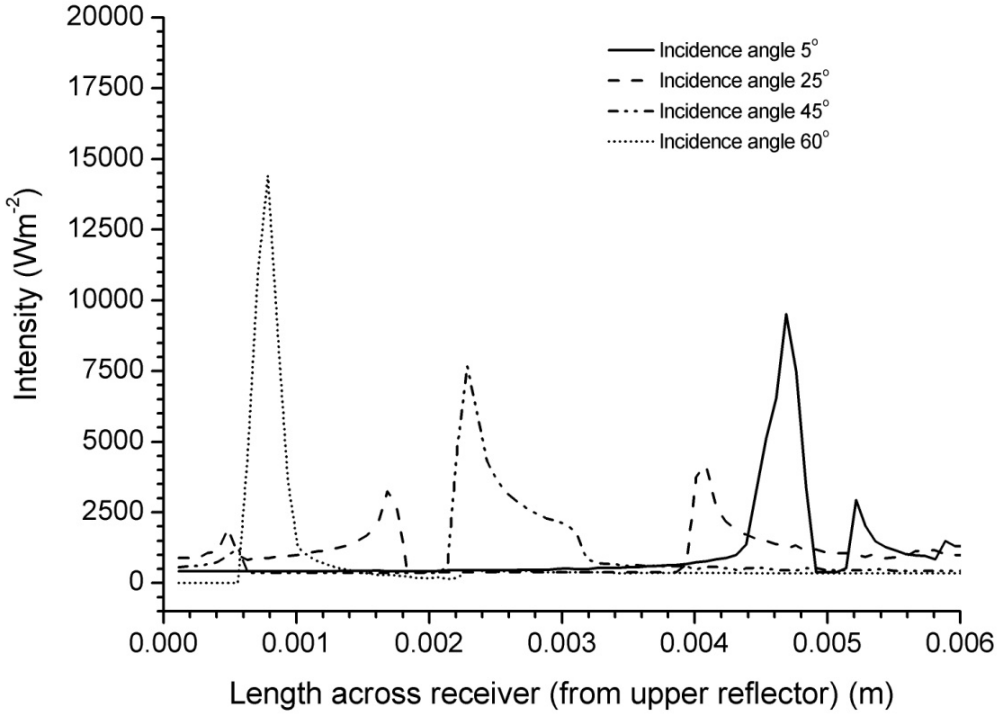

Figure 3.21 Energy flux distribution on receiver of DiACPC-66 for incidence radiation 5^o, 25^o, 45^o and 60^o

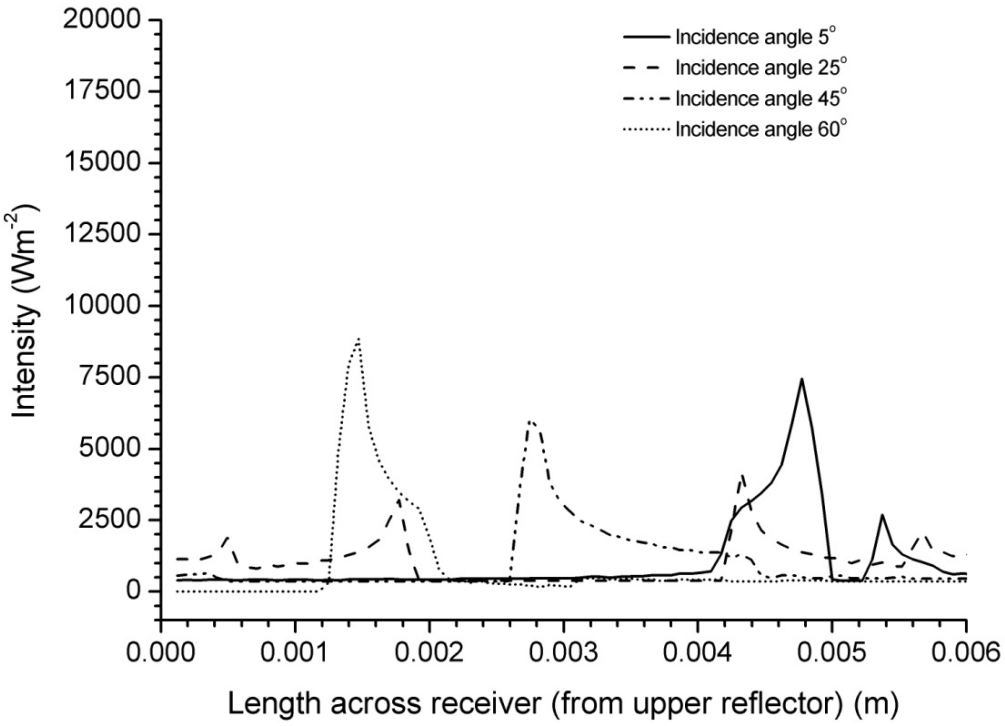

Figure 3.22 Energy flux distribution on receiver of DiACPC-77 for incidence radiation 5^o, 25^o, 45^o and 60^o.

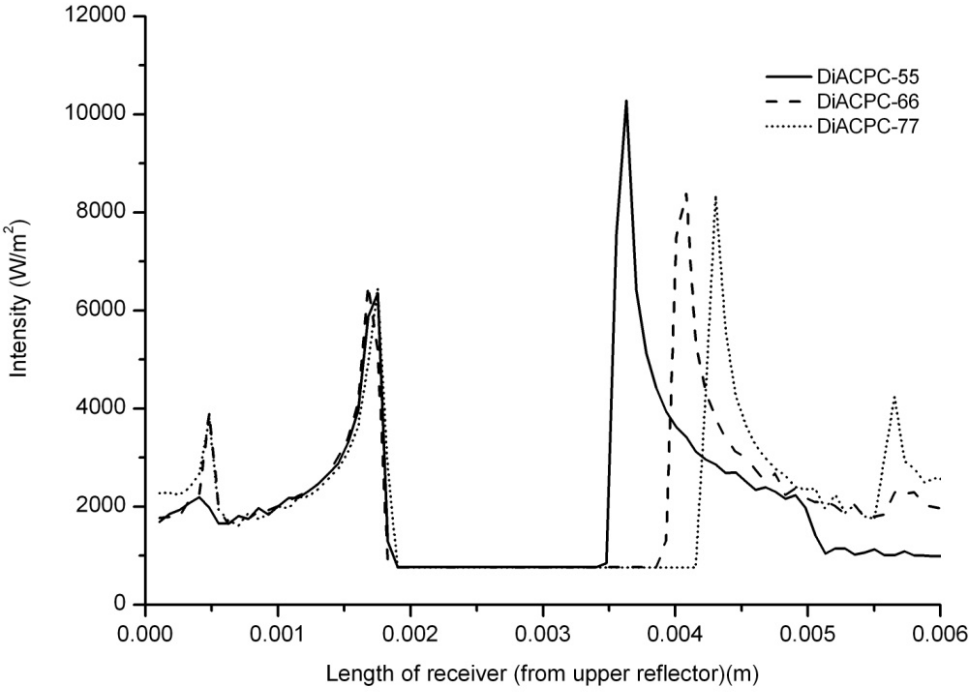

Figure 3.23 Energy flux distribution on receiver of DiACPC-55, DiACPC-66 and DiACPC-77 for incidence angle 25^o

The intensity distribution at receiver also changes with TAI of the concentrators. The change of the intensity distribution at receiver of DiACPC-55 with 0^o, 5^o and 10^o inclination is shown in figure 3.24 for incidence angle 25^o. Due to the change in profile with inclination, the position of the major peak shifts. The peaks shift towards the lower reflector for each degree of inclination and the minor peak is turned into major peaks for higher inclinations. The study shows in case of inclination requirements, 5^o TAI will be more effective for better optical performance of the concentrator.

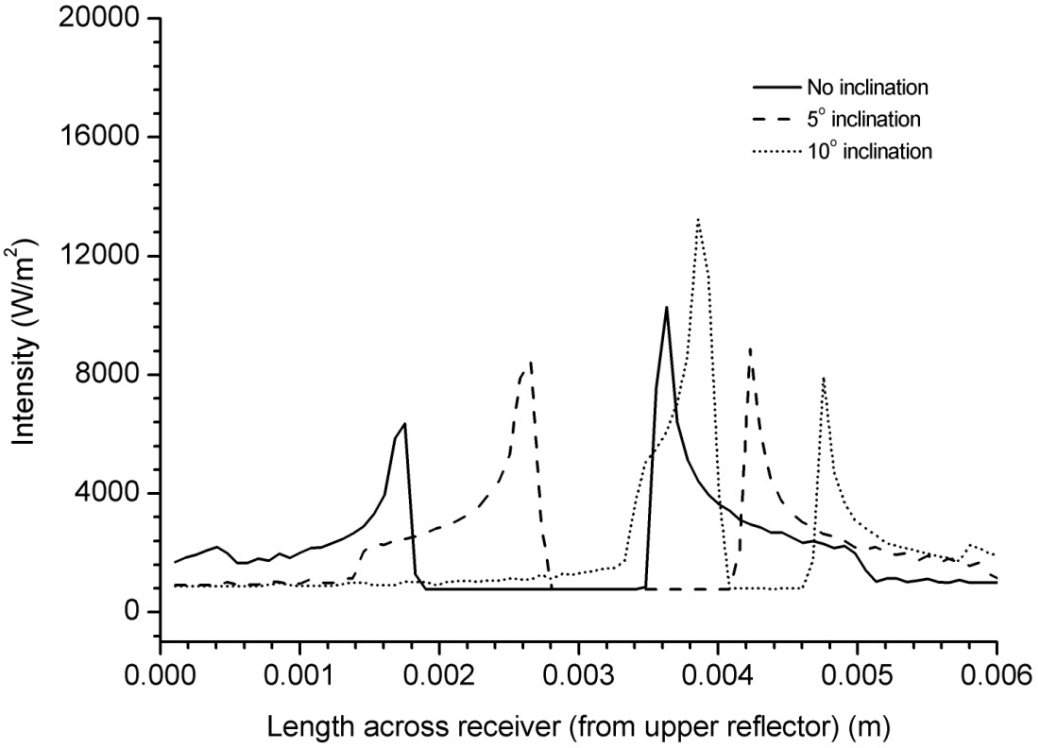

Figure 3.24 Variation of intensity distribution at the receiver of DiACPC-55 for incidence angle 25^o with TAI of 0^o, 5^o and 10^o.

3.9.2 Energy flux distribution at receiver due to diffuse irradiation

The diffuse part of solar radiation can contribute significantly to the performance of a dielectric concentrator. A study of angular acceptance shows that a wide range of incident rays can be accepted by the designed concentrators, especially by DiACPC-55, even outside the acceptance half angles. Therefore, diffuse radiation can still contribute to the optical efficiency, even though rays are incident at angles out of the defined acceptance range. Three different angular distributions of solar insolation are possible: isotropic, cosine and hybrid Gaussian are employed to estimate the optical performance of solar concentrators. A cosine distribution of diffuse radiation is considered in this

study as a suitable option for a non-tracking system. The normalised angular intensity in cosine distribution is shown below in Eqn. (3.7) [127]

$$I_{D,\phi} = \frac{\pi}{2} Cos\phi \tag{3.7}$$

Where, $I_{D,\phi}$ is the normalized angular intensity, φ is the angle of incidence (in degrees). The cosine distribution is the most realistic for low concentrating stationary dielectric concentrating systems where the insolation intensities for larger incidence angles are underestimated, unlike the hybrid Gaussian and isotropic distribution model [127].

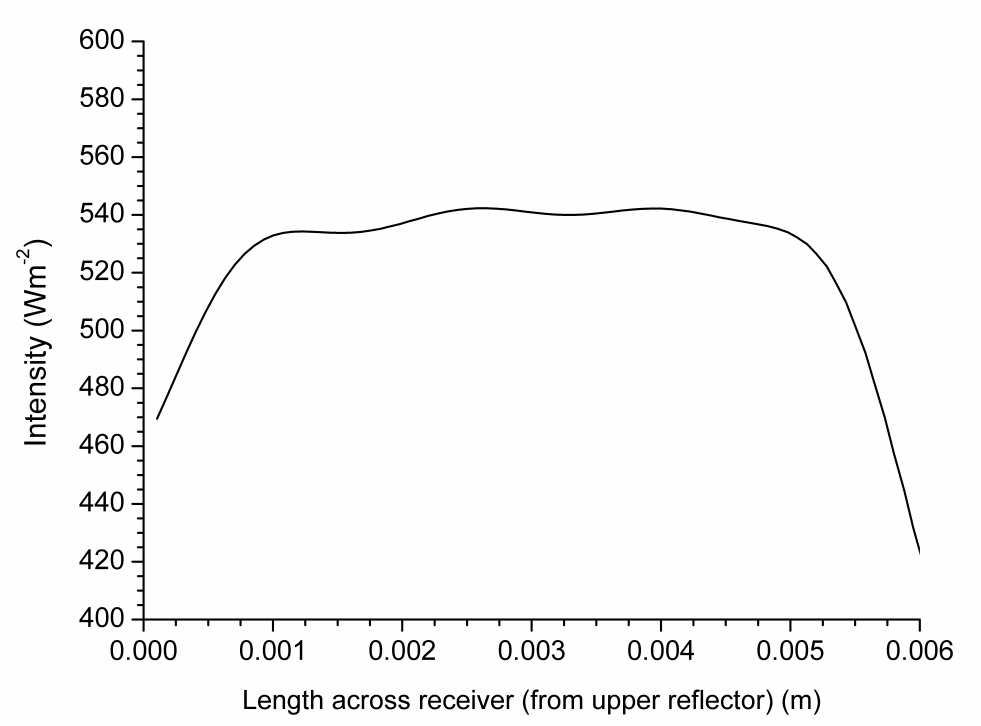

Figure 3.25 Energy flux distribution on receiver of DiACPC-55 with cosine diffuse radiation

The energy distribution at the receiver of the concentrator for diffuse radiation is shown in figure 3.25. Maximum diffuse radiation of 400 W/m^2, which is incident on sunny days in northern UK[248], has been considered in this study. The average intensity of 520 W/m^2 is found at the receiver for scattered diffuse radiation incident on the aperture of the concentrator, in the range of 180^o. From the angular acceptance study it is observed that the designed concentrator can only accept 40-46% of the total diffuse

radiation, which reduces the average energy flux at the receiver. Study shows that the DiACPC-55, DiACPC-66 and DiACPC-77 can collect 44.86%, 43.6% and 43.28% of the diffuse solar energy respectively, considering all the possible losses within the concentrators. The flux distribution at the receiver is found to be more uniform and well distributed compared to the direct insolation. However, if this kind of dielectric CPV system is exposed to the diffuse radiation only, it is more likely that the maximum power output and conversion efficiency of the CPV system will be less because of the low light intensity, and the losses within the concentrator [211].

3.10 Annual Energy Collection and System Optimisation

Estimation of annual energy collection by the concentrators helps in optimisation of the concentrator design for commercial application. The process flow diagram to optimise the designed concentrator is shown in figure 3.26.

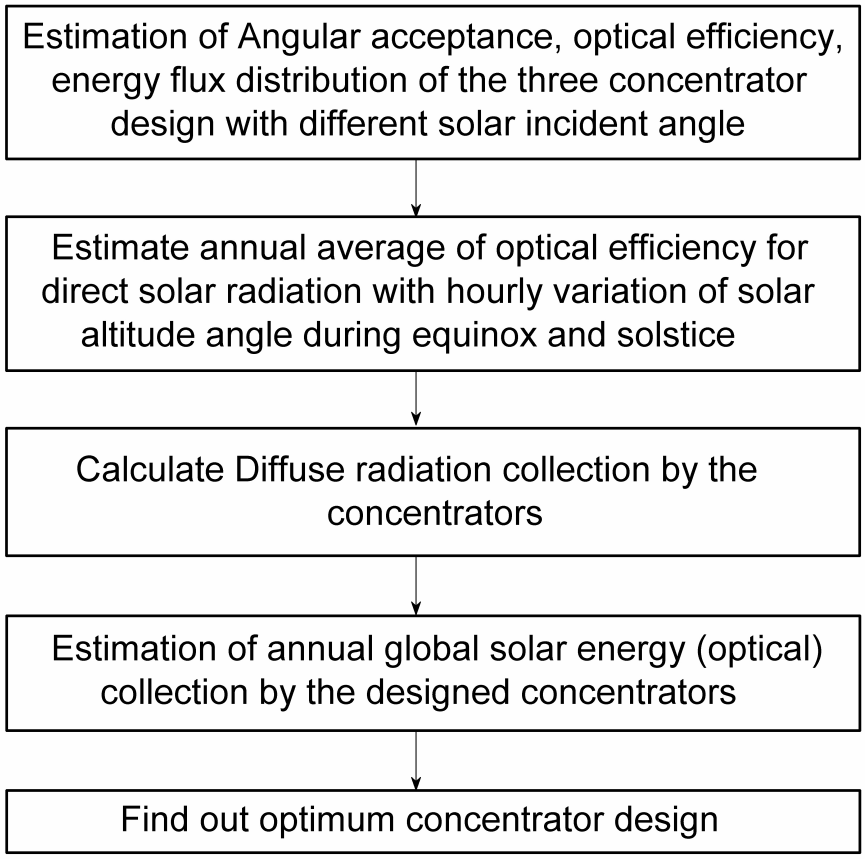

Figure 3.26 Optimisation process flow diagram for the designed concentrators.

The annual average optical efficiency of the three designed concentrators is calculated with hourly variation of incident angle (solar altitude angle) on the aperture of the

concentrator. The annual average of optical efficiency of the concentrators for direct solar radiation on the south facing walls has been calculated with variation of the solar altitude angle in every 15 minutes for the two equinox (21st March & 21st September) and two solstice (21st June and 21st December) of the year. The optical efficiency has been calculated for the altitude angles of the sun within solar azimuth angle -90^{o} to +90^{o} for a south facing wall in Edinburgh. The average optical efficiency of these four days with the extreme altitude angles can be represented as the average optical efficiency of the concentrator for the whole year. The calculations show that the annual hourly average of optical efficiency of DiACPC-55, DiACPC-66 and DiACPC-77 for a south facing wall in Edinburgh is respectively 78.35%, 77.55% and 75.59%. Since optical efficiency refers to the total optical energy collected by the system, the concentrator design can be optimized based on the total energy collection over a year, considering both direct and diffuse radiation.

The annual average of global horizontal solar energy in Edinburgh is 891 kWh/m^2, where, 327 kWh/m^2 is direct radiation and 564 kWh/m^2 is the diffuse part [248]. It is found that, with 44.86% collection of diffuse radiation and 78.35% annual average of optical efficiency for direct solar radiation, DiACPC-55 can collect 509.21 kWh/m^2 solar energy annually, in Edinburgh location, contributing 256.2 kWh/m^2 from direct radiation and 253.01 kWh/m^2 from diffuse radiation. The energy collected by DiACPC-55 is 1.64% (8.4 kWh/m^2) higher than DiACPC-66 and 3.53% (18 kWh/m^2) higher than DiACPC-77. Study reveals that DiACPC-55 is the optimum design to collect maximum solar irradiation for higher latitudes (>55^{o}) with a relatively smaller height, compared to the other two concentrator designs in consideration.

3.11 Thermal modelling CPV system

The basic principle of the CPV system is to collect the solar radiation in a small area to reduce the cost associated with the solar cell, which has a negative impact by increasing temperature. Due to the high solar flux, the temperature of the solar cell in a CPV module is higher than that of a flat plate module. The increase in temperature of the solar cell in the CPV modules can reduce the performance because of a decrease in fill factor and open circuit voltage. For high concentration system special attention for cooling is required to keep the solar cell temperature below a certain level for optimum performance. In low concentrating systems, the temperature of the solar cell is expected to be within the optimum operating range. However, detailed thermal modelling at the

system level can help in better understanding of the losses which occur due to the increase in temperature of the solar cell. The temperature of the module largely depends on the intensity of the solar radiation, ambient temperature and the heat transfer co-efficient of the surrounding air. These factors can vary depending on the weather condition in a real environment.

3.11.1 Numerical methods of thermal modelling of CPV module with DiACPC-55 concentrator

The solar cell temperature and thermal distribution within the CPV module with DiACPC-55 has been investigated using a numerical model. A computational fluid dynamics (CFD) software package called 'ANSYS cfx' is used for 3D simulation. A CFD technique can perform the thermal modelling analysing the fluid flow, heat transfer and chemical reaction with the help of computer based simulation. Similar to most of the CFD software tools, 'ANSYS cfx' also perform the thermal modelling in three steps process (a) Pre-processor (b) Solver and (c) Post-processor.

3.11.1.1 Pre-processor

In the pre-processor stage, the problem is defined by creating the geometry through a CAD interface. Use of finite element method to create sub-division and domains is also included in the pre-processor stage. The major steps of the pre-processor stage are:

- Import/draw the geometry to be used for thermal modelling into the ANSYS cfx
- Define the sub-division of the geometry and domain into non-overlapping smaller sub-domains or cells.
- Selection of the physical model
- Define material and fluid properties of the different components in the model
- Define the appropriate boundary conditions at domain boundaries and wherever appropriate

The accuracy of the CFD solution depends a lot on the definitions of the geometry, domains, sub-domains and cells. Higher sub-domains and cells number provides higher accuracy and detailed thermal distribution up to a very small area. However accuracy in defining sub domains and cells is very important. Any overlapping of sub-domain or

discontinued cells results wrong modelling results. Depending on the problem and geometry, defining optimum mesh can be crucial; which are very often non-uniform.

3.11.1.2 Solver

Solver is the different numerical techniques use to solve the fluid dynamic problems in the form of equations. The popular solver methods are finite difference, finite element and spectral methods. In general, the solver performed the following processes:

- Approximation of a unknown variable by means of simple function
- Discretisation by substituting the approximations into governing equations and subsequent mathematical calculation
- Solution of the algebraic equations

In the present work, finite element method is use through 'ANSYS cfx' package. Finite element methods use simple piecewise functions (e.g linear and quadratic) valid on elements to describe the local variations of unknown flow variables, say ϕ. The governing equation is precisely satisfied by the exact solution ϕ. If the piecewise approximating functions for ϕ are substituted into the equation it will not hold exactly and a residual is defined to measure the errors. Next the residuals are minimized by multiplying them by a set of weighting functions and followed by integrations. As a result, we obtain a set of algebraic equations for the unknown coefficients of the approximating functions. By using appropriate direct or iterative methods, the solution for the algebraic equations can be obtained.

3.11.1.3 Post-Processor

In the post-processing stage the modelling results obtained by the solver can be plotted and displayed. Various plotting and display methods in the post-processing stage in 'ANSYS cfx' includes:

- Domain geometry and grid display
- Vector plots
- Line and shaded contour plots
- Particle tracking
- View manipulation and colour postscript output

3.11.1.4 Theory of thermal modelling

The thermal modelling of the DiACPC-55 concentrator and the CPV module are carried out using the above described CFD technique. All the heat by means of conduction, convection and radiation of the given system has been considered in the thermal modelling. The results are obtained by solving the continuity, momentum and energy equations for the system. In vector form, these equations can be represented as [130, 249]

$$\nabla . V = 0 \tag{3.8}$$

$$\nabla . \nabla Z = X_g - \frac{\nabla P}{\rho_f} + \vartheta \nabla^2 \mathrm{Z} \tag{3.9}$$

$$\nabla . (k_f \nabla T) = 0 \tag{3.10}$$

In 2-D Cartesian coordinates, these equations can be written as;

Continuity equation

$$\frac{\partial \mathrm{u}}{\partial \mathrm{x}} + \frac{\partial \mathrm{v}}{\partial \mathrm{y}} = 0 \tag{3.11}$$

Momentum equations

X-Coordinates

$$\rho\left(\mathrm{u}\frac{\partial \mathrm{u}}{\partial \mathrm{x}} + \mathrm{v}\frac{\partial \mathrm{u}}{\partial \mathrm{y}}\right) = -\frac{\partial \mathrm{p}}{\partial \mathrm{x}} + \frac{\partial}{\partial \mathrm{x}}\left\{\mu\left[2\frac{\partial \mathrm{u}}{\partial \mathrm{x}} - \frac{2}{3}\left(\frac{\partial \mathrm{u}}{\partial \mathrm{x}} + \frac{\partial \mathrm{v}}{\partial \mathrm{y}}\right)\right]\right\} + \frac{\partial}{\partial \mathrm{y}}\left\{\mu\left[\frac{\partial \mathrm{u}}{\partial \mathrm{y}} + \frac{\partial \mathrm{v}}{\partial \mathrm{x}}\right]\right\} + \mathrm{X_g} \tag{3.12}$$

Y-Coordinates

$$\rho\left(\mathrm{u}\frac{\partial \mathrm{v}}{\partial \mathrm{x}} + \mathrm{v}\frac{\partial \mathrm{v}}{\partial \mathrm{y}}\right) = -\frac{\partial \mathrm{p}}{\partial \mathrm{y}} + \frac{\partial}{\partial \mathrm{y}}\left\{\mu\left[2\frac{\partial \mathrm{v}}{\partial \mathrm{y}} - \frac{2}{3}\left(\frac{\partial \mathrm{u}}{\partial \mathrm{x}} + \frac{\partial \mathrm{v}}{\partial \mathrm{y}}\right)\right]\right\} + \frac{\partial}{\partial \mathrm{x}}\left\{\mu\left[\frac{\partial \mathrm{u}}{\partial \mathrm{y}} + \frac{\partial \mathrm{v}}{\partial \mathrm{x}}\right]\right\} + \mathrm{Y_g} \tag{3.13}$$

Energy equation

$$\rho \mathrm{c_p}\left(\mathrm{u}\frac{\partial \mathrm{T}}{\partial \mathrm{x}} + \mathrm{v}\frac{\partial \mathrm{T}}{\partial \mathrm{y}}\right) = \frac{\partial}{\partial \mathrm{x}}\left(\mathrm{k_f}\frac{\partial \mathrm{T}}{\partial \mathrm{x}}\right) + \frac{\partial}{\partial \mathrm{y}}\left(\mathrm{k_f}\frac{\partial \mathrm{T}}{\partial \mathrm{y}}\right) \tag{3.14}$$

where, ∇ is the Laplace operator, Z is the vector function, P is the pressure, ρ and ρ_f are fluid density, k_f is the thermal conductivity of the fluid, u and v are velocities at x and y coordinates, T is the temperature.

This continuity, momentum and energy equations are used to solve for only laminar natural convection model. In order to include the radiative heat loss, radiosity equations

need to be considered for the specific geometry. The radiant heat loss from a given surface includes emitted and reflected thermal energy. Emissivity of the surface determines the emissive loss; while the reflected energy flux is dependent on the incident energy flux from the surroundings, which then can be expressed in terms of the energy flux from all the other surfaces of the geometry. The energy flux reflected from surface '*i*'' is given by [130];

$$q_{out,i} = \varepsilon_i \sigma T_i^4 + (1 - \varepsilon_i) q_{in,i} \quad (3.15)$$

The amount of incident energy upon a surface from another surface is a direct function of the surface-to-surface "view factor"F_{ji}. The incident energy flux $q_{in,i}$ can be expressed in terms of the energy flux leaving all other surfaces as:

$$A_i q_{in,i} = \sum_{j=1}^{N} A_j \, q_{out,j} F_{ji} \quad (3.16)$$

For *N* surfaces, view factor reciprocity theorem gives

$$A_j F_{ji} = A_i F_{ij} \quad (3.17)$$

Therefore $q_{in,i}$ is expressed as:

$$q_{in,i} = \sum_{j=1}^{N} F_{ij} \, q_{out,j} \quad (3.18)$$

Substituting Eq. (25) in Eq. (22),

$$q_{out,i} = \varepsilon_i \sigma T_i^4 + (1 - \varepsilon_i) \sum_{j=1}^{N} F_{ij} \, q_{out,j} \quad (3.19)$$

Eq. (26) can be re-written as:

$$J_i = E_i + (1 - \varepsilon_i) \sum_{j=1}^{N} F_{ij} J_j \quad (3.20)$$

Also

$$J_i = (1 - \varepsilon_i) \sum_{j=1}^{N} F_{ij} J_j = E_i \quad (3.21)$$

$$\sum_{j=1}^{N} (\delta_{ij} - (1 - \varepsilon_i) F_{ij}) J_j = E_i \quad (3.22)$$

Where,

$$\delta_{ij} = \begin{cases} 1 \; when \; i = j \\ 0 \; when \; i \neq j \end{cases}$$

The radiosity equation is expressed in vector form as:

$KJ = E$

where, K is an $N \times N$ matrix and $K = (\delta_{ij} - (1 - \varepsilon_i)F_{ij})$; J is the radiosity vector, and E is the emissive power vector.

3.11.1.5 Thermo-physical properties of the material for thermal modelling

The construction of the CPV module with DiACPC-55 concentrator is already describes in chapter 2. The thermal analysis has been carried out with the same design configuration of the CPV module. The solar cell is considered to be encapsulated in 0.5 mm thick sylgard material on the front and rear surfaces. The rear-plate is standard 3mm thick window glass, and the front glass is the 2 mm thick, low iron content soda-lime glass. The thermo-physical properties of the components in the CPV module used in this simulation is shown in table 3.2.

Table 3.2 Thermo-physical properties of the material used in CPV module

Component	Material	Thickness (mm)	Thermal Conductivity ($Wm^{-1}K^{-1}$)	Density ($Kg.m^{-2}$)	Specific Heat Capacity ($J.kg^{-1}.K^{-1}$)
Concentrator	Polyurethane	14.5	0.1875	1162	1465
Encapsulation	sylgard	0.5	0.16	1030	1100
Solar cell	Silicon	0.3	148	2330	712
Rear-plate/ Front glass	glass	2/3	1.4	2500	750

The simulation study has been carried out with the solar radiation that reaches the solar cell, which is calculated by the optical efficiency of the concentrator unit. For DiACPC-55 the optical efficiency is found to be 83% in the optical performance analysis. Therefore the source of the energy at solar cell is considered as 83% of the total solar radiation incident on the aperture. This study also investigates the change in temperature of the solar cell with the variation of the heat transfer co-efficient of the air that is in contact with the CPV unit.

The thermal simulation is carried out with a CPV configuration with single trough concentrator unit, 3 troughs concentrator unit and 8 trough concentrator units. The last

one is the module size modelling to predict the difference in temperature of the solar cells at the edges and in the middle of the module.

3.11.2 Thermal modelling results and discussion

The thermal modelling results of the CPV modules for different module configuration are discussed in the following sections. The initial thermal modelling is carried out for the single trough concentrator unit varying the heat transfer co-efficient of air. This is by modelling of followed by the CPV system configuration with 3 concentrator units. In the final approach a more realistic CPV configuration is considered as a framed CPV system including cover glass. A schematic diagram showing heat loss from the CPV module with 3 concentrator trough is shown in figure 3.27. The incident energy as solar radiation into the CPV modules increases the temperature of the solar cell. With the increase in temperature, heat from the solar cell dissipated within the different components of the modules and to the ambient. Heat from the solar cell is first dissipated to the encapsulation, rear plate and the concentrator by conduction and to the ambient by convection and radiation. A thermal network diagram of the designed CPV module is shown in figure 3.28

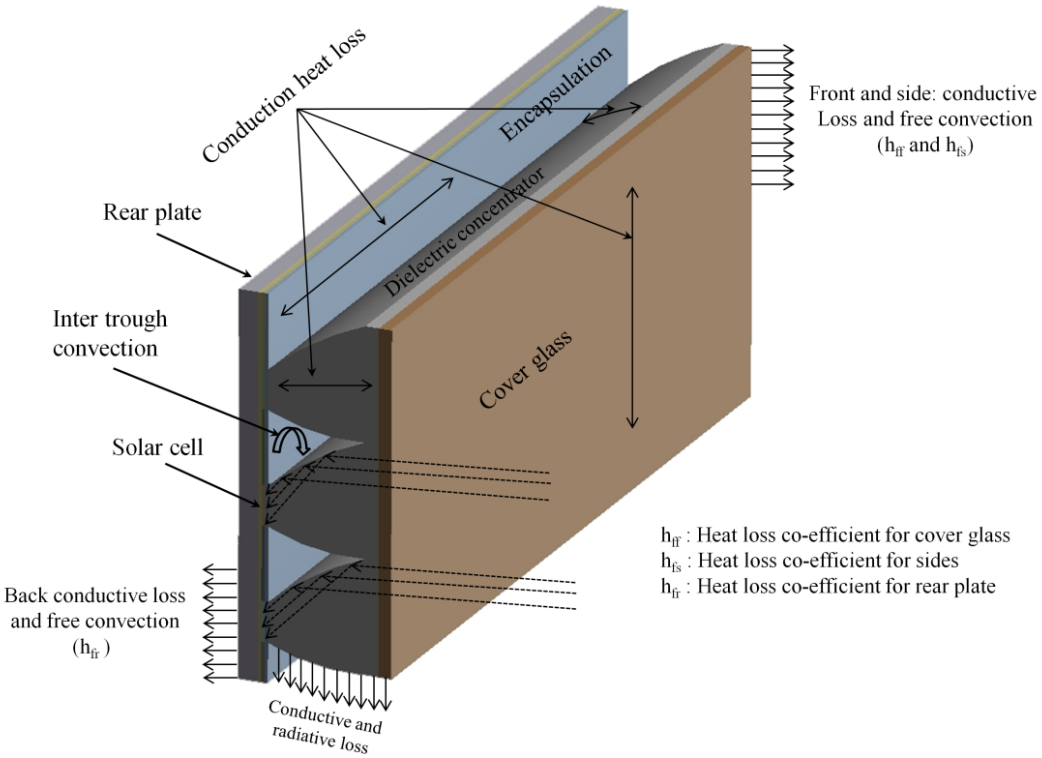

Figure 3.27 Schematic diagram of the CPV module with three troughs of concentrators showing heat loss mechanisms

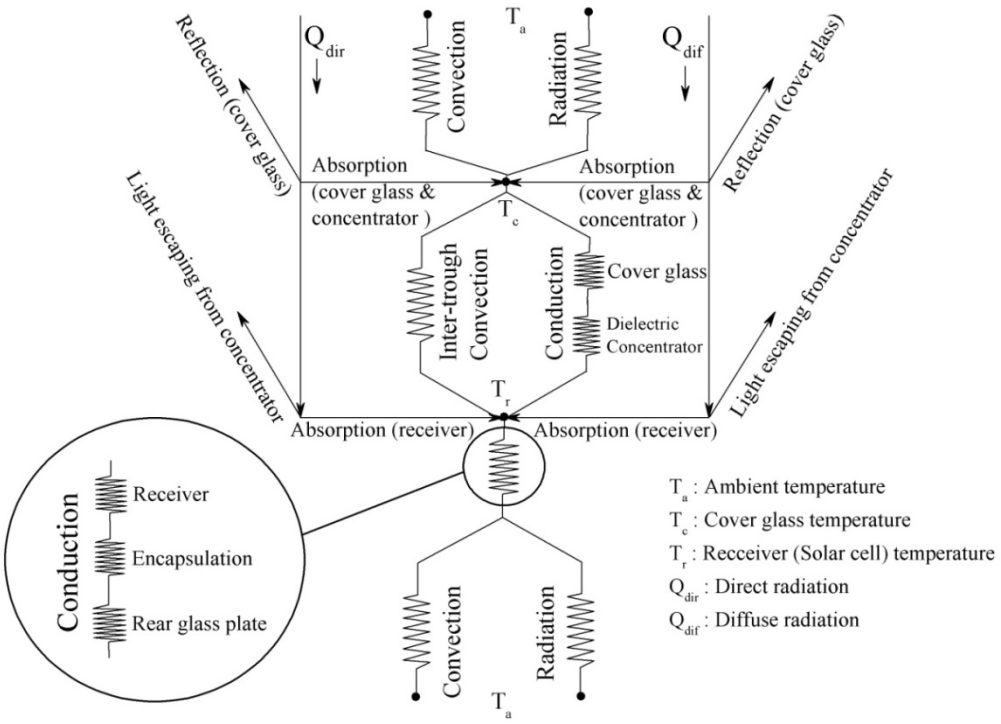

Figure 3.28 Thermal network diagram of the CPV module showing the input energy and heat resistances

3.11.3 Thermal modelling with single trough concentrator

The system configuration of the CPV module with single trough concentrator unit is shown in figure 3.29. The present study is carried out to determine the effect of an increase in solar irradiance and heat transfer co-efficient (HTC) of the surrounding air. To investigate the effect of increase in HTC of air, study has been carried out with HTC from 5 $Wm^{-2}K^{-1}$ to 20 $Wm^{-2}K^{-1}$ in 5$Wm^{-2}K^{-1}$ interval. The solar irradiance is considered from 500W/m^2 to 1000W/m^2 in 100W/m^2 interval for detailed investigation.

The images of the temperature distribution in the CPV unit with solar radiation 1000 W/m^2, when the HTC of air is equal to 5 $Wm^{-2}K^{-1}$, is shown in figure 3.30. The maximum temperature of the solar cell is found to be 81.9^o when the ambient temperature is 22^{o}C. At this solar radiation it is found that the temperature of the rear-plate is equal to solar cell. However, the temperature of the solar cell is not same as the rear-plate for the solar radiation of 500 W/m^2 and HTC of air 20 $Wm^{-2}K^{-1}$, as shown in figure 3.31.

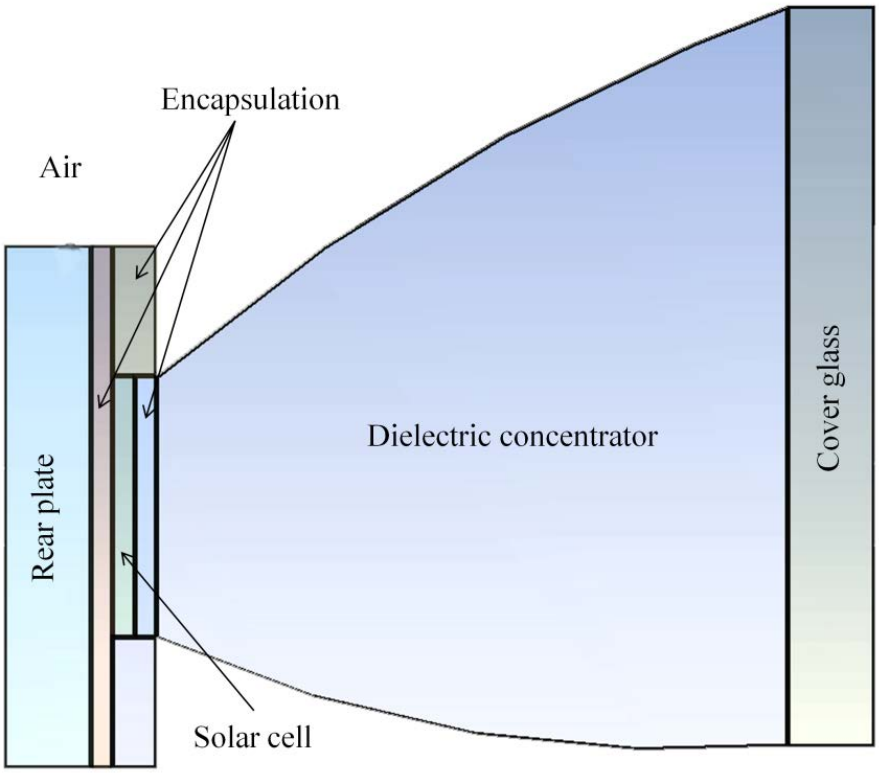

Figure 3.29 Configuration of the CPV module with single trough concentrator unit for thermal modelling

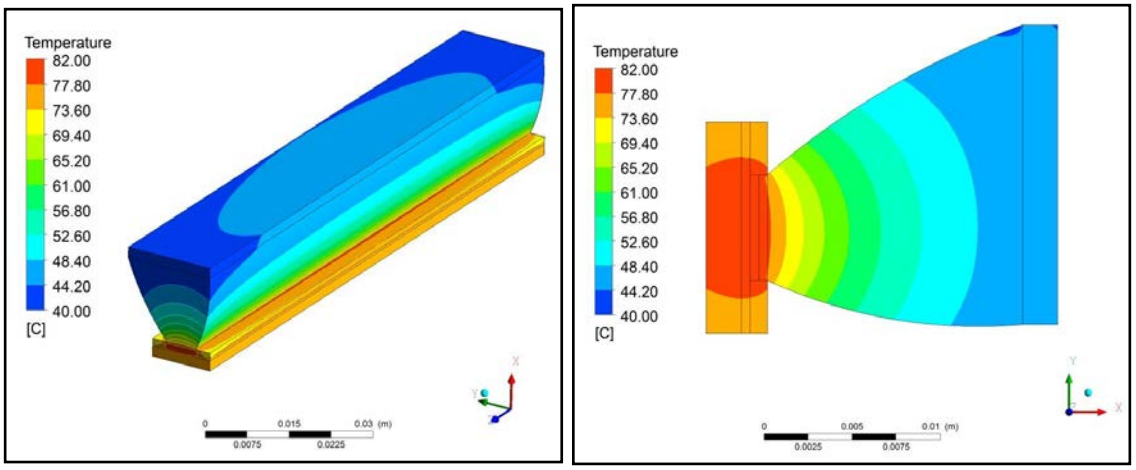

(a) (b)

Figure 3.30 Temperature distributions in the CPV unit with DiACPC-55, 1000 W/m^2 flux and HTC 5 Wm^{-2}K^{-1} of air (a) 3D view (b) cross sectional view

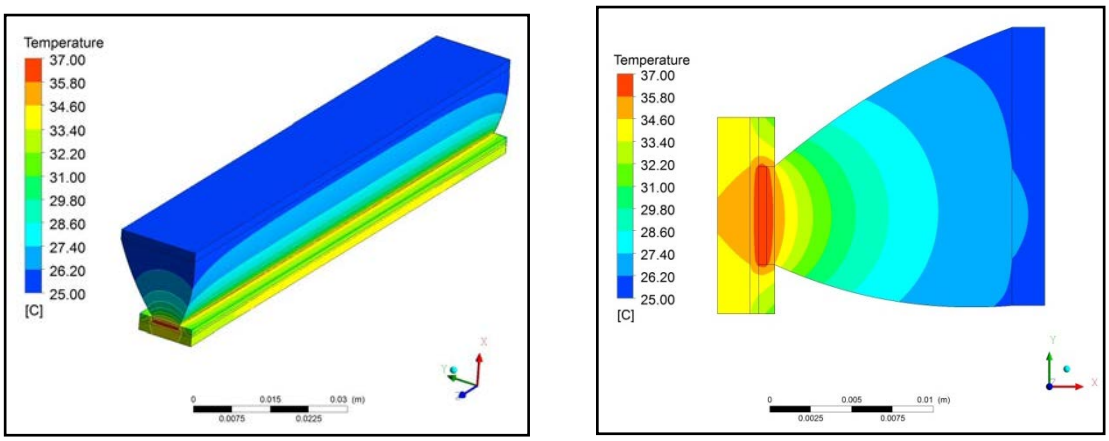

(a) (b)

Figure 3.31 Temperature distributions in the CPV unit with DiACPC-55, 500 W/m^2 flux and HTC 20 Wm^{-2}K^{-1} of air (a) 3D view (b) Cross-sectional view

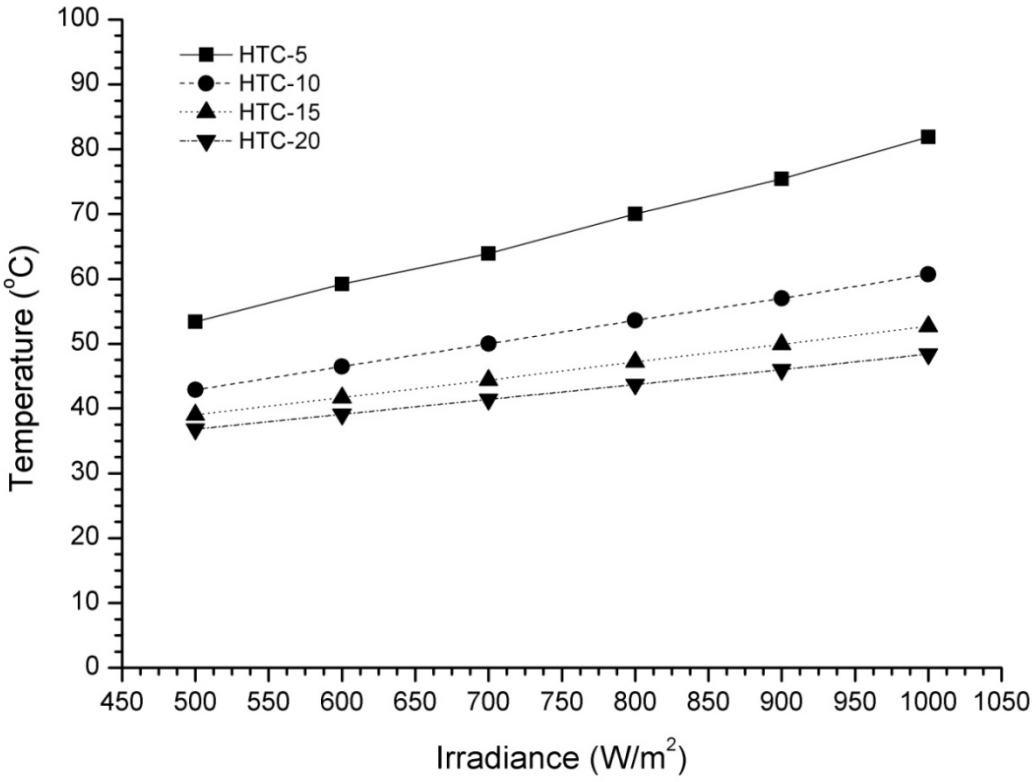

Figure 3.32 Variation of temperature of solar cell with the solar flux incident on the aperture for different HTC of air

It is found that the temperature of the solar cell can reach up to 53.4^o; with a HTC of 5 Wm^{-2}K^{-1} and solar irradiance 500W/m^2, when the ambient temperature is 22^{o}C. Figure 3.32 shows the variation of the temperature of the solar cell with variation solar

radiation for different HTC of air. It can be observed that the temperature reduces linearly with decrease in solar radiation and with increase in HTC of air.

3.11.3.1 Thermal modelling with three concentrator trough as one unit

This thermal modelling study has been carried out to compare the temperature of the solar cell with a non-concentrating unit. The 3D simulation results of predicted isotherms of the CPV system with 3 solar cells and 3 concentrator troughs for 1000 W/m^2 solar irradiation is shown in figure 3.33. The boundary condition considered in this study is air with an ambient temperature of 22^{o}C and HTC of 5 Wm^{-2}K^{-1}.

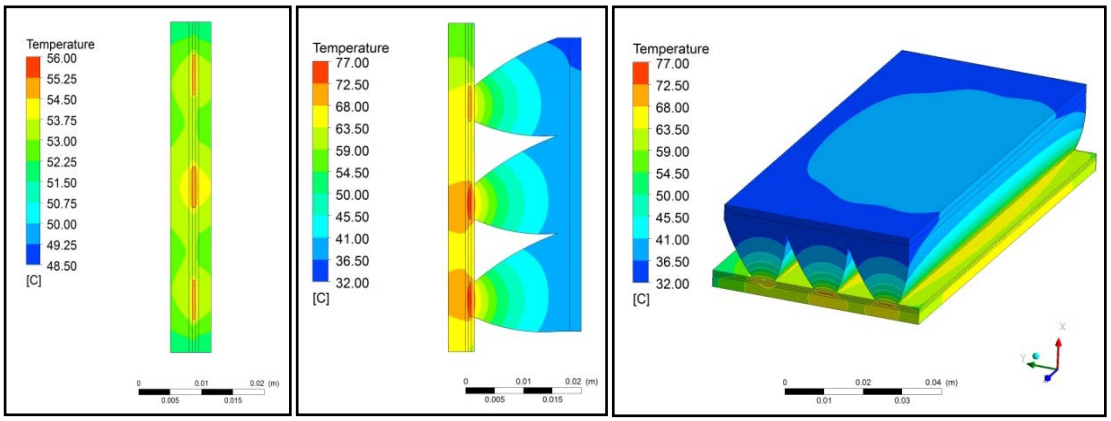

(a) (b) (c)

Figure 3.33 Predicted isotherm of (a) a non-concentrating PV module (b) 2D cross sectional view of CPV module with 3 concentrator trough (c) 3D view of the module for 1000 W/m^2 irradiance and heat transfer co-efficient 5 Wm^{-2}K^{-1}

The maximum temperature of the solar cell in the CPV system is found to be 77^{o}C, which is 55^o higher than the ambient temperature. The maximum solar cell temperature for a similar non-concentrating system is found to be 45^{o}C, which means a maximum 32^{o}C increase in temperature of the solar cell can be expected while using DiACPC-55 concentrator. The investigation of change in temperature with solar radiation shows that the solar cell reaches a maximum temperature of 46^{o}C for 500 W/m^2 as shown in figure 3.34.

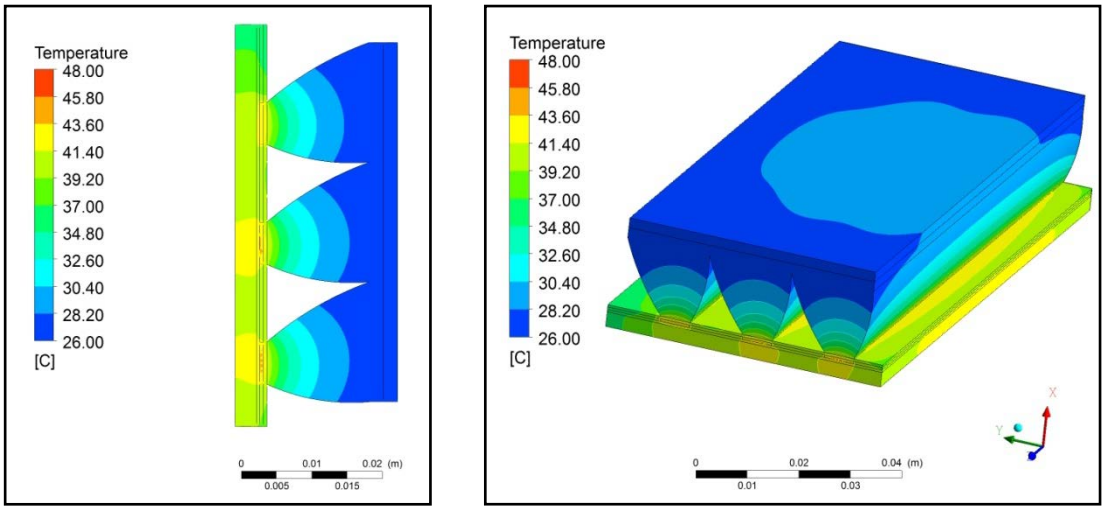

(a) (b)

Figure 3.34 a) 2D cross sectional view and (b) 3D view of the predicted isotherm of the CPV module with 3 concentrator troughs for 500 W/m^2 irradiance and heat transfer co-efficient 5 Wm^{-2}K^{-1}.

3.11.3.2 Thermal modelling with eight concentrator trough as one unit

Thermal modelling with 8 concentrator trough as one unit has been carried out as a realistic approach to predict the module and cell temperature of the CPV module in Edinburgh, with a the solar irradiance of 1000 W/m^2. Due to the weather conditions and the windy climate of Edinburgh, the HTC of air is considered to be 10 Wm^{-2}K^{-1} and ambient temperature as 10^{o}C. The CPV module is modelled to be in an enclosure with front glass and frame as shown in figure 3.35.

The temperature of the solar cell is found to be 41.6^{o}C for an irradiance of 1000 W/m^2, which is equal to the temperature of the rear-plate at the centre as shown in figure 3.36 (cross-sectional view of the simulated isotherm of the centre plane of the CPV module). Towards the edges of the rear-plate the temperature is found to be less than the solar cells by 3^{o}C. The temperature of the cell and the module is found to be less than the previous thermal modelling because of the combined effect of lower ambient temperature and higher HTC of air at the boundary of the module.

Due to the air trapped inside the enclosed module, air convection has also contributed to the reduction of temperature at the edges of the solar cell. The thermal modelling is

validated by outdoor characterisation of the CPV module as results closely match with those of the simulation.

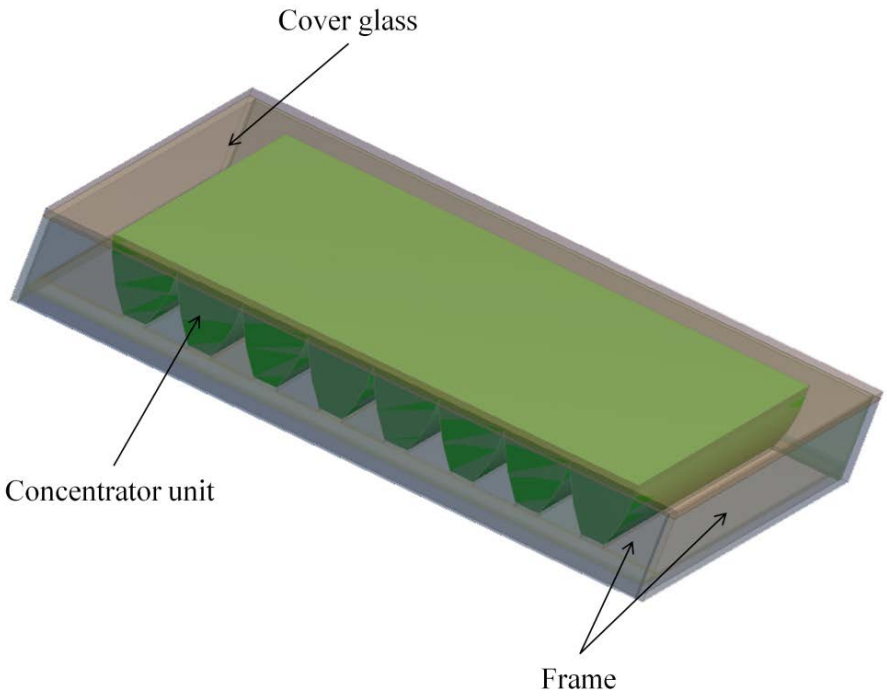

Figure 3.35 Schematic diagram of CPV module configuration with a concentrator unit of eight troughs enclosed with cover glass and frame

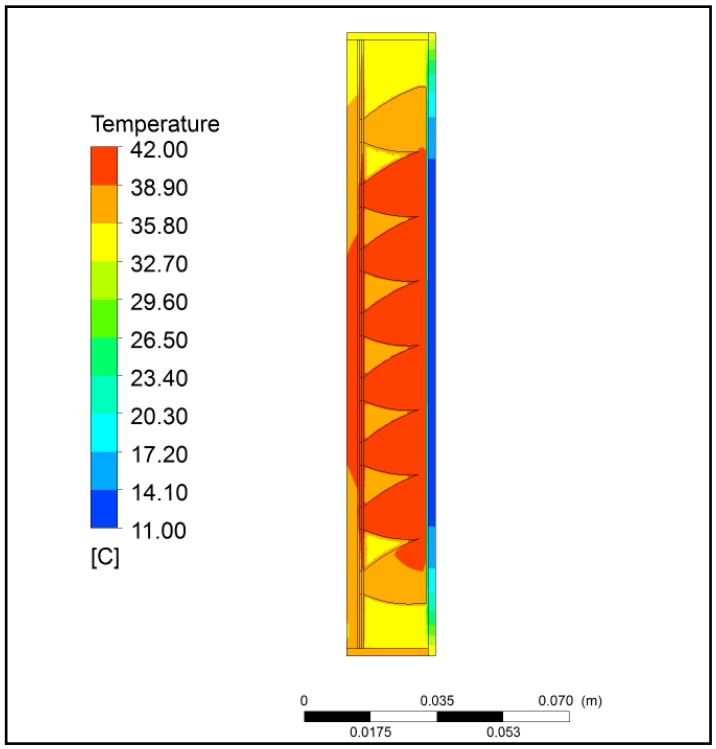

Figure 3.36 Predicted isotherm of the CPV module for irradiance 1000 W/m^2, HTC 10 Wm^{-2}K^{-1} and ambient temperature 10^{o}C

3.12 Thermo-electrical modelling of the CPV module with the DiACPC-55 concentrator

Basic electrical modelling of the designed CPV system has been carried out to estimate the power output of the system with the change in temperature. The thermal and electrical properties of the solar cell supplied by the manufacturer are used in an in-house MATLAB codes to simulate the IV characteristics. The study has been carried out for a $5.5W_p$ CPV module with 28 solar cells; 2 parallel strings of 14 solar cells in series (third prototype module of this project). The resulting IV characteristics of the concentrating and non-concentrating modules with a variation of solar radiation are shown in figure 3.37. The performance of the concentrating and non-concentrating module is compared with a similar system kept at a stable temperature of 22^oC, which is the standard temperature for the solar cell data supplied.

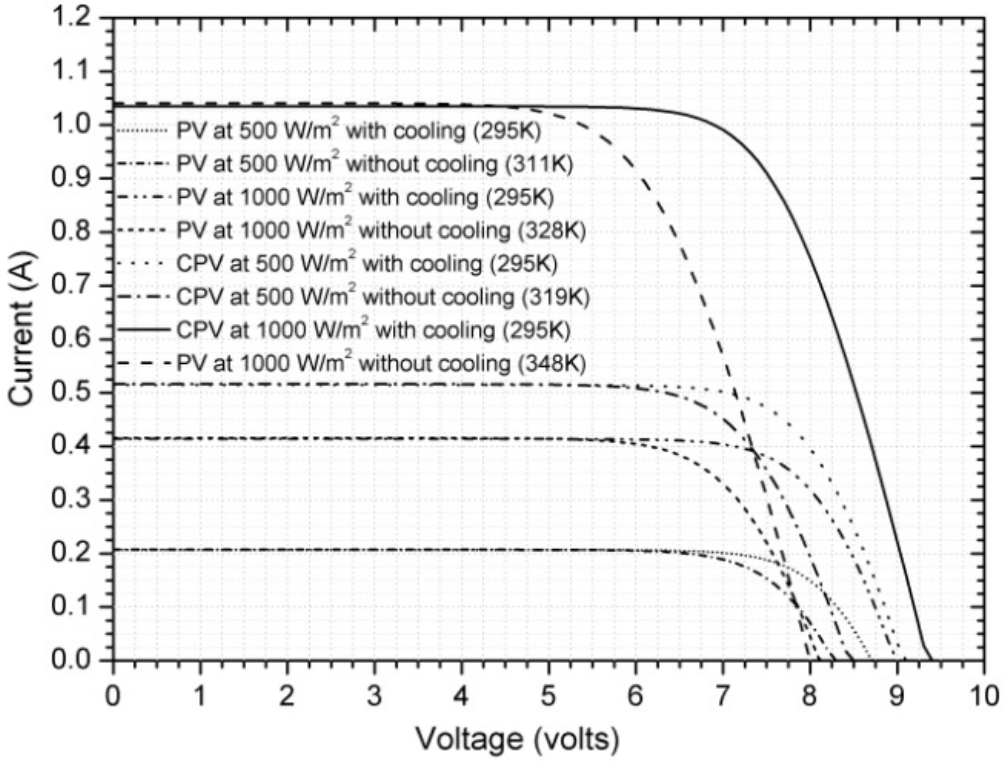

Figure 3.37 I-V characteristics of the prototype CPV and non-concentrating PV modules for different solar radiation

It was found that the open circuit voltage of the CPV system reduced by 14.9% (1.4 volts) at 75^oC compared to the similar CPV module at 22^oC. However, compared to a non-concentrating counterpart in similar conditions, the open circuit voltage of the CPV module is found to have decreased by only 2.4% (0.2V) for a solar radiation of 1000

W/m^2. For a lower solar radiation of 500 W/m^2 it is observed that the open circuit voltage of the CPV system is higher than the non-concentrating counterpart by 2.4% (0.2 volts). The higher short circuit current in the CPV module may be the reason to achieve higher open circuit voltage compared to non-concentrating module for 500W/m^2 irradiance; when the temperature difference of these two modules was only 8^{o}C. The change in open circuit voltage (V_{oc}), fill factor (FF), and short circuit current (I_{sh}) of the designed CPV system with incident solar radiation is shown in figure 3.38. The study shows that the FF of the CPV system is expected to reduce by 7% from 0.73 to 0.66 with an increase in solar radiation from 500 W/m^2 to 1000 W/m^2, whereas the short circuit current has increased by 2 times from 0.52 A to 1.04 A. This results in the maximum power of the CPV system increasing from 3.2 watt to 5.5 watt (71%).

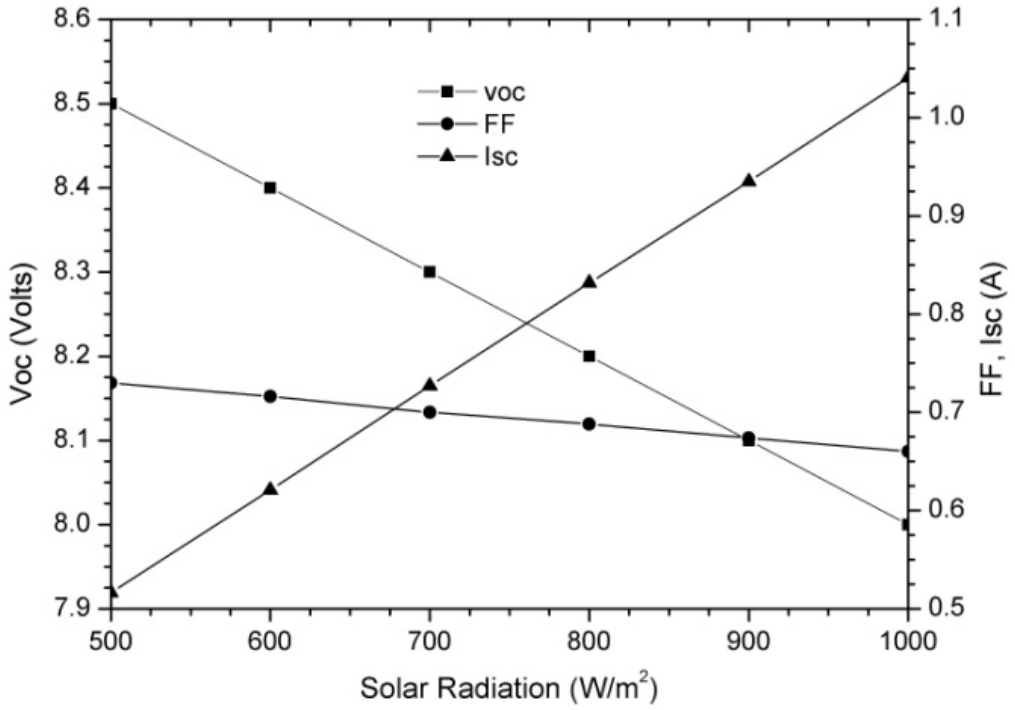

Figure 3.38 Dependence of open circuit voltage, short-circuit current and fill factor of CPV module with solar radiation

Compared to the non- concentrating PV module the short circuit current under 1 sun has increased by 2.5 times, whereas the maximum power ratio is only equal to 2.45. Therefore a loss of 2% is calculated due to the increase in solar cell temperature within the CPV system.

3.13 Conclusion

A detailed optical performance study has been presented to optimise a low concentrating line axis dielectric ACPC suitable for building façade integration. The present study has been carried out with three concentrator designs with acceptance half angles (0^o & 55^o), (0^o & 66^o) and (0^o & 77^o) termed as DiACPC-55, DiACPC-66 and DiACPC-77. The designed concentrators are realised by truncation of 68%, 55% and 40% of complete ACPC profiles with acceptance angles (0^o&33^o), (0^o&37^o) and (0^o&40^o) respectively. The concentration ratios of all the designed concentrators are equal to 2.82 for comparison of optical performance. Furthermore, the study investigated the optical performance of the designed concentrators integrated within a building façade, with seasonal variation of solar altitude angle for higher latitudes.

A maximum 2.2 times increase in range of acceptance angles for DiACPC-55 has been found with the truncation of complete dielectric ACPC profile. The angular acceptance is 100% within the acceptance half angle range; with an enhancement of angular acceptance to collect incident radiation both in positive and negative direction, outside the acceptance half angles. A maximum optical efficiency of 83% is found for DiACPC-55, which remains stable within ±7% throughout the range of acceptance angles. For DiACPC-66 and DiACPC-77 the maximum optical efficiency is found to be 82.4% and 81.7%, which decreases at larger incident angles and drops sharply after 55^o. Inclination of the designed concentrator shows that for a 5^o 'truncation after inclination' (TAI) of DiACPC-55, a 13% increase in the range of acceptance angles can be achieved with a value of 99% angular acceptance at 69^o incidence angle. However the optical efficiency drops to 71% at 69^o incidence angle. While several sharp intensity peaks can be observed at the receiver for direct solar radiation, the energy is found to be well distributed at the receiver for a wide range of incident angles. The energy flux distribution at the receiver with diffuse radiation is found to be homogeneous, with average intensity of 520 W/m^2. The study shows that, although the contribution of diffuse radiation is much less than direct radiation, it should not be ignored for northern Europe climates, where the number of sunny days is less. Based on the annual solar energy collection by all the systems it is concluded that DiACPC-55 can collect 1.64% and 3.53% higher energy compared to DiACPC-66 and DiACPC-77 respectively and is the optimum dielectric concentrator to use in building facades in higher northern latitude ($>55^o$).

The 3D thermal modelling of the CPV modules, with the designed concentrator DiACPC-55 was carried out and showed that the solar cell temperature can reach up to a maximum 81.9^{o}C; this was for conditions of 1000 W/m^{2} irradiance, HTC 5 Wm^{-2}K^{-1} and ambient temperature 22^{o}C. With the change in solar flux and heat transfer co-efficient of air, the temperature of the solar cell is found to vary linearly. In another thermal study, the temperature of the solar cell of the CPV module is found to be 32^{o} higher than a similar non-concentrating module for 1000W/m^{2} irradiance. Thermal modelling with realistic parameters to predict the temperature in Edinburgh shows that the maximum module and cell temperature can reach up to 41.6^{o}C.

The theoretical electrical characterisation of the CPV module, to investigate the effect of the rise in temperature of the solar cell shows that the open circuit voltage will drop by 2.4% compared to the non-concentrating modules under 1 sun. For a lower solar intensity at 500 W/m^{2} the temperature of CPV module is found to be only 8^{o}C higher than non-concentrating module. The fill factor drops by 7% with increase in solar radiation from 500 W/m^{2} to 1000 W/m^{2}. The study concludes a 2% higher loss in the power output of the CPV system compared to non-concentrating one, caused by the higher temperature of the solar cell.

Chapter 4

Indoor characterisation of dielectric concentrator

This chapter provides details of the indoor experimental characterisation of the DiACPC-55 concentrator to investigate the spectroscopic properties, optical loss and optical performance of the concentrator when integrated in a CPV system. The IV characterisation of the different prototype CPV modules is reported to optimise the module design. The performance of the CPV modules under the solar simulator is compared with the theoretical optical performance of the dielectric concentrator and with a non-concentrating counterpart. Finally the improvement in performance due to the different design modifications of the CPV modules is analysed and reported.

4.1 Introduction

The optical properties of the material used to manufacture the dielectric concentrator, in addition to the geometrical profile, plays significant roles in a photovoltaic concentrator. The optical properties include the transmission and absorption of solar radiation within the range of the spectral response of the solar cell. It is very important to maintain the required profile of the dielectric concentrator during the manufacturing process. Considering the possible machining error involved in the manufacturing of the concentrator, it is important to investigate the final profile of the manufactured concentrator to compare with the original design for loss analysis. Machining error and rough surfaces can cause optical losses by means of light scattering and escaping, which need to be investigated.

The performance of the photovoltaic concentrator can be experimentally analysed by evaluating the performance of a CPV module with the concentrator and comparing it with a non-concentrating counterpart. In an indoor controlled environment the module can be analysed for a variation in radiation intensity with different incident angle. For a static dielectric concentrator designed for a particular range of acceptance angles, it is

very important to evaluate the performance for all the incidence angles within the range. The indoor study with the different radiation intensities helps to understand the performance of the CPV module in the outdoor environment with variation of solar irradiation. The variation of all of the parameters, such as fill factor and conversion efficiency, with variation of radiation intensity can also be analysed thoroughly in the indoor environment.

4.2 Spectroscopic performance analysis of dielectric concentrator and CPV module

Spectroscopic analysis of the dielectric concentrator and CPV module provide detailed information of the absorption losses within the concentrator and the change in spectral response of the CPV module compared to the bare solar cell. A spectroscopic study has been undertaken to investigate the transmission of the different optical components used in the CPV module and the external quantum efficiency (EQE) of the module.

4.2.1 Transmission properties of the materials used in the CPV module

The transmittance of the different optical components of the CPV module is shown in figure 4.1. The transmittance of the concentrator material (polyurethane) is found to be 80%-90% over the wavelength range of 420nm to 1100nm, with a maximum transmittance of 89.6%. The transmittance is found to decreases sharply below 420nm and falls to zero at 400nm. The high absorption below 400 nm in this polyurethane material is due to the uv-stabilizer, which reduces the degradation of the material; therefore all light of wavelengths below 400nm is absorbed. The broad absorption peaks around 930 nm and 1030 nm are due to harmonics of CO and CH bond stretching in the polymer [250]. The transmittance of the encapsulation material (sylgard-184) is found to be higher than 90% within the range of 450nm to 1100nm, and slowly drops to 71% at 300nm. Two small absorption peaks at 910nm and 1020nm can be observed in the absorption spectrum of the sylgard-184 as well. The transmittance of the BF glass is found to be higher than 90% above 350nm with a maximum of 91.2%. However, at 300nm the transmittance drops to 62%.

Considering the known spectral response of the silicon solar cell used, an average AM1.5G weighted spectrum has been calculated to estimate the average transmittance within the range 300-1100nm. The average AM1.5G spectrum weighted transmittance

within this range for the 16.4 mm thick polyurethane concentrator is found to be 81.9%. The main reason for the decrease in average transmittance of the concentrator material is due to the high absorption below 420nm by the UV-stabiliser. The stabiliser is required to resist the photo-degradation of the plastic. The average AM1.5G spectrum weighted transmittance within the same spectral range for 0.3 mm thick encapsulation material (sylgard-184) and 2.75 mm thick cover glass (BF glass) is found to be 91.6% and 92% respectively

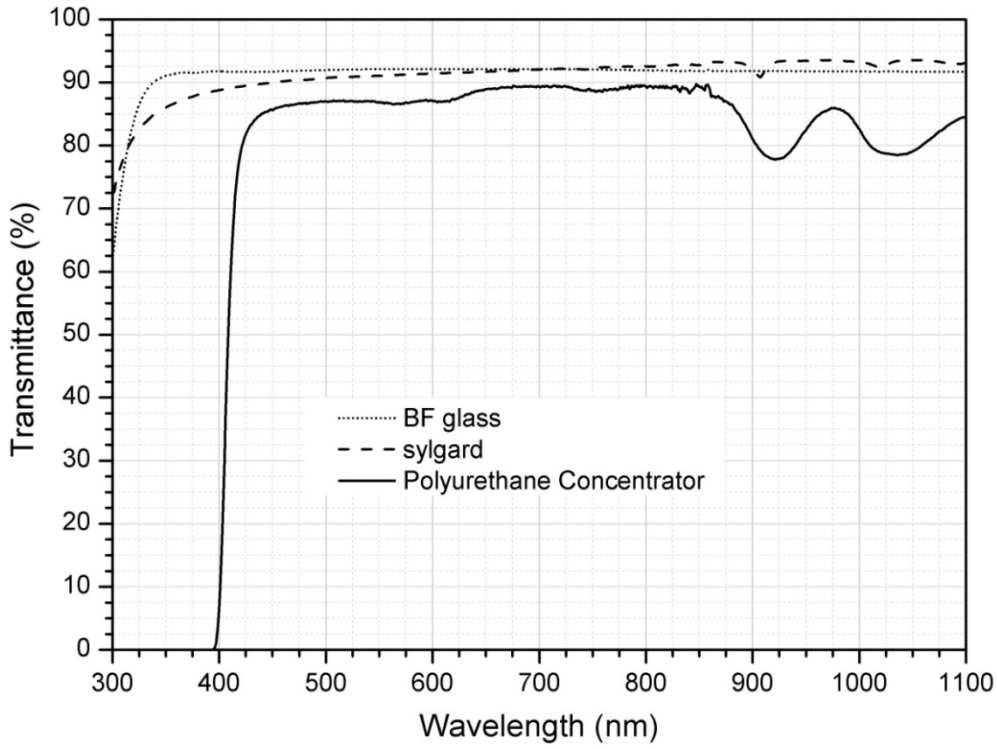

Figure 4.1 Transmission of the optical components used in the CPV module

4.2.2 External Quantum Efficiency study of the concentrating system

An EQE analysis of the bare, encapsulated crystalline solar cell and the prototype CPV has been undertaken to understand the change in spectral response of the module. Due to the absorption of the concentrator material, the EQE of the CPV module drops to zero at 400nm while the EQE of the both bare cell and encapsulated cell is found to be 73-74% (Figure 4.2). The decrease in EQE of the prototype CPV module over the range of 400 nm to 1100 nm is due to the optical losses in the concentrator. The reduction in EQE of the CPV module compared to the bare solar cell resembles the theoretical optical efficiency of the concentrating system reported earlier [251]. A drop in EQE of

the CPV module at ~ 930 nm can be observed, which is due to the absorption of the concentrator material as mentioned in Section 4.2.1.

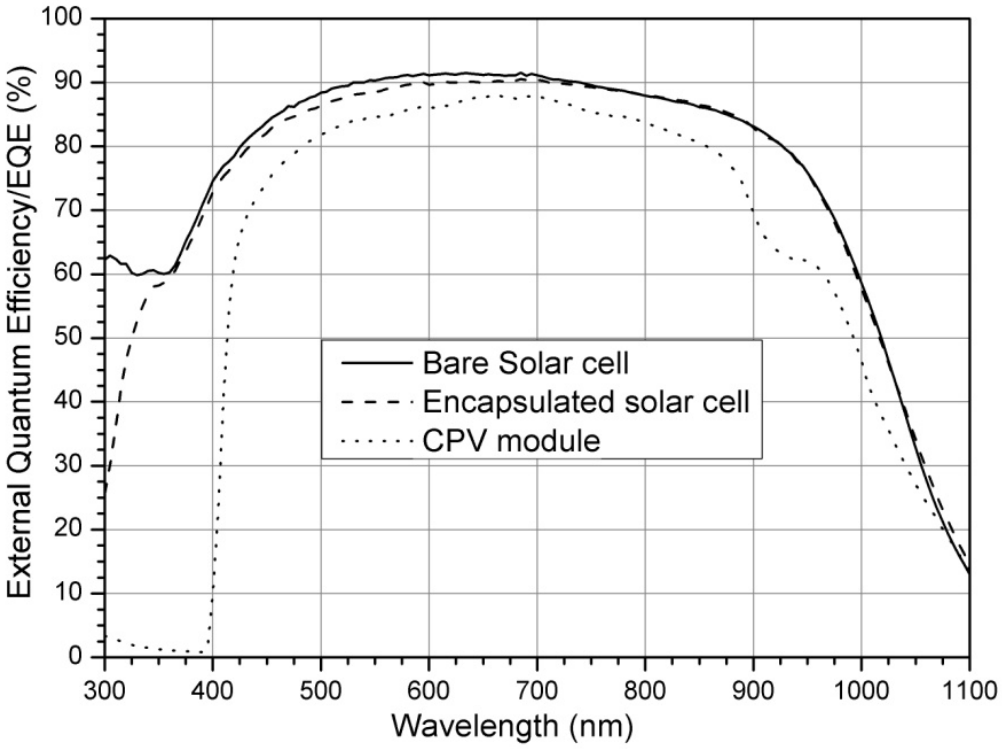

Figure 4.2 Quantum efficiency of the bare cell, encapsulated cell and CPV module

4.3 Optical loss analysis in a dielectric concentrator using the goniometer set-up

A detailed investigation of the optical losses in the concentrator caused by light escaping from the parabolic sides has been carried out to understand the difference between the theoretical and experimental optical efficiency of the CPV system. The parabolic surface of the casted concentrator has microscopic steps within the mould, due to the machining error. This caused a fraction of the light that reached the parabolic sides to escape, instead of reflecting back to the receiver. The detail of the goniometer set-up used is described in section 2.8.4. This study has been carried out to investigate the optical loss in the manufactured concentrator for different incidence angles and beam positions on the aperture of the concentrator. The light source (He-Ne laser) and the detector is positioned at 0^o, aligning the beam to be incident perpendicularly on both the aperture of the concentrator and the detector. The results are presented as negative and positive angles of the detector position for clockwise and anticlockwise rotation respectively as shown in figure 2.22 (page 88). The monochromatic light beam (630 nm) from the laser source is incident on the aperture of the dielectric concentrator and

the direction of the transmitted light is investigated by rotating the detector from -90^o to +90^o across the receiver. The angle of incidence is changed by rotating the source over the range of acceptance angles 0^o to 55^o in 10 degree intervals. Results have been measured for the light incident across different sections of the 17 mm aperture in 2 mm steps.

The experimental investigation of the optical losses due to light escaping from the dielectric concentrator is presented in terms of the optical efficiency of the light incident at different aperture positions with different angles of incidence, as shown in figure 4.3 and figure 4.4. The estimation of light escaping and scattering from the concentrator is investigated by comparing the ray trace diagram, theoretical optical efficiency and the optical efficiency measured across the receiver in the goniometer set-up.

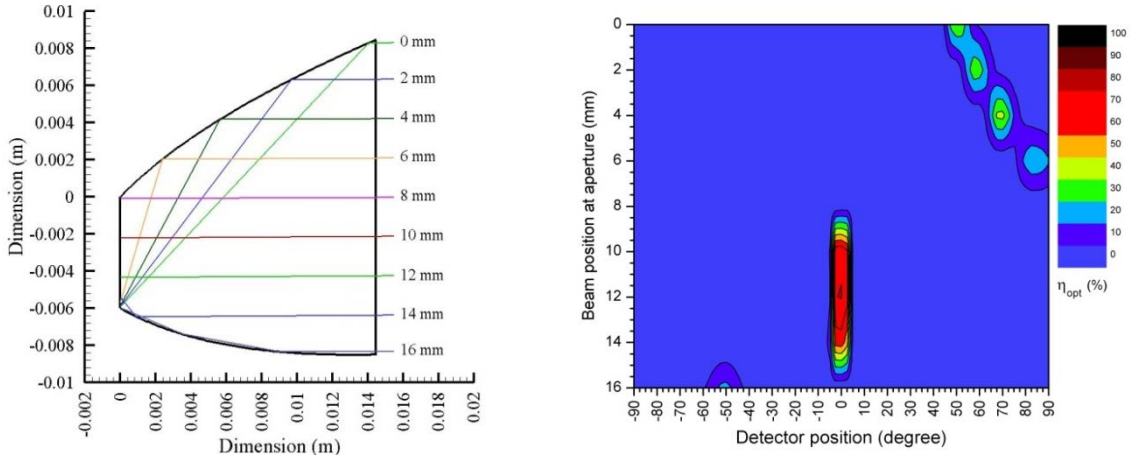

(a) (b)

Figure 4.3 (a) Ray-tracing image for ray incident on different sections of the aperture of the dielectric concentrator and (b) Optical efficiency of the concentrator for rays incident at different positions of the aperture with an angle of 0^o.

With perfect dielectric concentrator, the maximum optical efficiency should be measured at a particular detector position (angle) for a certain beam position at a given aperture and a certain incidence angle. The maximum optical efficiency is expected to be equal to the theoretical optical efficiency value for all aperture positions of a particular incidence angle. However, higher optical losses in the concentrator are observed compared to the theoretical study.

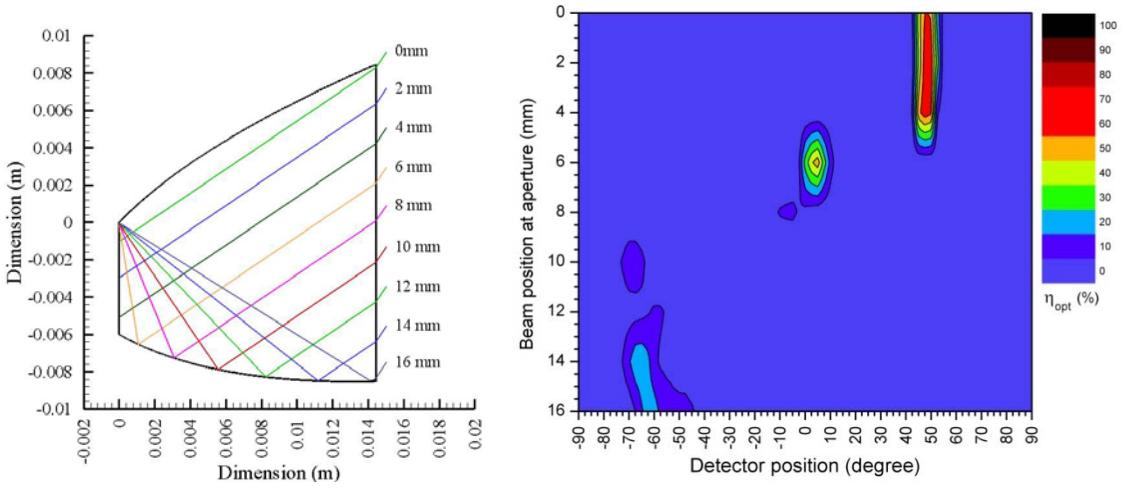

(a) (b)

Figure 4.4 (a) Ray-tracing image for ray incident on different sections of the aperture of the dielectric concentrator and (b) Optical efficiency of the concentrator for ray incident at different positions of the aperture with an angle of 55^o

The study shows that while reflecting from the parabolic sides, a fraction of light can also escape. It is also observed that most of the incident light reflected by TIR from the parabolic surfaces scatters within a specific range of angles. The surface roughness of the parabolic sides, caused during the casting of the concentrator, results in the light scattering and escaping. The scattering of the light may also be caused by the presence of micrometer-sized air bubbles in the dielectric material. It is observed that for the 0^o angle of incidence, some rays escape from the parabolic surfaces (beam position 2mm and 4mm in Figure 4.3 (a) & (b)), while others escape after multiple reflection within the concentrator from either the aperture or the parabolic sides (beam position 16mm in Figure 4.3 (a) & (b)). A maximum optical efficiency of 80.5% is achieved for the ray incident perpendicular (0^o incidence angle) to the aperture surface at the 10 mm position. The corresponding estimated theoretical optical efficiency of the CPV system is found to be 84.2% [251]. For the light rays reflecting from the parabolic sides, the optical efficiency is found to be distributed over a range of detector positions, instead of a sharp peak at a certain detector position (beam position 2mm and 4mm in Figure 4.3 (a) & (b)). For an increase in incidence angle, the rays are found to escape and scatter more from the parabolic surfaces which cause a reduction in the optical efficiency of the concentrator (beam position 14mm and 16mm in Figure 4.4 (a) & (b)). For a 55^o incidence angle the detector shows a 10^o scattering of the ray, with a peak optical efficiency of 66%, while the maximum estimated theoretical efficiency was 79%. For

higher incidence angles, the air-dielectric interface reflection losses at the aperture increase; this results in a further decrease of the optical efficiency of the concentrator. Some rays are found to be escaping due to the total internal reflection at the receiver (beam position 6mm and 8mm in Figure 4.3 (a) & (b)). The rays escaping from the aperture could not be detected, as they reflect back to the source position. However, with a solar cell, the encapsulation material and the receiver of the concentrator are attached together in a CPV module; these rays will reach the solar cell. The reflected rays coming out of the corners of the receiver and parabola increase the possibility of rays escaping from the concentrator-encapsulation interface of the CPV modules.

4.4 Validation of the dielectric concentrator profile using the profile scanning machine

The profile of the manufactured concentrator has been scanned to investigate any manufacturing defect in shape. The change in profile configuration can significantly alter the performance of the dielectric concentrator. Light can escape if the parabolic shape deviates from the designed profile. Because of the machining error the acceptance angle can change, which can increase or decrease the range of acceptance angles and the geometrical concentrator ratio. The surface profile of the manufactured concentrator and the designed concentrator profile are shown in Figure 4.5.

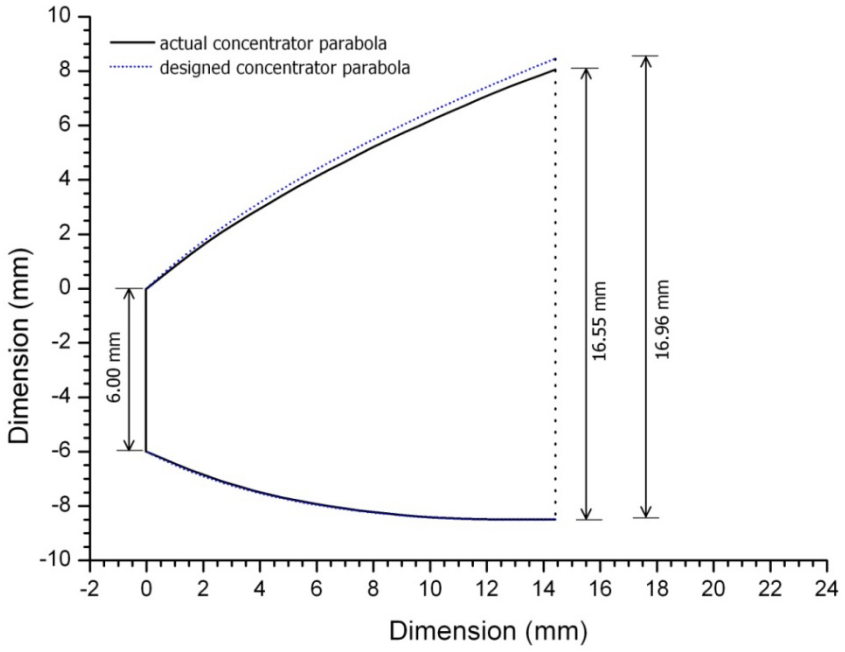

Figure.4.5 Designed concentrator profile and the profile of the manufactured concentrator trough.

A small variation of the position of one parabola at the aperture can be observed. Even though in two dimensional measurements the variation is only 0.41mm for a 116mm long concentrator trough, the total decrease in aperture area is 47.6mm^2. This corresponds to a 2.4% decrease in the aperture area, which in turn reduces the geometrical concentration ratio to 2.76. Even though the aperture area has decreased, the parabolic profile is found to be smooth, which indicates a change in the mounting angle of the parabola only. This will reduce the range of acceptance angles of the designed concentrator, changing the extreme acceptance angle to be less than 55^o.

4.5 IV characteristics of the first prototype module

The first prototype module is fabricated with 6 solar cells, consisting of two strings of three cells in series. The module includes three concentrator units with two concentrator troughs in each unit. The concentrator units haven't undergone post curing, so with the aperture surfaces still have the curved edges. For the first part of the experiment, the study has been carried out with a radiation intensity of 600 W/m^2, for inclination angles 0^o, 15^o, 30^o and 45^o. 600 W/m^2 is the minimum suggested radiation intensity from the ABET solar simulator for efficient use. The performance of the CPV-1 module is compared with a similar non-concentrating counterpart to investigate the performance of the DiACPC-55 concentrator. The IV-curve and the power curve of the non-concentrating module at 0^o are showing in figure 4.6. The maximum short circuit current is found to be 0.28A, with maximum power 0.31W. The fill factor is recorded to be 63.8%, which is considerably low for modules of crystalline silicon solar cells.

The I-V characteristics and the power curve of the CPV module for 0^o incidence angle are shown in figure 4.7. The maximum power of the CPV module is found to be 0.34W, which is very similar to the non-concentrating module (1.1 times higher). The short circuit current is found to be 0.38A, which is 1.36 times higher than the non concentrating counterpart. The reason for the lower power ratio compared to the short circuit current ratio is due to the decrease in fill factor of the CPV module compared to the non-concentrating counterpart. The fill factor is found to be considerably decreased to 53.7%, which reduces the maximum power of the CPV module. High optical loss and non-uniformity in the intensity distribution on the solar cell may be the major cause of the low fill factor observed in the CPV module.

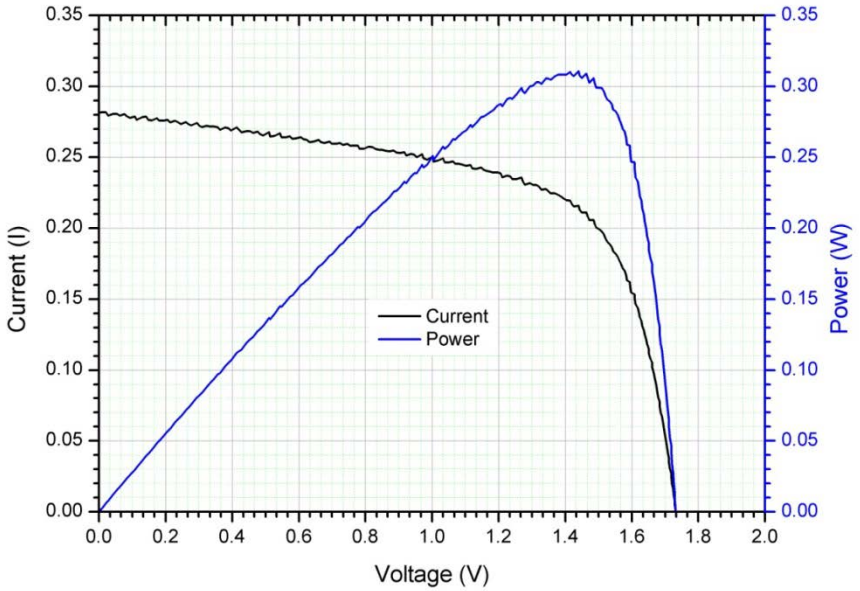

Figure 4.6 IV-characteristics and power curve of the first prototype non-concentrating module (FP-1) with 600 W/m^2 radiation intensity incident at 0^o

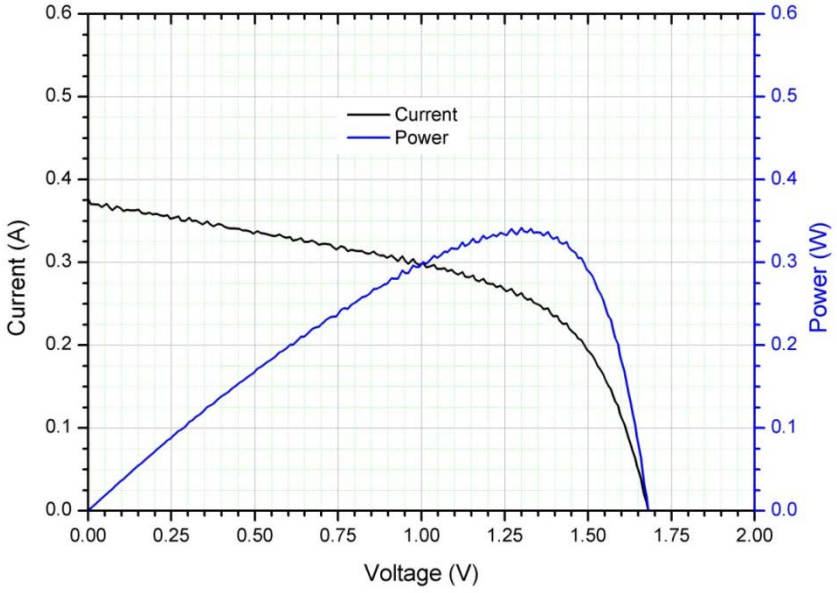

Figure 4.7 IV characteristics and power curve of the first prototype module with 600 W/m^2 radiation intensity incidents at 0^o incidence angle.

It is observed that with the increase in the incidence angle of the radiation, the short circuit current and the power ratio increases. As shown in figure 4.8, the short circuit current of the CPV module at 15^o and 30^o inclination angle is 0.48A and 0.49A respectively. The short circuit current is found to be 1.7 and 1.75 times higher than the non-concentrating module for incidence angles of 15^o and 30^o respectively. The maximum powers of the CPV module for these two incidence angle are 0.46W and

0.48W, both with fill factors of 56.7%. Compared to the designed concentration ratio of 2.8 the experimental power ratio is found to be only 1.6 and 1.7 respectively.

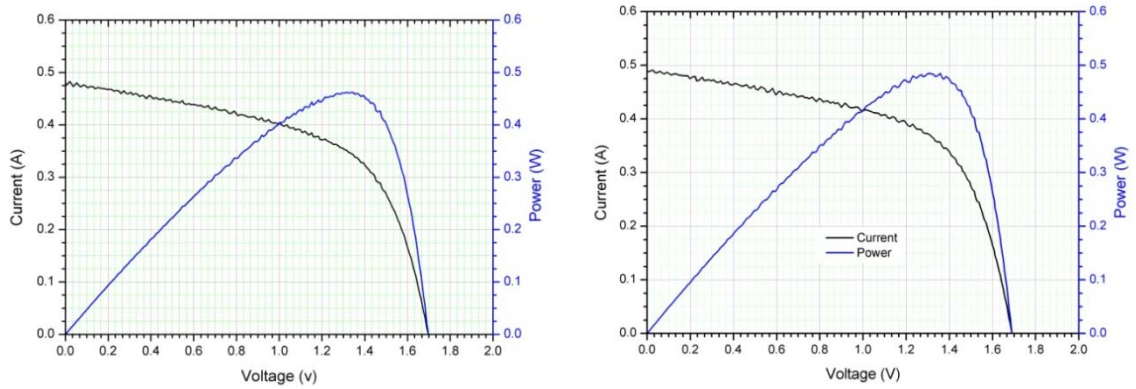

(a) (b)

Figure 4.8 IV characteristics and power curve of the first prototype module with 600 W/m^2 radiation intensity incidents at (a) 15^o incidence angle and (b) 30^o incidence angle

This clearly indicates significant losses in the CPV system. The increase in power of the CPV module for the incidence angles of 15^o and 30^o compared to 0^o implies a higher optical loss for the radiation incident perpendicular to the aperture of the CPV module. The higher optical loss can be attributed to the cured aperture surface and the misalignment of the receiver of the concentrator and the solar cell. With further increase in inclination angle it is found that the power of the module tends to decrease. For 45^o inclination angle, the power output of the module is recorded to be 0.32W, which is equal to the non-concentrating counterpart. The fill factor further decreases to 54%, while the short circuit current is found to be 0.35A. The IV characteristics and the power curve of the CPV module for 45^o inclination angle are shown in figure 4.9.

It is observed that a high optical loss occurs in the first prototype of the CPV module. The maximum power of the CPV module increases with increase in inclination angle until 30^o, which implies a reduction in optical loss. However a further increase in the incidence angle leads to decrease in the power output. This study indicates that the optical loss towards the extreme acceptance angles of the concentrator is higher than that of the incidence angles in the middle of the acceptance angle range. The comparative IV characteristic of the non-concentrating and the first prototype CPV module are shown in figure 4.10.

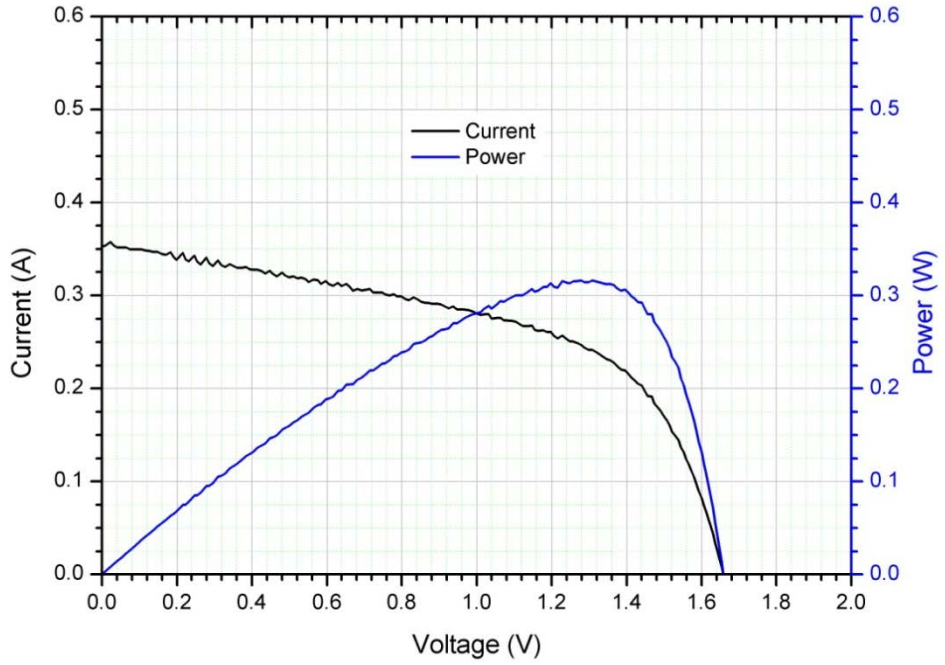

Figure 4.9 IV characteristics and power curve of the first prototype module with 600 W/m^2 radiation intensity incident at 45^o.

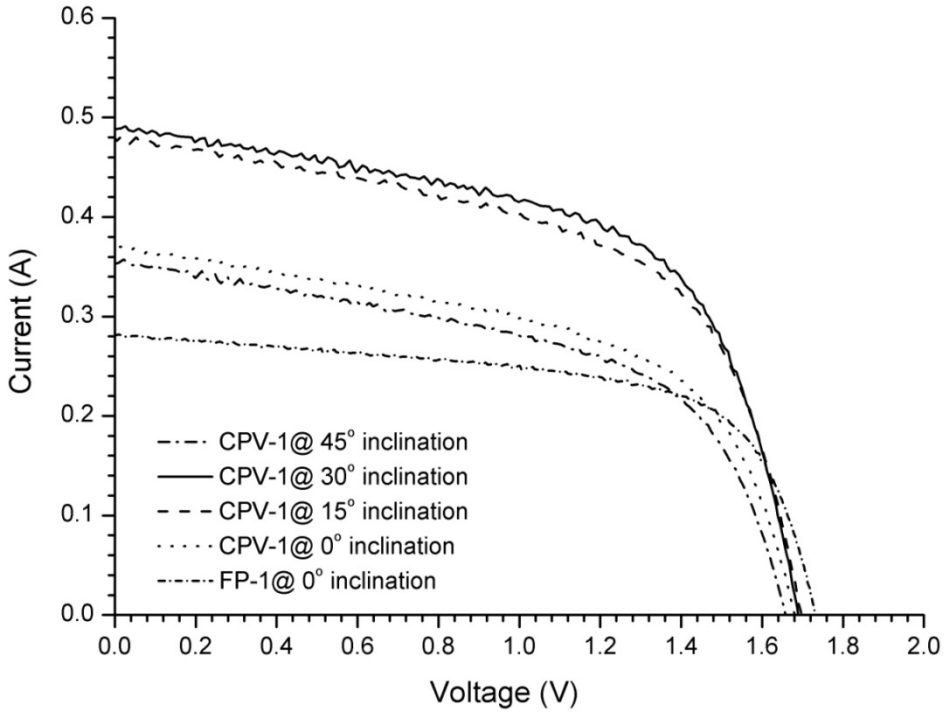

Figure 4.10 IV-characteristics of the first prototype non-concentrating and CPV modules at 600W/m^2 radiation intensity for different incidence angles

Further experiments have been carried out with radiation of 1000 W/m^2 to estimate the performance of the module with increase in solar irradiation. Considering the previous

study, these experiments have been carried out for 0^o and 30^o inclination angles only. Figure 4.11 shows the IV and power curves for non-concentrating module and CPV module for 0^o and 30^o inclination angle.

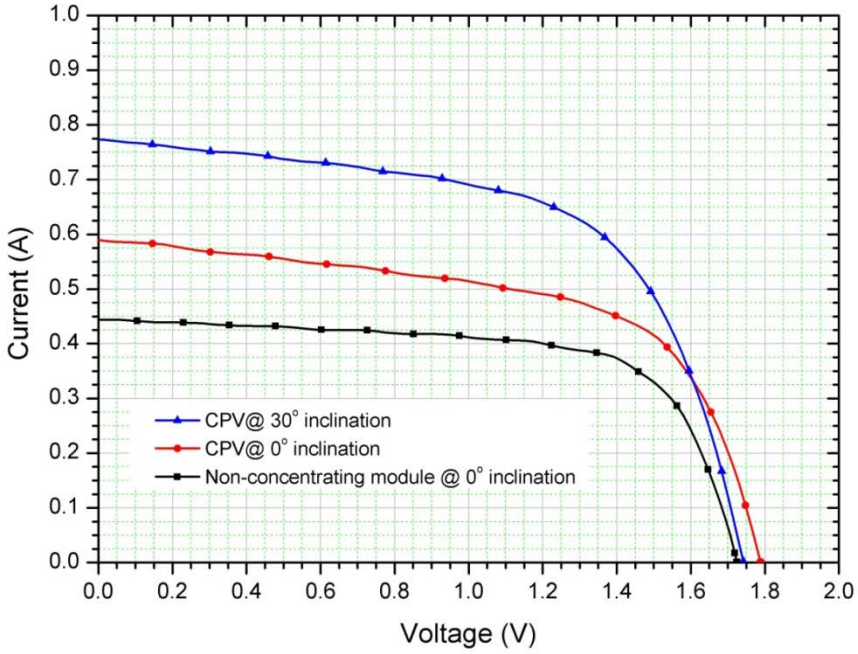

(a)

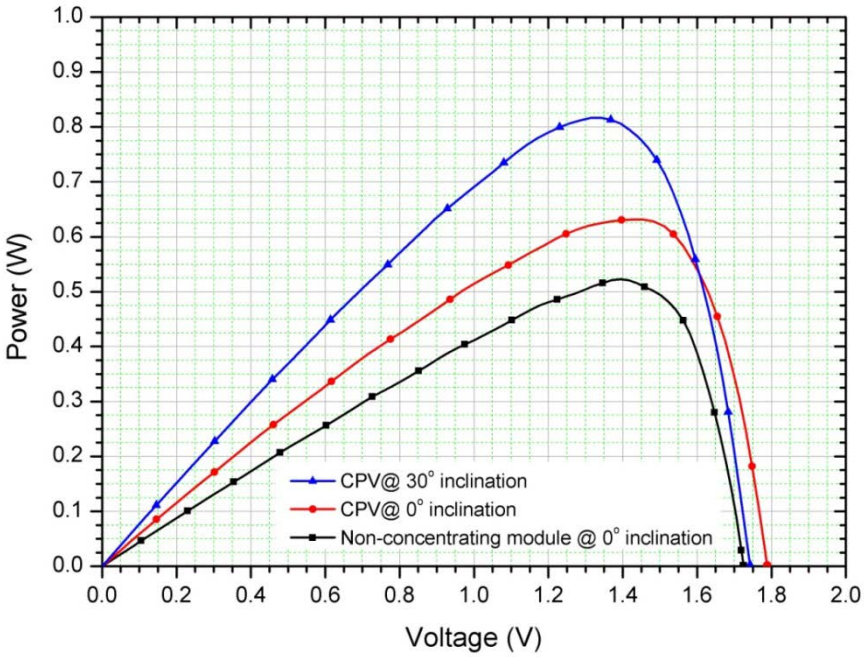

(b)

Figure 4.11 (a) IV curve (b) Power curve of the first prototype CPV module and non-concentrating counterpart at 1000W/m^2

A maximum 1.74 times increase in the short circuit current can be observed which increased from 444mA to 773mA with the introduction of the designed concentrator at 30^o inclination angle. The open circuit voltage of the non-concentrating system is found to be 1.72V, which increases to the maximum 1.74 for the concentrating system. The maximum power of the concentrating system is 1.56 times higher than the non-concentrating counterpart. However the increase in power and short circuit current is not significant for 0^o inclination angle. The short circuit current and maximum power is found to be increased by only 1.32 and 1.2 times respectively. The fill factor of the concentrating system is decreased to 60.6% compared to 68.2% for the non-concentrating system. This reduction in fill factor is attributed to an inhomogeneous distribution of light intensity on the solar cell in the concentrating system. This result demonstrates that only a 1.65 power concentration has been achieved whereas the theoretical study predicts an optical efficiency of ~ 2.3, considering all the transmission losses within the concentrator.

4.6 Electrical characterisation of second prototype modules

Extensive electrical characterisation of the second prototype has been carried out for a detailed investigation of the performance of the designed dielectric concentrator. Two different CPV modules are fabricated with modifications at the encapsulation-concentrator interface near the receiver and the concentrator-glass interface at the top surface. It is observed that the optical losses at the encapsulation-concentrator interface can be minimised by incorporating a thin reflective film in between and the loss at the top surface can be reduced by optically coupling the cover glass with the concentrator aperture surface. The process of optically coupling the glass and incorporating the reflecting film has been described in section 2.7.2. The two second prototype CPV modules with and without these modifications are termed as CPV-S1 and CPV-S2 for future reference which is described as:

- **CPV-S1 module**: Standard dielectric CPV module having an air gap between the cover glass and aperture of the concentrator; without a reflective film at the concentrator-encapsulation interface.
- **CPV-S2 module**: Modified dielectric CPV module with an optically coupled cover glass on the aperture of the concentrator and reflective film incorporated at the concentrator-encapsulation interface.

To compare the performance of the dielectric concentrator a similar non concentrating module has been fabricated as mentioned in section 2.7. The non-concentrating module has a similar electric configuration with 8 solar cells, where the cells are encapsulated between two glass layers using sylgard-184 as the encapsulation material (FP-2 module). The characterisation of the CPV systems has been carried out in terms of the increase in short circuit current (I_{sc}), the power ratio and the change in electrical conversion efficiency of the CPV module with the change in the incidence angle of the irradiance.

4.6.1 Short circuit current analysis

The short circuit current of the CPV systems is found to be a maximum at 20^o and decreases for both lower and higher incidence angles. This decrease of I_{sc} in the CPV systems is because of the higher optical losses from the parabolic sides and at the concentrator-encapsulation interfaces. The I_{sc} of the non-concentrating system is found to decrease with increasing angle of incidence. The reduction in I_{sc} of the non-concentrating system with the increase in incidence angle is due to the cosine effect and the increase in the reflecting component at the air-dielectric interface of the front glass. The maximum I_{sc} in the CPV-S1 and CPV-S2 modules is found to be 425mA and 513mA respectively for 1000 W/m^2 at 20^o incidence angle (Figure 4.12 (a)).

The maximum I_{sc} in the CPV-S2 and CPV-S1 module is 2.25 and 1.86 times higher respectively, compared to the non-concentrating counterpart at 20^o incidence angle. The I_{sc} in the CPV-S2 module increased by 17.2% at 20^o incidence angle and 10.66% at 0^o incidence angle compared to CPV-S1 because of the reduction in optical losses at the concentrator-encapsulation interface and cover glass. However, the I_{sc} of both CPV modules is found to be same at 50^o incidence angle, which indicates high optical losses even in the CPV-S2 module at higher incidence angles. Normalisation of the short circuit current shows that at a 55^o incidence angle, the I_{sc} of the CPV-S2 module is reduced to 40% of its maximum value, while for the non-concentrating system the I_{sc} is reduced to 60% (figure 4.12(b)). For a 0^o incidence angle the I_{sc} of the CPV-S2 is found to be 75% of its maximum value at a 20^o incidence angle. The study conducted using a goniometer shows that the light rays that are escaping from the parabolic sides increase the optical losses for higher incidence angles. The theoretical study investigating the concentrator-encapsulation interface losses shows that the drop in short circuit current in the CPV system towards the extreme acceptance half angles (0^o & 55^o) of the

designed concentrator is mostly due to the scattering and light escaping from the concentrator-encapsulation interface. For higher incidence angles (towards 55^{o}), reflection loss at the air-dielectric interface and the cosine effect further reduces the short circuit current.

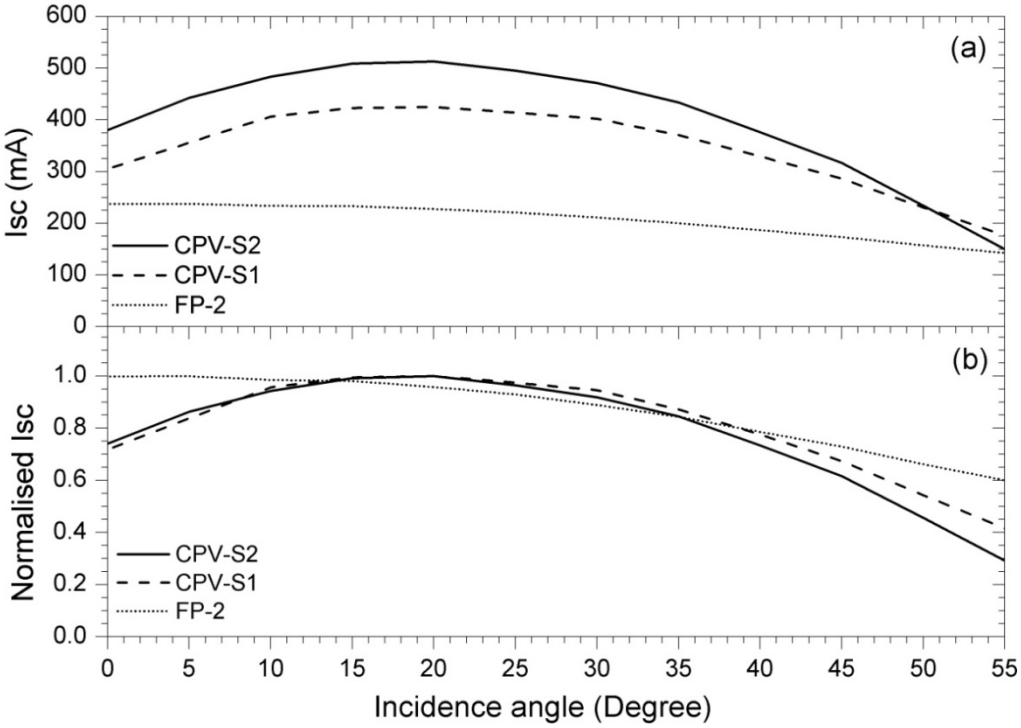

Figure 4.12 (a) Variation in short circuit current (I_{sc}) of the dielectric CPV modules and non concentrating module with change in the incidence angle at 1000 W/m^2 (b) normalised short circuit current (I_{sc})

4.6.2 Theoretical and experimental optical efficiency of the CPV modules

The theoretical and experimental optical efficiency of the CPV system are found to be in good agreement between 10^{o} and 45^{o} incidence angles as shown in figure 4.13. The experimental optical efficiency is calculated in terms of the I_{sc} of the non-concentrating and CPV modules using the equation [252]:

$$Optical\ Efficiency = \frac{(I_{sc})_{CPV}}{\{(I_{sc})_{pv}\} \times CR} \times 100$$

where $(I_{sc})_{cpv}$ is the short circuit current of CPV module, $(I_{sc})_{pv}$ is the short circuit of the non-concentrating system and CR is the geometrical concentration ratio. The theoretical optical efficiency is calculated by considering the reflection losses at the air-dielectric

interface on the cover glass, the absorption losses within the dielectric materials and the light escaping from the concentrator-encapsulation interface at both ends of the receiver. The average absorption co-efficient is considered to be 6.1 cm^{-1}, 1 cm^{-1} and 1.2 cm^{-1} for the polyurethane (concentrator), cover glass and sylgard (encapsulation material) respectively for the wavelength range 400-1100 nm.

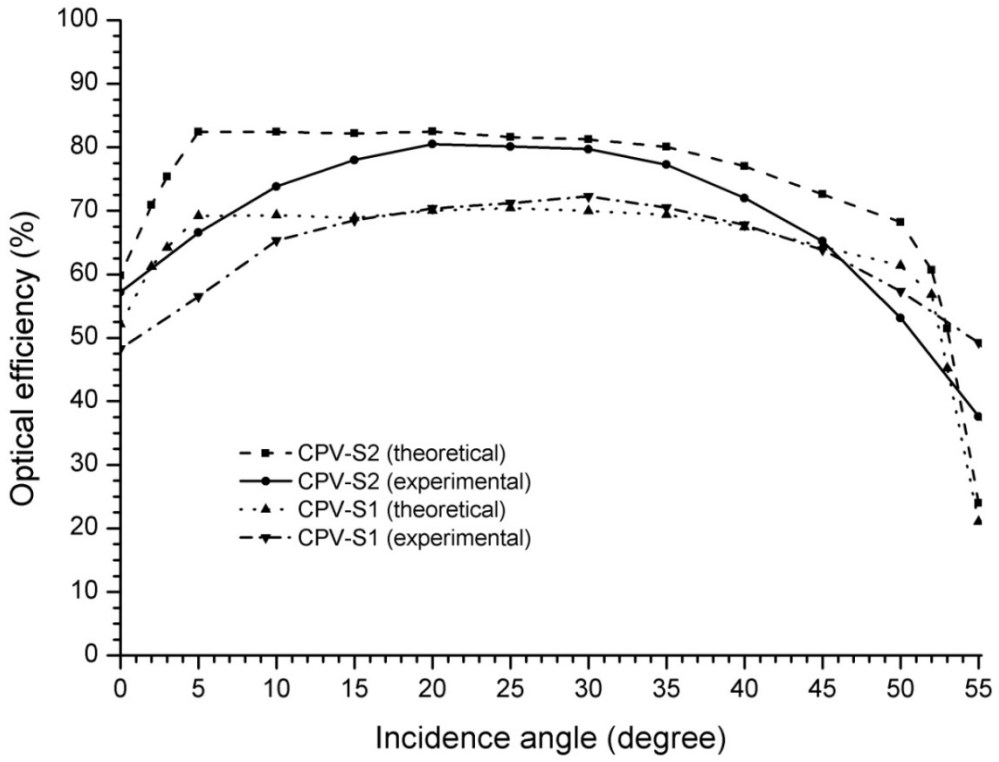

Figure 4.13 Theoretical and experimental Optical efficiency of CPV-1 and CPV-2 module with dielectric concentrator

The study shows that for the CPV-S1 module, the maximum experimental optical efficiency is 72.3% at 30^o, which is higher than the maximum theoretical value of 70.4% at 25^o incidence angle (figure 4.13). The scattering of the light in the concentrator and the collimation error of the solar simulator may be the reason behind the higher experimental values at these angles. However for the incidence angles less than 20^o the experimental optical efficiency is found to be lower than the theoretical. For incidence angles higher than 50^o, a sharp drop in the theoretical optical efficiency can be noticed due to most of the concentrated light escaping from the edges of the receiver at the concentrator-encapsulation interface. For the CPV-S2 module, the maximum experimental optical efficiency is found to be 80.5% at a 20^o incidence angle, while the theoretical maximum is 82.5% at the same angle of incidence. The theoretical

optical efficiency decreases sharply for incidence angles less than 5^o and higher than 50^o, while the experimental counterpart follows a smooth increase until 20^o and decreases thereafter. The maximum differences between the theoretical and experimental optical efficiencies can be observed at the incidence angles of 5^o and 50^o. For these two angles (near the acceptance half angles) the light concentrates from one of the parabolic surfaces towards the edge of the receiver. So the possibility of light escaping from the corners of the receiver increases, even for a small manufacturing error. For a 0^o incidence angle the theoretical optical efficiency is found to be higher than the experimental values, whereas for a 55^o incidence angle the experimental optical efficiency is found to be higher than the theoretical estimation. Scattering of the reflected light from the parabolic surface due to the surface roughness can be a reason of this mismatch. For extreme half acceptance angles the possibility of high scattering and optical losses increases, as most of the rays reflect from one surface. The beam collimation error (~4%) of the solar simulator may also contribute to the mismatch between the theoretical and experimental optical efficiencies at the extreme acceptance half angles.

4.6.3 Power ratio of the CPV modules

The power ratio is defined as the ratio of the power output of the CPV module and the non concentrating counterpart. The power ratio is not same as the optical concentration ratio of the system. Unlike the optical concentration ratio, power ratio has effect of the change in fill factor and open circuit voltage in a CPV system compared to the non-concentrating counterpart while exposed to similar conditions. The power ratio reveals the performance of the concentrator in a CPV module in terms of the increase in the total power output. A study has been undertaken to estimate the change in the power ratio of the CPV-S1 and CPV-S2 modules with change in solar incidence angle for different radiation intensities. Figure 4.14 shows the power ratio of CPV-S1 and CPV-S2 for the range of incidence angles from 0^o to 55^o for radiation intensities $600W/m^2$, $800W/m^2$ and $1000W/m^2$. The power ratio of the CPV-S1 module is found to vary between 1.48 and 2.09 for different irradiance and incidence angles. The maximum power ratio is found to occur at 25^o incidence angle for a radiation intensity of 600 W/m^2, whereas the lowest is recorded for 1000 W/m^2 at 55^o inclination. For the CPV-S2 module the maximum power ratio is found to be 2.32 for $600W/m^2$ at incidence angle 20^o.

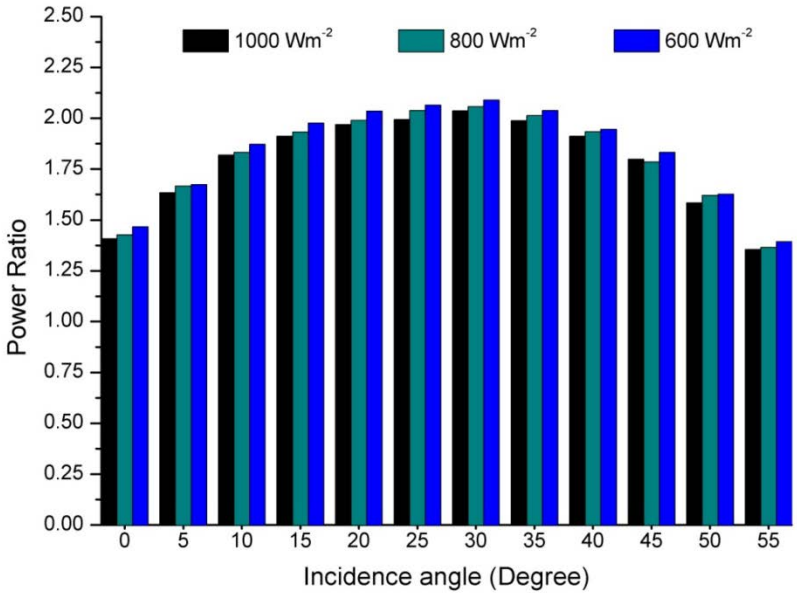

(a)

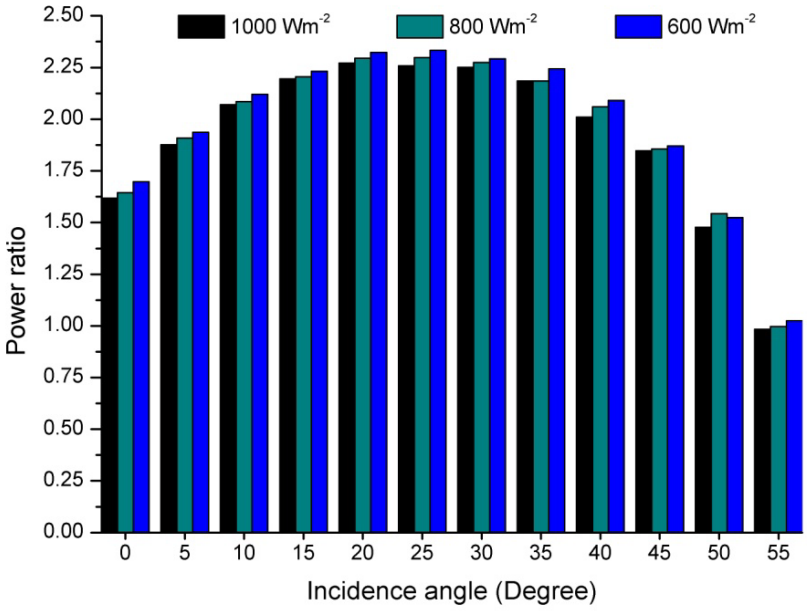

(b)

Figure 4.14 Power ratio of the (a) CPV-S1 module (b) CPV-S2 for different radiation intensities.

The study shows that the power ratio is higher for lower radiation intensities, which may be due to the lower solar cell temperature at lower radiation intensities. A comparison of the power ratio of the two designed CPV modules under 1000 W/m^2

irradiation shows that the CPV-S2 module can achieve a maximum power ratio of 2.27 at a 20^o incidence angle, while CPV-S1 reaches 1.97 (figure 4.15).

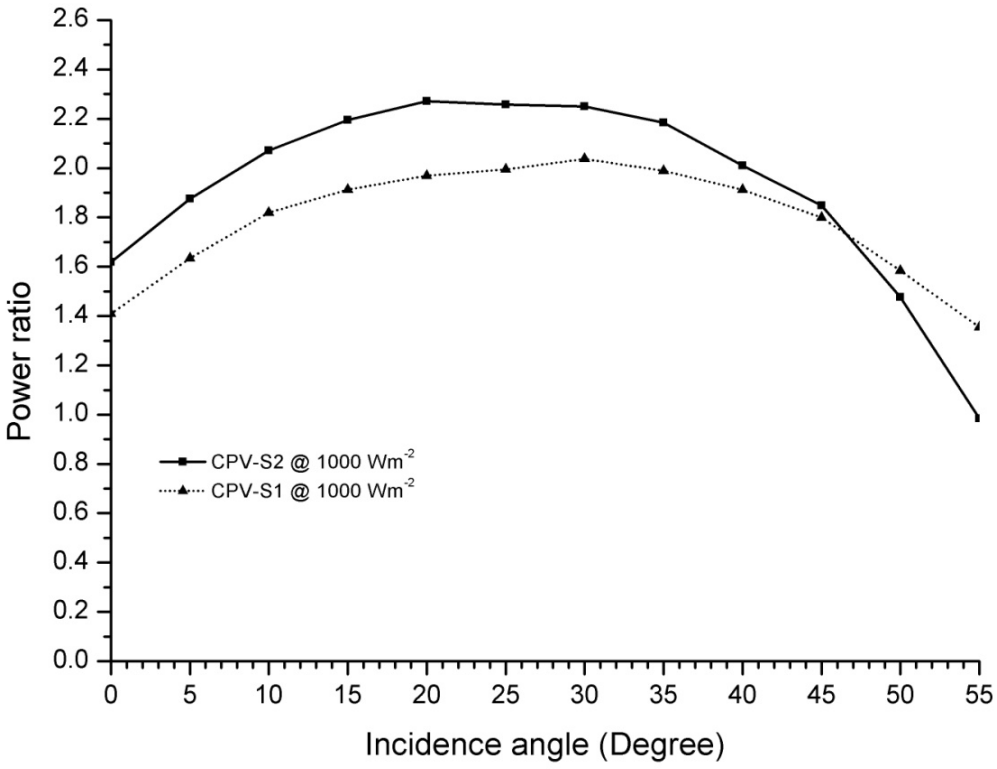

Figure 4.15 Comparison of the power ratio of CPV modules with variation of incidence angle

The power ratio of the CPV-S2 module is enhanced by 12.9% and 13% compared to CPV-S1 module at 0^o and 20^o incidence angles respectively. However, the drop in the power ratio is found to be higher for CPV-S2 compared to CPV-S1 for incidence angles higher than 47^o. The drop in the power ratio of the CPV-S2 module for higher incidence angles may be due to the higher optical losses, which can occur due to the imperfect optical-coupling of the reflective film and concentrator. It has also been found that the optical coupling of the front glass layer with concentrator results in an improvement of 4.8% in the power ratio at 20^o incidence angle.

A higher open circuit voltage and lower fill factor are observed in the CPV modules compared to the non-concentrating counterpart for the same radiation intensity. Figure 4.16 shows the open circuit voltage and fill factor of the CPV-S2 and non-concentrating modules at 1000 W/m^2.

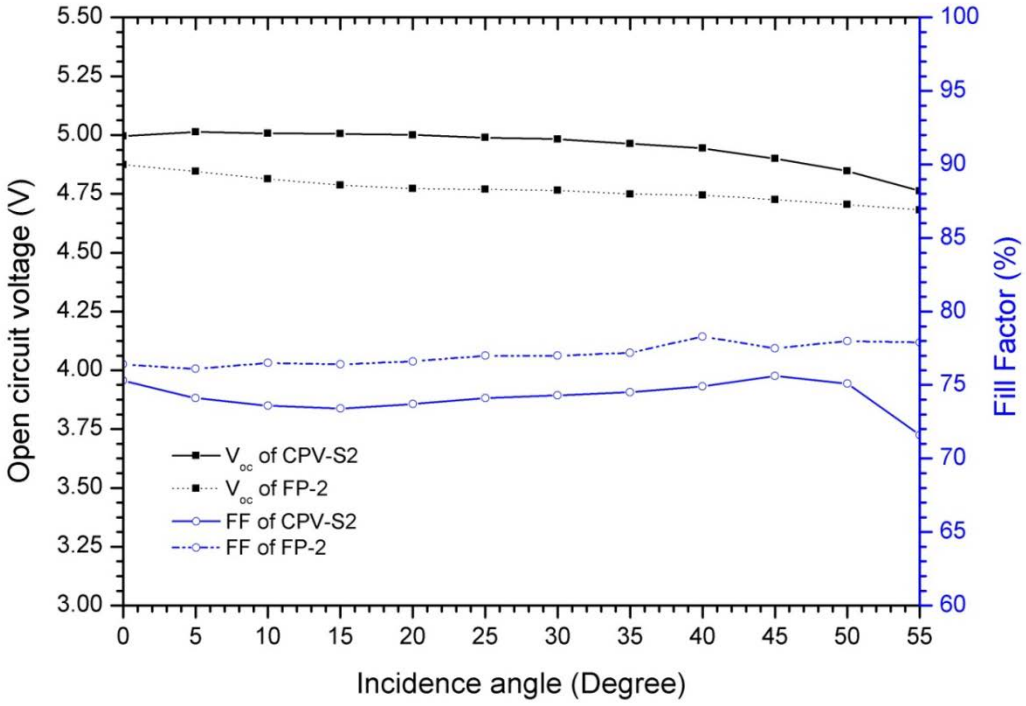

Figure 4.16 Variation of open circuit voltage and fill factor of non-concentrating and CPV-S2 module with change in incidence angle at 1000 W/m^2

A 4.8% variation in the open circuit voltage can be observed in the CPV system with a change in the incidence angle from 0^o to 55^o, while the variation for the non-concentrating system is 3.9%. The open circuit voltage (V_{oc}) of the CPV-S2 module is found to vary from 5 to 4.7 volts within the range of incidence angles 0^o to 55^o. The V_{oc} of the CPV-S2 module at 20^o incidence angle is found to be 5V, which is 4.6% higher than the non-concentrating counterpart. The increase in I_{sc} with increasing light intensity on the cells of CPV system is the reason for the increase in V_{oc}. For a 55^o incidence angle the V_{oc} of the CPV-S2 module is found to be 1.7% higher than the non-concentrating system. The fill factor is found to be within the range of 73.4% to 75.3%, which is 3% less than non-concentrating system for respective incidence angles. The increase in resistive losses with increase in current has reduced the fill factor in CPV system. Higher optical losses at extreme acceptance angles can be another reason of reduction in fill factor at extreme acceptance half angles.

4.6.4 Electrical conversion efficiency of the CPV modules

An investigation of the electrical conversion efficiency of both the non-concentrating and CPV modules shows that the maximum system efficiency of the CPV-S2 module decreases by 24% compared to the maximum of the non-concentrating system. The

electrical conversion efficiency of the CPV modules and the non concentrating module are calculated by considering the active area of the concentrator aperture and the active area of the solar cells respectively. The maximum efficiency of the non-concentrating system is found to vary from 15.9% to 9.4%, with an average of 13.6% within the range of acceptance half angle of the designed concentrator as shown in figure 4.17.

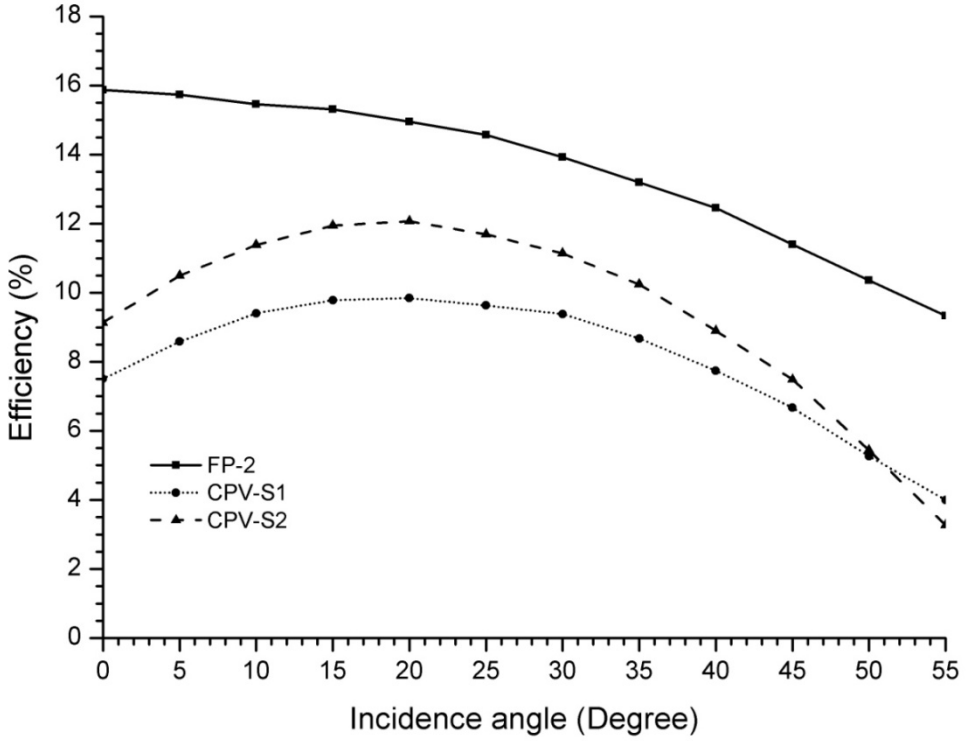

Figure 4.17 System efficiency of the non-concentrating and CPV modules with variation of incidence angle

The system efficiency of the CPV-S2 module is found to be 9.2% for a 0^o incidence angle, which increases to 12.1% at 20^o and then decreases to 3.3% for the extreme acceptance half angle (55^o). The average system efficiency of the CPV-S2 system within the range of the acceptance half angle is 9.5%.

4.6.5 Indoor electrical characterisation of CPV-S3 module

The CPV-S3 module is constructed with the concentrator manufactured from PMMA and having the same configuration as the CPV-S1 module. The electrical performance of the CPV module shows a maximum short circuit current of 439mA at a 15^o incidence angle, which is 2 times higher than the non-concentrating counterpart (Figure 4.18).

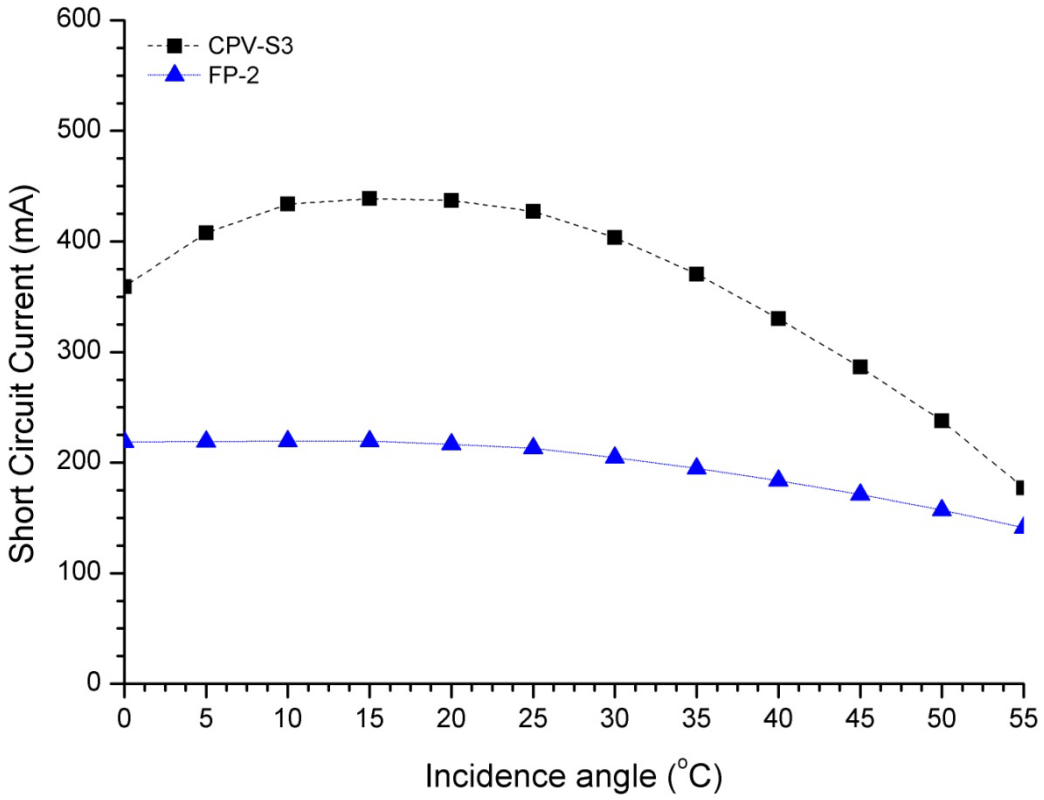

Figure 4.18 Variation in the short-circuit current with angle of incidence of the CPV-S3 and FP-2 modules

The experimental optical efficiency based on the short circuit current of the CPV-S3 module shows that the maximum optical efficiency at a 15^{o} incidence angle is 2.9% higher than the theoretical value (figure 4.19). The theoretical simulation considers all possible optical losses including the possibility of light escaping from the concentrator-encapsulation interface. Near the extreme acceptances angles (0^{o} & 55^{o}) the theoretical optical efficiency is found to be higher, then drops sharply at 0^{o} and 55^{o} due to light escaping from the concentrator-encapsulation interface.

The maximum power output of the CPV-S3 module for 1000 W/m^2 illumination is 1.6W at a 15^{o} incidence angle, which is 2.1 times higher than the non-concentrating counterpart (figure 4.20). However the average power ratio of the CPV-S3 module within the range of the acceptance angles is found to be only 1.6. This is because of the drop in the power output of the CPV module near the extreme acceptance angles, especially towards the acceptance angle of 55^{o}. At 0^{o} the power ratio is found to be 1.7, whereas the power ratio at 55^{o} incidence is 1.2. It can be concluded that there are higher optical loss towards the acceptance angle of 55^{o}. The manufacturing error during the

machining of the concentrator and the fabrication of the CPV-S3 module are possible reasons for the higher optical loss.

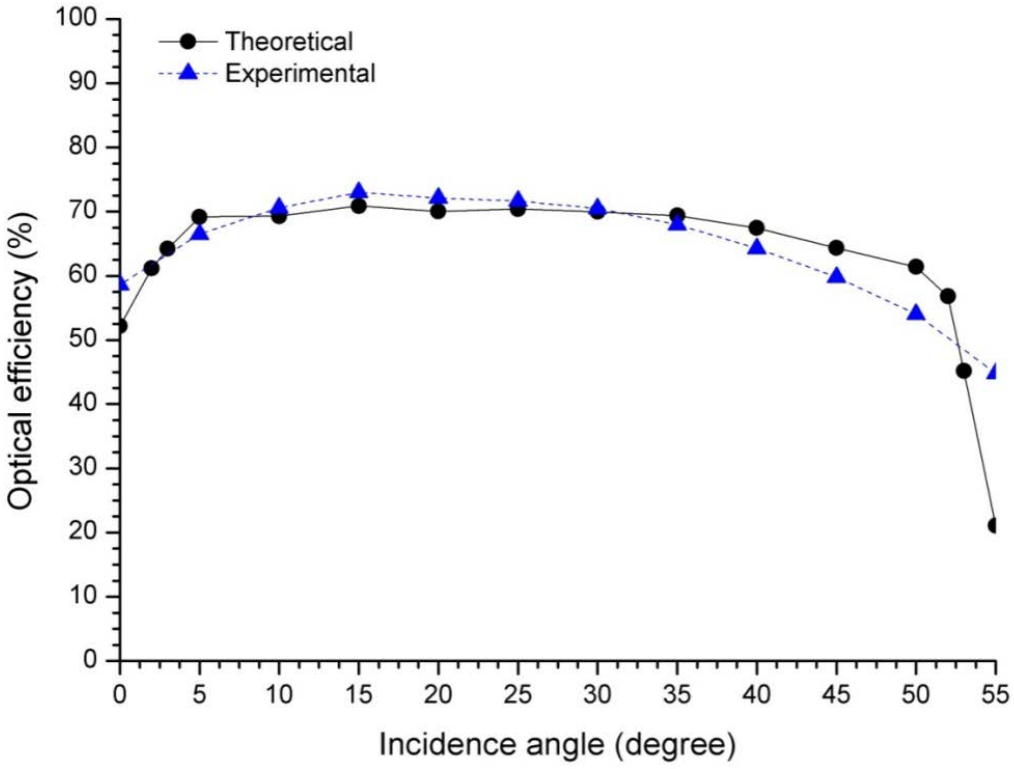

Figure 4.19 Theoretical and experimental optical efficiencies of the CPV-S3 module

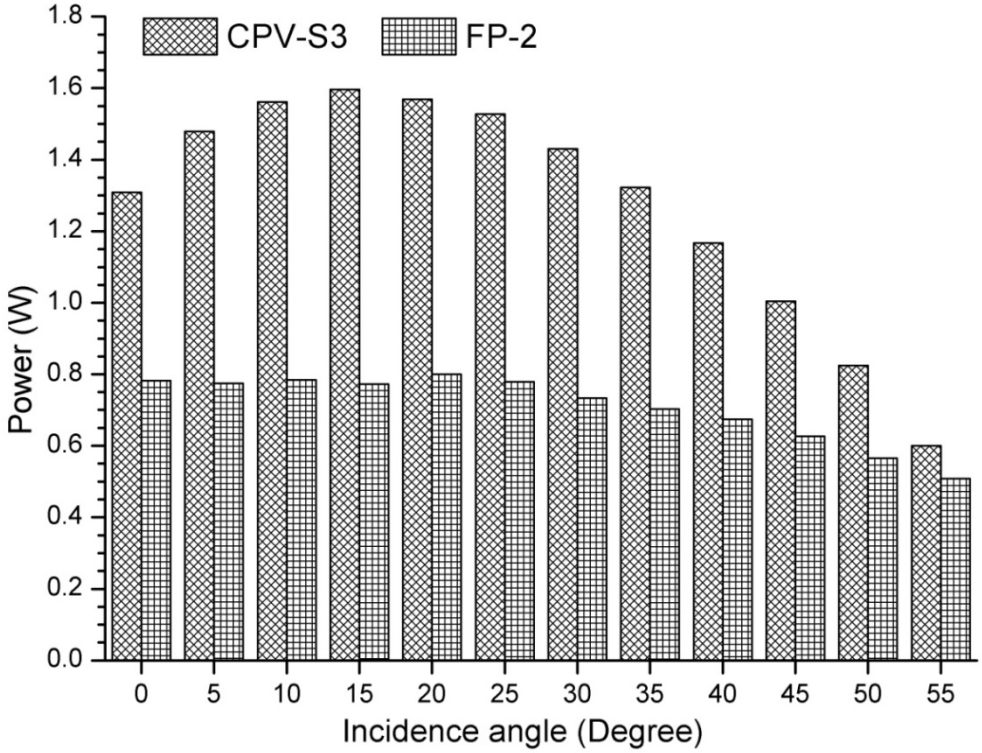

Figure 4.20 Variation of the maximum power output with incidence angle

4.7 Electrical characterisation of third prototype (CPV-T1) module using large area solar simulator

The third prototype module is fabricated mainly for outdoor characterisation with two parallel strings of 14 solar cells in series. However to evaluate the variation in performance of the CPV module with change in incident angle, the third prototype module is characterised using the large area solar simulator. Even though the optically coupled cover glass reduces the optical loss in the module, it is very critical to couple the cover glass with more than one concentrator units. So the large area modules are fabricated with an air gap between the concentrator and the cover glass. The reflective film at the encapsulation-concentrator interface has not been used in the prototype modules for this preliminary study.

The study has been carried out with a radiation intensity of 800 W/m^2 for two incident angles. To evaluate the performance of the concentrator, a similar non-concentrating module has been fabricated and characterised. It is important to mention that the large solar simulator set-up is covered by curtains, which leads to increase in the diffuse component of the radiation compared to the set-up without curtains. The measured 800 W/m^2 radiation intensity is a combination of the direct and diffuse light from solar simulator.

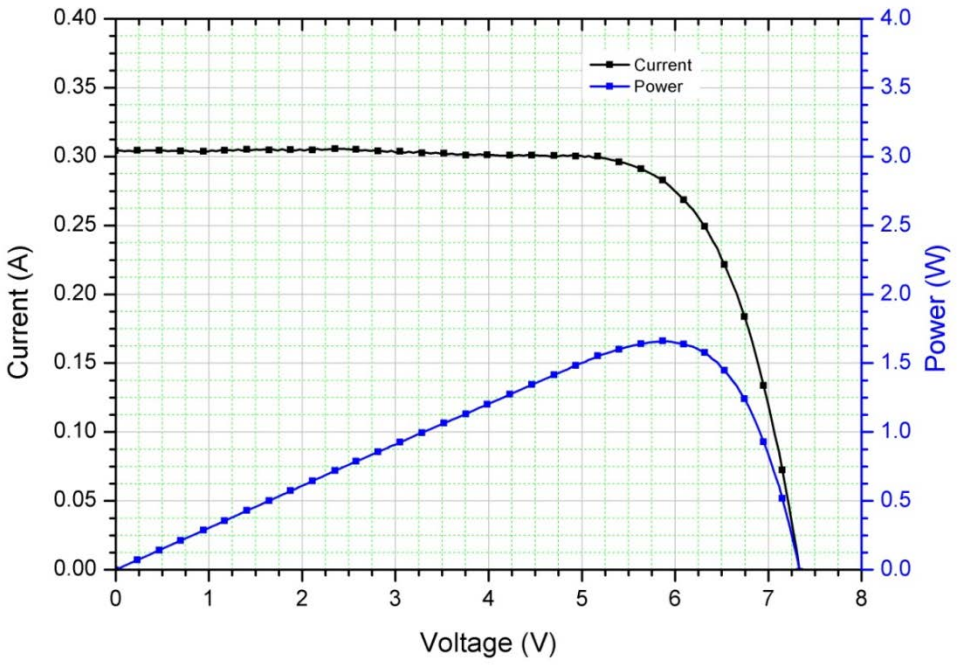

Figure 4.21 IV characteristics and power curve of the CPV-T1 module with 800 W/m^2 radiation intensity incident at 0^o

The IV characteristic of the FP-3 module under the solar simulator for a 0^o incident angle (radiation incident perpendicular to the aperture) is shown in figure 4.21. The short circuit current and open circuit voltage is found to be 0.3A and 7.3V respectively with a fill factor of 74.4%. The maximum power recorded is 1.66W. The conversion efficiency of the non-concentrating module, considering the active solar cell area (6.96 cm^2), is found to be 10.65%. The conversion efficiency is lower than that observed from the earlier study with the second prototype using the ABET simulator. This is because of the difference in the spectrum between the in-house built and ABET solar simulator. Unlike the ABET solar simulator, the in house built large area solar simulator uses HMI lamps (instead of Xenon lamps) and AM1.5G filter has not been used. Since this study is intended for comparative analysis of non-concentrating and CPV modules, these results give a clear understanding of the performance of the dielectric concentrator for different incidence angles.

The CPV-T1 module has been characterised under the large solar simulator for two incident angles 0^o and 30^o. The short circuit current at 0^o and 30^o is found to be 0.5A and 0.52A respectively (Figure 4.22).

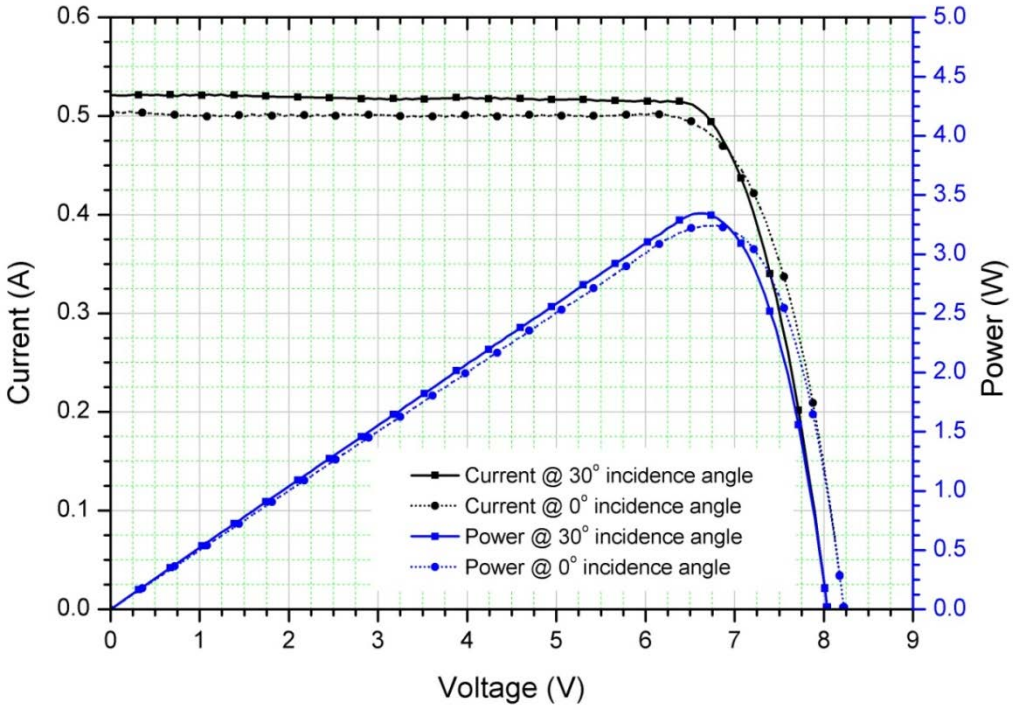

Figure 4.22 IV characteristics and power curve of the third prototype module with 800 W/m^2 radiation intensity incidents at 0^o and 30^o incidence angle

The short circuit current is 67% and 73% times higher than the non-concentrating counterpart for 0^o and 30^o incidence angle respectively. This indicates high optical losses from the cover glasses and at the encapsulation-concentrator interface. However the manufacturing error related to the misalignment of the solar cell and the receiver of the solar cell while fabricating the first unit of third prototype CPV module cannot be ignored. The maximum power output of the CPV-T1 module at 0^o incidence angle is found to be 3.24W with an open circuit voltage of 8.2V and fill factor 78.4%. For a 30^o incidence angle the maximum power output is found to be 3.35W, while the open circuit voltage is 8V and the fill factor is 80%. The decrease in open circuit voltage is because of the increase in temperature of the solar cell in the CPV module. The cell temperature during the experiment at 0^o incident angle was found to be 31.3^oC, which increased to 39^oC while characterising the CPV-T1 module for a 30^o incidence angle.

4.8 Conclusion

A study of the spectroscopic performance of the concentrator material and the CPV module has been carried out and analysed in terms of the transmittance and EQE. The transmission of the concentrator material is found to be very good within the range of 420nm to 1100nm with a maximum transmittance of 89.6%. The average AM1.5G spectrum weighted transmittance with the spectral response range of the silicon solar cells (300nm to 1100nm) is found to be 81.9%. The reason for the significant decrease in average AM1.5G spectrum weighted transmittance compared to the maximum transmittance is due to the UV-stabiliser, which absorbs wavelengths below 400nm. The average AM1.5G spectrum weighted transmittance of the other components of the CPV module including the encapsulation material and the cover glass is found to be 91.6% and 92% respectively. The variation in EQE of the CPV module compared to the bare solar cell is found to correspond to the transmittance.

The optical losses due to light escaping from the dielectric concentrator have been investigated using a goniometer set-up. This experimental optical loss analysis shows that the light reflected from the parabolic sides may scatter over the range of angles 30^o to 50^o and can escape from the parabolic sides and aperture. As the incidence angle increased, rays were found to escape and scatter more within the concentrator, resulting in a reduction in the optical efficiency of the CPV module.

The indoor IV-characterisation of the 3 prototype modules using solar simulator shows that higher optical losses occur at extreme acceptance angles (0^o and 55^o) of the concentrators. A maximum power ratio of 2.27 can be achieved for the solar radiation incident at 20^o for 1000 W/m^2 irradiance. For lower irradiance ($600W/m^2$) the power ratio is found to be increased to 2.32. The theoretical and experimental optical efficiencies are found to be in accordance with each other within the range of acceptance angles, except for the extreme acceptance angles.

Chapter 5

Outdoor experimental characterisation of CPV modules

This chapter provides details of outdoor characterisation of CPV modules to evaluate the performance of DiACPC-55 concentrator in Edinburgh (55°55′N, 3°10′ W) location. The power output of the CPV module for different weather conditions has been compared with a similar non-concentrating counterpart. The diurnal variation of CPV module characteristics with sun position and irradiation has been analysed. The durability in terms of the power output of the CPV module with the DiACPC-55 concentrators has also been monitored and reported.

5.1 Introduction

Outdoor characterisation of the CPV module provides real performance data of a designed concentrator in collecting both direct and diffuse radiations. The effect of diurnal variation of sun position on the performance of the CPV system can also be tracked. Monitoring the increase in the temperature of the module is another issue to be addressed. This is necessary to estimate the loss due to the temperature effect and evaluate the actual optical performance of the concentrator in the CPV module. However it is not very convenient for real time measurement of the solar cell temperature in a CPV module; a thermal modelling helps better understanding of the temperature distribution in the CPV module and to predict the cell temperature. The CPV module degrades with long term exposure to the outdoor environment, due to UV-light, humidity and variation in temperature throughout the day. Degradation of the CPV modules with long term exposure to the outside environment also needs to be taken into consideration for a detailed analysis.

5.2 Outdoor experimental measurement conditions of the CPV module

The fabrication details of the CPV module used for outdoor characterisation are discussed in chapter 2 (section 2.6). Characterisation method and details of the

mounting of the modules have been also detailed in chapter 2. The modules were characterised on the roof and in the SE test site of Heriot-Watt University, Edinburgh ($55^{o}55^{/}$N, $3^{o}10^{/}$W). The solar irradiation and IV-data of the modules were collected in 1 minute intervals, throughout the duration of the day. The Study was carried out with the modules mounted vertically and with 10^{o} inclination to the vertical, to comparatively investigate the energy yield for these configurations. The rear plate temperature behind the solar cell position was measured to understand the effect of temperature. The wind speed data for a 10 minute average has been reported, which was collected from the Edinburgh airport situated 5km away.

Three CPV modules (CPV-T1, CPV-T2 and CPV-4) and one flat plate module (FP-3) were used in analysing outdoor electric performance of the dielectric concentrator. The outdoor experiment was carried out in 3 phases, as shown in table 5.1.

Table 5.1 List of the outdoor experimental characterisation phases and modules used

Experiments	**Modules used**	**Time of the experiment**	**Location of the experiment**
OE-First phase	FP-3, CPV-T1	9th June 2011	HWU building roof
OE-Second phase	FP-3, CPV-T1, CPV-T2	1st – 30th October 2011	SE test site, HWU
OE-Third phase	CPV-4	1st – 31st March 2012	SE test site, HWU

In the first phase of the experiment carried out in June 2011, only CPV-T1 and FP-2 modules were used. In the second phase of the experiment carried out in SE test site, CPV-T1, CPV-T2 and FP-3 modules were used for detailed electrical performance analysis and to investigate the performance of CPV modules compared to the flat-plate module. In the third phase of the experiment CPV-4 module was used to investigate the effect of scaling up the module and the energy yield with continuous power output.

5.2.1 OE-First phase: Electrical performance analysis

The weather during the first phase of the outdoor experiment was typical Scottish summer days, with sunshine, rain and clouds. There was not a sunny day during May-June 2011, after several attempts the 1st phase of the outdoor experiment was carried out on 9th June 2011, which was also a day of sunny intervals with rain showers. The diurnal variation of the solar radiation on the vertical plane facing south and the power output of the CPV-T1 system are shown in figure 5.1. The maximum power output of the system was found to be 4.3W, corresponding to maximum solar radiation of 886 W/m^2 at 10:42 am. The fill factor was recorded as 79% for the CPV system and 73% for the non-concentrating system during the maximum power output. The maximum open circuit voltage was found to be 8.5V during the time of maximum solar radiation. The systematic study on the effect of the increase in temperature could not be carried out because of the rapid change in solar radiation. However, when the solar irradiation was more than 800 W/m^2 and remained steady for 2-3 minutes, the open circuit voltage in CPV module tends to decrease. The maximum solar cell temperature of the CPV module was found to be 27^{o}C, while the ambient temperature was 15^{o}C. The diurnal variation of power output follows a similar pattern to diurnal variation of solar radiation, as shown in figure 5.1.

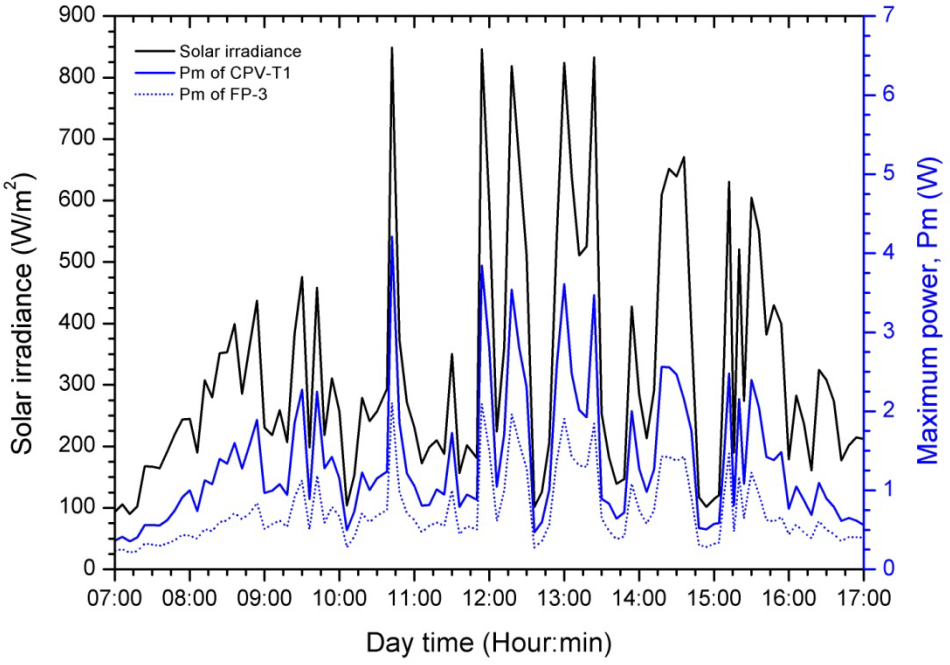

Figure 5.1 Diurnal variation of solar radiation and maximum power of the designed CPV and flat-plate modules.

The variation of short circuit current of the CPV-T1 and FP-3 modules are shown in figure 5.2. The results are given as 15 minute averages of data collected in 1 minute intervals, due to the rapid change in solar radiation and electrical output of the system. For the maximum solar radiation 886 W/m^2 at 10:42 am, the maximum short circuit current of the CPV system is found to be 641 mA, while the non-concentrating system results to be 329 mA. The minimum short circuit current recorded was 80.4 mA at 12:36 pm, for solar radiations of 104 W/m^2.

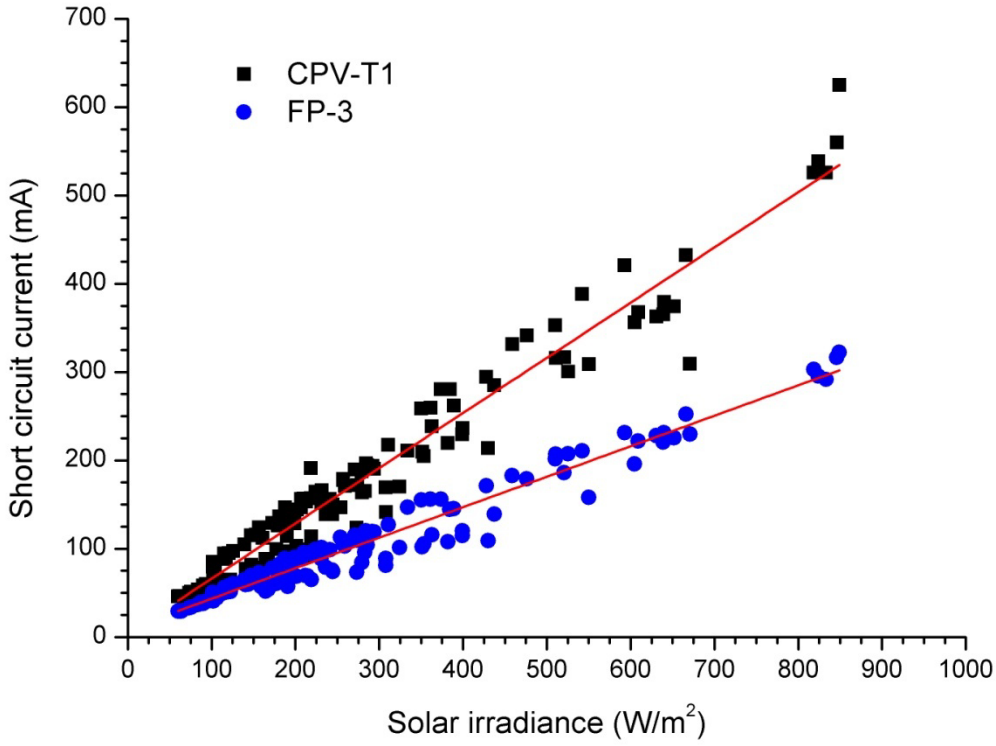

Figure 5.2 Variation of short circuit current of the designed CPV and flat-plate modules over a day, with variation of solar irradiation

The variation of power ratio of the CPV system, over the non-concentrating counterpart for different solar radiation intensities is shown in figure 5.3. It is observed that the power ratio for lower intensities was 1.6 at 91 W/m^2, while for higher intensities it was found to be a maximum of 2.3 at 530 W/m^2. Study shows that the designed dielectric concentrator performance for both direct and diffuse irradiation correlates very well with the theoretical analysis [251].

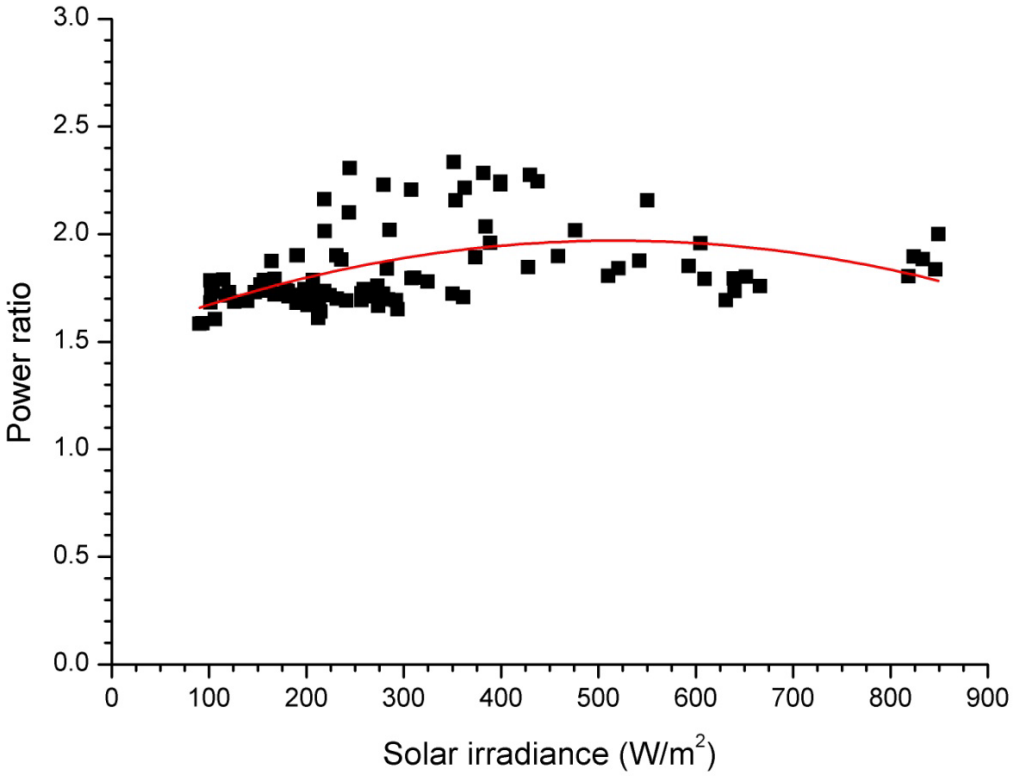

Figure 5.3 Power ratio of the concentrating system over the non-concentrating with diurnal variation of solar irradiation

The system efficiency of the designed CPV module and the non-concentrating system for different solar radiation intensities over the day is shown in figure 5.4. The system efficiency of the CPV module is calculated considering the effective aperture area of the concentrators, while the total area of the solar cells in use are considered in the case of the non-concentrating system. The maximum system efficiency of the CPV module was found to be 9.2% at 500W/m^2 irradiation, compared with 14.2% for the non-concentrating system. The system efficiency of the both CPV and non-concentrating system increases with increase in solar radiation intensities up to 500 W/m^2 and decreases for higher intensities. The increase in temperature of the system with increase in radiation intensity may have lead to the decreases in system efficiency. To reduce significant errors due to fluctuation in solar radiation intensities, the system efficiencies are calculated based on an instantaneous measurement of power at a particular time.

Study shows that output power of the CPV-T1 modules increased by a maximum of 2.3 times compared to the FP-3 module. The power ratio is found to be inconsistent over the range of acceptance angle of the designed concentrator (0^o & 55^o). For extreme acceptance half angles concentrated rays may escape from the concentrator-

encapsulation-cell interfaces, which lead to the lower short circuit current and system efficiency.

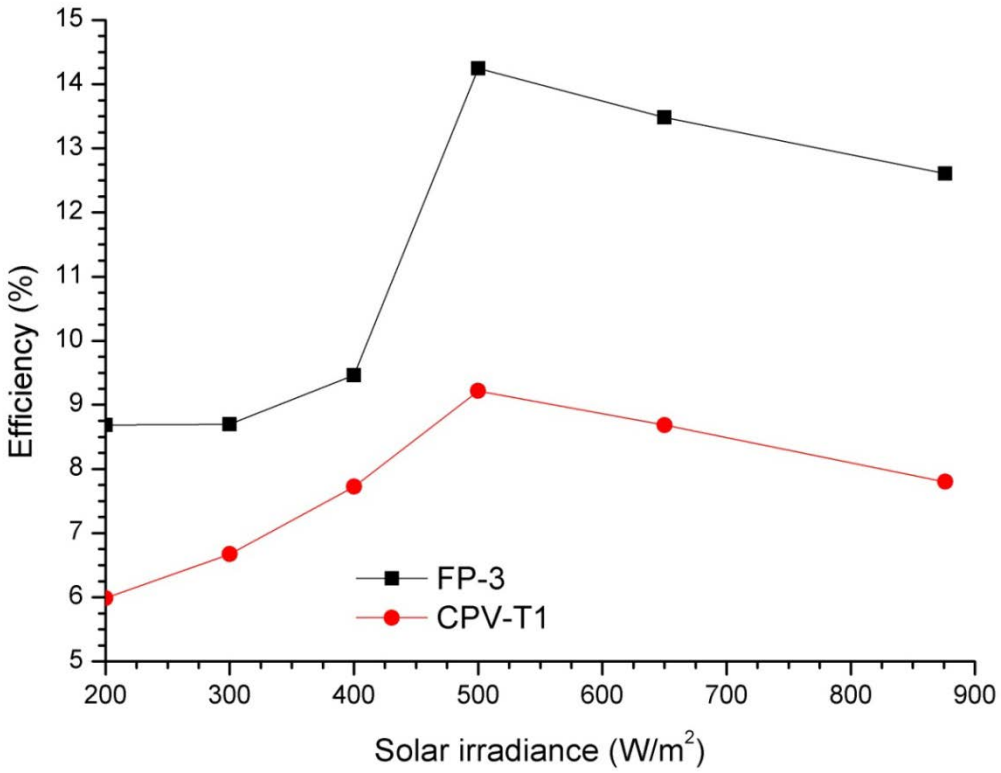

Figure 5.4 Variation of system efficiency of CPV-T1 and FP-3 for different solar radiation intensities

5.2.2 OE-second phase: Electrical performance analysis of the third prototype of CPV modules in the SE test site

The second phase of the outdoor experiment has been carried out in the month of October 2011, for 30 days. During this period, there was not a clear and sunny day. Therefore, the electrical performance of the CPV-T1 and CPV-T2 modules has been reported for four days of month: one cloudy day, two sunny interval days and one rainy day, on 4th, 7th, 16th and 17th of October respectively. This will help in understanding the performance of the dielectric concentrator under direct, diffuse radiation and also in rainy seasons. For the duration of the four days the modules were mounted vertically. The outdoor experiment has also been carried out mounting the modules with 10^{o} inclination to the vertical for few days, one of which was the 28th of October 2011. The results for this day have also been reported. The overview of the variation of the solar radiation, wind speed and the ambient temperature of the first four days is shown in figure 5.5. Detailed contribution of the direct and diffuse radiation for the global

irradiance will be discussed, along with the electrical performance of the modules on the reported days.

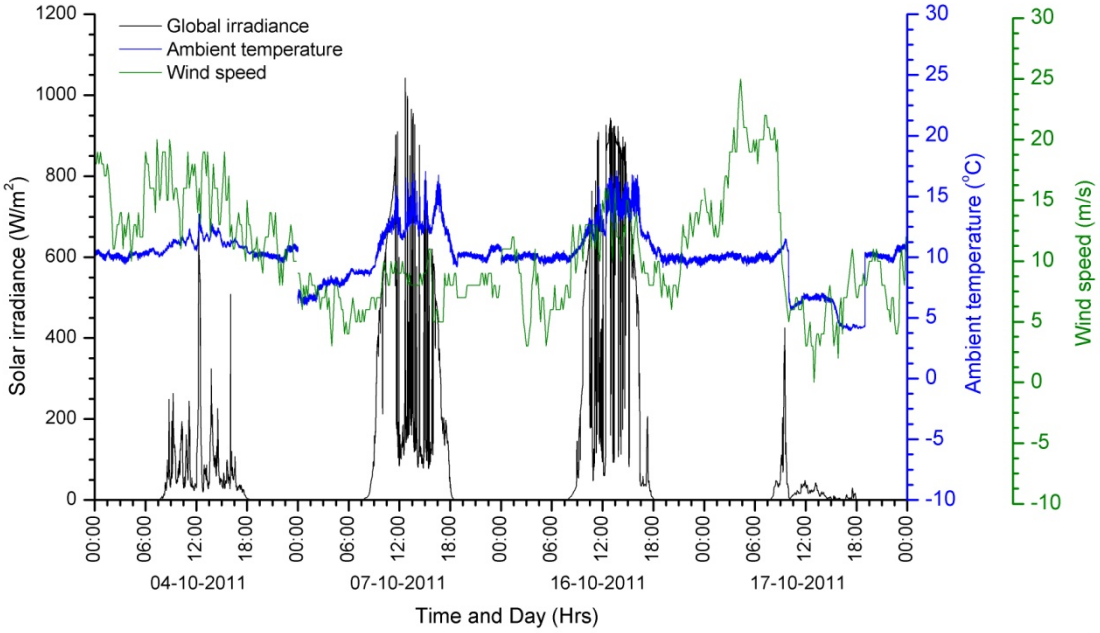

Figure 5.5 The variation of the global solar irradiance, ambient temperature and wind speed of the four reported days of the outdoor study

The ambient temperature of all four days was found to vary with the sunshine and rain. While the ambient temperature on 4th of October was almost steady, sudden increases and decreases in ambient temperature with sunshine and clouds can be noted for the rest of the days. A sudden drop in ambient temperature and wind on 17th of October can also be observed at 10:00am. The ambient temperature and wind speed played a significant role in reducing the module temperature and eventually increasing the power output of the modules.

5.2.2.1 Electrical performance of the CPV modules on a cloudy day (4th October 2011)

The diurnal variation of the solar irradiance on the cloudy day, 4th of October 2011, is shown in figure 5.6. Since the radiation was predominantly diffuse, with the exception of a short interval of time, the contribution of the direct irradiation has not been reported.

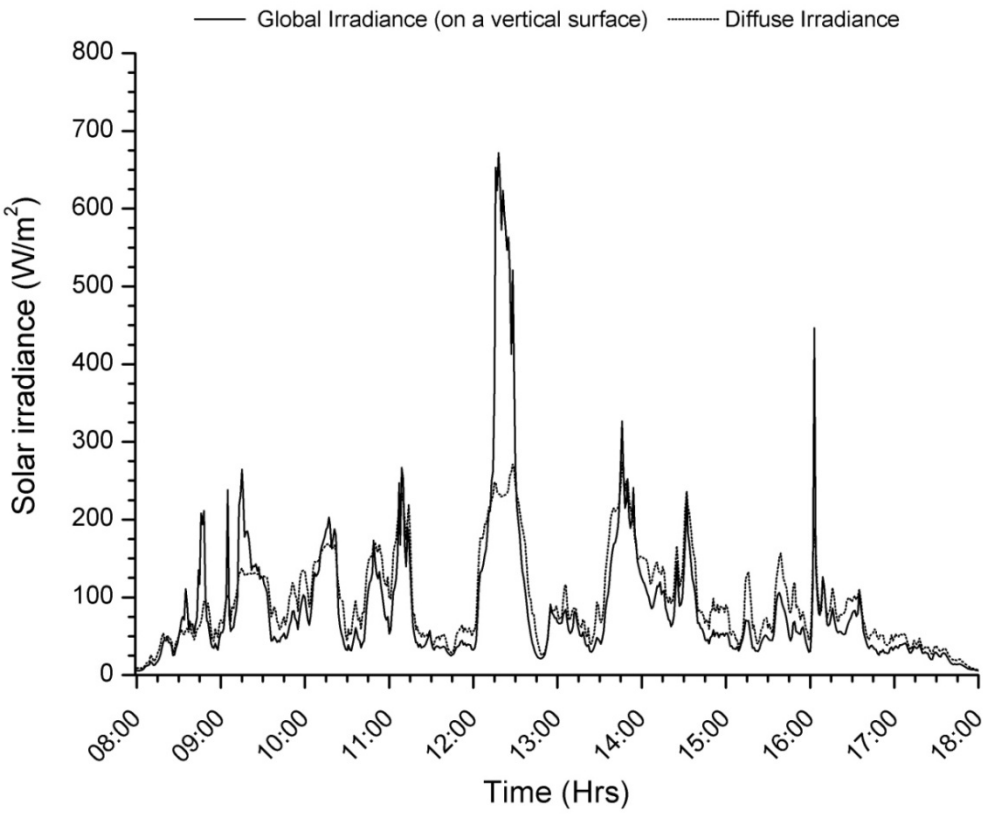

Figure 5.6 Diurnal variation of the global and diffuse solar irradiance on a vertical plane on 4th of October 2011

It was a typical cloudy days of Scotland with a bit sunshine for a while between 12:00 pm to 1:00 pm. The maximum global solar radiation on a vertical plane facing south is measured 680 W/m^2 at 12:20pm. Most of the time of the day, the global irradiance is found to be equivalent to the diffuse radiation. The diffuse solar radiation is found to be fluctuating between 30 W/m^2 to 300 W/m^2 depending on the clouds and rain. The module temperatures are varied according to the change in solar irradiance. Figure 5.7 shows the variation of the module temperature and ambient temperature over the day. The average irradiance over the day is 84.7 W/m^2. The rear plate temperature of the CPV and flat-plate modules varied with the increase in solar radiation. The maximum temperature of the CPV-2 module is found to be 19.3^{o}C at 12:30pm, while the ambient temperature was 12.4^{o}C.

The effect of thermal inertia of the module can be observed as it takes some time to increase the temperature of the module after increase in solar irradiance. The rear plate temperature of the CPV-T1 module is found to be 1^o C less than CPV-T2 module, which is because of higher optical loss in the CPV-1 module, which eventually reduces

the concentration of the light on the solar cell. The rear plate temperature of the CPV-T2 module was 4^{o} higher than the flat-plate module at 12:30pm, while for the rest of the day the temperature of the CPV and flat-plate module was found to be within a difference of ±1^{o}C. The ambient temperature was found to be within 10-13.2^{o}C on that day.

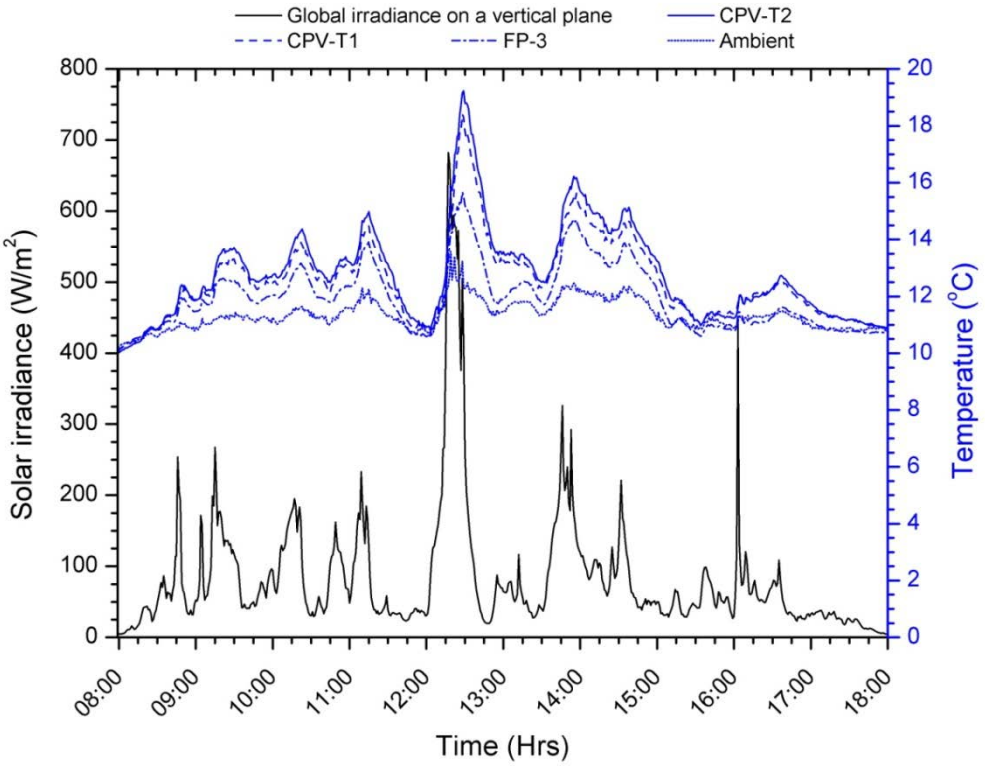

Figure 5.7 Diurnal variation of the module and ambient temperature with the solar irradiance on 4th of October 2011

The short circuit current of all the modules varied with the change in solar irradiance, as shown in figure 5.8. Maximum short circuit current of the CPV-T2 module was found to be 624 mA for solar irradiance 669 W/m^2, while for the same period of time the short circuit current of the CPV-T1 and flat-plate module is found to be 590 mA and 280 mA, respectively. The short circuit current of the CPV-T2 module for this irradiation was 2.23 time higher than the flat-plate module. The average short circuit current of the CPV-T2 and CPV-T1 module was 2 times and 1.97 times higher than the flat-plate module over the day from 8am to 6pm, respectively.

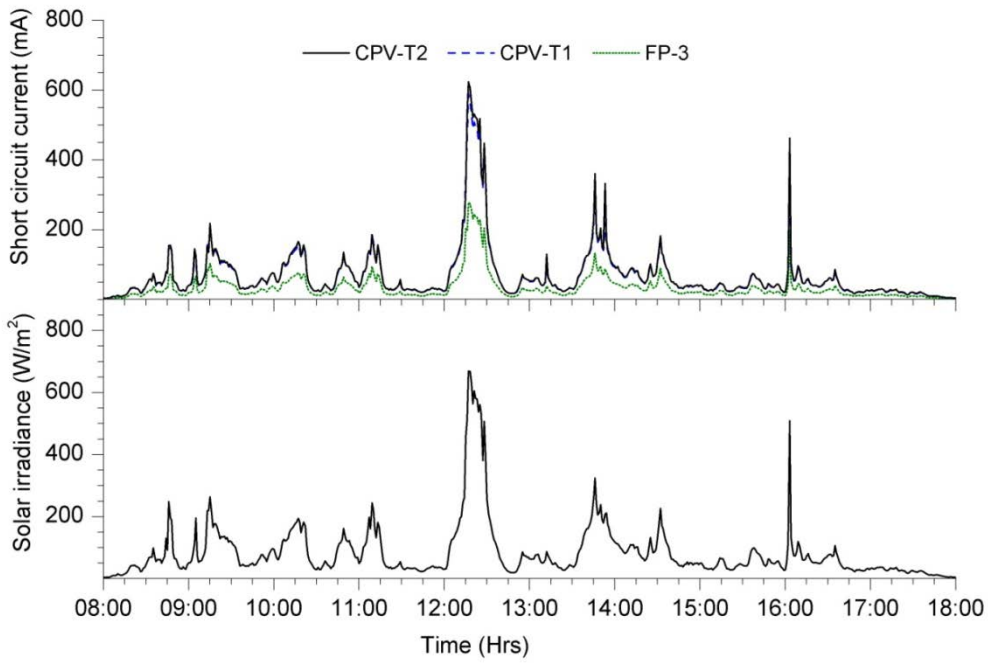

Figure 5.8 Diurnal variation in the short circuit current of the CPV-T2, CPV-T1 and flat-plate modules with solar irradiance on 4th of October

The variation in open circuit voltage and fill factor with the solar irradiance is shown in figure 5.9. The open circuit voltage of both the CPV and flat-plate module varied with the solar irradiance. The open circuit voltage of the CPV-T2 and CPV-T1 module was found to be almost equal and recorded between 8.8V to 6.7V over the day. The open circuit voltage of the flat-plate module was found to be insignificantly less than CPV modules for corresponding solar irradiations and recorded between 8.6V to 6.2V. The average open circuit voltages of the CPV and flat-plate modules over the day are found to be 7.9 and 7.6 respectively. The fill factor of all the modules was between 64.5% and 80.7% during the day. The average fill factor of the CPV module over the day was found to be higher than flat plat module by 5.3%. The fill factor increased with higher solar radiation. The fill factor of the CPV-T2, CPV-T1 and flat-plate module for 50W/m^2 irradiance was found to be 76.5%, 77.6% and 72.4%, while for the irradiance 680 W/m^2, the fill factor was measured as 79.5%, 80.3% and 79.6% respectively.

The maximum power output over the day from the CPV-T2, CPV-T1 and flat-plate module was recorded to be 4.38W, 4.17W and 1.9W for the solar irradiance 680 W/m^2 (figure 5.10). While the average irradiance over the day was 84.5W/m^2, the average maximum power output of the CPV-T2, CPV-T1 and flat-plat module was found to be 0.45W, 0.44W and 0.2W.

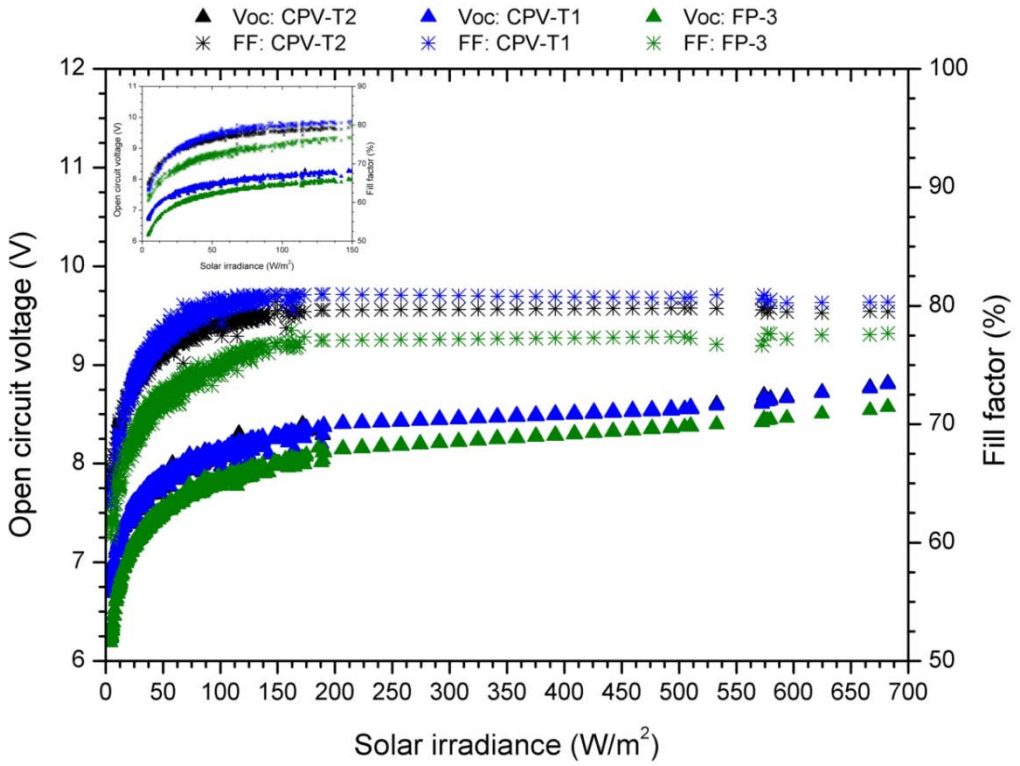

Figure 5.9 Variation of open circuit voltage and fill factor of the modules with solar irradiance.

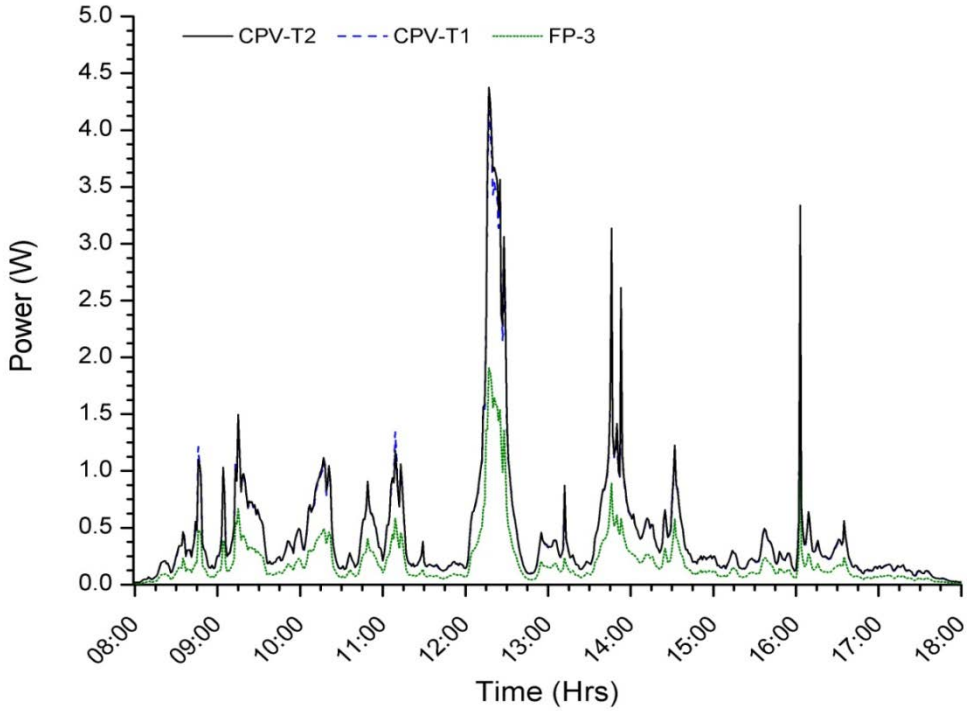

Figure 5.10 Diurnal variation of power output of the modules.

As shown in figure 5.11, the power output of all the modules increase linearly. Most of the contribution of higher intensities came from direct radiation, so a better power

output of the CPV modules compared to the flat plate module was achieved with increased irradiance. The theoretical study shows that the DiACPC-55 concentrator can achieve an optical concentration ratio of 2.28 considering all possible losses in the system, while the concentrator is designed for geometric concentration ratio 2.8. The theoretical study also showed that the concentrator could achieve an optical concentration ratio of 1.3 for diffuse radiation. In the experimental investigation unexpected increase or decrease in power output was observed for some irradiance data points, which was due to the mismatch of recording in solar irradiance and power output due to the fluctuation of solar irradiance.

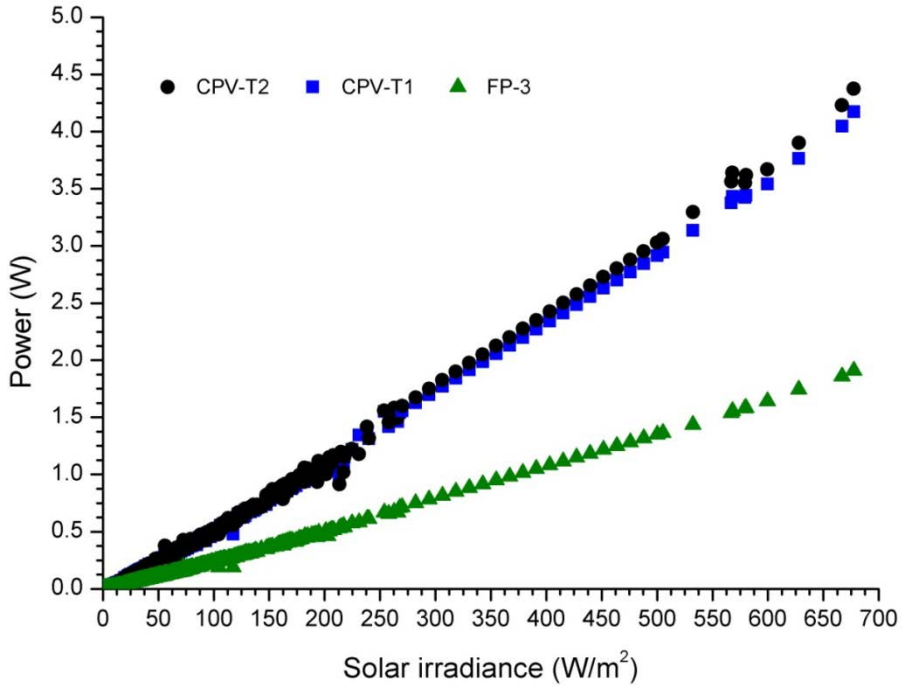

Figure 5.11 Variation of the power output of the modules with increase in solar irradiance over the day

Fluctuations were observed in the power ratio of the CPV-T2 and CPV-T1 modules, within the range of 1.9 to 2.3 (figure 5.12). The average power ratio of the CPV-T2 and CPV-T1 module on the rainy day was found to be 2.2 and 2.1. For a range of consistent solar radiation of few minutes on this rainy day, the average power ratio of 2.22 and 2.19 for CPV-T2 and CPV-T1 module corresponding to the average irradiance 138 W/m^2 has been recorded between 9:10am to 9:30am. With an increase in solar irradiance the average power ratio of CPV-T2 and CPV-T1 was found to be 2.2 and 2.15 respectively for average irradiance 423 W/m^2 within 12:10pm to 12:30pm.

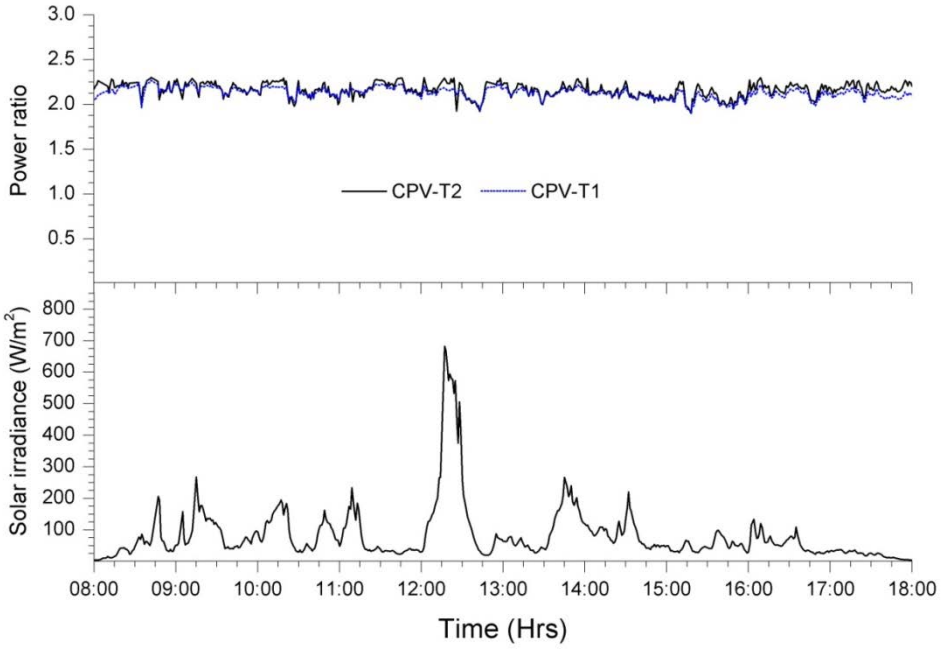

Figure 5.12 Diurnal variation of the power ratio of CPV-T2 and CPV-T1 module over the day with the variation of the solar irradiance.

The average efficiency of the CPV-T2, CPV-T1 and the flat-plate module over the day was found to be 8.92%, 8.76% and 11.63% as shown in figure 5.13. For maximum irradiation 680 W/m^2, the corresponding efficiency of the CPV-T2, CPV-T1 and flat-plate module is 10.7%, 10.4% and 13.9%, respectively.

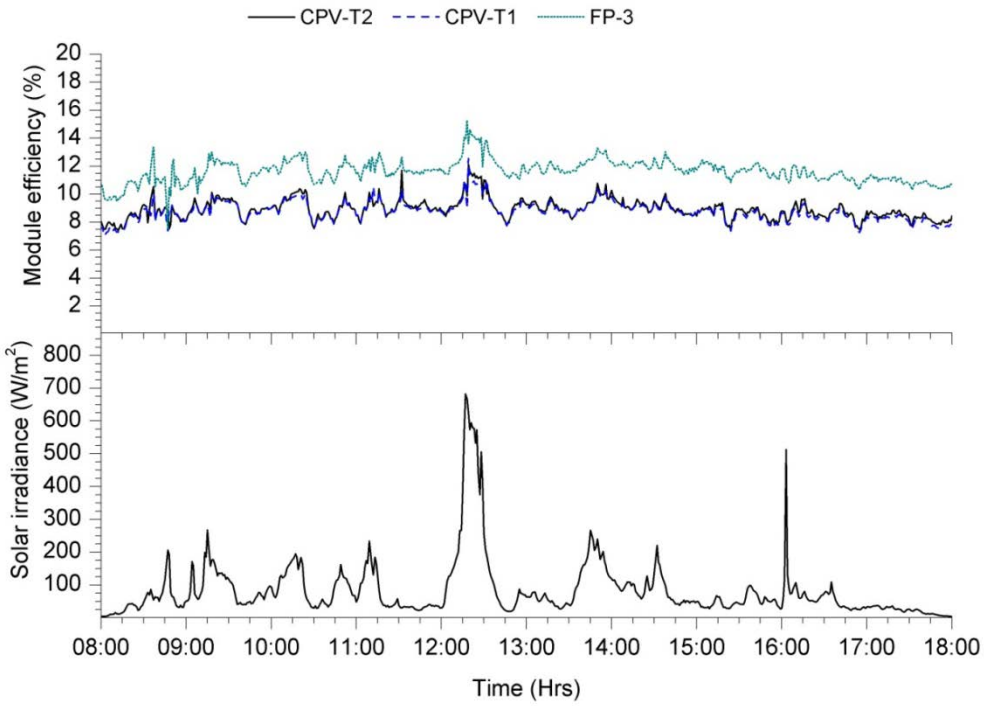

Figure 5.13 Diurnal variation of module efficiency of the modules with solar irradiance

For a range of consistent solar radiation for few minutes on this rainy day, the average module efficiency of 9.5%, 9.3% and 12% for CPV-T2, CPV-T1 and flat-plat module corresponding to an average irradiance 138 W/m^2 has been recorded between 9:10am to 9:30am. With an increase in solar irradiance the average module efficiency of CPV-T2, CPV-T1 and flat-plat module is found to be 10.6%, 10.36% and 13.54% respectively for an average irradiance 423 W/m^2 during 12:10pm to 12:30pm. The output of the characterisation on 4th October 2011 is summarised in table 5.2.

Table 5.2 Summary of the characterisation of the CPV modules on 4th October 2011

	Parameters	-	FP-3	CPV-1	CPV-2
4th October	Solar Irradiance (W/m^2)	Maximum	669.79	669.79	669.79
		Minimum	4.14	4.14	4.14
		Average	84.49	84.49	84.49
	Short circuit current (mA)	Maximum	279.6	590	623.9
		Minimum	2.3	4.4	4.5
		Average	34.1	67.3	69.7
	Open Circuit voltage (V)	Maximum	8.58	8.8	8.82
		Minimum	6.19	6.7	6.74
		Average	7.56	7.89	7.88
	Maximum Power (W)	Maximum	1.9	4.17	4.38
		Minimum	0.009	0.02	0.02
		Average	0.2	0.44	0.45
	Fill factor (%)	Maximum	77.7	80.2	80.7
		Minimum	64.5	64.8	64.5
		Average	72.5	77.2	76.4
	Efficiency (%)	Maximum	14.3	11.1	12.1
		Minimum	9.5	7	7.43
		Average	11.63	8.8	8.95

5.2.2.2 Electrical performance of the CPV modules on a sunny interval day-1(7th October 2011)

The diurnal variation of the solar irradiance on the day with sunny intervals, the 7th of October 2011, is shown in figure 5.14. The global irradiance on a vertical plane and the contribution of direct and diffuse radiation has been observed.

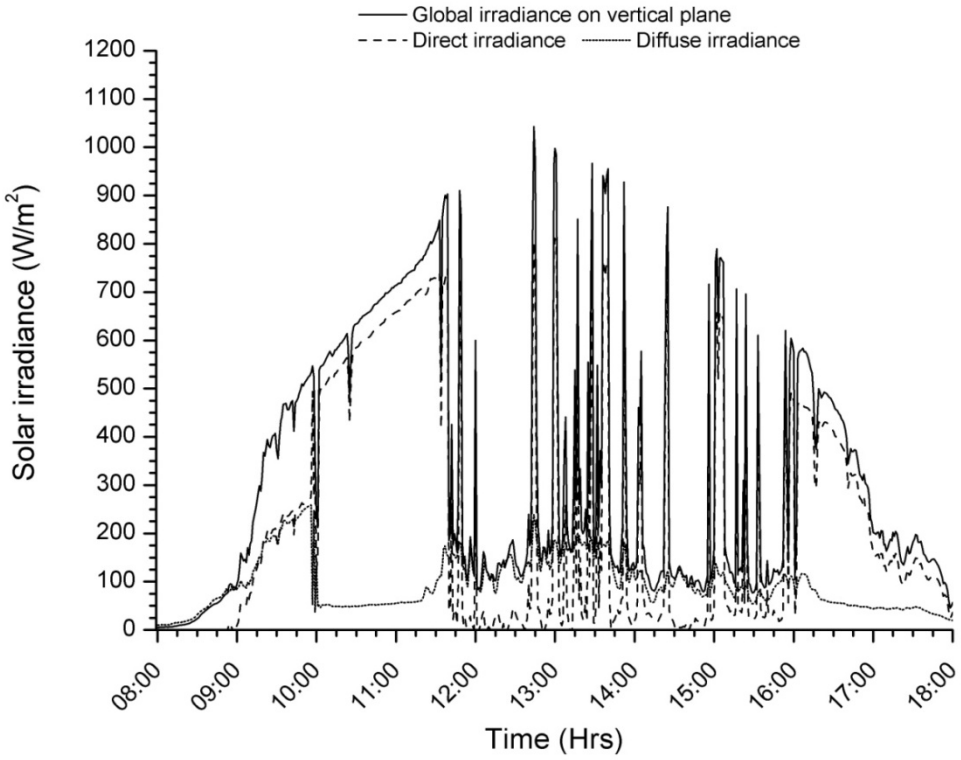

Figure 5.14 Diurnal variation of the Global, direct and diffuse irradiance on a vertical plane on7th of October 2011

Maximum global irradiance on the vertical surface was found to be 997 W/m^2, with 811W/m^2 of direct irradiance and 185W/m^2 of diffuse radiation. The day consisted of sunny interval with clear sky in the morning and in the afternoon. The average global, direct and diffuse irradiance over the day was found to be 375.5 W/m^2, 267 W/m^2 and 108.5 W/m^{2,} respectively. The ambient temperature and the module temperature have also varied with the solar irradiance which is shown in figure 5.15.

The module temperature varied in all cases, with the solar irradiance at a maximum of 35.2^{o}C for the CPV-T2 module, 28.1^{o}C for the CPV-T1 module and 24 ^{o}C for the flat-plate module. While the ambient temperature and wind speed was 14.7^{o}C (at 11:34am) and 10m/s respectively. The maximum temperature of the CPV-T2 module was found

to be 11.2^{o}C higher than the flat-plate module, and 6^{o}C higher than the CPV-T1 module. The CPV-T1 module temperature varied from 8.3^{o}C to 35.2^{o}C, while the ambient temperature varied from 8.5^{o}C to 17^{o}C. Higher module temperature of the CPV-T2 compared with the CPV-T1 module were observed, resulting from higher optical losses and also may be due to the moisture trapped inside the CPV-T1 module.

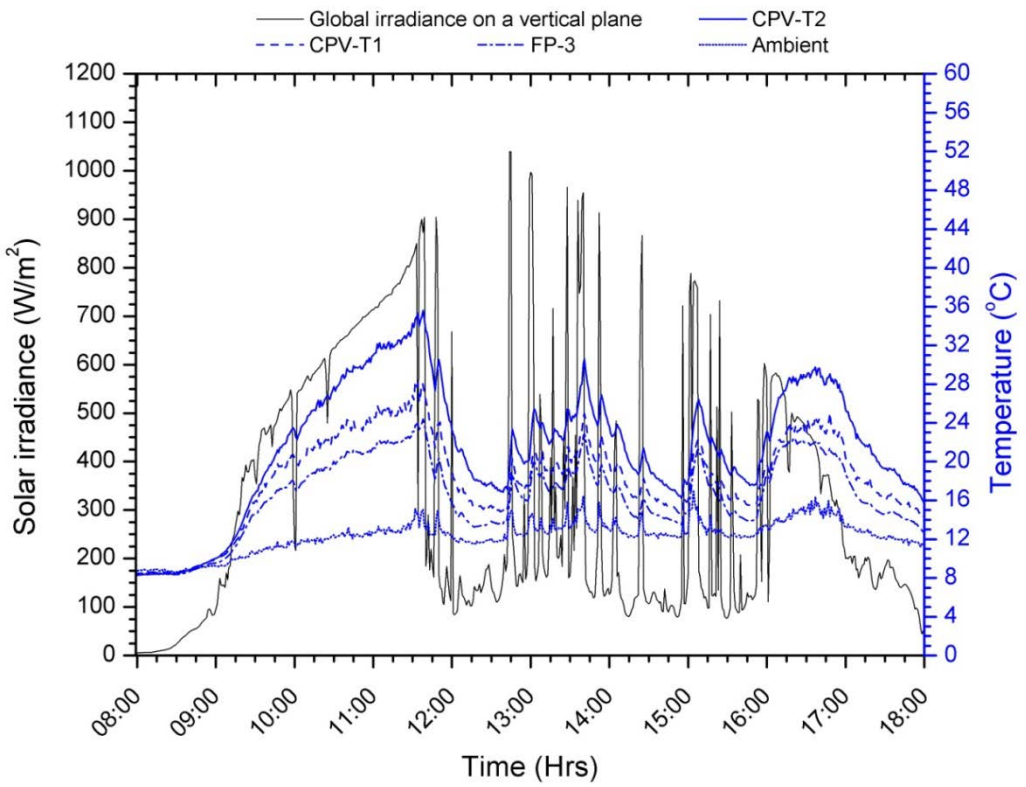

Figure 5.15 Variation of the module temperature with solar irradiance throughout the day.

The diurnal variations of the short circuit currents of the modules are shown in figure 5.16. The maximum short circuit current of the CPV-T2 module was recorded as 933.5mA, while the same for CPV-T1 and flat-plate module was found to be 870mA and 421.5mA at 997 W/m^2. The maximum short circuit current of the CPV-T2 module was 2.21 times and CPV-T1 module was 2.1 times higher than the flat-plate module for the same solar irradiance. During 12:00am to 12:40pm, in the cloudy weather, while solar irradiance was diffuse with the average value 134 W/m^2, the average short circuit current of the CPV-T2, CPV-T1 and flat-plate module was 113mA, 107.1mA and 51.6mA, respectively. During the continuous solar irradiance between 10:30am to 11:30, the average solar irradiance was 717 W/m^2, and the average short circuit current

of the CPV-T2, CPV-T1 and flat-plate module was 677mA, 632.5mA and 305.5mA, respectively.

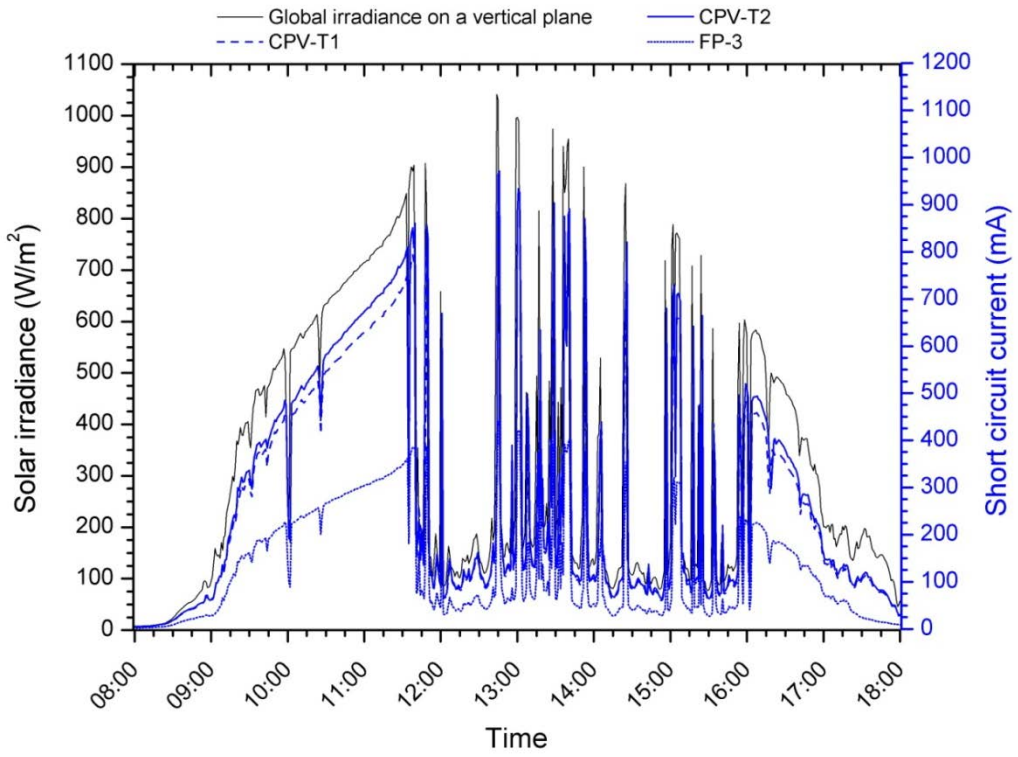

Figure 5.16 Diurnal variation of the short circuit current of the modules with solar irradiance.

The variation of the open circuit voltage and fill factor over the day, with the variation of the solar irradiance, is shown in figure 5.17. The open circuit voltage of the CPV-T2 and CPV-T1 module was found similar and recorded between 8.8V to 6.8V over the course of the day. The open circuit voltage of the flat-plate module was slightly less than CPV modules for corresponding solar irradiations and recorded between 8.6V to 6.4V. The average open circuit voltages of the CPV and flat-plate module over the day are found to be 8.16 and 7.96, respectively. It can be noticed that with decrease in solar irradiance the open circuit voltage decreases. During 12:00am to 12:40pm, in the cloudy weather, while solar irradiance was diffuse with an average of 134 W/m^2, the average open circuit voltage was found to be 8.1V for both CPV-T2 and CPV-T1 and 7.9 for the flat-plate module. The fill factor of the modules was observed to fluctuate with the solar irradiance, which contributes to the maximum power output of the CPV and the flat plate system. During the steady increase or decrease in solar irradiation the fill factor varied steadily, decreasing with increase in solar irradiance. This may be due to the change in temperature of the module.

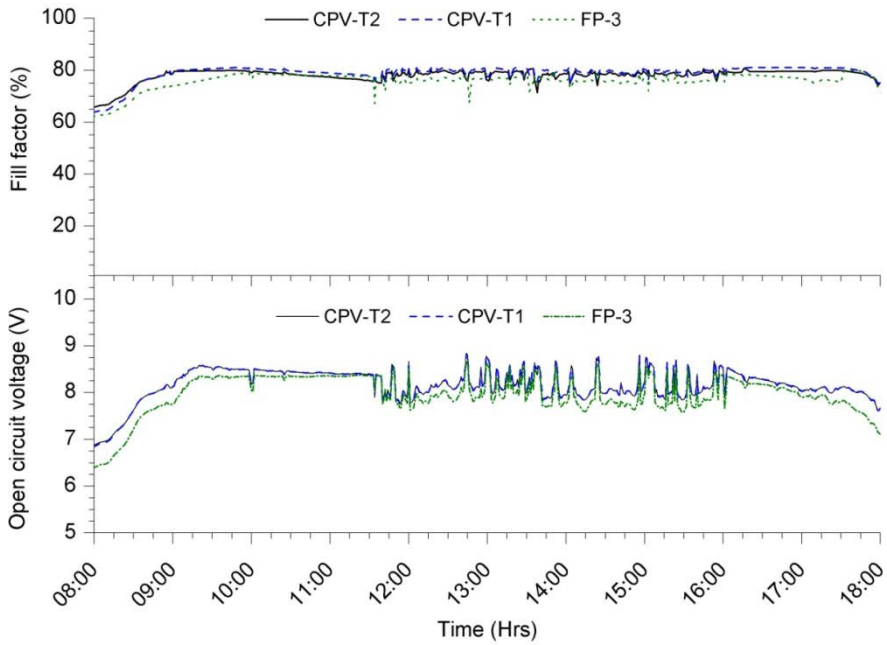

Figure 5.17 Variation of open circuit voltage and fill factor over the day with change in solar irradiance

The fill factor of all the modules was found to be within 67.2% to 80.9% throughout the duration of the day. The fill factors of the CPV modules were very close for corresponding solar irradiance and higher than the flat-plate module. Higher load current in the CPV modules compared to the flat-plate module could be the reason for the increase in fill factors. With increase in radiation during the morning hours (which is mostly diffuse radiation) the fill factor increases. With increase in direct radiation after 9am, the fill factor tends to be decreased (till 11:30am). After which it fluctuates with variation in solar irradiance. The average fill factor of the CPV-T2, CPV-T1 and flat-plate module during steady increase of solar irradiance between 10:00am to 11:30am was found to be 77.8%, 79.3% and 78% respectively for an average irradiance of 677 W/m^2. The average fill factor of the CPV-T2, CPV-T1 and flat-plate module in a cloudy condition between 12:00am to 12:40am was 79%, 79.9% and 76.3% respectively, for an average irradiance 131.9 W/m^2. The change in fill-factor and the open circuit voltage of the module changes the maximum power output of the module. The diurnal variation of the power output of the modules on the 7th of October is shown in figure 5.18. The maximum power output over the day from the CPV-T2, CPV-T1 and flat-plate module was 6.5W, 6.2W and 2.96W for the solar irradiance 997 W/m^2. The average maximum power output of the CPV-T2, CPV-T1 and flat-plat module was found to be 1.83W, 1.74W and 0.8W, for the average daily irradiance of 318.6W/m^2.

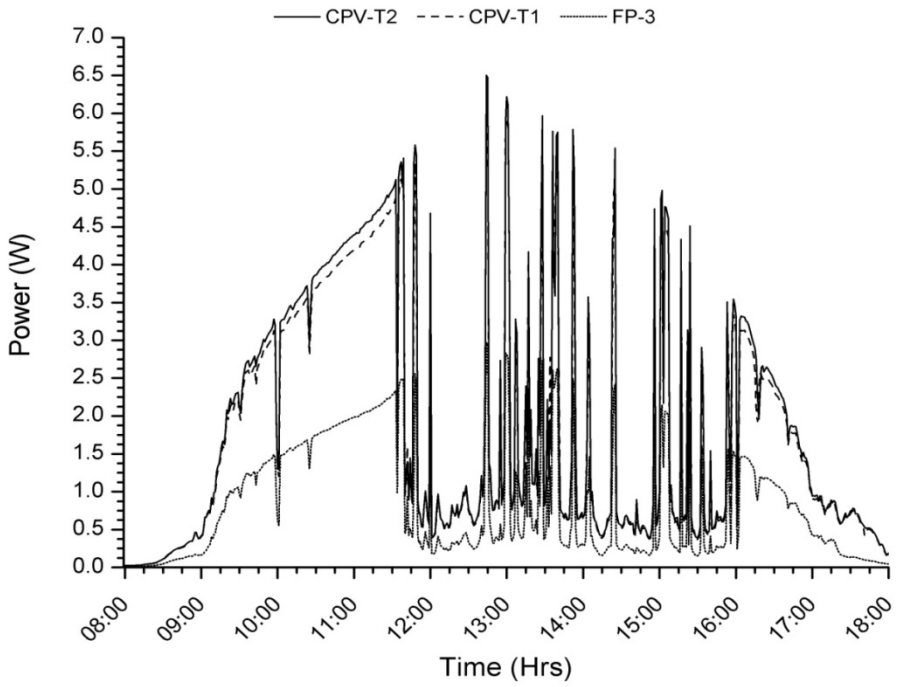

Figure 5.18 Diurnal variation of the power output of the modules on the sunny interval day 7th of October 2011.

The variation of the maximum power output with the solar irradiance is shown in figure 5.19. A linear increase in power output of the CPV and the flat-plat module can be observed. The power output of the CPV modules are found to be higher in all conditions compared to the flat-plate module, which is a significant outcome for effective use of the dielectric concentrator in diffuse radiation. Due to the fluctuation of the solar irradiance, the power output from CPV-T2 module was found to be less than the CPV-T1 module for few data points. This is mainly because of the switching delay of the IV-tracer instrument, which causes a mismatch. The power ratio of the CPV-T2 and CPV-T1 module was observed to fluctuate within 1.35 to 2.33. The fluctuation of the solar irradiance caused by the shadow of the clouds leads to a mismatch in the power output of the modules, which results in a wider range of fluctuation in power ratio calculations. The average power ratio of the CPV-T2 and CPV-T1 module on this sunny interval day was found to be 2.2 and 2.1. The average power ratio of the CPV-T2, CPV-T1 module during steady increase of solar irradiance between 10:00am to 11:30am is also found to be 2.2 and 2.1 respectively, for an average irradiance of 677 W/m^2. The average power ratio of the CPV-T2 and CPV-T1 module in a cloudy condition between 12:00am to 12:40am was 2.26 and 2.2 respectively, for average irradiance 131.9 W/m^2. This demonstrates a better performance of the dielectric concentrators for diffuse radiation. Even though the power output of the CPV modules has increased, the module efficiency

of the flat-plate module is found to be higher for all the range of irradiance over the course of the day.

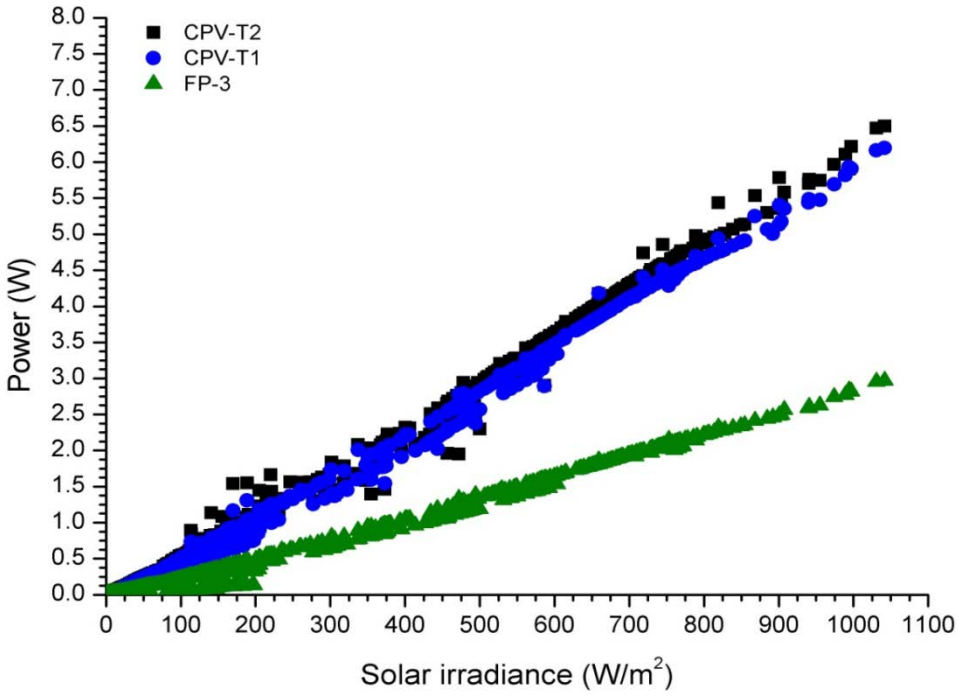

Figure 5.19 Variation of the power output of the module with solar irradiance.

The diurnal variation of the module efficiency of all the three modules in study is shown in figure 5.20. The average efficiency of the CPV-T2, CPV-T1 and the flat-plate module over the day was found to be 10%, 9.56% and 12.44%.

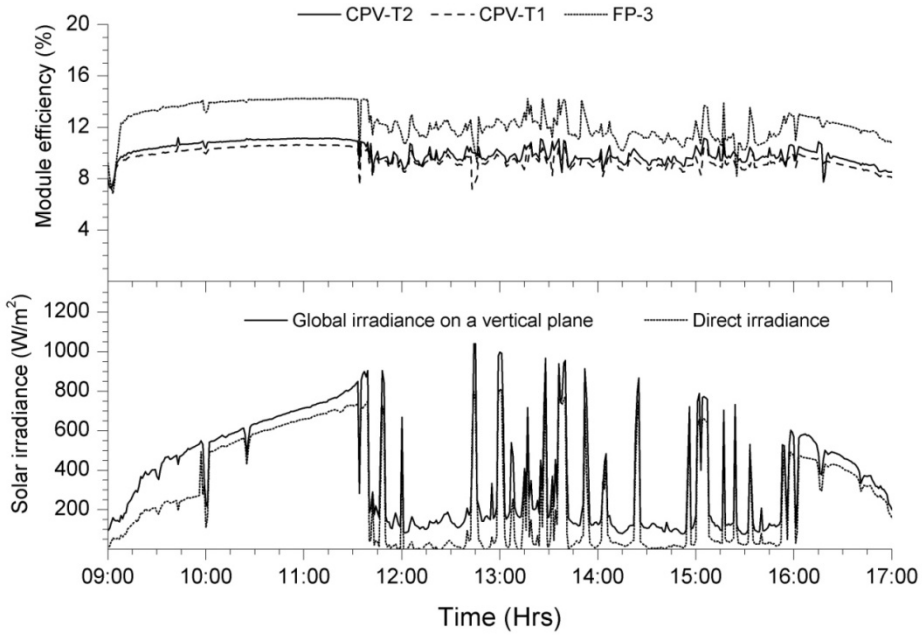

Figure 5.20 Diurnal variation of the module efficiency with the variation of global and direct solar irradiance on a vertical plane.

The average module efficiency of the CPV-T2, CPV-T1 and flat-plat module during steady increase of solar irradiance between 10:00am to 11:30am was measured as 11%, 10.55% and 14.15% respectively, for an average irradiance of 677 W/m^2. The average fill factor of the CPV-T2, CPV-T1 and flat-plate module in cloudy conditions between 12:00am to 12:40am, was found to be 9.7%, 9.33% and 11.8% respectively, for average irradiance 131.9 W/m^2. The output of the characterisation on 7th October 2011 is summarised in table 5.3.

Table 5.3 Summary of the characterisation of the CPV modules on 7th October 2011

	Parameters	-	FP-3	CPV-1	CPV-2
7th October	Solar Irradiance (W/m^2)	Maximum	997	997	997
		Minimum	8.4	8.4	8.4
		Average	318	318	318
	Short circuit current (mA)	Maximum	421.5	870	933.5
		Minimum	2.7	9.3	5.3
		Average	126.1	260.2	278.02
	Open Circuit voltage (V)	Maximum	8.6	8.8	8.8
		Minimum	6.4	6.8	6.8
		Average	7.96	8.16	8.16
	Maximum Power (W)	Maximum	2.96	6.2	6.5
		Minimum	0.01	0.023	0.024
		Average	1.83	1.74	0.8
	Fill factor (%)	Maximum	79.2	80.1	80.9
		Minimum	62.3	63.9	65.9
		Average	76.1	79.4	78.3
	Efficiency (%)	Maximum	14.3	11.7	12
		Minimum	3	5.4	5.7
		Average	12.44	9.65	10

5.2.2.3 Electrical performance of the CPV modules on a sunny interval day-2 (16th October 2011)

The outdoor performance analysis of the CPV modules has been carried out on another sunny interval day to investigate the consistency of the performance. The diurnal variation of the solar irradiance on 16th of October is shown in figure 5.21.

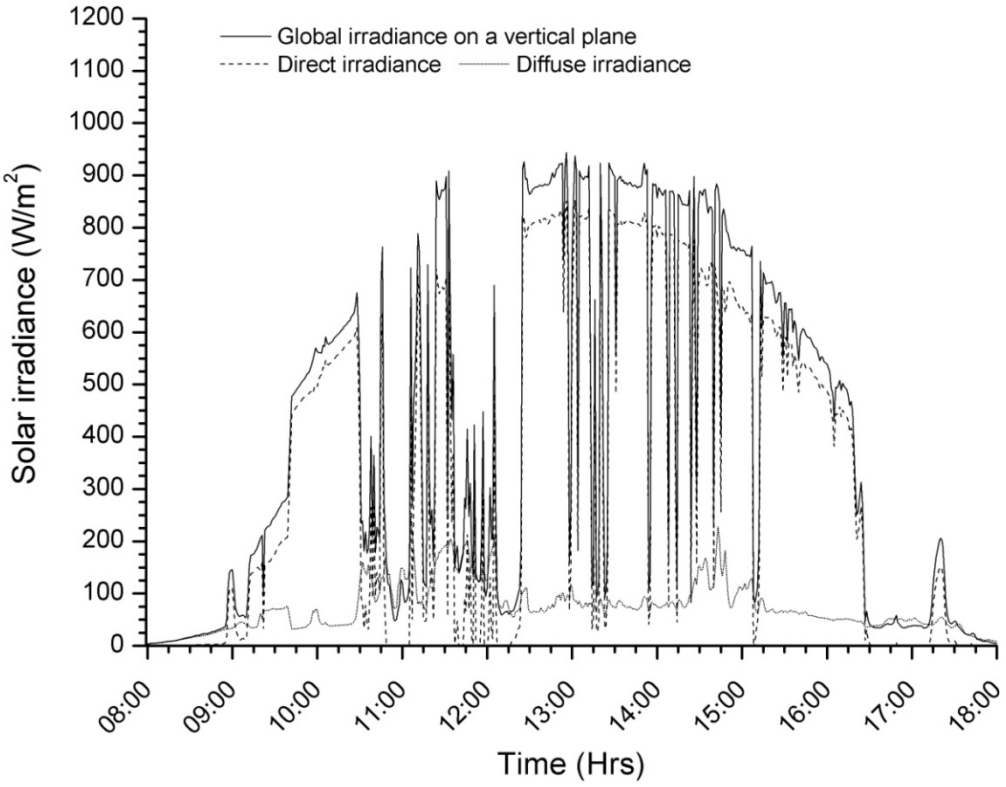

Figure 5.21 Diurnal variation of the global, direct and diffuse solar irradiance on a sunny interval day 16th of October 2011

The day was basically sunny with white clouds interrupting the direct solar irradiance. The maximum global irradiance on the vertical surface was 943 W/m^2, with 851.3W/m^2 direct irradiance and 92.55 W/m^2 diffuse radiation. The average irradiance over the day was 398.5 W/m^2 as global irradiance on the vertical surface, 325.7W/m^2 as direct irradiation and 72.87W/m^2 as diffuse radiation. The module temperature has also varied with the irradiance, which is shown in figure 5.22. The rear plate temperature of all the modules rose with the increase in solar irradiance. The rear plate temperature of the CPV-T2 module varied from 11.6^{o}C to 39.8^{o}C, while the ambient temperature varied from 9.4^{o}C to 16.6^{o}C. In the morning hours between 8:00am to 9:30am, the temperature of the CPV and the flat-plate module was found to be almost same, while the irradiance was predominantly diffuse radiation. However, during the rest of the day, the temperature of the CPV-T2 module was found to be higher than the flat-plate module. The average temperature of the CPV-T2 and flat-plate module from 12:30pm to 16:30pm was 33.5^{o}C and 23.4^{o}C respectively, which is 23% higher than the flat-plate module temperature. The average ambient temperature, solar irradiance and wind speed during this period was 14.6^{o}C, 670W/m^2 and 13m/s, respectively.

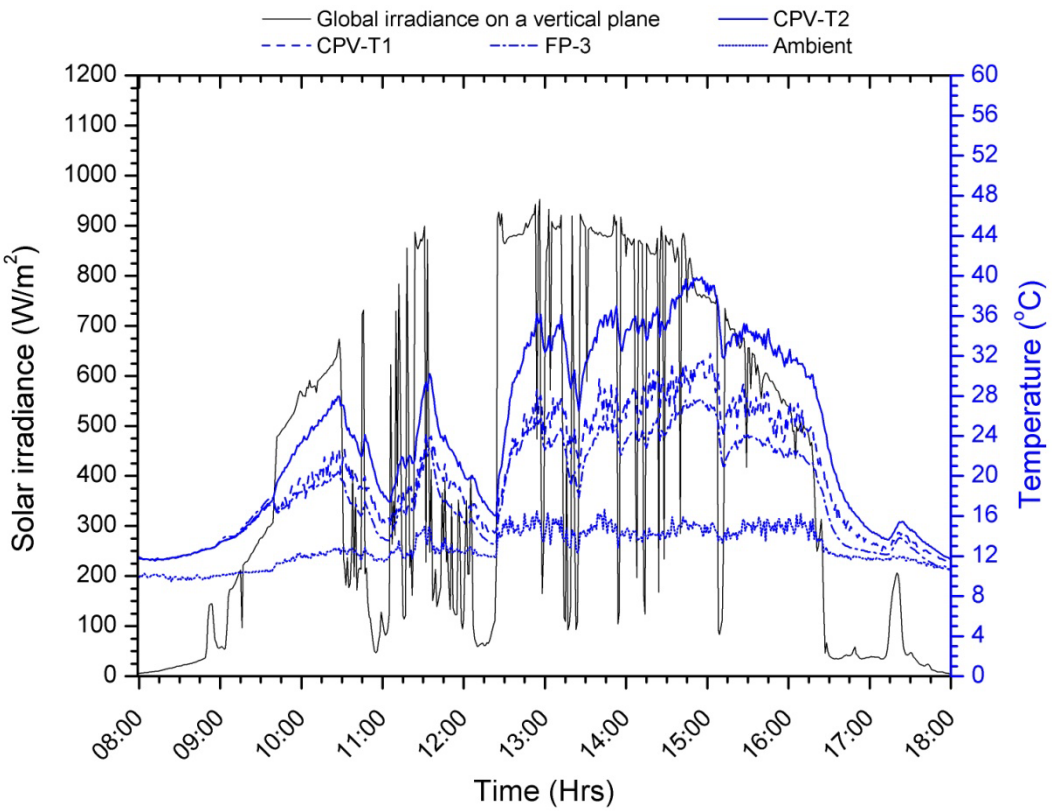

Figure 5.22 Diurnal variation of the module temperatures and ambient temperature over the day.

The diurnal variation of short-circuit current is shown in figure 5.23. The maximum short circuit current of CPV-T2, CPV-T1 and the flat-plat module was recorded to be 898mA, 815mA and 399.2mA, for the maximum global solar irradiance of 943W/m^2 on a vertical surface. The short circuit current of the CPV-T2 and CPV-T1 module was found to be 2.25 and 2.04 times higher than the flat-plat module, for maximum irradiance. The average short circuit current of the CPV-T2, CPV-T1 and flat-plat module over the day was 355.6mA, 325.1mA and 160mA respectively, while the average solar global irradiance was 399.4W/m^2. The average short circuit current of the CPV-T2 and CPV-T1 module was observed to be 2.22 and 2 times higher than the flat plat module. Over the period of 12:30pm to 4:30pm, while the solar irradiance was mostly direct irradiance, the average short circuit current of the CPV-T2 and CPV-T1 module was 633.5mA and 575.4mA respectively. This is 2.23 and 2 times higher than the flat-plat module for the average solar irradiance 693.6W/m^2 during this period.

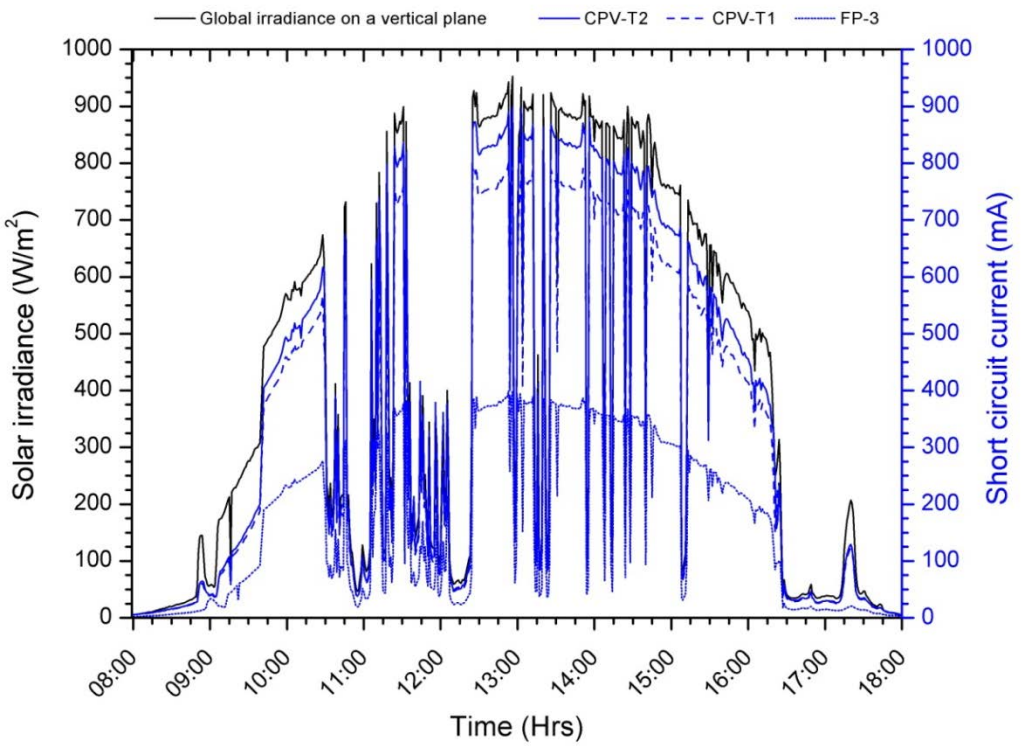

Figure 5.23 Diurnal variation of the short circuit current of the CPV and flat plate module with the variation in solar irradiance

The open circuit voltage performed as expected; it was generally consistent over the day, with small fluctuations due to the fluctuating solar irradiance, as shown in figure 5.24. The open circuit voltage was lower during the morning and evening time, while the solar irradiance was less and mainly contributed by diffuse radiation. With increase in temperature during mid day, the open circuit voltage of all the modules decreased. The average open circuit voltage over the day of the CPV-T2, CPV-T1 was ~8V; while the open circuit voltage of FP-3 module was 7.87V. During 10:00am to 4:00pm, the average open circuit voltage of all the three modules was approximately 8.2V.

The fill factor of the all the modules varied with an increase in solar irradiance and the temperature of the module (figure 5.24). During the morning and evening hours, when the module temperature was low, the fill factor of the CPV-T2 modules was higher than the flat plat module. Whereas during 12:30pm to 4:00pm, while the solar irradiance was predominantly direct radiation, the fill factors of the CPV modules were found to be less than flat plate module. The average fill factor of the CPV-T2 and flat plate module within 8:00am to 9:30am was 74.7% and 71.5%. While during 12:30pm to 4:3pm the average fill factor of these two modules was 76.2% and 77.3%. The average fill factor

of the CPV-T2, CPV-T1 and flat plate modules over the day was observed as 76.2%, 77% and 75%, respectively.

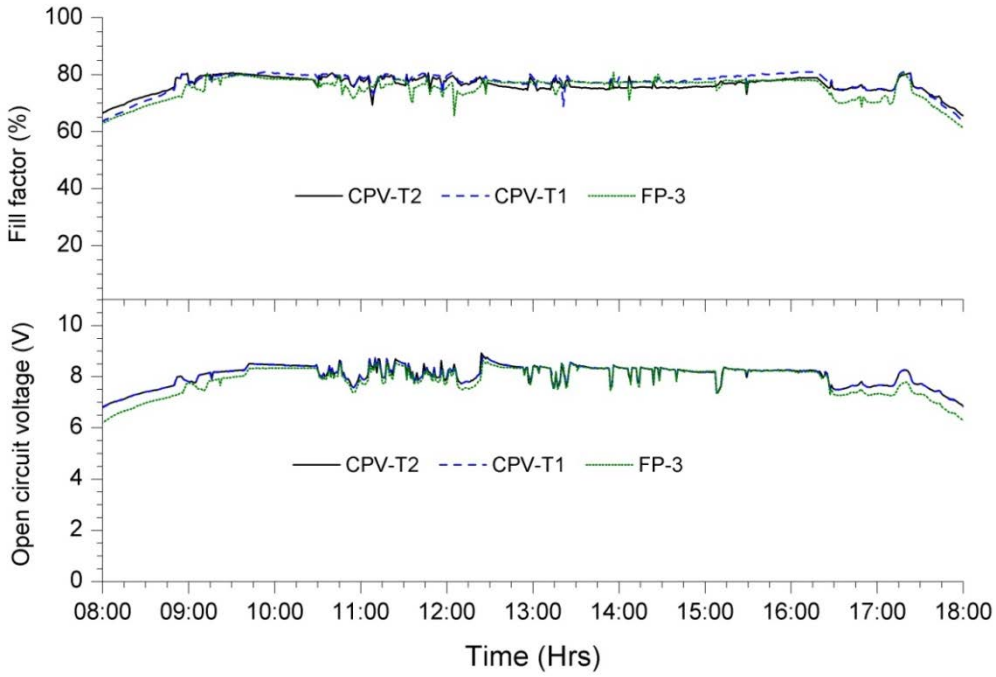

Figure 5.24 Diurnal variation of open circuit voltage and fill factor of the module on 16th of October 2011.

The diurnal variation of the maximum power output of the three modules is shown in figure 5.25. The average power output of the three modules, CPV-T2, CPV-T1 and the flat-plat over the day, was 2.28W, 2.14W and 1.02W respectively, for the average irradiance 399.4W/m^2. In the morning hours, while there was a continuous increase in solar irradiance from 8:00am to 9:30am, the average power output of the CPV-T2, CPV-T1 and flat-plat module was 0.3W, 0.28W and 0.11 respectively, for an average irradiance 84W/m^2. During 12:30pm to 4:00pm, with an average global irradiance of 693W/m^2, the average power output of the CPV-T2, CPV-T1 and flat plat module was 4.14W, 3.87W and 1.88W, respectively.

The power output of all the modules varied linearly with increase in solar irradiance, as shown in figure 5.26. The maximum power output of the CPV-T2, CPV-T1 and the flat plate module over the day was recorded as 5.88W, 5.47W and 2.59W respectively, for the corresponding irradiance of 943W/m^2.

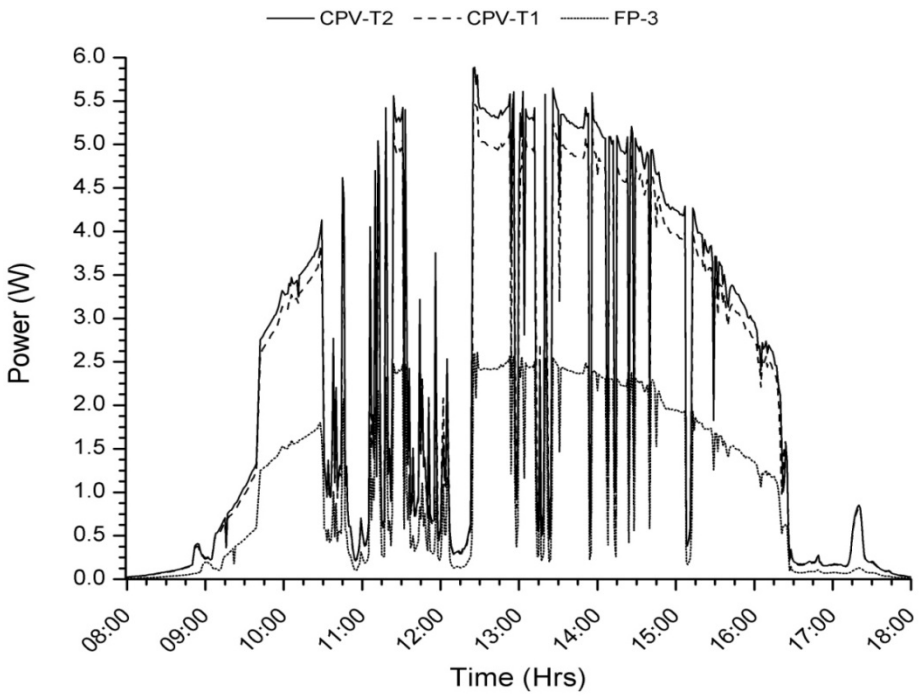

Figure 5.25 Diurnal variation of the power output of the modules throughout the day

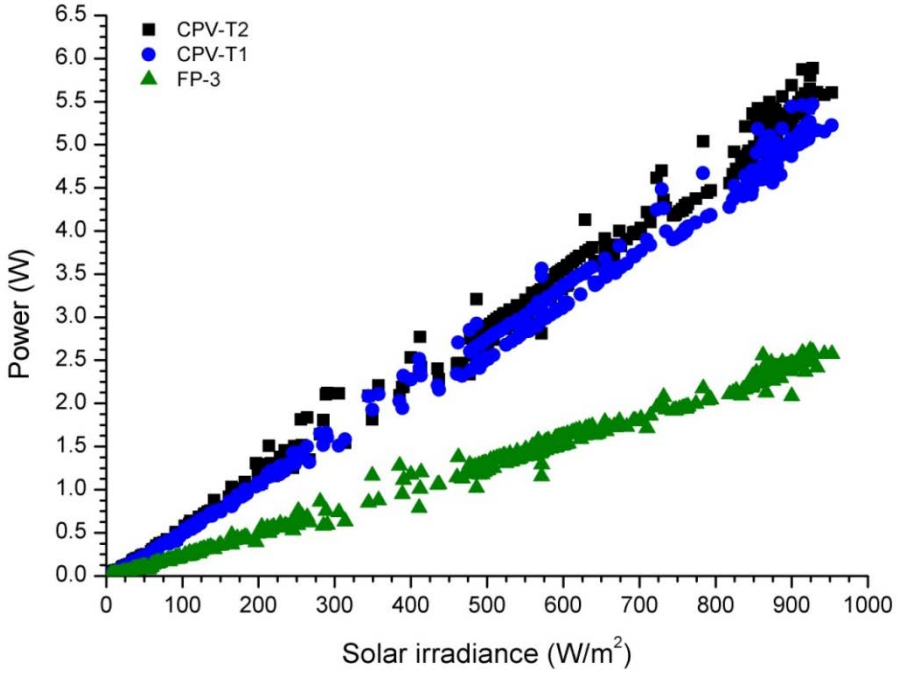

Figure 5.26 Variation of the power output of the modules with the solar irradiance.

The power ratio of the CPV-T2 and CPV-T1 module was in agreement with the theoretical study and indoor characterisation of the modules (figure 5.27). The power ratio of the CPV modules varied between 1.67 to 2.29 depending on the solar irradiance and the fluctuation of the solar radiation due to clouds. The average power ratio over the day for the CPV-T2 and CPV-T1 module was found to be 2.19 and 2.07. During the

morning hours from 9:00am to 10:30am, while the solar irradiance was increasing without much disruption, the average power ratio was recorded as 2.19 and 2.07 respectively for CPV-T2 and CPV-T1 modules. From 12:30pm to 4:00pm while the irradiation was largely attributed to direct radiation, the average power ratio was found to be the same for both the modules.

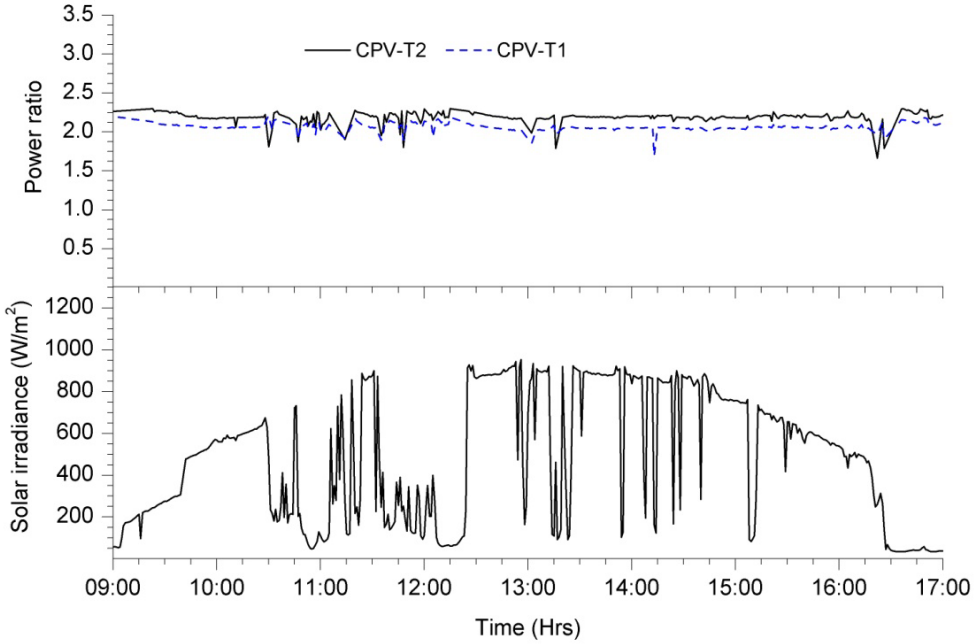

Figure 5.27 Variation of the power ratio of CPV-T2 and CPV-T1 modules over the day on 16th of October 2011.

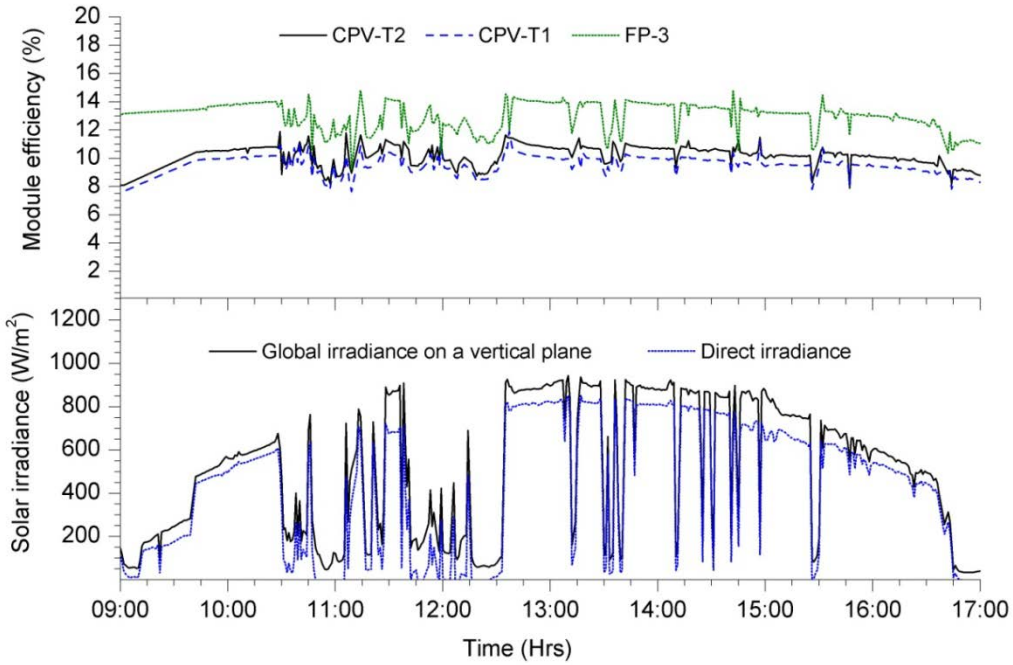

Figure 5.28 Diurnal variation of the module efficiency with change in solar irradiance on a sunny interval day 16th of October 2011.

The diurnal variation of the module efficiencies with the change in solar irradiance is shown in figure 5.28. The average module efficiencies of the CPV-T2, CPV-T1 and the flat-plate module over the day were 10.01%, 9.4% and 12.67%, respectively. The average module efficiency of the CPV-T2, CPV-T1 and the flat-plate module from 12:30pm to 4:00pm were 10.49%, 9.79% and 13.36%, while the irradiation was mostly contributed by direct irradiance. Because of the higher fluctuation in the solar irradiance from 10:30am to 12:30pm compared to the rest of the day, the average module efficiency over the day has been reduced. For a complete sunny day the average efficiency of the module is expected to be increased. The output of the characterisation on 16th October 2011 is summarised in table 5.4.

Table 5.4 Summary of the characterisation of the CPV modules on 16th October 2011

	Parameters	-	FP-3	CPV-1	CPV-2
16th October	Solar Irradiance (W/m^2)	Maximum	943	943	943
		Minimum	3.6	3.6	3.6
		Average	398.5	398.5	398.5
	Short circuit current (mA)	Maximum	399.2	815	898
		Minimum	2.1	5.4	5.6
		Average	160	325.1	355.6
	Open Circuit voltage (V)	Maximum	8.64	8.8	8.82
		Minimum	6.2	6.8	6.83
		Average	7.87	8	8
	Maximum Power (W)	Maximum	2.59	5.47	5.88
		Minimum	0.008	0.02	0.03
		Average	1.02	2.14	2.28
	Fill factor (%)	Maximum	80.8	80.8	81.02
		Minimum	57.6	63.7	46.1
		Average	75	77	76.2
	Efficiency (%)	Maximum	16.5	12.4	13.2
		Minimum	3.2	4	3.83
		Average	12.76	9.4	10.01

5.2.2.4 Electrical performance of the CPV modules on a rainy day (17th October 2011)

The CPV module has also been characterised on a rainy day to investigate the performance of the concentrator for diffuse radiations and overall performance of the module in a different weather condition. The diurnal variation of the global and diffuse irradiance on a vertical plane is shown in figure 5.29. The global irradiance was mostly diffuse with rain showers, so direct irradiance is not shown in the figure.

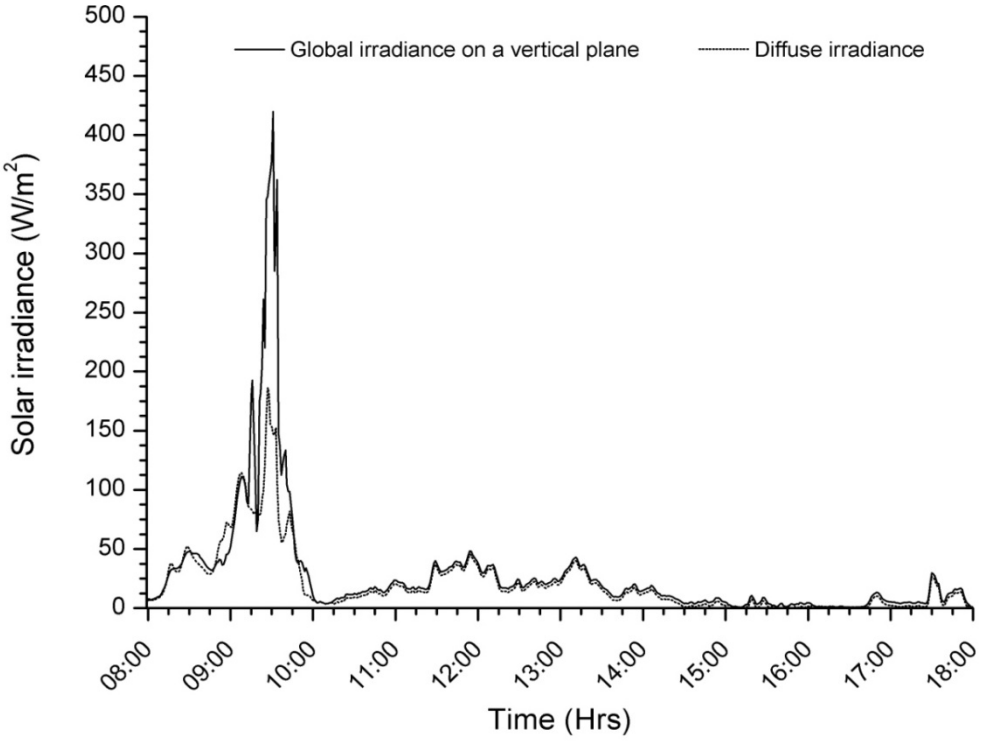

Figure 5.29 Diurnal variation of the global and diffuse irradiance on a vertical plane on 17th of October 2011

The average global and diffuse irradiance on the cloudy day (17th October2011) was found to be 28W/m^2 and 20W/m^2, respectively. The global irradiance is higher because of the increase in direct irradiance for almost half an hour in-between 9:15am to 9:45am. For the rest of the day from 10:00am to 6:00pm the average global and diffuse irradiance was 14W/m^2 and 11W/m^2 respectively. The ambient and the module temperature during the day were very close, except during higher irradiance. The ambient temperature drops significantly at around 10:00am while grey clouds covered the sky followed by drizzling. The change in module and ambient temperature is shown in figure 5.30.

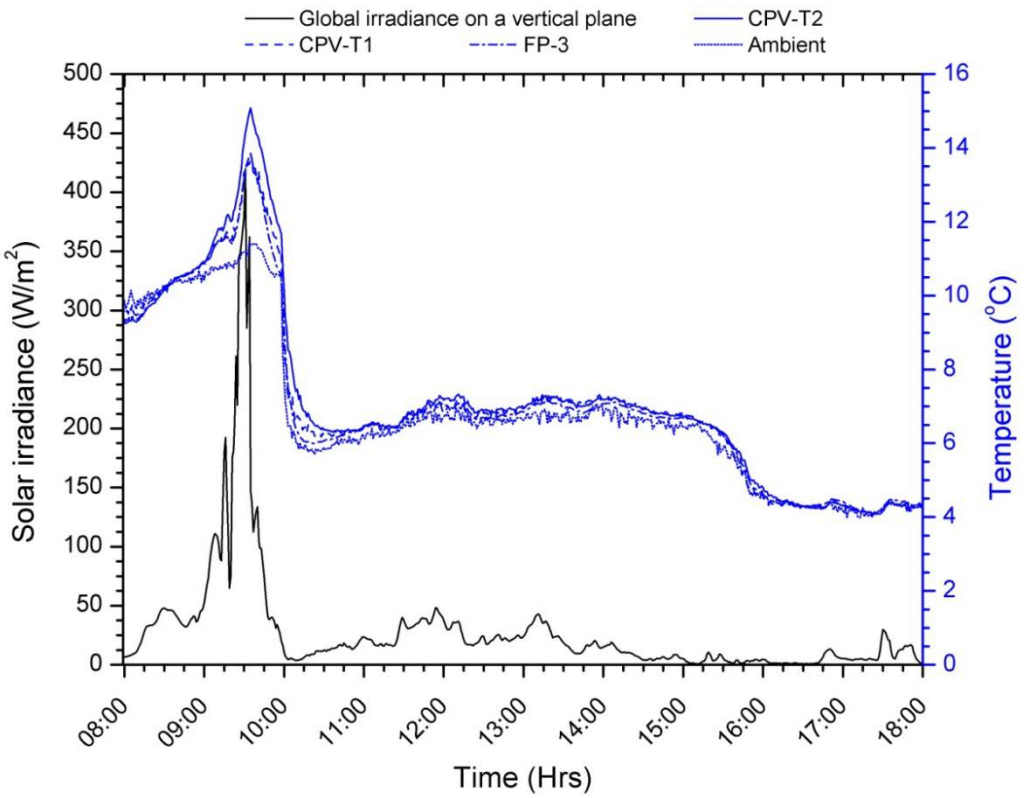

Figure 5.30 Variation of the module temperature and ambient temperature over the day with the variation of solar irradiance

The maximum temperatures of the CPV-T2, CPV-T1 and flat-plate module were recorded to be 15.1°C, 13.9°C and 13.9°C, while the ambient temperature was 11.4°C. The average temperature of the CPV-T2, CPV-T1 and flat-plate module was 7.2°C, 7.1°C, and 7°C, respectively. During the day the average ambient temperature and wind speed was 6.8°C and 7.2m/s. From 8:00am to 10:00am, the average temperatures of the CPV-T2, CPV-T1, FP-3 module and the ambient temperature were 11.3°C, 11.1°C, 19.9°C and 10.5°C. During this period, the average wind speed was 13.3m/s. However with drop in temperature, from 10:00am to 6:00pm, the average temperature of the CPV-T2, CPV-T1, flat-plate module and the ambient temperature were recorded as 6.2°C, 6.1°C, 6°C and 5.9°C, respectively.

The average short circuit current of the CPV-T2, CPV-T1 and the flat-plate module over the day was 21.7mA, 20.6 mA and 10.8mA respectively, while the average irradiance was 28W/m^2. In between 10:00am to 6:00pm, when the irradiance was completely diffuse and only 14W/m^2, the average short circuit currents of the three modules CPV-

T2, CPV-T1 and FP-3 modules were 11.9mA, 11.2 mA and 6.3 mA, respectively (shown in figure 5.31).

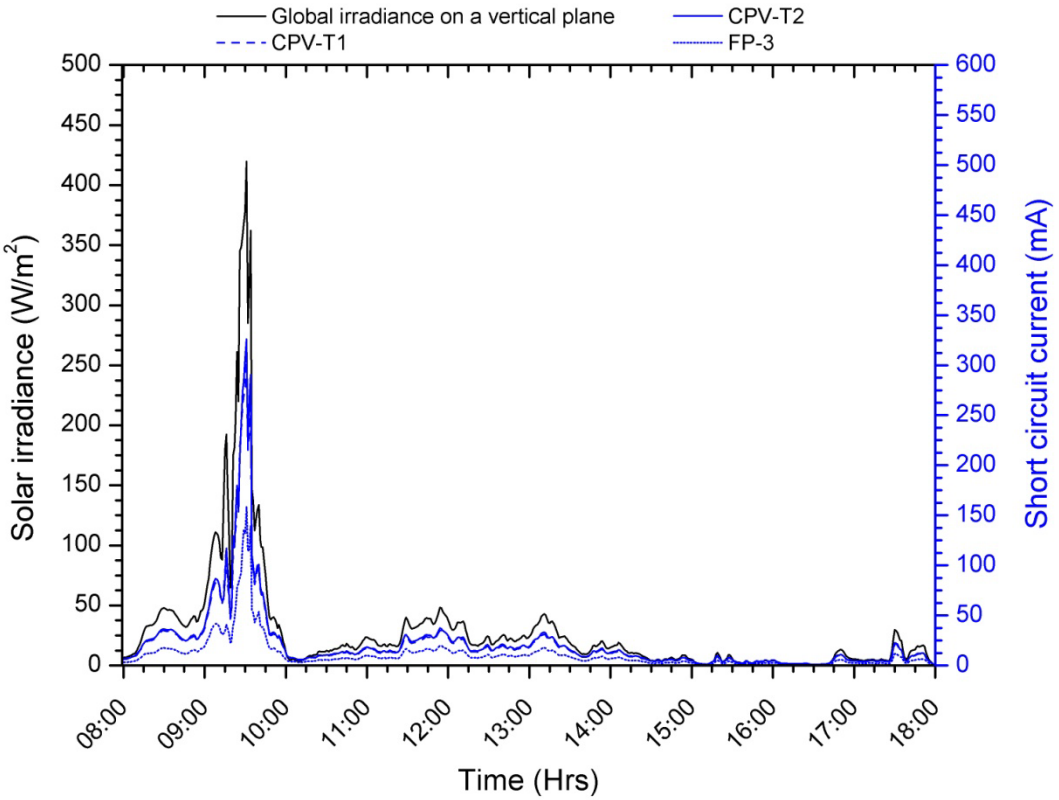

Figure 5.31 Diurnal variation of the short circuit current of the modules under study on 17th of October 2011

The average short circuit current of the CPV-T2 and CPV-T1 module was found to be 1.9 and 1.8 times higher than the flat-plate module. This shows that the dielectric concentrator can collect almost 68% diffuse radiation, considering all possible optical losses in the system. The maximum short circuit current of the CPV-T2 and the flat-plate module was 326.2mA and 158.7mA, for the maximum global solar irradiance 419.6W/m^2 on that day.

The open circuit voltage of the CPV modules was found to be higher for very low solar radiation intensities (<50W/m^2) and also for higher intensities of diffuse radiation (at 9:30am in the figure 5.32). The open circuit voltage of the CPV modules fluctuated between 5.1V to 8.6V with the solar irradiance fluctuating from 0.7W/m^2 to 419.6W/m^2. The average open circuit voltage of the CPV modules and the flat-plate module over the day was found to be 7.4V and 6.9V, while the average global

irradiance was 28W/m^2. From 10:00am to 6:00pm, when the solar irradiance is consistently low (less than 50W/m^2), the average open circuit voltage of the CPV modules and the flat plate modules was 7.2V and 6.7V.

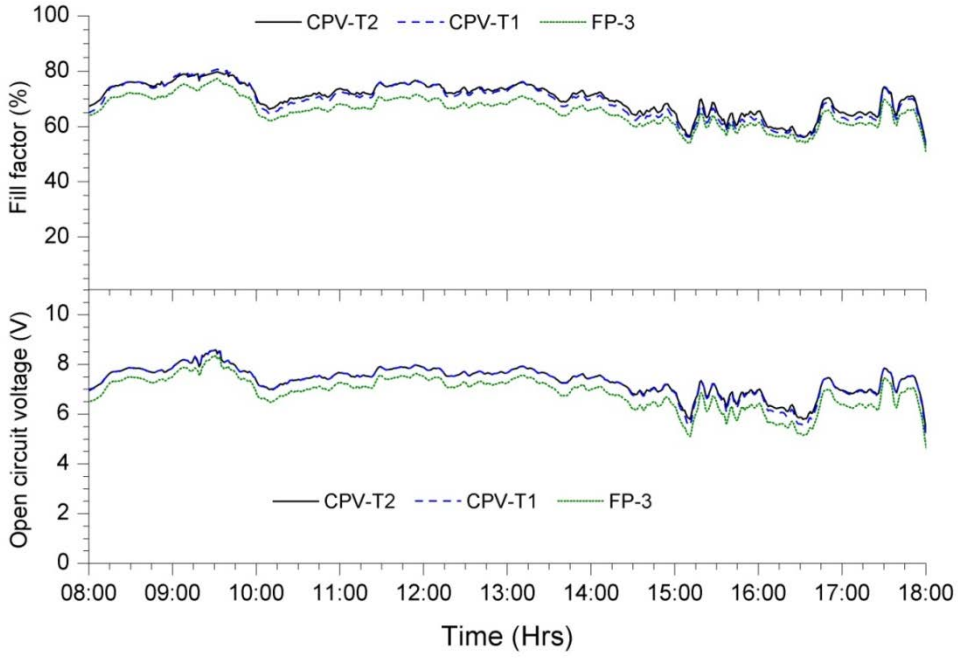

Figure 5.32 Variation of the open circuit voltage and fill factor on the 17th of October 2011

The fill factor was lower than on a sunny day and fluctuated within a range with the change in solar irradiation, as shown in figure 5.32. The average fill factor of the CPV-T2, CPV-T1 and the flat-plate module over the day was 69.9%, 68.9% and 65.4%. For the drop in intensity of solar irradiance, the reduction of fill factor for all the modules can be observed at 10:00am. While the solar irradiance dropped from 419W/m^2 to 10.7W/m^2, the fill factor of the CPV module dropped from 76.1% to 68.2%, while the fill factor of the flat-plate module dropped from 71.9% to 63.4%. The average fill factor of the CPV-T2, CPV-T1 and the flat-plate module from 10:00am to 6:00pm was recorded as 68.7%, 67.5% and 64.2%, respectively.

The diurnal variation of the power out of the three modules is shown in figure 5.33. The average power output over the day of the CPV-T2, CPV-T1 and flat-plate module was 0.13W, 0.12W and 0.06W respectively, while the average global irradiance was 28W/m^2. During 10:00am to 6:00pm, the average power output of the CPV-T2, CPV-T1 and the flat-plate module was 0.07W, 0.06W and 0.03W respectively, corresponding

to the average irradiance 14W/m^2. During 10:00am to 6:00pm, while the solar irradiance was fluctuating between 0.7W/m^2 to 48.3W/m^2, the maximum power output of the CPV-T2 module varied within 0.002W to 0.23W and the flat-plate module power output varied from 0.001W to 0.11W.

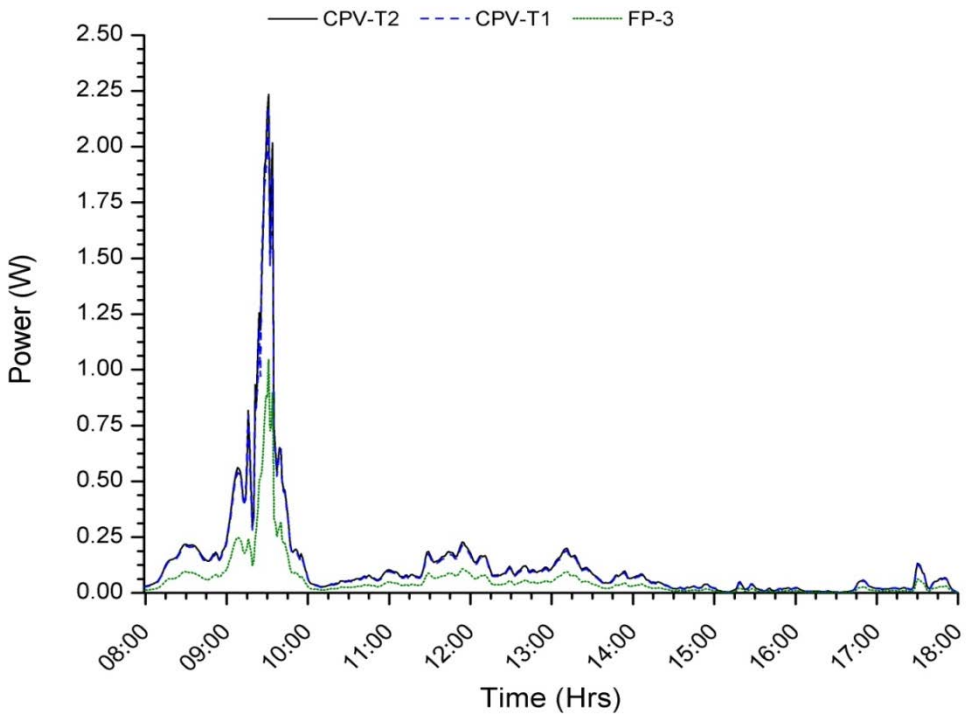

Figure 5.33 Diurnal variation of the power output of the modules on 17th of October 2011.

The increase in power output of all three modules is shown in figure 5.34, which shows a linear relationship with rise in solar irradiance. The drop of power output at some points, such as 150W/m^2, 175W/m^2 and 192W/m^{2,} may be due to the partial shading caused by the clouds movement. The variation of power output of the modules with increase in solar irradiance from 0 to 50W/m^2 is shown in the inset picture. Even for low diffuse radiation, higher power output of the CPV modules compared to the flat-plate module can be observed. The power ratio calculation shows a better performance of the dielectric concentrator and the CPV module compared to the theoretical analysis for diffuse radiation.

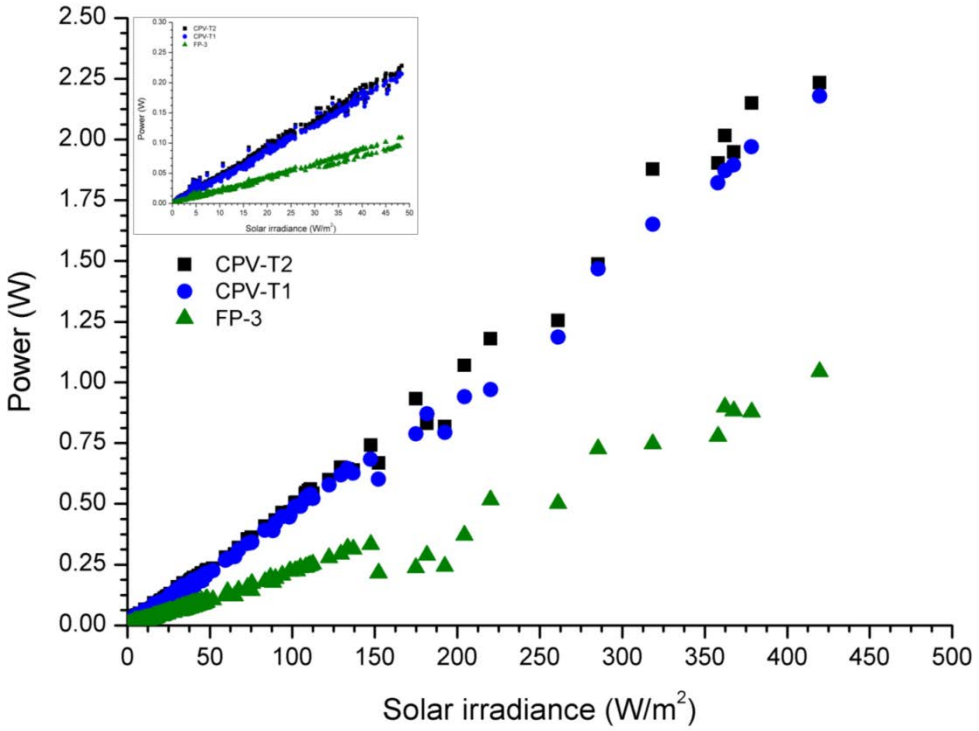

Figure 5.34 Variation of the power output of the modules with the increase in irradiance. Inset picture shows the variation of power output for the lower radiations (below 50W/m^2).

The diurnal variation of power ratio of the two CPV modules is shown in figure 5.35. The average power ratio of the CPV-T2 and CPV-T1 module for the whole day (from 9:00am to 5:00pm) was found to be 2.16 and 2, respectively. However the efficiency of all the modules was low for diffuse radiation. The average power ratios were found to be within the same order, even during the time period from 10:00am to 17:00pm while the solar irradiance was very low. However the efficiency of all the modules was found to be lower when compared to a sunny day.

The diurnal variation of the efficiency of the modules under study is shown in figure 5.36. The average efficiency of the CPV-T2, CPV-T1 and the flat-plate module over the day was 8.7%, 8% and 11.4%, respectively. After 2:30pm the module efficiency was fluctuating and showing higher values, which may have resulted from the measurement error. Since the solar irradiation was very low, it can be below the calibration limit of the pyranometer resulting in erroneous data (very low irradiation values) from the pyranometer.

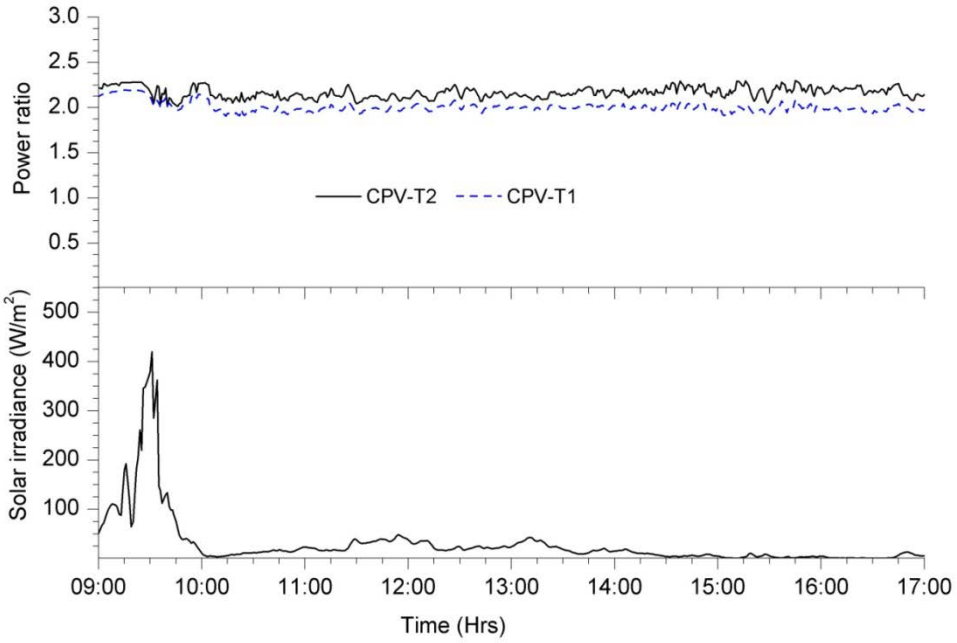

Figure 5.35 Diurnal variation of the power output of the CPV-T2 and CPV-T1 module with the solar irradiance

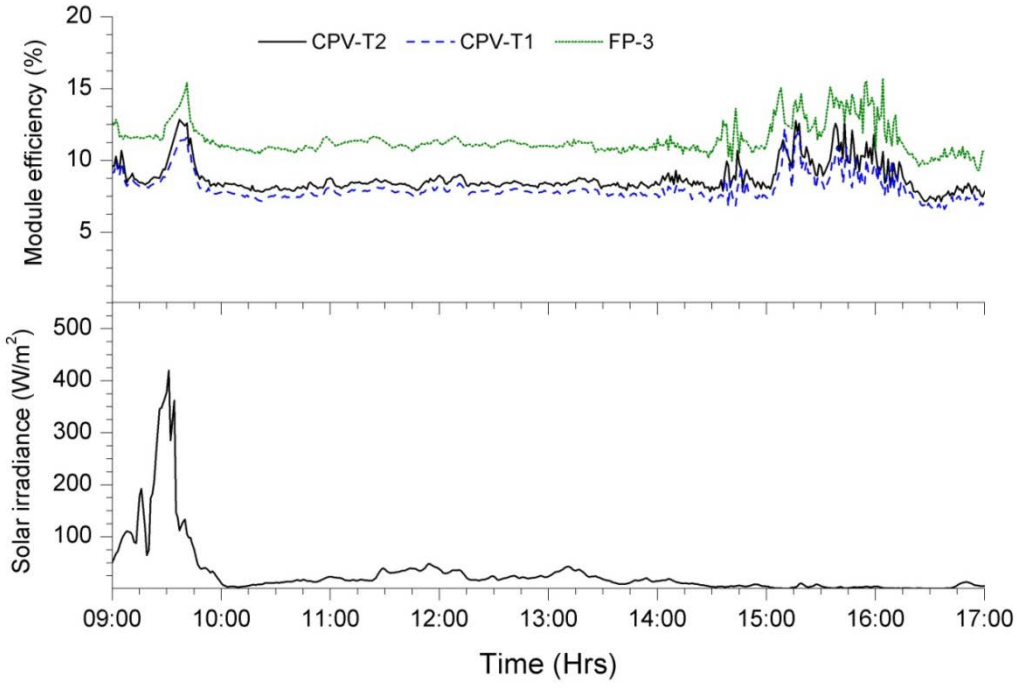

Figure 5.36 Diurnal variation of the module efficiencies on a rainy day (17th of October 2011)

The average efficiency within the low solar radiation intensity from 10:00 am to 2:00pm of the CPV-2, CPV-1 and the flat-plate module was found to be 8.34%, 7.77% and

11.05%, respectively. The output of the characterisation on 17th October 2011 is summarised in table 5.5.

Table 5.5 Summary of the characterisation of the CPV modules on 17th October 2011

	Parameters	-	FP-3	CPV-1	CPV-2
17th October 2012	Solar Irradiance (W/m^2)	Maximum	425	425	425
		Minimum	0.6	0.6	0.6
		Average	28	28	28
	Short circuit current (mA)	Maximum	158.7	309.6	326.2
		Minimum	0.44	0.8	0.8
		Average	10.8	20.6	21.7
	Open Circuit voltage (V)	Maximum	8.4	8.6	8.6
		Minimum	4.7	5.1	5.4
		Average	6.7	7.2	7.2
	Maximum Power (W)	Maximum	1.04	2.2	2.23
		Minimum	0.001	0.002	0.002
		Average	0.06	0.12	0.13
	Fill factor (%)	Maximum	77.7	80.5	80.3
		Minimum	51	53.9	53.2
		Average	65.4	68.9	69.9
	Efficiency (%)	Maximum	13.3	11	13.1
		Minimum	5.9	5.7	4.95
		Average	11.4	8	8.7

5.2.2.5 Electrical performance of the CPV modules with 10^{o}inclination to the vertical on a sunny interval day (28th October 2011)

The performance of CPV modules with 10^o inclination to the vertical has also been investigated. It was found that during the autumn season, in the month of October, the CPV modules are performing better while mounted vertically rather than the 10^o inclination. The experiment has been carried out on 28th of October 2011, which was a day with sunny intervals. The diurnal variation of the global, direct and diffuse irradiance on 28th of October 2011 is shown in figure 5.37.

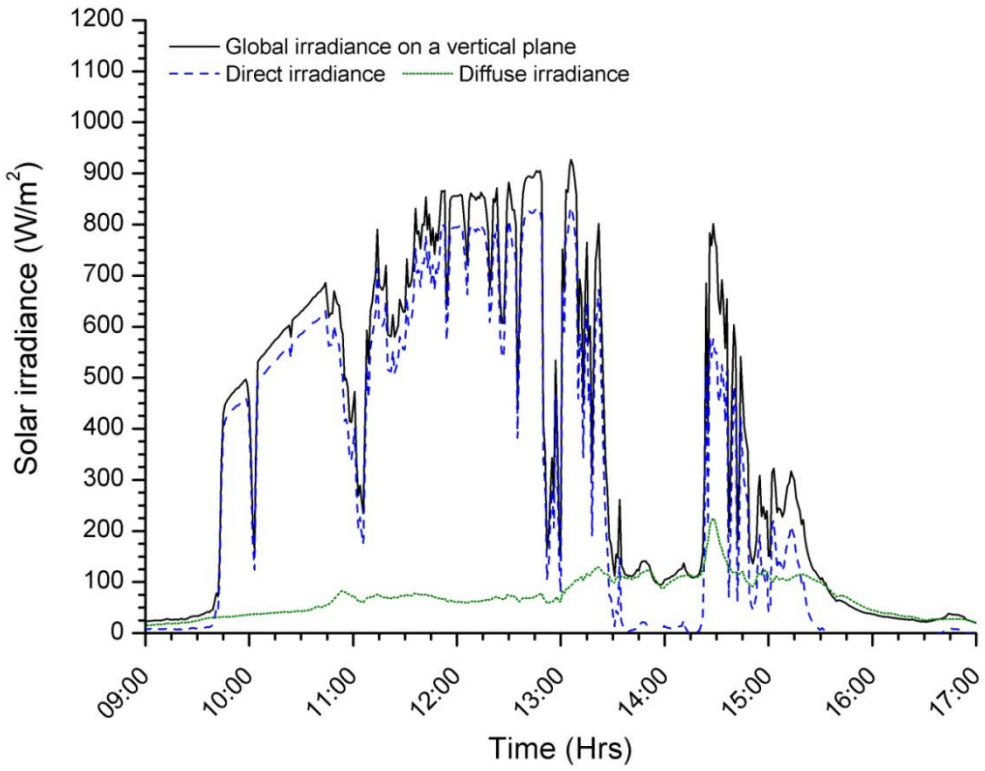

Figure 5.37 Diurnal variation of the global, direct and diffuse irradiance on a plane 10^{o} inclined to the vertical

The average global, direct and diffuse solar irradiance from 9:00am to 5:00pm was observed as 372W/m^2, 301.4W/m^2 and 70.6W/m^2. However for the duration of 9:45am to 1:30pm, when the solar irradiation was mostly direct, the average global irradiation was 648.8W/m^2. The short circuit current in all the modules varied accordingly with the solar irradiance, with a daily average short circuit current of the CPV-T2, CPV-T1 and FP-3 modules as 304.5mA, 280.9mA and 144mA, respectively. The diurnal variation of the short circuit current of the modules is shown in figure 5.38. The average short circuit current of the CPV-T2, CPV-T1 modules are respectively 2.1 times and 1.95 times higher than flat-plate module. The maximum short circuit current of the CPV-T2, CPV-T1 and flat-plate modules were 787.7mA, 714.3mA and 368.5mA respectively at 1:06pm, while the maximum solar global irradiance was 927W/m^2. The maximum short circuit current of the CPV-T2 module was found to be 2.13 times higher than the FP-3 module. The average short circuit current ratio of the CPV modules mounting with 10^{o} inclination to the vertical was less than mounting vertically during the month of October. A study on 16th of October showed that the CPV-T2 and CPV-T1 modules are producing 2.22 times and 2 times higher short circuit current compared to the flat-plate module, while the average irradiance was 399W/m^2.

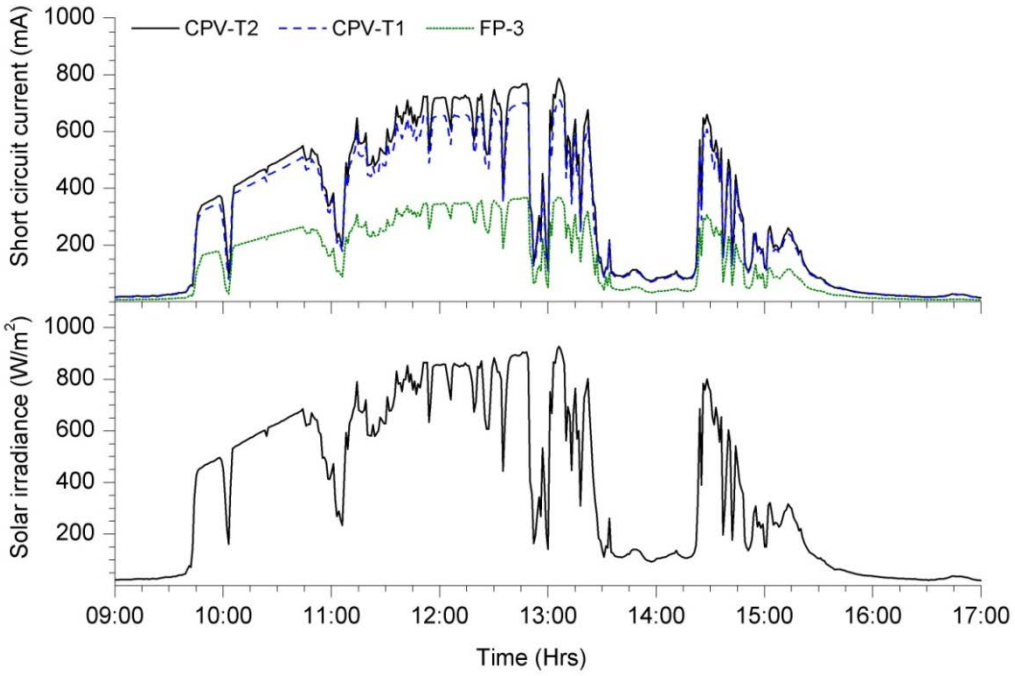

Figure 5.38 Diurnal variation of the short circuit current of the modules with the variation in solar irradiance

The variation of the power output and the open circuit voltages of the modules are shown in figure 5.39. The maximum power output of the CPV-T2, CPV-T1 and the flat-plate module was 5.1W, 4.8W and 2.4W respectively, for the solar irradiance 927W/m^2. The average power output of the CPV-T2, CPV-T1 and the flat plate modules over the day was 2W, 1.9W and 0.93W respectively for the average solar irradiance 372 W/m^2. For the average diurnal solar irradiance of 399W/m^2 on 16th of October with the modules mounted vertically, the power output of the CPV-T2 module was found to be 2.28W. The power output of the same module with 10^o inclination was comparatively lower for the almost same average irradiance. Even though the solar path has changed and the maximum altitude angle has decreased during this time from 16th to 28th of October, the decrease in power output has been caused by the inclination of the module. This can be justified from the insignificant change in comparative power out of the modules between the two days 7th and 16th of October.

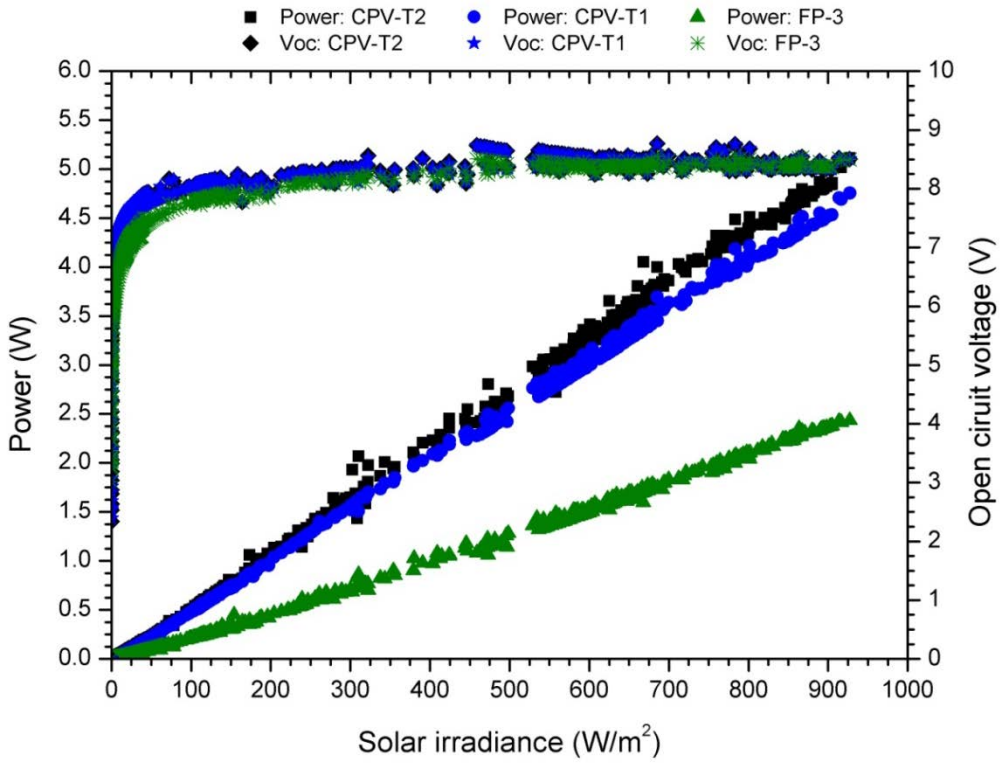

Figure 5.39 Variation of the power output and the open circuit voltage with the solar irradiance over the day on 28th of October 2011

The change in the open circuit voltage of all the modules was less depended on the variation of the solar irradiance. The average open circuit voltage of all the CPV modules was found to be 2.6% higher than the flat-plate modules for all radiation above 20W/m^2. The average open circuit voltage of the CPV and the flat-plate module was 8.14V and 7.93V over the day. The maximum open circuit voltage of the CPV-T2 modules was 8.76V at 685W/m^2, while the minimum was 7.4V for 20W/m^2. The open circuit voltage of the CPV modules decreased due to increase in module temperature with the increase in solar irradiance. So the open circuit voltage of the CPV-T2 module decreases for irradiance higher than 685W/m^2. The diurnal variation of the module temperature with the solar irradiance is shown in figure 5.40. The maximum temperature of the CPV-T2 module was found to be 34.9^{o}C at 12:46pm while the ambient temperature was 11.5^{o}C and the wind speed was 12m/s. The maximum temperature of the CPV module was found to be 10.4^{o}C higher than the flat plate module. The module temperature always has an offset to the irradiance because of the thermal inertia of the materials in the module.

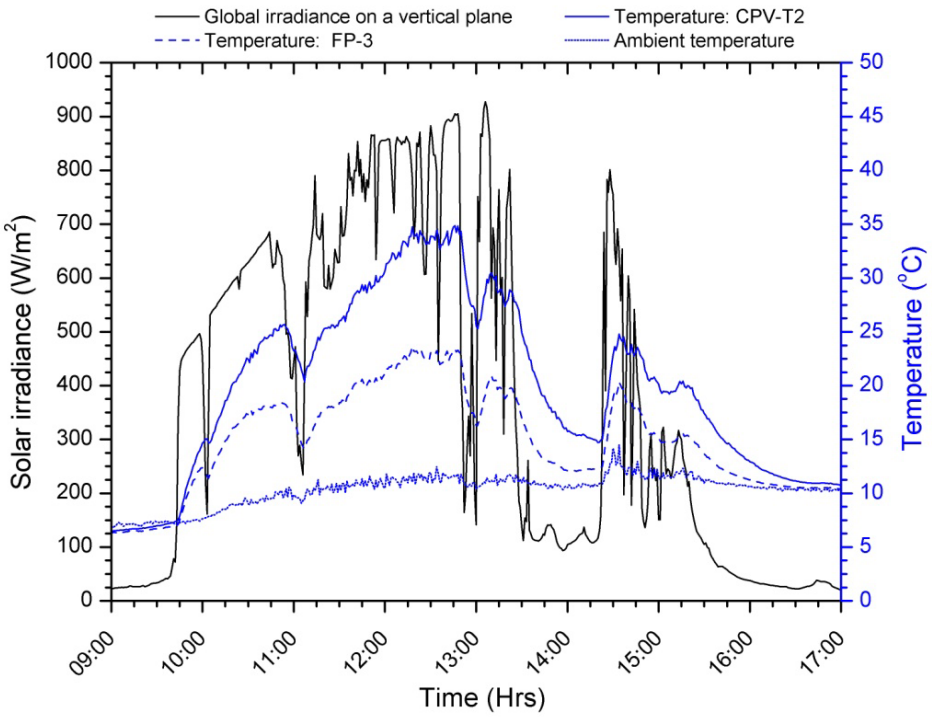

Figure 5.40 Variation of module temperature and the ambient temperature over the day with the solar irradiance

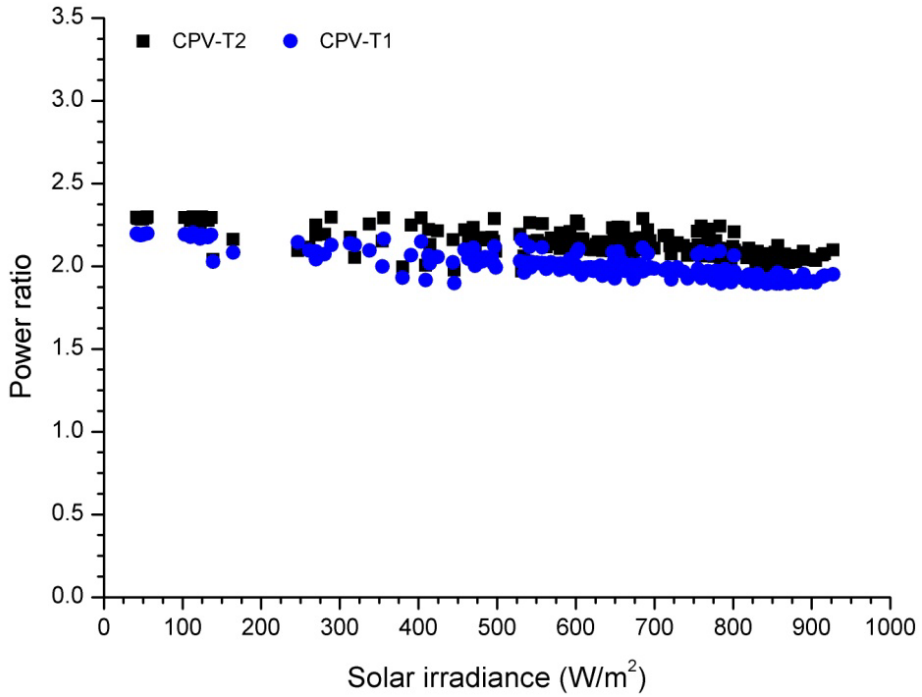

Figure 5.41 Variation of the power ratio of the CPV-T2 and CPV-T1 module with the solar irradiance

The change in power ratio of the CPV-T2 and CPV-T1 modules for an increase in solar irradiance is shown in figure 5.41. The average power ratio of the CPV-T2 and CPV-T1

modules was 2.13 and 2 respectively. Higher optical losses have reduced the power ratio of the CPV-T1 module compared to the CPV-T2 module. The power ratio of both the CPV modules was found to decrease with increase in solar radiance, which may be due to the decrease in open circuit voltage and fill factor caused by the increase in temperature of the module. For maximum irradiance 927W/m^2, the power ratio of the CPV-T2 and CPV-T1 modules was 2.1 and 1.95 respectively.

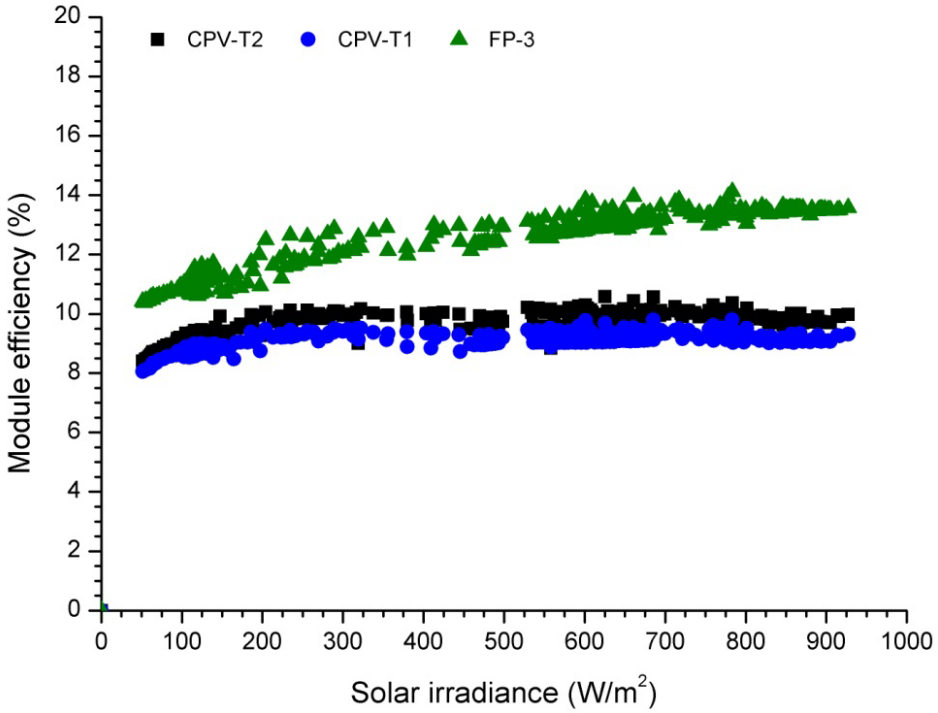

Figure 5.42 Variation of the module efficiency with the solar irradiance on 28th of October 2011

Figure 5.42 shows the variation of the module efficiency with global irradiance. The average module efficiency of the CPV-T2, CPV-T1 and the flat-plate module over the day was 9.67%, 9.1% and 12.5%, respectively. While the flat plate module efficiency has increased with solar irradiance, the CPV modules efficiencies are found to be steady for irradiance above 200W/m^2. Degradation of the module over time and the effect of the inclination may have prevented the increase in module efficiency with irradiance.

5.2.3 OE-Third phase: Electrical performance analysis of the fourth prototype CPV modules

In the third phase of the outdoor experiment the fourth prototype module is characterised at the SE test site of Heriot-Watt University. The IV characteristics of the

CPV module were monitored for a month from 1st to 31st of March 2012 to investigate the long term performance and the issues related to scaling up the module.

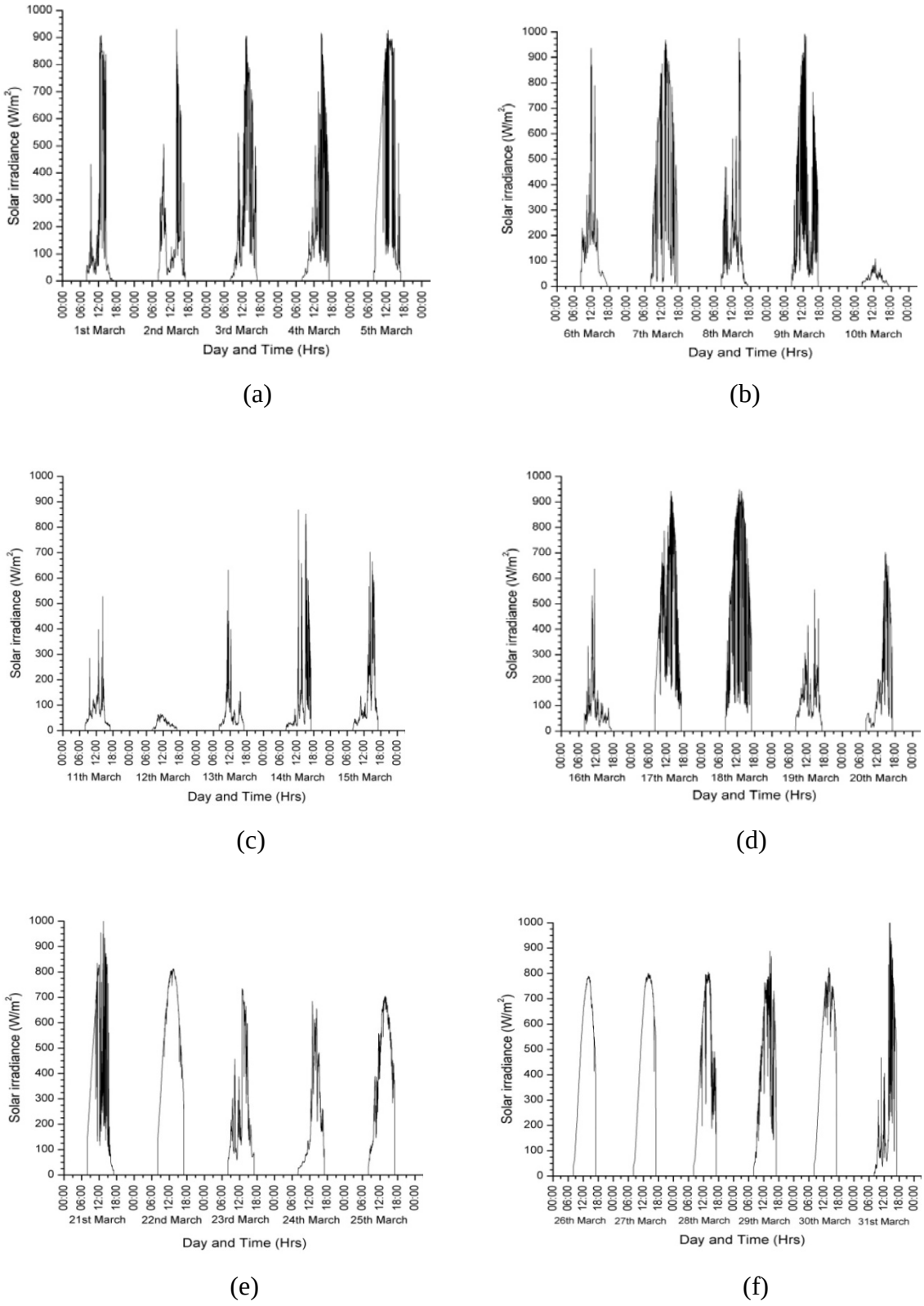

Figure 5.43 Daily solar irradiation during the month of March 2012

The variation of solar irradiance for all the days of March 2012 is shown in figure 5.43. Most of the days during the experiment are 'sunny interval' and cloudy; except for 5 completely sunny days (22nd, 25th, 26th, 27th and 30th March). The maximum solar irradiation on a sunny day (22nd March) was recorded as 813 W/m2. Some higher intensity peaks on a sunny interval day can be observed (during large fluctuation in solar radiation intensities) for short period of time, which can be because of the clear sky after rain.

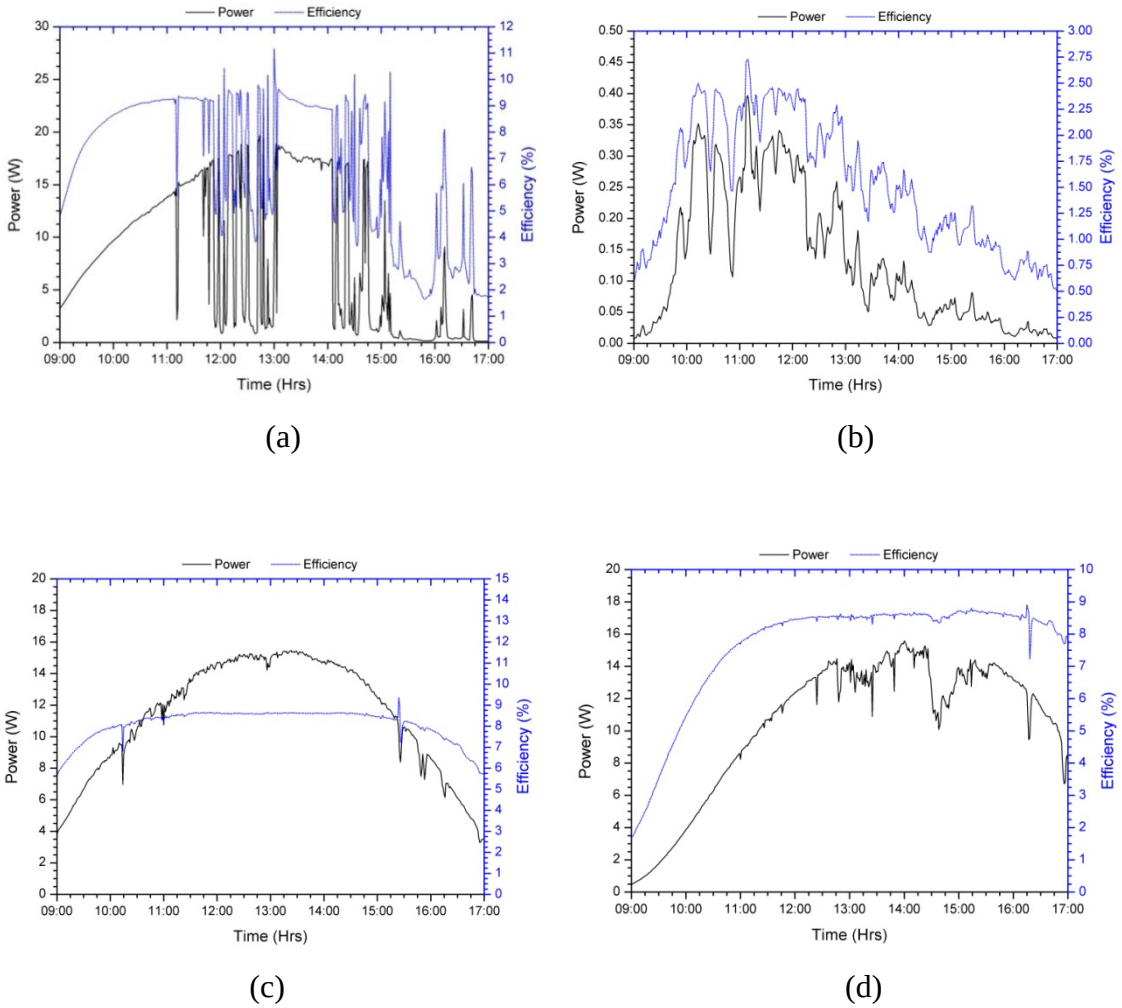

Figure 5.44 Variation of maximum power and efficiency of CPV-4 module over the day on (a) 5th March (b) 12th March (c) 22nd March (d) 30th March

The variation of maximum power output and efficiency of the CPV-4 module for 4 days during March 2012 is shown in figure 5.44. On 5th March (sunny interval day) the maximum power out of the CPV module was 19.7W at 12:44 pm while the solar irradiance was 928 W/m^2. The efficiency of the module for the maximum power output

was 9.65%. However the average power output of the module on 5th March was 7.32W with an average efficiency 6.26% due to the fluctuation of solar irradiance over the day. On a rainy day with dark clouds (12th March) the maximum power of the CPV module was found to be 0.3W, while the solar irradiance was 66W/m^2 at 11:07am. The maximum efficiency over the day was recorded as 2.73%. The average power output and the efficiency over the day were 0.12W and 1.43% respectively, while the average solar irradiance was 30W/m^2. On a clear sunny day (22nd March) a nice variation of power output and efficiency over the day can be noticed (figure 5.44 (c)). A maximum power output of 15.5W was found while the irradiance was 813 W/m^2. The efficiency of the module was steady at ~ 8.6% during 10:30am to 3:30pm, which drops for lower irradiance during early morning and late afternoon. The average power output and efficiency of the CPV-4 module on 22nd of March was found to be 10.25W and 7.53 respectively, while the average solar irradiance was 578.81 W/m^2. During another sunny interval day (30th March) the maximum power output of the CPV-4 module was 15.6W with maximum efficiency 8.9%, while the irradiance was 820.3W/m^2. However the average power output and efficiency over the day was 9.37W and 6.93%, respectively.

The daily average of the electrical output of the CPV-4 module corresponding to the daily average of the solar irradiance of March 2012 is shown in table 5.6. Considering the suns path during the month of March in Edinburgh, the electrical data of the module is averaged from 9am to 5pm to evaluate the optimum performance of the module. The average monthly irradiance and power output of CPV-4 module during March 2012 was found to be 284.4W/m^2 and 4.69W. The average open circuit voltage for the month was 13.13V and the short circuit current was 0.47A.

Table 5.6 Daily averages of the IV parameters of CPV- 4 module over the month of March 2012

Parameters	Solar Irradiance	Open Circuit Voltage	Short Circuit Current	Maximum Power	Conversion Efficiency
Day	**W/m2**	**V**	**A**	**W**	**%**
01/03/2012	205.19	10.85	0.36	3.54	3.78
02/03/2012	176.04	12.66	0.28	2.52	4.09
03/03/2012	276.05	13.16	0.47	4.75	5.12
04/03/2012	227.71	13.31	0.37	3.63	4.77
05/03/2012	402.62	14.74	0.69	7.32	6.26
06/03/2012	163.82	13.16	0.26	2.22	4.23
07/03/2012	405.93	14.51	0.70	7.75	6.49
08/03/2012	169.89	12.70	0.28	2.44	4.18
09/03/2012	312.21	14.41	0.53	5.52	5.77
10/03/2012	34.81	6.90	0.05	0.13	1.47
11/03/2012	75.34	10.67	0.11	0.55	2.50
12/03/2012	30.01	6.38	0.05	0.12	1.43
13/03/2012	72.99	9.68	0.11	0.65	2.46
14/03/2012	129.31	10.27	0.21	1.78	3.21
15/03/2012	131.05	11.57	0.21	1.68	3.45
16/03/2012	91.92	11.15	0.15	0.92	2.92
17/03/2012	446.38	16.15	0.74	7.86	7.06
18/03/2012	492.38	15.76	0.83	9.03	7.04
19/03/2012	128.08	13.65	0.20	1.33	3.78
20/03/2012	196.98	12.68	0.32	3.00	4.34
21/03/2012	390.29	14.77	0.65	6.82	6.22
22/03/2012	578.81	15.80	0.97	10.25	7.53
23/03/2012	249.23	14.81	0.40	3.70	5.18
24/03/2012	219.52	13.16	0.35	3.26	4.68
25/03/2012	415.35	14.91	0.68	6.89	6.45
26/03/2012	519.23	14.74	0.86	8.83	6.68
27/03/2012	548.50	14.99	0.89	9.46	6.78
28/03/2012	457.88	15.19	0.73	7.66	6.51
29/03/2012	453.77	15.38	0.73	7.80	6.71
30/03/2012	531.60	15.43	0.86	9.37	6.93
31/03/2012	283.54	13.51	0.46	4.49	4.82
Average	284.40	13.13	0.47	4.69	4.93

A decrease in the maximum efficiency and the power output of the CPV module with time was observed. The maximum efficiency during the initial days of the month was ~9.6% for irradiance higher than 600W/m^2, which decreases to 8.9% towards the end of the month. Growing white spots on the encapsulation material between solar cell and concentrator trough leads to decrease in current from the string of the cells and

eventually from the whole module. The white spot in the encapsulation material in between the solar cell and the concentrator can be seen in figure 5.45. The white spot could be uncured silicone material, which turns into a white spot with increase in temperature. Certain chemicals or materials can inhabit the sylgard from curing and the flux solvent used for soldering the solar cell with tabbing wire is one such chemical [253]. Another reason of reduction in overall power output of the CPV module is condensation between the concentrator and the cover glass.

Figure 5.45 White spots in between solar cell and concentrator

5.3 Conclusion

The CPV modules with the dielectric concentrator 'DiACPC-55' were characterised in outdoor environment to investigate the realistic performance for both direct and diffuse radiations. The modules were mounted vertically for two sunny interval days, a rainy day and a cloudy day, to evaluate the performance in different weather conditions. Since there was not a sunny day during the days of the experiment, the sunny interval days are considered to be the best performance taking into account the long sunny spells on those days. Study shows that the CPV-T2 modules manufactured to reduce the optical losses in the CPV modules with the dielectric concentrator DiACPC-55, has better performance in all weather conditions over the CPV-T1 module (conventional dielectric CPV module with higher optical losses). The maximum power output of the CPV-T2

module was found to be 6.5W for 997W/m^2 at 12:45pm on 7th of October (Table 5.3). The average power ratio of the CPV-T2 module was observed between 2 to 2.25 in different weather conditions. The maximum theoretical power ratio for direct irradiation was 2.28, while for the diffuse radiation the theoretical power ratio was only 1.3. The outdoor characterisation of the CPV modules with the dielectric concentrator shows a better performance for diffuse radiation to achieve power ratio ~ 2.

The study also shows that the CPV modules attain better performance in the month of October in Edinburgh while mounted vertically compared to the 10^o inclination to the vertical. The average power output of the vertically mounted CPV-T2 module over a day with an average irradiance of 399 W/m^2 was found to be 2.28W, while for the average irradiance of 372W/m^2 the CPV-T2 module mounted 10^o inclination to vertical was only 2W. Linear conversion of the average power output for 399W/m^2 with 10^o inclination on 28th of October will be 2.15W. Though the results are from two different days (16th and 28th of October), the change in mounting angle from vertical to 10^o inclination has played the significant role in decreasing the average power output of the CPV-T2 module.

Outdoor characterisation of 600mm×600mm CPV module (CPV-4 module) during the month of March 2012 showed a maximum power output of 19.7W with a conversion efficiency of 9.65%. The maximum daily average of the power output of 10.25W was recorded with an average conversion efficiency of 7.53% on 22nd of March, while the average irradiance was 578.81W/m^2. However, the maximum power output and the efficiency on 22nd March were found to be 15.5 and 8.6%. Degradation of the encapsulation material was observed, which may be because of the uncured sylgard in between solar cell and concentrator.

Chapter 6

Cost assessment of the CPV module

This chapter provides cost analysis details of the designed CPV module for building façade integration. The cost and the embodied energy of the CPV module is compared with the commercial glass-glass laminated modules.

6.1 Introduction

The cost of the solar PV system is still a big challenge to compete with the conventional sources of energy. The designed building integrated concentrating system with the optimum concentrator for Edinburgh and higher latitude locations is mainly targeted to replace the conventional PV modules for building façade integration. The conventional building façade PV systems are the thin film amorphous silicon modules and crystalline silicon modules consisting of glass-glass lamination. In the glass-glass laminated PV modules for building integration, standard silicon cells are laminated between two thick glass plates (4mm thick) for structural rigidity. Sometimes solar cells of different shape and colours are used, as per the aesthetic and architectural requirements. The glass-glass modules for building façade integration are normally designed to be used during daylight, keeping gaps between the solar cells.

In this study, the cost analysis and embodied energy of the designed CPV modules is compared with the standard commercial glass-glass PV modules for building integration. The cost analysis is carried out according to the outdoor test performance of the CPV modules. The performance of the flat plate modules are considered as the performance of the glass-glass laminated PV modules. The embodied energy analysis is performed with the data available for the embodied energy of the materials using different sources. The embodied energy can provide information of the carbon emission and energy required for the manufacturing of the materials used in the CPV system and its effect to the environment. The labour, processing and manufacturing cost of the CPV module is ignored as it is largely an unknown cost and may vary in different countries.

6.2 Cost and embodied energy of the module components

The primary cost analysis of the CPV module is carried out with the Polyurethane material being used. However, a comparative study with the PMMA was also completed to analyse the cost if the PU is replaced by the commercial PMMA manufactured by the casting process. The PMMA is being used in CPV industries for its high transmittance and resistance to photo degradation. The commercially available PMMA are cheaper than the urethane monomers bought for casting the concentrators.

The electrical conversion efficiency of the designed CPV module considered in this cost analysis is the average efficiency and power output of the CPV module characterised in different weather conditions in Edinburgh, Scotland. The frame used to construct the designed CPV module is not commercially available frame. Its custom built frame with the aluminium angles. However the material requirement for commercial frame should not be very different from the current material used. In study highly transmittance BF glass (even in UV-range) is used as cover glass. However it is observed that due to the presence of UV-stabiliser in the concentrator material (Polyurethane) the transmittance of BF glass in the UV range do not cause significant difference in enhancing the performance of the CPV module.

In cost comparison of the designed CPV module with the glass-glass laminated module, it is important to take into account the transparency of the modules. The transparency of the glass-glass laminated modules for building integration is controlled by the spacing between the solar cells. With increase in spacing the transparency increases. However with the increase in solar cell spacing the overall module efficiency decreases.

To calculate the cost and embodied energy in the designed CPV module, the cost and embodied energy of the material is calculated to manufacture a CPV module with aperture area $1m^2$ and expressed in £/m^2 and MJ/m^2. The cost and the embodied energy of the each component is calculated separately and added up to determine the total cost and embodied energy of the designed CPV module. The cost of the material varies depending on the quantity of purchasing. In this cost analysis the cost of the bulk material is considered wherever possible and for the rest the quotation price, while purchasing the material during fabrication of the CPV module is considered. For some materials like glass, the increase in size increase the cost of the significantly. The cost of

the unit piece to manufacture the large area module (CPV-T1 & CPV-T2) is considered in this study. The cost and embodied energy of most of the material is referred to the thesis of Dr. Lindsay Wilson in 2010. Any minor change in cost and embodied energy of the material during the period of 2010 to 2012 has been ignored. The details of the cost and the embodied energy analysis of the different component of the CPV module are shown below:

1. Concentrator material (PU): A single trough of the DiACPC-55 concentrator manufactures by polyurethane have an aperture area of 19.49cm^2 and the weight 27.75gm. So 513 trough of concentrator required for 1m^2 module. The price of per kilogram of clear polyurethane is £3 [254]. So the cost of the one concentrator trough will be £0.083 and the cost of the concentrator material in a module of 1m^2 size will be £42.58/m^2. The embodied energy of the polyurethane is 70MJ/Kg [255]. So the bulk embodied energy per unit area of the 14.5mm thick polyurethane plastic in the CPV module will be 996.7MJ/m^2.

2. Encapsulation Material (Sylgard-184): The thickness of the encapsulation material is 1mm. The cost of per kilogram sylgard-184 is £54.9 [254]. This results the cost of the encapsulation material is £5.14/m^2 in a 1m^2 size CPV module. The embodied energy of the sylgard-184 is 200-300MJ/m^3. The average value 250MJ/m^2 is considered in this study.

3. Clear float glass: Chemically toughen clear float window glasses are used for higher rigidity than standard ones. The cost of the 1m × 1m size and 3mm thick glass sheet is £15 [254]. The embodied energy of the float glass is considered to be 20MJ/kg [215]. While the density of this glass is 2.5g/cm^3, the embodied energy per unit area of the glass is found to be 200MJ/m^2.

4. BF33 borosilicate glass: It's a light weight highly transparent clear glass, with better properties than a standard soda lime glass float glass (Datasheet, SCHOTT). The density of the glass is 2.2g/cm^3. The bulk embodied energy is reported to be 20MJ/kg. For 2.75mm thick glass the embodied energy will be 111.1MJ/m^2. The cost of the 1m × 1m size glass sheet is considered to be £53/m^2 [254]. However experimentally it is found that the difference in power

output of the CPV modules with BF-glass and normal window glass is negligible, due to the presence of uv-stabiliser in the concentrator material. So for the cost analysis the normal window glass has been considered.

5. Solar cells: The mono-crystalline solar cells used in this project are LGBC solar cell by BP termed as 'SATURN' solar cell. Since those cells were manufactured long before, for cost analysis price quoted by NaREC for LGBC cells in 2009 is used. Bulk cost of the 5-inch semi square wafer is £6, which is equivalent to £2.6/W [215]. So the cost of the solar cell per unit area will be £372/m^2 and the cost of a solar cell having an area of 6.96 cm^2 (11.6cm long and 0.6cm wide) will be £0.26. Each cell of 6.96cm^2 can generate 0.1W power with 1 sun irradiance. However in the CPV module of 1m^2 apertures, the total area of the solar cell to be used is 0.36m^2 (since geometrical concentration ratio of the concentrator is 2.8), making the cost of the solar cell in the CPV module to be £133.9. The embodied energy of the silicon solar cell is reported as 2800MJ/m^2 [256].

6. Tabbing material: The tabbing strips used to connect the solar cells are from Ulbrich. The 2mm wide and 0.25mm thick tabbing strips have density of 8.6gm/cm^3. The bulk cost of this material is £0.50/m and the embodied energy is 0.3MJ/m, considering the embodied energy of copper as 70.6MJ/kg [255]. 5 meter long tabbing wire is needed for the CPV module resulting total cost £2.50 per module.

7. Reflecting film: The cost of the reflective film quoted by Reflectech in 2009 was £225 for 14m^2 [257]. So the cost per unit area is £16.1/m^2. In each trough of concentrators two 2mm wide and 116mm long strips are used. So the total area of the reflective films used in one trough is 0.0005m^2 and for one module of 1m^2 the amount of reflective film needed is 0.26m^2. So the cost of the reflective film in a 1m × 1m size module is £4. The embodied energy of the reflective films is unknown.

8. Framing material: The framing cost can be a crucial factor to analysis the overall cost of the module. In the lab scale manufacturing process a frame by aluminium

angle constructed. However, to compare the cost with the glass-glass laminated BIPV modules, commercial framing for building integration need to be considered. The framing will cost £250-300/m^2 considering the thickness of the CPV module [215]. An average value £275/m^2 is being considered in this study. The embodied energy of the frame will be same as aluminium, which is 153MJ/kg. The mass per length is 4kg/m, which results the embodied energy per meter to be 612MJ/m. So for the perimeter of 4 meter the embodied energy will be 2448MJ/m^2 [215].

In summary the cost and the embodied energy of the materials used in the designed CPV module of 1m^2 size is shown in table 6.1

Table 6.1 Summary of the cost and the embodied energy of the components in the CPV module of 1m^2 size

Component	Embodied Energy	Cost
3 mm thick front cover glass	111.1 MJ/m^2	£15/m^2
Concentrator: Polyurethane	996.7 MJ/m^2	£42.58/m^2
Encapsulation: Sylgard-184	250MJ/m^2	£5.14/m^2
Solar cell	2800MJ/m^2	£133.9/m^2
4mm thick Rear glass	200MJ/m^2	£18/m^2
Tabbing	0.3MJ/m	£2.50/m^2
Reflective film	-	£3.86/m^2
Framing	2448MJ/m	£275/m^2

6.3 Cost comparison with conventional glass-glass laminated modules

While comparing the cost of the designed CPV module with glass-glass laminated module for building integration, transparency of these modules to use the day light effectively can be an important factor. Some of the commercial glass-glass modules for building are designed to allow the daylight to pass through by controlled spacing of the solar cells. The transparency of the designed CPV modules can also be controlled by a gap between the strings of the solar cell and the concentrator units. However for cost analysis closely packed concentrator units in the CPV module and closely packed solar cells in glass-glass laminated module is considered. Rather than comparing the market price of the glass-glass laminated module, sum of the cost of the components is

considered as the total cost of the system. Table 6.2 shows the material cost and the embodied energy of the glass-glass laminated module

Table 6.2 Cost of the materials for the component of glass-glass laminated module [215]

Component	**Embodied energy**	**Cost**
Glass-glass laminated module		
Front glass cover (4mm)	200 MJ/m^2	£18/m^2
EVA Lamination film for both side of the cell (0.5mm + 0.5mm)	250 MJ/m^2	£6.8/m^2
Solar cell	45 MJ/cell	£372/m^2
Tabbing	0.3 MJ/m	£0.5/m^2
Rear soda-lime glass (4mm thick)	200 MJ/m^2	£14/m^2
Frame	612 MJ/m^2	£275/m^2

The comparison of the cost of the designed CPV module and glass-glass laminated module is carried out based on the size and the power generated by the module differently. Table 6.3 shows the cost of the modules based on the size in per square meter.

Table 6.3 Cost and embodied energy comparison of the designed CPV module with glass-glass laminated BIPV module of same size

Modules	**Size**	**Cost**	**Embodied energy**
CPV module with DiACPC-55	1m^2	£496	9165.2 MJ
Glass-glass laminated module	1m^2	£686.3	5889.5 MJ

A cost analysis of the designed CPV module, glass-glass laminated module of similar power output has been considered to evaluate the cost per peak power output. The average efficiency of the designed CPV module while tested in outdoor environment is considered to be 10%. The reported module efficiency of a glass-glass laminated module is 12.5% (average efficiency of the non-concentrating module in this study). So for a 100W_p module the active are of the designed CPV module, glass-glass laminated module need to be 1m^2 and 0.8m^2. Table 6.4 shows the cost per watt peak of the CPV and glass-glass laminated modules. It is found that the cost per watt peak of the CPV

module is less than the glass-glass laminated modules manufactured using the similar crystalline silicon solar cells. The cost per watt peak of the CPV module is £0.53 cheaper than the glass-glass laminated modules.

Table 6.4 Cost comparison of the designed CPV module with the glass-glass laminated BIPV module of same power rating

Modules	**Size**	**Power**	**Cost/W_p**
CPV module with DiACPC-55	$1.0m^2$	100W	£4.96
Glass-glass laminated module	$0.8m^2$	100W	£5.49

6.4 Cost comparison of CPV module with change in solar cell cost

The solar cell price is continuously decreasing since its commercial deployment, due to the technological development. More specifically, the silicon price has drop significantly in recent times. In last 18 months the crystalline silicon solar cell price dropped from £1.54 to £0.52 per watt peak. So it is found that the low concentrating CPV modules with dielectric concentrator may not be a viable option in today's market. However the fluctuation of the silicon solar cell cost in last 8 years indicates that the cost of the solar cell can be increased depending on the silicon feedstock and government policies. So an estimation of the cost per watt peak of the manufactured CPV module has been carried out in comparison to glass-glass laminated modules with variation of the solar cell cost. The cost of the solar cell for the range of £5/W_p to the present value £0.5/W_p has been taken into consideration in this study. Table 6.5 shows the variation of the cost of the designed CPV module and glass-glass laminated modules with variation in solar cell cost. The cost of the other components and the efficiency of the solar cell are considered to be fixed in this analysis.

It can be observed from the table 6.5 that the cost the cost per unit energy output of the CPV module is less than the glass-glass laminated modules until the solar cell price is higher than £2/W. With further decrease in solar cell price at £1.5/W, CPV module is no longer a cost efficient choice compared to the glass-glass laminated module for building integration. Figure 6.1 shows the variation of the cost of the glass-glass laminated module and CPV module with the variation of the solar cell cost. It is found that, while the cost of the solar cell is £1.75/W, the cost per unit energy output of the glass-glass laminated module and the CPV module is same.

Table 6.5 Cost comparison of the glass-glass laminated module and the CPV module with the variation of the solar cell cost

Solar cell cost (Cost/W_p)	**Glass-glass laminated module cost (Cost/m^2)**	**CPV module cost (Cost/m^2)**	**Glass-glass laminated module cost (Cost/W_p)**	**CPV module cost (Cost/W_p)**
£5	£1030	£619.86	£8.24	£6.2
£4.5	£958.75	£594.08	£7.67	£5.94
£4	£887.15	£568.3	£7.1	£5.68
£3.5	£815.54	£542.53	£6.52	£5.42
£3	£743.93	£516.75	£5.95	£5.16
£2.5	£672.33	£490.97	£5.38	£4.9
£2	£600.72	£465.19	£4.8	£4.65
£1.5	£529.12	£439.41	£4.23	£4.39
£1	£457.51	£413.64	£3.66	£4.14
£0.5	£385.9	£387.86	£3.09	£3.88

In this study the major component cost next to the solar cell is of the frame. However in commercial large scale production and depending on requirement of the modules for building application, the cost of the frame will be significantly reduced, which eventually reduces the overall cost of the CPV system.

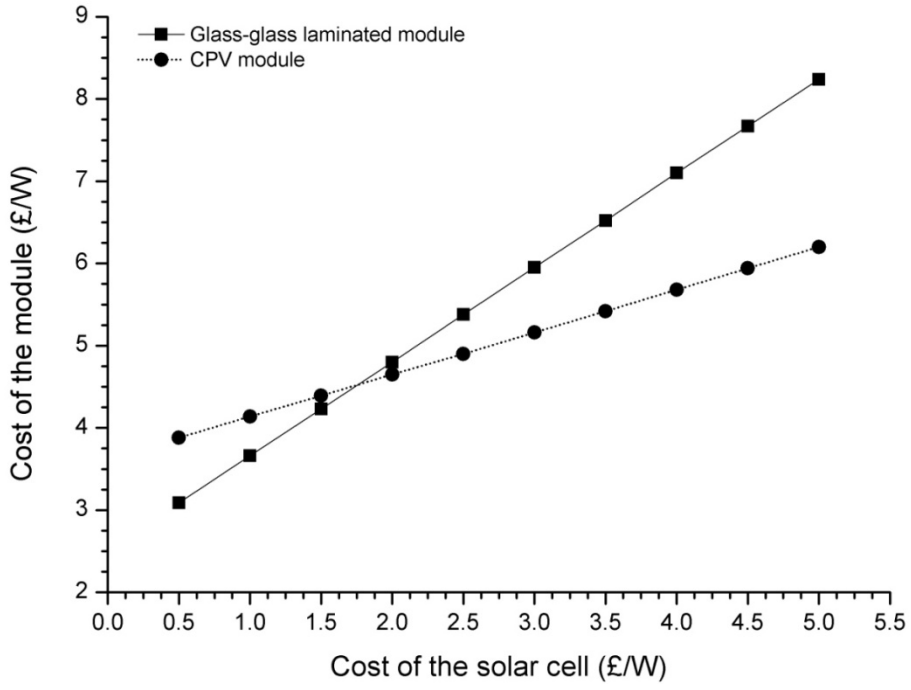

Figure 6.1 The cost of the glass-glass laminated module and the CPV module with the variation of the cost of the solar cell.

6.5 Conclusion

An analytical cost analysis of the designed CPV module with DiACPC-55 concentrator was undertaken and compared with the commercially designed glass-glass laminated modules. The total cost of the modules is considered as the sum of the cost of the different components in the module. Considering the cost of the components in 2010 (when the components were bought) the cost of a $1m^2$ size CPV module is found to be £496, which is £190.3 cheaper than glass-glass laminated module. For per watt (peak) power generation, CPV module is found to be £0.53/W_p cheaper than conventional glass-glass laminated modules. Even though the difference in cost of the CPV module and glass-glass laminated module for per watt peak do not appear trivial, for large installations this difference will have significant impact for energy pay-back period. For every kWh production the energy from the CPV module will be £280 cheaper than glass-glass laminated module. Study reveals that a CPV module with the designed dielectric concentrators is a cost effective alternative to the conventional glass-glass laminated modules; however depending on the cost of the solar cell.

Chapter 7

Conclusions

7.1 Summary

A detail theoretical optimisation and experimental investigation of dielectric compound parabolic concentrator for building façade integration in higher latitudes (>55^{o}) have been reported in this thesis. The stationary concentrator designed with low concentration ratio can face tough challenges with the commercial flat plate modules in terms of the cost. However in the specific applications, such as building façade integration, there is still huge potential for low concentrating CPV system. The performance of the dielectric concentrator reported in this thesis will assist in increasing interest towards the low concentrating dielectric concentrator for PV application. Some important findings of this project are summarised below:

Concentrator design and optimisation

Three compound parabolic concentrator designs with different range of acceptance angles (0&55^{o}), (0&66^{o}) and (0&77^{o}) termed as DiACPC-55, DiACPC-66 and DiACPC-77 were considered for optimisation study. The dielectric concentrator designs DiACPC-55, DiACPC-66 and DiACPC-77 are achieved after truncation of three different complete CPC profiles by 68%, 55% and 40% respectively. The optical simulation result shows:

- All the designed dielectric concentrators are capable of collecting the solar radiation incident within the range of acceptance angles.
- After truncation the range of acceptance angle of the DiACPC-55 increases by 2.2 times compared to the untruncated profile of dielectric concentrator.
- Two dimensional optical simulations show a maximum optical efficiency of the DiACPC-55 as 83%, while the maximum optical efficiency of the DiACPC-66 and DiACPC-77 is found to be 82.4% and 81.7%.
- The intensity distribution at the receiver of the dielectric concentrator is found to be inhomogeneous but well distributed over the receiver area.

- The localised intensity of the peaks changes with the variation in incident angle and results to have a better performance during autumn and spring than winter and summer.
- Optical simulation results DiACPC-55 as optimum concentrator design for building façade integration in Edinburgh and higher latitudes.

Thermal and electrical simulation

Thermal simulations of the CPV system were carried out to estimate the temperature of the solar cell and the rear-plate. The thermal modelling has been carried out with different configuration, single trough, three trough in one unit and 8 troughs as one unit. Variation of the module and cell temperature with heat transfer co-efficient of air and solar irradiance for all the configurations has also been analysed. A basic electric modelling has been carried out to estimate the effect in total power output of the CPV module with the increase in temperature. The thermal and electrical modelling results shows

- The module temperature can reach up to 81.9^{o}; while heat transfer co-efficient (HTC) of surrounding air is 5 $Wm^{-2}K^{-1}$, solar irradiance is 1000 W/m^2, and the ambient temperature is 22^{o}C.
- System level thermal modelling of the designed CPV module with realistic approach for Edinburgh location results a maximum of 41.6^{o}C rear-plate temperature at 1000 W/m^2 irradiance.
- The system level thermal modelling results of the CPV module with 8-trough of concentrator units were found to have a good match with the experimental results.
- Electrical simulation results shows that the open circuit voltage of the CPV system at 75^{o}C can reduced by 14.9% (1.4 volts) compared to the similar CPV module at 22^{o}C. However the comparison of the concentrating and non-concentrating system shows only a 0.2 volt (2.4%) reduction in open circuit voltage for solar radiation 1000 W/m^2.

Performance of the CPV module in indoor environment

The indoor characterisations were undertaken to investigate the optical losses and electrical performance of the CPV module with dielectric concentrators. Optimisation of

concentrator manufacturing criterion and modification in the construction process of the CPV modules for minimum optical losses are two basic outcomes of the indoor characterisation. Based on the initial indoor characterisation results, CPV modules are fabricated to reduce the optical losses at concentrator-encapsulation interface. To understand the optical losses and the variation in theoretical and experimental results, manufactured concentrator profile has been scanned using precision measurement set-up. Detail optical loss analysis in the dielectric concentrator trough is investigated using spectrophotometer (transmission losses) and a goniometer set-up (escaping light). The significant findings of the indoor characterisation of the dielectric concentrator and the CPV module are given below:

- The average AM1.5G spectrum weighted transmittance of the DiACPC-55 concentrator within the spectral response range of the crystalline solar cell (300nm – 1100nm) was 81.9%, results 18.1% transmission losses including partial reflection loss at air-dielectric interface.
- The EQE of the CPV module is only affected by the transmittance of the concentrator compared to a bared cell.
- The maximum experimental optical efficiency of the CPV module was found to be 80.5% at 20^{o} incidence angle, while the system level theoretical optical efficiency considering the optical losses is 82.5% at the same incidence angle.
- The short circuit current of the CPV module was found to be a maximum of 2.25 times higher than similar non-concentrating counterpart.
- The power output of the CPV module was found to be 2.32 (maximum) times higher than non concentrating counterpart at $600W/m^2$ irradiance.
- The average efficiency for the entire range of acceptance angle was found to be 9.5%, while the average efficiency of the non-concentrating module is 13.6%.
- The profile scanning of the concentrator shows that the aperture area of the manufactured concentrator is 2.4% less than the designed concentrator due to the machining error
- Detailed optical loss analysis shows that light can escape from the parabolic sides, due to the rough surface. The light escaping from the parabolic sides increases for extreme acceptance angle, while the light concentrates at the edge of the receiver.

Performance of the CPV modules in outdoor environment

The characterisation of the CPV modules evaluates the actual performance of the dielectric concentrator in real environment with the change in sun angle every hour and every season. A comparison study of the performance of the CPV module with similar non-concentrating counterpart in different weather conditions reveals that the dielectric concentrator is very well capable to work with diffuse irradiance as well. The study carried out in a cloudy, rainy and sunny interval days. There was not any complete sunny day during the experiments for comparative analysis. The study has been undertaken mounting the modules vertically and with 10^{o} inclination to the vertical. Some important findings of the outdoor characterisation are:

- The maximum output the CPV module of 300mm × 300mm with active CPV area 552 cm^2 was found to be 6.5W for solar irradiance 997 W/m^2.
- The short circuit current of the CPV module was found to be 2 times higher than the similar non concentrating counterpart on a cloudy day. The short circuit current of the CPV and the non-concentrating module for sunny interval day and rainy day is found to be 2.22 and 1.9 times higher than the similar non-concentrating counterpart.
- It was found that the designed dielectric concentrator can collect 68% of the diffuse radiation, to achieve a power ratio of 2.16 compared to the non-concentrating counterpart.
- The average fill factor and the open circuit voltage of the CPV module was found to be insignificantly higher than the non-concentrating module. However for higher radiations (>500W/m^2) the fill factor and the open circuit voltage of both the modules is almost similar. This is because of the higher temperature of the CPV module compared to the non-concentrating module for higher irradiance the fill factor and the open circuit voltage drops.
- The average module efficiency of the CPV modules for all weather conditions was found to be 21% less than the non concentrating module, while the module efficiency of the non-concentrating module is found to be 12%, the CPV module efficiency is 9.4%.
- The temperature of the module rear-plate temperature reached up to maximum 39.8^{o}C, while the ambient temperature was 15^{o}C and the non-concentrating module temperature was 27^{o}C.

- Delamination in the module reduces the power output of the module. The delamination occurred because of the thin layer of the encapsulation material between the solar cell and the receiver of the concentrator. With the increase in temperature this thin layer turns to off-white which prevents the collect solar flux to reach the solar cell. Increasing the thickness of the encapsulation material this problem can be eliminated.

Cost analysis

The cost will be the biggest factor to bring the developed technology to the market. With the drop in prices of flat plate PV modules, the challenge to the low concentrating CPV is very high. However, for certain applications like building integration the flat plate modules need to be specially designed. So the cost of the designed CPV module is compared with the glass-glass laminated module which has specific application of building façade integration. The cost, embodied energy analysis shows the following outcomes

- The CPV module with the dielectric concentrator is cost effective alternative to the conventional glass-glass laminated module.
- The CPV module is £0.53/W_p cheaper than the glass-glass laminated module.
- For similar size 1m^2 modules designed CPV module is £190.3 cheaper than glass-glass laminated module.
- For a module of the same power output the embodied energy of the CPV module is also found to be higher than the glass-glass module.

7.2 Achievements and further design considerations

This thesis work demonstrates an extensive optimisation study and performance analysis of the designed dielectric concentrator for BICPV applications. The detail study also identified the scopes of possible improvements in the design and fabrication of the dielectric concentrators and CPV modules. Those modifications have been incurred and demonstrated with the extensive experimental analysis. The reduction in optical losses in the different components of the CPV module is the most prominent modification in the CPV module design compared to the previous studies. **The extensive investigation of the truncation effect on the angular acceptance of dielectric ACPC concentrator has not been done before, which is a significant**

outcome of this thesis work. The optimum truncation can significantly reduce the amount of the material used to manufacture the concentrator with minimum compromise in the performance. The results of the indoor and outdoor characterisation of the CPV modules are milestones for future research in dielectric concentrating system.

All the objectives those were underlined for the project has been achieved and reported in this thesis. However during the project, the harvesting of knowledge has led to new ideas and scope for further improvement in the design of the CPV module. Even though the concentrator design considered in this study has been optimised for high latitudes, the possibility of improvement in the concentrator and solar cell design cannot be ignored. The scope of increase in performance of the designed CPV module is to design the solar cell specifically for the optimised concentrators. The design and layout of the bus bars and finger in a solar cell plays an important role in the performance of the solar cell. While using with concentrating system, optimum solar cell design can enhance the performance significantly. The solar cell used in this study was designed for optimum performance up to the concentration ratio 10 with any type of concentrators. So, if the solar cell can be designed based on the energy flux distribution at the receiver of the designed concentrator, an enhancement in performance can be expected. The optical modelling result carried out in this study for the energy flux distribution with the variation in solar incidence angle (Section 3.9.1; page 132) provides the required information for optimum solar cell design for this type of concentrator.

In broader perspective, the increase in concentration ratio can further decrease the area of the solar cell in the CPV module and can further reduce the cost. One of the reasons to use low-concentrating system for BICPV application, considered in this thesis, is to avoid active cooling requirement. With high concentration, the temperature of the solar cell increases which reduces the conversion efficiency of the system because of the drop in open circuit voltage. However for a location like Edinburgh, where the number of sunny days in a year is very less and ambient temperature is moderate, a higher concentration ratio (CR=5) compared to 2.8 will have benefits in terms of annual energy generation for a time duration 10 years. Even though during the complete sunny days the conversion efficiency of the CPV system with concentration ratio 5 will be less than the designed system in this study, considering the less number of complete sunny days, the average conversion efficiency over the year will be very comparable to the CPV

system with concentration ratio 2.8. Even though the concentration ratio of up to 3.5 can only be achieved with the truncated dielectric ACPC while maintaining the acceptance half angle (0^o and 55^o), but the proposed concentration ratio of 5 is certainly achievable with a degree of compromise in the design and performance of the system, where the range of acceptance angle will decrease by 34% (given by Equation (1.14)). It can be assumed that the complete sunny day in Edinburgh is approximately 25 days, considering the total annual average of sunshine in Scotland as 1200hrs. So considering the adverse effect the complete sunny days can bring to the dielectric ACPC system with concentration ratio 5, viz. material (sealing and encapsulation) degradation, thermal stresses in the PV devices etc., it appears that the system can still withstand itself for 10 odd years without much appreciable damage. This needs a separate investigation through life-time testing analysis of the system over longer periods, through accelerating testing facilities for a favourable market penetration possibility of the product as this could generate overall higher power.

7.3 Recommendation for future work

The low concentrating PV modules cannot replace the standard commercial glass-glass modules unless it is cheaper and aesthetically accepted by the architectures. The only possible ways to reduce the cost of the unit energy output is to use durable, cheap dielectric material with good transmission properties. Reducing the optical loss in the system level and the increase in performance of the modules by homogeneous distribution of the solar flux at the receiver could be other options to be considered. The following further research works can be interesting to investigate in order to bring the low concentrating technology to the market for building integration:

- Detail investigation of the same concentrator design manufactured with clear casted PMMA. PMMA has better optical properties and easily available. Machining of a thick PMMA sheet (thicker than the concentrator height) cause higher surface roughness; however a better optical clarity can be achieved, which can enhance the performance and the cost of the CPV system significantly.
- Diurnal variation of sun spectrum is an important factor to estimate the annual energy output of the CPV modules. Investigation of the spectral dependence on

the performance of the dielectric concentrator and its effect in power generation with the diurnal variation of sun spectrum is required.

- The performance of the dielectric concentrators with diffuse radiation need to be investigated in details. Explicit optical simulation with diffuse radiation is required to estimate the performance of the CPV modules. Long term outdoor experimental characterisation with special interest to diffuse radiation is required.
- Detail investigation of the effect of the inhomogeneous distribution of the solar flux distribution in low concentrating modules and designing solar cells with optimum fingers and bus-bars positions for the better module performance.
- Details investigation of the outdoor performance of the CPV module near equator locations, where the season variation sun position is not significant to use these modules as standalone system.
- Replacing the expensive encapsulation material sylgard by low cost EVA to reduce the cost of the CPV module.
- Manufacturing dielectric concentrator in a single sheet of dielectric material, which will be suitable for optical coupling of the cover glass and the concentrator aperture. This will reduce the optical loss and also provide more rigidity to the CPV system while integration as a façade.
- Use of downshifting dyes in the dielectric concentrator can enhance the optical performance and electrical output of the CPV modules. Details investigation of the optical performance of the dielectric concentrator with different dyes and different dye concentration is required.
- Energy analysis of a building with the BICPV system.
- Detailed thermal performance investigation to evaluate the overall heat loss coefficient is required in order to use the CPV modules as a building fenestration.
- Accelerated weathering test is required to understand the stability and durability of the CPV system.
- Detailed investigation by incorporating different refractive index materials can be carried out to improve the overall efficiency of the CPV system.

The above mentioned recommendations can enhance the performance of the CPV system while reducing the cost. Due to the time constraints in PhD all these

recommendations are out of the scope of this PhD project. With optimisation in module fabrication process with cheap material and by reducing the optical loses, the low concentrating stationary CPV system will be a better choice for building integration in the near future.

Bibliography

[1] T. Muneer, C. Gueymard, H. Kambezidis, Solar Radiation & Daylight Models, Elsevier Butterworth Heinemann, (2004).

[2] R.E.H. Sims, Renewable energy: a response to climate change, Solar Energy, 76 (2004) 9-17.

[3] M.I. Hoffert, K. Caldeira, G. Benford, D.R. Criswell, C. Green, H. Herzog, A.K. Jain, H.S. Kheshgi, K.S. Lackner, J.S. Lewis, H.D. Lightfoot, W. Manheimer, J.C. Mankins, M.E. Mauel, L.J. Perkins, M.E. Schlesinger, T. Volk, T.M.L. Wigley, Advanced Technology Paths to Global Climate Stability: Energy for a Greenhouse Planet, Science, 298 (2002) 981-987.

[4] S. Roaf, D. Crichton, F. Nicol, Adapting Buildings and Cities for Climate Change: A 21st Century Survival Guide, Elsevier, (2009).

[5] D. Schimmelpfenning, The option value of renewable energy The case of climate change, Energy Economics, 17 (1995) 311-317.

[6] M. Hankins, Stand-alone Solar Electric Systems: "The Earthscan Expert Handbook for Planning, Design and Installation", Taylor & Francis, (2012).

[7] N.S. Lewis, D.G. Nocera, Powering the planet: Chemical challenges in solar energy utilization, Proceedings of the National Academy of Sciences, 103 (2006) 15729-15735.

[8] M.A. Green, Solar cells: operating principles, technology, and system applications, Prentice-Hall, (1982).

[9] C.F. Campen, Handbook of Geophysics, Macmillan, (1960).

[10] J.A. Duffie, W.A. Beckman, Solar engineering of thermal processes, Wiley, 2006.

[11] M.A. Green, Solar cells: operating principles, technology, and system applications, Prentice-Hall,, Englewood Cliffs, (1982).

[12] D.Y. Goswami, J.F. Kreider, Principles of Solar Engineering, Taylor & Francis, (2000).

[13] J.F. Kreider, F. Kreith, Solar energy handbook, McGraw-Hill, (1981).

[14] S. Kalogirou, Solar Energy Engineering: Processes and Systems, Elsevier/Academic Press, (2009).

[15] G.N. Tiwari, Solar Energy: Fundamentals, Design, Modelling and Applications, CRC Press, (2002).

[16] S. Fonash, Solar Cell Device Physics, Elsevier Science, (2010).

[17] A. Luque, S. Hegedus, Handbook of Photovoltaic Science and Engineering, Wiley, (2003).

[18] D.M. Chapin, C.S. Fuller, G.L. Pearson, A New Silicon p-n Junction Photocell for Converting Solar Radiation into Electrical Power, Journal of Applied Physics, 25 (1954) 676-677.

[19] M. Wolf, H. Rauschenbach, Series resistance effects on solar cell measurements, Advanced Energy Conversion, 3 (1963) 455-479.

[20] W.G. Pfann, W. Van Roosbroeck, Radioactive and Photoelectric p-n Junction Power Sources, Journal of Applied Physics, 25 (1954) 1422-1434.

[21] M.B. Prince, Silicon Solar Energy Converters, Journal of Applied Physics, 26 (1955) 534-540.

[22] M.D. Archer, R. Hill, Clean Electricity from Photovoltaics, Imperial College Press, (2001).

[23] R. Hull, INSPEC, Properties of Crystalline Silicon, INSPEC, The Institution of Electrical Engineers, (1999).

[24] M.A. Green, M.J. Keevers, Optical properties of intrinsic silicon at 300 K, Progress in Photovoltaics: Research and Applications, 3 (1995) 189-192.

[25] S. Kolodinski, J.H. Werner, T. Wittchen, H.J. Queisser, Quantum efficiencies exceeding unity due to impact ionization in silicon solar cells, Applied Physics Letters, 63 (1993) 2405-2407.

[26] M. Wolf, The influence of heavy doping effects on silicon solar cell performance, Solar Cells, 17 (1986) 53-63.

[27] J. Nelson, The Physics of Solar Cells, Imperial College Press, (2003).

[28] R.W. Miles, K.M. Hynes, I. Forbes, Photovoltaic solar cells: An overview of state-of-the-art cell development and environmental issues, Progress in Crystal Growth and Characterization of Materials, 51 (2005) 1-42.

[29] M.A. Green, K. Emery, Y. Hishikawa, W. Warta, E.D. Dunlop, Solar cell efficiency tables (version 39), Progress in Photovoltaics: Research and Applications, 20 (2012) 12-20.

[30] S. Wenham, Buried-contact silicon solar cells, Progress in Photovoltaics: Research and Applications, 1 (1993) 3-10.

[31] M.A. Green, S.R. Wenham, J. Zhao, S. Bowden, A.M. Milne, M. Taouk, F. Zhang, Present status of buried contact solar cells, In proceedings of the 22nd IEEE Photovoltaic Specialists Conference, (1991), pages 46-53.

[32] L.L. Kazmerski, Photovoltaics: A review of cell and module technologies, Renewable and Sustainable Energy Reviews, 1 (1997) 71-170.

[33] A. McEvoy, T. Markvart, L. Castañer, Practical Handbook of Photovoltaics: Fundamentals and Applications, Academic Press, 2011.

[34] M.A. Green, S.R. Wenham, C.B. Honsberg, D. Hogg, Transfer of buried contact cell laboratory sequences into commercial production, Solar Energy Materials and Solar Cells, 34 (1994) 83-89.

[35] C.B. Honsberg, F. Yun, A. Ebong, M. Taouk, S.R. Wenham, M.A. Green, 685 mV open-circuit voltage laser grooved silicon solar cell, Solar Energy Materials and Solar Cells, 34 (1994) 117-123.

[36] K. Ardani, R. Margolis, Solar Technologies Market Report, NREL report, (2010)

[37] A. Shah, E. Vallat-Sauvain, P. Torres, J. Meier, U. Kroll, C. Hof, C. Droz, M. Goerlitzer, N. Wyrsch, M. Vanecek, Intrinsic microcrystalline silicon (μc-Si:H) deposited by VHF-GD (very high frequency-glow discharge): a new material for photovoltaics and optoelectronics, Materials Science and Engineering: B, 69–70 (2000) 219-226.

[38] M. Lipiński, P. Panek, Z. Świątek, E. Bełtowska, R. Ciach, Double porous silicon layer on multi-crystalline Si for photovoltaic application, Solar Energy Materials and Solar Cells, 72 (2002) 271-276.

[39] K. Shirasawa, H. Yamashita, K. Fukui, M. Takayama, K. Okada, K. Masuri, H. Watanabe, Large area high efficiency multicrystalline silicon solar cell, In proceedings of the 21st IEEE Photovoltaic Specialists Conference, (1990), pages 668-673.

[40] G. Willeke, H. Nussbaumer, H. Bender, E. Bucher, A simple and effective light trapping technique for polycrystalline silicon solar cells, Solar Energy Materials and Solar Cells, 26 (1992) 345-356.

[41] A.G. Aberle, Surface passivation of crystalline silicon solar cells: a review, Progress in Photovoltaics: Research and Applications, 8 (2000) 473-487.

[42] R.W. Birkmire, E. Eser, POLYCRYSTALLINE THIN FILM SOLAR CELLS: Present Status and Future Potential, Annual Review of Materials Science, 27 (1997) 625-653.

[43] J. Poortmans, V. Arkhipov, Thin Film Solar Cells: Fabrication, Characterization and Applications, Wiley, (2006).

[44] K. Zweibel, Thin films: Past, present, future, NREL report, (1995).

[45] K. Zweibel, Thin film PV manufacturing: Materials costs and their optimization, Solar Energy Materials and Solar Cells, 63 (2000) 375-386.

[46] K. Zweibel, Harnessing solar power: the photovoltaics challenge, Plenum Press, (1990).

[47] J.H. Scofield, A. Duda, D. Albin, B.L. Ballard, P.K. Predecki, Sputtered molybdenum bilayer back contact for copper indium diselenide-based polycrystalline thin-film solar cells, Thin Solid Films, 260 (1995) 26-31.

[48] B.M. Başol, V.K. Kapur, A. Halani, C. Leidholm, Copper indium diselenide thin film solar cells fabricated on flexible foil substrates, Solar Energy Materials and Solar Cells, 29 (1993) 163-173.

[49] J.F. Guillemoles, P. Cowache, S. Massaccesi, L. Thouin, S. Sanchez, D. Lincot, J. Vedel, Solar cells with improved efficiency based on electrodeposited copper indium diselenide thin films, Advanced Materials, 6 (1994) 379-381.

[50] G. Fulop, M. Doty, P. Meyers, J. Betz, C.H. Liu, High-efficiency electrodeposited cadmium telluride solar cells, Applied Physics Letters, 40 (1982) 327-328.

[51] X. Wu, High-efficiency polycrystalline CdTe thin-film solar cells, Solar Energy, 77 (2004) 803-814.

[52] R.W. Miles, M.T. Bhatti, K.M. Hynes, A.E. Baumann, R. Hill, Thin films of CdTe produced using stacked elemental layer processing for use in CdTe/CdS solar cells, Materials Science and Engineering: B, 16 (1993) 250-256.

[53] B. O'Regan, M. Gratzel, A low-cost, high-efficiency solar cell based on dye-sensitized colloidal TiO2 films, Nature, 353 (1991) 737-740.

[54] R.J. Komp, Practical photovoltaics: electricity from solar cells, Aatec Publications, (1995).

[55] H. Hoppe, N.S. Sariciftci, Organic solar cells: An overview, Journal of Materials Research, 19 (2004) 1924-1945.

[56] D. Wöhrle, D. Meissner, Organic Solar Cells, Advanced Materials, 3 (1991) 129-138.

[57] M. Pagliaro, G. Palmisano, R. Ciriminna, Flexible Solar Cells, Wiley, (2008).

[58] J.L. Segura, N. Martin, D.M. Guldi, Materials for organic solar cells: the C60/[small pi]-conjugated oligomer approach, Chemical Society Reviews, 34 (2005) 31-47.

[59] G.A. Chamberlain, Organic solar cells: A review, Solar Cells, 8 (1983) 47-83.

[60] F. Dimroth, S. Kurtz, High-Efficiency Multijunction Solar Cells, MRS Bulletin, 32 (2007) 230-235.

[61] C.H. Henry, Limiting efficiencies of ideal single and multiple energy gap terrestrial solar cells, Journal of Applied Physics, 51 (1980) 4494-4500.

[62] J.M. Olson, S.R. Kurtz, A.E. Kibbler, P. Faine, A 27.3% efficient Ga[sub 0.5]In[sub 0.5]P/GaAs tandem solar cell, Applied Physics Letters, 56 (1990) 623-625.

[63] T. Takamoto, E. Ikeda, T. Agui, H. Kurita, T. Tanabe, S. Tanaka, H. Matsubara, Y. Mine, S. Takagishi, M. Yamaguchi, InGaP/GaAs and InGaAs mechanically-stacked triple-junction solar cells, In proceedings of the 26th IEEE Photovoltaic Specialists Conference, (1997), pages 1031-1034.

[64] N.H. Karam, R.R. King, B.T. Cavicchi, D.D. Krut, J.H. Ermer, M. Haddad, C. Li, D.E. Joslin, M. Takahashi, J.W. Eldredge, W.T. Nishikawa, D.R. Lillington, B.M. Keyes, R.K. Ahrenkiel, Development and characterization of high-efficiency Ga_{0.5}In_{0.5}P/GaAs/Ge dual- and triple-junction solar cells, IEEE Transactions on Electron Devices, 46 (1999) 2116-2125.

[65] J.M. Olson, D.J. Friedman, S. Kurtz, High-Efficiency III-V Multijunction Solar Cells, in: Handbook of Photovoltaic Science and Engineering, John Wiley & Sons, Ltd, 2005, pp. 359-411.

[66] M. Yamaguchi, T. Takamoto, K. Araki, M. Imaizumi, N. Kojima, Y. Ohshita, Present and Future of High Efficiency Multi-Junction Solar Cells, In proceedings of the CLEO Conference, (2011).

[67] S. Philipps, W. Guter, E. Welser, J. Schöne, M. Steiner, F. Dimroth, A. Bett, Present Status in the Development of III–V Multi-Junction Solar Cells, Next Generation of Photovoltaics: New concept, Springer, (2012), pages 1-21.

[68] S. Kurtz, Opportunities and Challenges for Development of a Mature Concentrating Photovoltaic Power Industry (Revision), NREL report, (2011).

[69] R. Winston, H. Hinterberger, Principles of cylindrical concentrators for solar energy, Solar Energy, 17 (1975) 255-258.

[70] W.T. Xie, Y.J. Dai, R.Z. Wang, K. Sumathy, Concentrated solar energy applications using Fresnel lenses: A review, Renewable and Sustainable Energy Reviews, 15 (2011) 2588-2606.

[71] J.S. Bodenheimer, N.P. Eisenberg, J. Gur, Testing the figure of parabolic reflectors for solar concentrators, Appl. Opt., 21 (1982) 4434-4438.

[72] J. Chaves, M. Collares-Pereira, Ideal Concentrators with Gaps, Appl. Opt., 41 (2002) 1267-1276.

[73] H. Kaiyan, Z. Hongfei, L. Yixin, C. Ziqian, An Imaging Compounding Parabolic Concentrator, In proceedings of the ISES World Congress, (2007).

[74] J.L. Richter, Optics of a two-trough solar concentrator, Solar Energy, 56 (1996) 191-198.

[75] E.A. Igel, R.L. Hughes, Optical analysis of solar facility heliostats, Solar Energy, 22 (1979) 283-295.

[76] R. Zaibel, E. Dagan, J. Karni, H. Ries, An astigmatic corrected target-aligned heliostat for high concentration, Solar Energy Materials and Solar Cells, 37 (1995) 191-202.

[77] C.S. Sangani, C.S. Solanki, Experimental evaluation of V-trough (2 suns) PV concentrator system using commercial PV modules, Solar Energy Materials and Solar Cells, 91 (2007) 453-459.

[78] M.A.M. Shaltout, A. Ghettas, M. Sabry, V-trough concentrator on a photovoltaic full tracking system in a hot desert climate, Renewable Energy, 6 (1995) 527-532.

[79] W.P. Mulligan, A. Terao, S.G. Daroczi, O. Chao Pujol, M.J. Cudzinovic, P.J. Verlinden, R.M. Swanson, P. Benitez, J.C. Minano, A flat-plate concentrator: micro-concentrator design overview, In proceedings of the 28th IEEE Photovoltaic Specialists Conference, (2000), pages 1495-1497.

[80] W.T. Welford, R. Winston, The optics of nonimaging concentrators : light and solar energy, Academic Press, New York, 1978.

[81] P.A. Davies, Edge-ray principle of nonimaging optics, J. Opt. Soc. Am. A, 11 (1994) 1256-1259.

[82] R. Winston, J.C. Miñano, P. Benítez, Nonimaging Optics, in, Elsevier, 2005.

[83] A. Rabl, Comparison of solar concentrators, Solar Energy, 18 (1976) 93-111.

[84] R. Winston, W.T. Welford, Design Of nonimaging concentrators as second stages in tandem with image-forming first-Stage concentrators, Appl. Opt., 19 (1980) 347-351.

[85] T.K. Mallick, Optics and heat transfer for asymmetric compound parabolic photovoltaic concentrators for building integrated photovoltaics, in: Faculty of Engineering, University of Ulster, Newtownabbey, UK, 2003.

[86] D.E. Prapas, B. Norton, S.D. Probert, Thermal Design of Compound Parabolic Concentrating Solar-Energy Collectors, Journal of Solar Energy Engineering, 109 (1987) 161-168.

[87] D.E. Prapas, B. Norton, P.E. Melidis, S.D. Probert, Convective heat transfers within air spaces of compound parabolic concentrating solar-energy collectors, Applied Energy, 28 (1987) 123-135.

[88] D.R. Mills, J.E. Giutronich, Ideal prism solar concentrators, Solar Energy, 21 (1978) 423-430.

[89] T. Uematsu, Y. Yazawa, Y. Miyamura, S. Muramatsu, H. Ohtsuka, K. Tsutsui, T. Warabisako, Static concentrator photovoltaic module with prism array, Solar Energy Materials and Solar Cells, 67 (2001) 415-423.

[90] D. Chemisana, M. Ibáñez, J. Barrau, Comparison of Fresnel concentrators for building integrated photovoltaics, Energy Conversion and Management, 50 (2009) 1079-1084.

[91] D.C. Miller, S.R. Kurtz, Durability of Fresnel lenses: A review specific to the concentrating photovoltaic application, Solar Energy Materials and Solar Cells, 95 (2011) 2037-2068.

[92] D. Krüger, Y. Pandian, K. Hennecke, M. Schmitz, Parabolic trough collector testing in the frame of the REACt project, Desalination, 220 (2008) 612-618.

[93] T. Tao, H. Zheng, Y. Su, S.B. Riffat, A novel combined solar concentration/wind augmentation system: Constructions and preliminary testing of a prototype, Applied Thermal Engineering, 31 (2011) 3664-3668.

[94] G. Mittelman, A. Kribus, O. Mouchtar, A. Dayan, Water desalination with concentrating photovoltaic/thermal (CPVT) systems, Solar Energy, 83 (2009) 1322-1334.

[95] K.J. Weber, V. Everett, P.N.K. Deenapanray, E. Franklin, A.W. Blakers, Modeling of static concentrator modules incorporating lambertian or v-groove rear reflectors, Solar Energy Materials and Solar Cells, 90 (2006) 1741-1749.

[96] K. Sakuta, S. Sawata, M. Tanimoto, Luminescent concentrator module of a practical size, In proceedings of the 24th IEEE Photovoltaic Specialists Conference, (1994), pages 1115-1118.

[97] N. Fraidenraich, C. Tiba, B.B. Brandão, O.C. Vilela, Analytic solutions for the geometric and optical properties of stationary compound parabolic concentrators with fully illuminated inverted V receiver, Solar Energy, 82 (2008) 132-143.

[98] H.P. Garg, R.S. Adhikari, Performance analysis of a hybrid photovoltaic/thermal (PV/T) collector with integrated CPC troughs, International Journal of Energy Research, 23 (1999) 1295-1304.

[99] E.M. Kritchman, A.A. Friesem, G. Yekutieli, Highly concentrating Fresnel lenses, Appl. Opt., 18 (1979) 2688-2695.

[100] A.W. Bett, B. Burger, F. Dimroth, G. Siefer, H. Lerchenmuller, High-Concentration PV using III-V Solar Cells, In proceedings of the 4th IEEE World Conference on Photovoltaic Energy Conversion, (2006), pages 651-620.

[101] D. Feuermann, J.M. Gordon, High-concentration photovoltaic designs based on miniature parabolic dishes, Solar Energy, 70 (2001) 423-430.

[102] K.S. Reddy, N. Sendhil Kumar, Combined laminar natural convection and surface radiation heat transfer in a modified cavity receiver of solar parabolic dish, International Journal of Thermal Sciences, 47 (2008) 1647-1657.

[103] P. Schramek, D.R. Mills, Heliostats for maximum ground coverage, Energy, 29 (2004) 701-713.

[104] S. Kalogirou, Use of parabolic trough solar energy collectors for sea-water desalination, Applied Energy, 60 (1998) 65-88.

[105] G. Sala, J.C. Arboiro, A. Luque, J.C. Zamorano, J.C. Minano, C. Dramsch, T. Bruton, D. Cunningham, The EUCLIDES prototype: An efficient parabolic trough for PV concentration, In proceedings of the 25th IEEE Photovoltaic Specialists Conference, (1996), pages 1207-1210.

[106] K. Ryu, J.-G. Rhee, K.-M. Park, J. Kim, Concept and design of modular Fresnel lenses for concentration solar PV system, Solar Energy, 80 (2006) 1580-1587.

[107] F.H. Koltz, PV systems with V-trough concentration and Passive tracking-concept and economic potential in Europe, In proceedings of the 13th European PV Solar Energy Conference, (1995), pages 1060-1063.

[108] T.K. Mallick, P.C. Eames, T.J. Hyde, B. Norton, The design and experimental characterisation of an asymmetric compound parabolic photovoltaic concentrator for building façade integration in the UK, Solar Energy, 77 (2004) 319-327.

[109] J. Nilsson, Optical Design and Characterization of Solar Concentrators for Photovoltaics, PhD Thesis, Department of Architechture and Built Environment Lund University, Lund, (2005).

[110] A. Luque, G.L. Araújo, Solar cells and optics for photovoltaic concentration, A. Hilger, (1989).

[111] J. O'Gallagher, Nonimaging Optics in Solar Energy, Morgan & Claypool Publishers, (2008).

[112] H. Ries, A. Rabl, Edge-ray principle of nonimaging optics, J. Opt. Soc. Am. A, 11 (1994) 2627-2632.

[113] A. Luque, Nonimaging Optics in Solar Energy, Synthesis Lectures on Energy and the Environment Technology Science and Society, 2 (2008).

[114] R. Winston, Principles of solar concentrators of a novel design, Solar Energy, 16 (1974) 89-95.

[115] N.B. Goodman, R. Ignatius, L. Wharton, R. Winston, Solid-Dielectric Compound Parabolic Concentrators: On Their Use With Photovoltaic Devices, Appl. Opt., 15 (1976) 2434-2436.

[116] D.P. Grimmer, A comparison of compound parabolic and simple parabolic concentrating solar collectors, Solar Energy, 22 (1979) 21-25.

[117] J.A. Manrique, A compound parabolic concentrator, International Communications in Heat and Mass Transfer, 11 (1984) 267-273.

[118] D. Suresh, J. O'Gallagher, R. Winston, Thermal and optical performance test results for compound parabolic concentrators (CPCs), Solar Energy, 44 (1990) 257-270.

[119] J.M. Gordon, A. Rabl, Nonimaging Compound Parabolic Concentrator-Type Reflectors With Variable Extreme Direction, Appl. Opt., 31 (1992) 7332-7338.

[120] R. Oommen, S. Jayaraman, Development and performance analysis of compound parabolic solar concentrators with reduced gap losses – oversized reflector, Energy Conversion and Management, 42 (2001) 1379-1399.

[121] P.C. Eames, M. Smyth, B. Norton, The experimental validation of a comprehensive unified model for optics and heat transfer in line-axis solar energy systems, Solar Energy, 71 (2001) 121-133.

[122] S.C. Mullick, A. Malhotra, S.K. Nanda, Optimization of the geometry of a seasonally adjusted solar concentrator by the discrete maximum principle, Solar & Wind Technology, 4 (1987) 195-199.

[123] B. Norton, P.C. Eames, Y.P. Yadav, Symmetric and asymmetric linear compound parabolic concentrating solar energy collectors: The state-of-the-art in optical and thermo-physical analysis, International Journal of Ambient Energy, 12 (1991) 171-190.

[124] G. Almonacid, A. Luque, Truncation effects in bifacial compound parabolic concentrators, Solar Cells, 22 (1987) 47-54.

[125] A. Rabl, Optical and thermal properties of compound parabolic concentrators, Solar Energy, 18 (1976) 497-511.

[126] C.K. Hsieh, Thermal analysis of CPC collectors, Solar Energy, 27 (1981) 19-29.

[127] D.E. Prapas, B. Norton, S.D. Probert, Optics of parabolic-trough, solar-energy collectors, possessing small concentration ratios, Solar Energy, 39 (1987) 541-550.

[128] T.C. Chew, A.O. Tay, N.E. Wijeysundera, A Numerical Study of the Natural Convection in CPC Solar Collector Cavities with Tubular Absorbers, Journal of Solar Energy Engineering, 111 (1989) 16-23.

[129] T.C. Chew, N.E. Wijeysundera, A.O. Tay, An Experimental Study of Free Convection in Compound Parabolic Concentrator (CPC) Cavities, Journal of Solar Energy Engineering, 110 (1988) 293-298.

[130] F.P. Incropera, D.P. De Witt, Fundamentals of heat and mass transfer, 2nd edition, Wiley, (1985).

[131] R.A. Tatara, G. Thodos, Experimental natural convective studies within a compound parabolic concentrator enclosure, Technical report, Northwestern University, Evanston, (1983).

[132] P.C. Eames, B. Norton, Detailed parametric analyses of heat transfer in CPC solar energy collectors, Solar Energy, 50 (1993) 321-338.

[133] E.C. Bose, A. Luque, Renewable energy : sources for fuels and electricity, Island Press, Washington, D.C., (1993).

[134] R. Leutz, A. Suzuki, A. Akisawa, T. Kashiwagi, DESIGN OF A NONIMAGING FRESNEL LENS FOR SOLAR CONCENTRATORS, Solar Energy, 65 (1999) 379-387.

[135] G. Sala, I. Anton, J.C. Arboiro, A. Luque, E. Camblor, E. Mera, M. Gasson, M. Cendagorta, P. Valera, M.P. Friend, J. Monedero, S. Genzales, F. Dobon, I. Luque, The 480 kW(p) EUCLIDES-THERMIE Power Plant: Installation, Set-UP and First Results, In proceedings of the 16th European PV Solar Energy Conference, (2000), pages 2071-2077.

[136] I. Antón, Sala, G., The EUCLIDES Concentrator, Concentrator Photovoltaics, Springer Berlin / Heidelberg, (2007), pages 279-299.

[137] I. Antón, G. Sala, Losses caused by dispersion of optical parameters and misalignments in PV concentrators, Progress in Photovoltaics: Research and Applications, 13 (2005) 341-352.

[138] http://www.amonix.com/technology_description.html

[139] K.W. Stone, V. Garboushian, D. Dutra, H. Hayden, Operation of 350 kW of Amonix High Concentration PV Systems at Arizona Public Service, In proceedings of the ASME Conference, (2003), pages 433-438.

[140] M. Hein, F. Dimroth, G. Siefer, A.W. Bett, Characterisation of a 300× photovoltaic concentrator system with one-axis tracking, Solar Energy Materials and Solar Cells, 75 (2003) 277-283.

[141] F.J. Vorster, E.E. van Dyk, Current-voltage characteristics of high-concentration, photovoltaic arrays, Progress in Photovoltaics: Research and Applications, 13 (2005) 55-66.

[142] A. Royne, C.J. Dey, D.R. Mills, Cooling of photovoltaic cells under concentrated illumination: a critical review, Solar Energy Materials and Solar Cells, 86 (2005) 451-483.

[143] D.J. Mbewe, H.C. Card, D.C. Card, A model of silicon solar cells for concentrator photovoltaic and photovoltaic/thermal system design, Solar Energy, 35 (1985) 247-258.

[144] V.L. Dalal, A.R. Moore, Design considerations for high-intensity solar cells, Journal of Applied Physics, 48 (1977) 1244-1251.

[145] S.M. Vernon, W.A. Anderson, Temperature effects in Schottky-barrier silicon solar cells, Applied Physics Letters 26 (1975) 707-709.

[146] Z. Ye, Q. Li, Q. Zhu, W. Pan, The cooling technology of solar cells under concentrated system, In proceedings of the IEEE 6th International Power Electronics and Motion Control Conference, (2009), pages 2193-2197.

[147] M. Cao, S. Butler, J.T. Benoit, Y. Jiang, R. Radhakrishnan, Y. Chen, S. Bendapudi, S. Horne, Thermal Stress Analysis/Life Prediction of Concentrating Photovoltaic Module, Journal of Solar Energy Engineering, 130 (2008) 021011-021019.

[148] M.J. O'Leary, L.D. Clements, Thermal-electric performance analysis for actively cooled, concentrating photovoltaic systems, Solar Energy, 25 (1980) 401-406.

[149] J.C. Minano, J.C. Gonzalez, I. Zanesco, Flat high concentration devices, In proceedings of the 24th IEEE Photovoltaic Specialists Conference and 1st World conference on Photovoltaic Energy Conversion, (1994), pages 1123-1126.

[150] A. Akbarzadeh, T. Wadowski, Heat pipe-based cooling systems for photovoltaic cells under concentrated solar radiation, Applied Thermal Engineering, 16 (1996) 81-87.

[151] F. Chenlo, M. Cid, A linear concentrator photovoltaic module: analysis of non-uniform illumination and temperature effects on efficiency, Solar Cells, 20 (1987) 27-39.

[152] J.K. Tonui, Y. Tripanagnostopoulos, Air-cooled PV/T solar collectors with low cost performance improvements, Solar Energy, 81 (2007) 498-511.

[153] S. Kurtz, J. Granata, M. Quintana, Photovoltaic Reliability R&D toward a Solar-Powered World, In proceedings of the SPIE Conference, (2009), pages 7412 - 7415.

[154] G. Peharz, F. Dimroth, Energy payback time of the high-concentration PV system FLATCON®, Progress in Photovoltaics: Research and Applications, 13 (2005) 627-634.

[155] F. Sick, T. Erge, I.E.A.S. Heating, C. Programme, Photovoltaics in Buildings: A Design Handbook for Architects and Engineers, James & James (Science Publishers) Limited, (1996).

[156] S.F. Barkaszi, J.P. Dunlop, Discussion of strategies for mounting photovoltaic arrays on rooftops, In proceedings of the Solar Forum: Solar Energy: The Power to choose, Washington, D.C., (2001).

[157] B. Petter Jelle, C. Breivik, H. Drolsum Røkenes, Building integrated photovoltaic products: A state-of-the-art review and future research opportunities, Solar Energy Materials and Solar Cells, 100 (2012) 69-96.

[158] B. Norton, P.C. Eames, T.K. Mallick, M.J. Huang, S.J. McCormack, J.D. Mondol, Y.G. Yohanis, Enhancing the performance of building integrated photovoltaics, Solar Energy, 85 (2011) 1629-1664.

[159] M.D. Archer, Clean electricity from photovoltaics, Imperial College Press, London, (2005).

[160] J. Strong S, The dawning of solar electric architecture : Feature : Photovoltaics in buildings, Sunworld, 20 (1996) 3-5.

[161] I. Hagemann, PV in buildings - the influence of pv on the design and planning process of a building, Renewable Energy, 8 (1996) 467-470.

[162] H. Maurus, M. Schmid, B. Blersch, P. Lechner, H. Schade, PV for buildings: Benefits and experiences with amorphous silicon in BIPV applications, Refocus, 5 (2004) 22-27.

[163] J. Benemann, Multifunctional solar facades-a new challenge for photovoltaic, In proceedings of the 24th IEEE Photovoltaic Specialists Conference, (1994), pages 784-787.

[164] C. Peng, Y. Huang, Z. Wu, Building-integrated photovoltaics (BIPV) in architectural design in China, Energy and Buildings, 43 (2011) 3592-3598.

[165] B.H. Chowdhury, S. Muknahallipatna, J.J. Cupal, J.C. Hamann, T. Dinwoodie, D. Shugar, A 50 kilowatt distributed grid-connected photovoltaic generation system for the University of Wyoming, In proceedings of the 26th IEEE Photovoltaic Specialists Conference, (1997), pages 1369-1372.

[166] Y. Nitta, T. Hatukaiwa, T. Yamawaki, Y. Matumura, S. Mizukami, Development of photovoltaic modules integrated with roofing materials (heat insulated roof panel), In proceedings of the 24th IEEE Photovoltaic Specialists Conference, (1994), pages 073-976.

[167] J. Bonvin, C. Roecker, P. Affolter, A. Muller, SOLBAC flat roof system and first installations, In proceedings of the 14th European Photovoltaic Solar Energy Conference, (1997), pages 1849-1850.

[168] A.N. Muller, P. Affolter, J. Bonvin, J.B. Gay, C. Roecker, The DEMOSITE and PV building integration activities, In proceedings of the 4th European Conference on Solar Energy in Architecture and Urban Planning, (1996), pages 575-578.

[169] T.L. Dinwoodie, D.S. Shugar, Optimizing roof-integrated photovoltaics: a case study of the PowerGuard roofing tile, In proceedings of the 24th IEEE Photovoltaic Specialists Conference, (1994), pages 1004-1007.

[170] M. Posnansky, T. Szacsvay, A. Eckmanns, J. Jürgens, New electricity construction materials for roofs and façades, Renewable Energy, 15 (1998) 541-544.

[171] T. Matsuoka, H. Yagi, Y. Waki, K. Honma, S. Sakai, M. Ohnishi, H. Kawata, S. Nakano, Y. Kuwano, A new solar cell roofing tile, Solar Cells, 29 (1990) 361-368.

[172] S.J. Strong, World overview of building-integrated photovoltaics, In proceedings of the 25th IEEE Photovoltaic Specialists Conference, (1996), pages 1197-1202.

[173] Y. Ichikawa, T. Ihara, T. Hama, Y. Watanuki, S. Kato, H. Ota, H. Sakai, N. Sakai, J. Kurihara, O. Ishikawa, A new flexible a-Si PV module and its application to rooftop PV systems, In proceedings of the 24th IEEE Photovoltaic Specialists Conference, (1994), pages 986-989.

[174] K. Murata, T. Yagiura, K. Takeda, M. Tanaka, S. Kiyama, New type of photovoltaic module integrated with roofing material (highly fire-resistant PV tile), Solar Energy Materials and Solar Cells, 75 (2003) 647-653.

[175] C. Meier, A. Hasler, Solar tile: a special PV-module integrated in clay tile roofs, In proceedings of the 11th European Photovoltaic Solar Energy Conference, (1992), pages 1664-1667.

[176] M. Sala, M. Brissoni, G. Franci, Network re-integrated bus shelter in regional development, In proceedings of the 13th European Photovoltaic Solar Energy Conference, (1995), pages 533-536.

[177] N. Mosko, D. Niephaus, Bypass support system designed as an electrical distribution frame and a basic triangle solar cell module for constructing solar power plants, In proceedings of the 13th European Photovoltaic Solar Energy Conference, (1995), pages 537-538.

[178] F. Shinjo, R&D of photovoltaic modules integrated with construction materials, In proceedings of the 24th IEEE Photovoltaic Specialists Conference, (1994), pages 778-780.

[179] S. Toyokawa, S. Uehara, Overall evaluation for R&D of PV modules integrated with construction materials, In proceedings of the 26th IEEE Photovoltaic Specialists Conference, (1997), pages 1333-1336.

[180] S. Roberts, N. Guariento, Building Integrated Photovoltaics: A Handbook, Birkhäuser, (2009).

[181] R.D. Scott, B.E. Lord, F.J. Crick, J.P. Louineau, R. Noble, D. Anderson, A study of the integration of PV modules into building cladding components in the UK, In proceedings of the 11th European Photovoltaic Solar Energy Conference, (1992), pages 1491-1494.

[182] R. Coons, Dow: Solar shingles could generate $5 billion by 2015, Chemical week, 171 (2009) 9.

[183] C. Breyer, A. Gerlach, Global overview on grid-parity, Progress in Photovoltaics: Research and Applications, (2012).

[184] M. Pagliaro, R. Ciriminna, G. Palmisano, BIPV: merging the photovoltaic with the construction industry, Progress in Photovoltaics: Research and Applications, 18 (2010) 61-72.

[185] R. Dones, C. Bauer, R. Bolliger, B. Burger, M. Faist Emmenegger, R. Frischknecht, T. Heck, N. Jungbluth, A. Roder, M. Tuchschmid, Life cycle inventories of energy systems: Results for current systems in Switzerland and other UCTE countries, Swiss Centre for Life Cycle Inventories, Duebendorf , Switzerland, 2007.

[186] G.P. Hammond, H.A. Harajli, C.I. Jones, A.B. Winnett, Whole systems appraisal of a UK Building Integrated Photovoltaic (BIPV) system: Energy, environmental, and economic evaluations, Energy Policy, 40 (2012) 219-230.

[187] R.M. Swanson, The promise of concentrators, Progress in Photovoltaics: Research and Applications, 8 (2000) 93-111.

[188] T. Reijena, Photovoltaics in the built environment, In proceedings of the 2nd world solar electric buildings conference, (2000).

[189] D. Chemisana, Building Integrated Concentrating Photovoltaics: A review, Renewable and Sustainable Energy Reviews, 15 (2011) 603-611.

[190] V.I. Kabakov, L.B. Levin, A choice of the position of receiver with photocells in parabolic trough concentrator, Solar Energy Materials and Solar Cells, 33 (1994) 45-49.

[191] D.R. Mills, J.E. Giutronich, Asymmetrical non-imaging cylindrical solar concentrators, Solar Energy, 20 (1978) 45-55.

[192] R.H. Smith, Solergy collector concept, In proceedings of the International conference on Heliotechnique and development, (1975), pages 251-264.

[193] D.R. Mills, J.E. Giutronich, New ideal concentrators for distant radiation sources, Solar Energy, 23 (1979) 85-87.

[194] A. Rabl, Solar Concentrators With Maximal Concentration For Cylindrical Absorbers, Appl. Opt., 15 (1976) 1871-1873.

[195] M. Adsten, Solar Thermal Collectors at High Latitudes: Design and Performance of Non-Tracking Concentrators, PhD Thesis, Faculty of Science and Technology, Uppsala University, Uppsala, (2002).

[196] M. Adsten, A. Helgesson, B. Karlsson, Evaluation of CPC-collector designs for stand-alone, roof- or wall installation, Solar Energy, 79 (2005) 638-647.

[197] M. Adsten, B. Hellström, B. Karlsson, Measurement of radiation distribution on the absorber in an asymmetric CPC collector, Solar Energy, 76 (2004) 199-206.

[198] T.K. Mallick, P.C. Eames, B. Norton, Non-concentrating and asymmetric compound parabolic concentrating building façade integrated photovoltaics: An experimental comparison, Solar Energy, 80 (2006) 834-849.

[199] N.C. Shaw, S.R. Wenham, Design of a novel static concentrator lens utilising total internal reflection surfaces, In proceedings of the 16th European Photovoltaic Solar Energy Conference, (2000), pages 2342-2345.

[200] S.R. Wenham, S. Bowden, M. Dickinson, R. Largent, N. Shaw, C.B. Honsberg, M.A. Green, P. Smith, Low cost photovoltaic roof tile, Solar Energy Materials and Solar Cells, 47 (1997) 325-337.

[201] S. Bowden, S.R. Wenham, P. Coffey, M. Dickinson, M.A. Green, High efficiency photovoltaic roof tile with static concentrator, In proceedings of the 23th IEEE Photovoltaic Specialists Conference, (1993), pages 1068-1072.

[202] S. Bowden, S.R. Wenham, W.R. Dickinson, M.A. Green, High efficiency photovoltaic roof tiles with static concentrators, In proceedings of the 24th IEEE Photovoltaic Specialists Conference, (1994), pages 774-777.

[203] T. Uematsu, Y. Yazawa, T. Joge, S. Kokunai, Fabrication and characterization of a flat-plate static-concentrator photovoltaic module, Solar Energy Materials and Solar Cells, 67 (2001) 425-434.

[204] T. Uematsu, Y. Yazawa, K. Tsutsui, Y. Miyamura, H. Ohtsuka, T. Warabisako, T. Joge, Design and characterization of flat-plate static-concentrator photovoltaic modules, Solar Energy Materials and Solar Cells, 67 (2001) 441-448.

[205] M. Brogren, Optical efficiency of low-concentrating solar energy systems with parabolic reflectors, PhD Thesis, Faculty of Science and Technology, Uppsala University, Uppsala, (2004).

[206] M. Brogren, J. Wennerberg, R. Kapper, B. Karlsson, Design of concentrating elements with CIS thin-film solar cells for façade integration, Solar Energy Materials and Solar Cells, 75 (2003) 567-575.

[207] H. Gajbert, M. Hall, B. Karlsson, Optimisation of reflector and module geometries for stationary, low-concentrating, façade-integrated photovoltaic systems, Solar Energy Materials and Solar Cells, 91 (2007) 1788-1799.

[208] R. Winston, Dielectric compound parabolic concentrators, Appl. Opt., 15 (1976) 291-292.

[209] A. Zacharopoulos, P.C. Eames, D. McLarnon, B. Norton, Linear Dielectric Non-Imaging Concentrating Covers For PV Integrated Building Facades, Solar Energy, 68 (2000) 439-452.

[210] O. Korech, J.M. Gordon, E.A. Katz, D. Feuermann, N. Eisenberg, Dielectric microconcentrators for efficiency enhancement in concentrator solar cells, Opt. Lett., 32 (2007) 2789-2791.

[211] T.K. Mallick, P.C. Eames, Design and fabrication of low concentrating second generation PRIDE concentrator, Solar Energy Materials and Solar Cells, 91 (2007) 597-608.

[212] B.C. Rowan, L.R. Wilson, B.S. Richards, Advanced Material Concepts for Luminescent Solar Concentrators, Selected Topics in Quantum Electronics, IEEE Journal of, 14 (2008) 1312-1322.

[213] J.C. Goldschmidt, M. Peters, A. Bösch, H. Helmers, F. Dimroth, S.W. Glunz, G. Willeke, Increasing the efficiency of fluorescent concentrator systems, Solar Energy Materials and Solar Cells, 93 (2009) 176-182.

[214] L.H. Slooff, E.E. Bende, A.R. Burgers, T. Budel, M. Pravettoni, R.P. Kenny, E.D. Dunlop, A. Büchtemann, A luminescent solar concentrator with 7.1% power conversion efficiency, physica status solidi (RRL) – Rapid Research Letters, 2 (2008) 257-259.

[215] L.R. Wilson, Luminescent Solar Concentrators: A Study of Optical Properties, Re-absorption and Device Optimisation, PhD Thesis, Mechanical Engineering, Heriot-Watt University, Edinburgh, (2010).

[216] S.J. Gallagher, B.C. Rowan, J. Doran, B. Norton, Quantum dot solar concentrator: Device optimisation using spectroscopic techniques, Solar Energy, 81 (2007) 540-547.

[217] P.R. Rempp, E.D. Merrill, Polymer Synthesis, Hutting&Wepf Verlag, New York, USA, (1986).

[218] Anon, Data sheet, crystal clear series, Smooth-On (Ed.), Easton, USA, 2008.

[219] G.T. Howard, Biodegradation of polyurethane: a review, International Biodeterioration & amp; Biodegradation, 49 (2002) 245-252.

[220] A.W. Czanderna, F.J. Pern, Encapsulation of PV modules using ethylene vinyl acetate copolymer as a pottant: A critical review, Solar Energy Materials and Solar Cells, 43 (1996) 101-181.

[221] B. Ketola, K.R. McIntosh, A. Norris, M.K. Tomalia, Silicones for photovoltaic encapsulation, In proceedings of the 23rd European Photovoltaic Solar Energy Conference (2008), pages 2969-2973.

[222] Anon, Information about Dow Corning Brand Silicone Encapsulants,: Dow Corning (Ed.), Midland, USA, 2008.

[223] A. Cole, K.C. Heasman, A. Mellor, S. Roberts, T.M. Bruton, Laser Grooved Buried Contact Solar Cells for Concentration Factors up to 100x, In proceedings of the IEEE 4th World Conference on Photovoltaic Energy Conversion, (2006), pages 834-837.

[224] K.C. Heasman, A. Cole, S. Roberts, M. Brown, I. Baistow, S. Devenport and T.M. Bruton, Development of LGBC solar cells for use at concentration factors up to 100x, In proceedings of the 4th International Conference on Solar Concentrators for the generation of Hydrogen, (2007).

[225] M.I. L. Serenelli SDI, M. Tucci, E. Salza, L. Pirozzi, A. Cole, L.M. Brown, S. Devenport, K. Drew, K. Heasman, D.J. Morrison, T. Bruton, S. Dewallef, Screen Printing in Laser Grooved Buried Contact Solar Cells: the LAB2LINE Hybrid Processes, In proceedings of the 25th European Photovoltaic Solar Energy Conference (2010).

[226] K. Drew, L.M. Brown, A. Cole, K.C. Heasman, T.M. Bruton, Design considerations for silicon solar cells as part of the ASPIS concentrator concept, In proceedings of the 26th European Photovoltaic Solar Energy Conference (2011),

[227] A. Cole, I. Baistow, L. Brown, S. Devenport, K.C. Heasman, D. Morrison, G. Whyte, T.M. Bruton, Technological and financial aspects of laser grooved buried contact silicon solar cell based concentrator systems, In proceedings of the 2nd international Workshop on Concentrating Photovoltaic Power Plants: Optical Design and Grid Connection, Darmstadt, (2009).

[228] S. Eager, N. Mason, T. Bruton, J. Sherborne, R. Russell, Environmentally friendly processes in the manufacture of Saturn solar cells, In proceedings of the 29th IEEE Photovoltaic Specialists Conference (2002), pages 62-65.

[229] M. Vivar, C. Morilla, I. Antón, J.M. Fernández, G. Sala, Laser grooved buried contact cells optimised for linear concentration systems, Solar Energy Materials and Solar Cells, 94 (2010) 187-193.

[230] T.K. Mallick, P.C. Eames, Electrical performance evaluation of low-concentrating non-imaging photovoltaic concentrator, Progress in Photovoltaics: Research and Applications, 16 (2008) 389-398.

[231] Anon, Mutronic Prazisionsmaschinen, GmbH & Co. KG. (Ed.), Avilable from http://www.mutronic.de/, (2010).

[232] Anon, Datasheet: Dow Conring (R) 92-023 Primer, Dow-Corning, Midland, USA, (2008).

[233] Anon, Datasheet: ReflecTech mirror film, ReflecTech, http://www.reflectechsolar.com/technical.html, Arvada, USA, (2008).

[234] Anon, Datasheet: Perkin Elmer Lambda 900 UV-Vis spectrometer, Perkin. Elmer (Ed.), Massachusetts, USA, (2010).

[235] S. Svanberg, Atomic and Molecular Spectroscopy: Basic Aspects and Practical Applications, Springer, (2004).

[236] Anon, Datasheet: Renishaw Cyclone, Renishaw (Ed.), Gloucestershire, UK, (2009).

[237] Anon, Datasheet: ABET sun2000 class-A, ABET Technologies Inc, Milford, USA, (2009).

[238] Anon, Datasheet: EKO MP-160 IV-curve tracer, EKO Instruments Co. (Ed.), Tokyo, Japan, (2010).

[239] Anon, Datasheet: EKO MI-520 Module selector, EKO Instruments Co. (Ed.), Tokyo, Japan, (2010).

[240] Anon, Datasheet: SOLYS 2, Kipp & Zonen, Delft, The Netherlands, (2010).

[241] Anon, Datasheet: CMP-11 pyranometer, Delft, The Netherlands, Delft, The Netherlands, (2010).

[242] Anon, Technical information: Metal Halide Lamp: HMI 1200 W/SEL, OSRAM (Ed.), Munchen, Germany, (2008).

[243] Anon, Manual: Optics Lab, Optical Ray Tracing Software, http://www.optics-lab.com/, Carlsbad, CA, USA, (2008).

[244] Anon, Datasheet: Si-photodiode, S3477-series, Hamamatsu, http://sales.hamamatsu.com/en/products/solid-state-division/si-photodiode-series/si-photodiode/part-s3477-04.php, (2010).

[245] Anon, Datasheet: ND30A - Reflective Ø25 mm ND Filter, Thorlabs, Cambridgeshire, UK, (2010).

[246] L.G. Rainhart, W.P. Schimmel Jr, Effect of outdoor aging on acrylic sheet, Solar Energy, 17 (1975) 259-264.

[247] Anon, Techplot manual, A.E. Bellevue (Ed.), Washington, U.S.A, (2008).

[248] Meteorology Data, PVSYST, Switzerland, (2008).

[249] Anon, Training mannual for ANSYS-cfx,, ANSYS, (2010).

[250] J. Ballato, S.H. Foulger, J.D.W. Smith, Optical properties of perfluorocyclobutyl polymers. II. Theoretical and experimental attenuation, J. Opt. Soc. Am. B, 21 (2004) 958-967.

[251] N. Sarmah, B.S. Richards, T.K. Mallick, Evaluation and optimization of the optical performance of low-concentrating dielectric compound parabolic concentrator using ray-tracing methods, Appl. Opt., 50 (2011) 3303-3310.

[252] T.K. Mallick, P.C. Eames, B. Norton, Power losses in an asymmetric compound parabolic photovoltaic concentrator, Solar Energy Materials and Solar Cells, 91 (2007) 1137-1146.

[253] Personal communication, Dow-corning, UK, (2011).

[254] Personal communication, Shanghai Xinyutian International Trade Co., Shanghai, (2010).

[255] Embodied energy coefficient, Available from www.victoria.ac.nz/cbpr/documents/pdfs/ee-coefficients.pdf, (2012).

[256] E.A. E.A. Alsema, M.J.d. Wild-Scholten, Reduction of the environmental impacts in crystalline silicon module manufacturing, In proceedings of the 22nd European Photovoltaic Solar Energy Conference (2007), pages 829-836.

[257] Personal communication, ReflecTech Inc., Arvada, USA, (2009).